(2)

ESL-TR-88-74

PORTABLE TANDEM MASS SPECTROMETER ANALYZER

R. YOST, M. K. JOHNSON, M. HAIL

UNIVERSITY OF FLORIDA
CHEMISTRY DEPARTMENT
GAINESVILLE FL 32611

JULY 1991

FINAL REPORT

DECEMBER 1984 - DECEMBER 1987

APPROVED FOR PUBLIC RELEASE: DISTRIBUTION UNLIMITED

AIR FORCE ENGINEERING & SERVICES CENTER
ENGINEERING & SERVICES LABORATORY
TYNDALL AIR FORCE BASE, FLORIDA 32403

NOTICE

PLEASE DO NOT REQUEST COPIES OF THIS REPORT FROM HQ AFESC/RD (ENGINEERING AND SERVICES LABORATORY). ADDITIONAL COPIES MAY BE PURCHASED FROM:

NATIONAL TECHNICAL INFORMATION SERVICE
5285 PORT ROYAL ROAD
SPRINGFIELD, VIRGINIA 22161

FEDERAL GOVERNMENT AGENCIES AND THEIR CONTRACTORS REGISTERED WITH DEFENSE TECHNICAL INFORMATION CENTER SHOULD DIRECT REQUESTS FOR COPIES OF THIS REPORT TO:

DEFENSE TECHNICAL INFORMATION CENTER
CAMERON STATION
ALEXANDRIA, VIRGINIA 22314

UNCLASSIFIED
SECURITY CLASSIFICATION OF THIS PAGE

REPORT DOCUMENTATION PAGE

Form Approved
OMB No. 0704-0188

1a. REPORT SECURITY CLASSIFICATION	1b. RESTRICTIVE MARKINGS
2a. SECURITY CLASSIFICATION AUTHORITY	3. DISTRIBUTION/AVAILABILITY OF REPORT Approved for Public Release Distribution Unlimited
2b. DECLASSIFICATION/DOWNGRADING SCHEDULE	
4. PERFORMING ORGANIZATION REPORT NUMBER(S)	5. MONITORING ORGANIZATION REPORT NUMBER(S) ESL-TR-88-74
6a. NAME OF PERFORMING ORGANIZATION Chemistry Department University of Florida 6b. OFFICE SYMBOL (If applicable)	7a. NAME OF MONITORING ORGANIZATION Air Force Engineering & Services Center
6c. ADDRESS (City, State, and ZIP Code) Gainesville FL 32611	7b. ADDRESS (City, State, and ZIP Code) Tyndall AFB FL 32403
8a. NAME OF FUNDING/SPONSORING ORGANIZATION HQ AFESC 8b OFFICE SYMBOL (If applicable) RDVS	9. PROCUREMENT INSTRUMENT IDENTIFICATION NUMBER F08635-83-C-0136
8c. ADDRESS (City, State, and ZIP Code) HQ AFESC/RDVS Tyndall AFB FL 32403-6001	10. SOURCE OF FUNDING NUMBERS PROGRAM ELEMENT NO. 62601F; PROJECT NO. 1900; TASK NO 20; WORK UNIT ACCESSION NO. 71

11. TITLE (Include Security Classification)
(U) Portable Tandem Mass Spectrometer Analyzer

12. PERSONAL AUTHOR(S)
Yost, R., Johnson, Matuszak, K., and Hail, M.

13a. TYPE OF REPORT	13b. TIME COVERED	14. DATE OF REPORT (Year, Month, Day)	15. PAGE COUNT
Final	FROM 84 12 TO 87 12	July 1991	281

16. SUPPLEMENTARY NOTATION
Availability of this report is specified on reverse of the front cover

17. COSATI CODES			18. SUBJECT TERMS (Continue on reverse if necessary and identify by block number)
FIELD	GROUP	SUB-GROUP	Mass Spectrometer; Portable Mass Spectrometer; Tandem Mass Spectrometer; Atmospheric Pressure Ionization

19. ABSTRACT (Continue on reverse if necessary and identify by block number)

This report documents Phase 1 of a two-phased project to develop a portable tandem mass spectral analyzer to be used in environmental characterizations of contaminated and suspected contaminated sites of Air Force properties. Phase 1 was a laboratory prototyping study and Phase 2 was to entail the construction of an actual portable prototype instrument. Phase 1 accomplishments include the development of an atmospheric pressure ionization source for a compact commercial mass spectrometer, fundamental studies of the atmospheric pressure ionization processes, and the development of rapid gas chromatographic pre-separation methods intended to enhance the instrument's performance when analyzing complex samples.

20. DISTRIBUTION/AVAILABILITY OF ABSTRACT	21 ABSTRACT SECURITY CLASSIFICATION	
☐ UNCLASSIFIED/UNLIMITED ☐ SAME AS RPT ☐ DTIC USERS	Unclassified	
22a NAME OF RESPONSIBLE INDIVIDUAL Dr Howard T. Mayfield	22b TELEPHONE (Include Area Code) (904) 283-6049	22c OFFICE SYMBOL HQ AFESC/RDVC

DD Form 1473, JUN 86 *Previous editions are obsolete* SECURITY CLASSIFICATION OF THIS PAGE

(The reverse of this page is blank.)

SUMMARY

This effort was a laboratory study to develop techniques and equipment for use in building a portable tandem mass spectrometer analyzer. The planned instrument was to be small enough to be portable in small vehicles and was to be able to use either an atmospheric pressure ion source or a conventional electron impact/chemical ionization ion source. In order to accomplish these developments an atmospheric pressure ionization source was developed for a compact, commercially available tandem quadrupole mass spectrometer. This ion source could be readily exchanged with the conventional electron impact/chemical ionization ion source without modifications to the instrument mainframe. Additionally, techniques for introducing samples into the instrument using either the atmospheric pressure ion source or conventional ion sources were developed and tested. One of the sample introduction developments was the use of a short length of a capillary gas chromatography column as a sample introduction device. The capillary column served as an inlet restrictor but was also able to separate mixed component samples that simulated environmental mixtures. The short inlet column was shown to be able to generate reasonable separations of jet fuels within only a few minutes. Since the vacuum system of the mass spectrometer evacuated most of the inlet capillary column, theoretical aspects of separating mixtures in an open tubular column under reduced pressure were also investigated.

(The reverse of this page is blank.)

PREFACE

This report was prepared by the Chemistry Department, University of Florida, Gainesville Florida, under Contract No. F08635-83-C-0136, Subtask 85-2, for the US Air Force Engineering and Services Center, Engineering and Services Laboratory, Tyndall Air Force Base, Florida 32403-6001. Dr Richard A. Yost of the University of Florida, was the principal investigator. This report summarizes work accomplished between 1 December 1984 and 31 December 1987.

Although this report does not meet all format standards for this laboratory, it is being published because of its interest to the scientific and technical community.

This report has been reviewed by the Public Affairs Office (PA) and is releasable to the National Technical Information Service (NTIS). At NTIS, it will be available to the general public, including foreign nationals.

This technical report has been reviewed and is approved for publication.

HOWARD T. MAYFIELD, GS-12
Project Officer

Neil J. Lamb, Lt Col, USAF
Chief, Environics Division

WAYNE P. CHEPREN, Capt, USAF
Chief, Environmental Compliance R&D

Frank P. Gallagher III, Colonel, USAF
Director, Engineering and Services Laboratory

(The reverse of this page is blank.)

Final Report

PORTABLE TANDEM MASS SPECTROMETRIC ANALYZER

Table of Contents

(The reverse of this page is blank.)

Final Report

PORTABLE TANDEM MASS SPECTROMETRIC ANALYZER

Executive Summary

This is the final report on our three-year Phase I project to perform research which could lead to the development of a portable tandem mass spectrometric (MS/MS) analyzer for environmental monitoring in the field. As originally prescribed, our research was initially oriented specifically towards a triple quadrupole tandem mass spectrometer with atmospheric pressure ionization (API) for direct atmospheric monitoring of compounds of environmental concern to Air Force programs. During the course of this project, the objectives have been broadened to include consideration of analysis of environmental samples other than ambient air (e.g., soil and groundwater), including alternative methods of sample introduction and ionization. A further extension has been investigation of the quadrupole ion trap as an alternative to the triple quadrupole instrument for MS/MS. The sections which follow detail our research in each of these areas. A number of significant accomplishments are reported, as summarized below.

We have developed a working API source which is compatible with a conventional triple quadrupole tandem mass spectrometer. Not only does this make API available on an instrument that is also capable of general purpose MS/MS studies (e.g., traditional electron ionization and chemical ionization methods, as well as GC and probe introduction of complex mixtures), it also makes available API capabilities on modern, state-of-the-art, triple quadrupole instruments. This represents a significant advantage over current commercial

API instruments. A further accomplishment is the realization of declustering and prevention of orifice clogging with a simple gas jet design and control of ion velocity in the source/analyzer interface region.

Our studies of the ion optics and ion transmission in the triple quadrupole mass spectrometer have led to a significant improvement in our ability to operate such an instrument to reproducibly obtain maximum sensitivity. We have observed significant mass dependencies in the transmission of ions through the entrance and exit lenses of mass-filtering quadrupoles, as well as in the effects of collision energy and RF potential on the center quadrupole collision cell. Our research has clearly demonstrated that the computer-controlled TSQ 70 is the best instrument for performing these investigations and characterizing these ion optical effects. Moreover, the TSQ 70 is the only MS/MS instrument with the capability to utilize these observations to optimize mass transmission and reduce mass dependencies within each mass spectral scan.

Our research into alternative sample introduction and ionization methods for non-air samples has emphasized developments in rapid chromatographic separation on short open tubular (capillary) gas chromatographic (OTGC) columns. Important features of this work have included detailed theoretical and experimental characterization of the analytical performance of short OTGC columns operated with vacuum outlet conditions, extensions to vacuum inlet conditions, and development of exponential flow rate programming as an alternative to temperature programming for rapid GC separations. This research points toward the development of a small probe-type capillary gas chromatograph which could permit rapid switching from direct probe analyses to GC analyses on a small portable field instrument.

Our research in the area of tandem-in-time (e.g., quadrupole ion trap) as an alternative to tandem-in-space (e.g., triple quadrupole) MS/MS has clearly

indicated potential advantages and limitations of this approach. The advantages include the potential for small, simple, low cost MS/MS instrumentation with remarkably high MS/MS sensitivity, all important features for a portable environmental monitor. Trade-offs include restrictions on ionization methods (currently limited to electron ionization and chemical ionization, not API) and potential interferences and selectivity problems from ion-molecule interactions during the relatively long residence times of ions in the single ionization/MS/MS region.

In conclusion, these research efforts have provided a solid foundation for the development of a portable tandem mass spectrometric analyzer for environmental monitoring. Details of the research are presented in the following sections.

1. CHARACTERIZATION AND OPTIMIZATION OF ION TRANSMISSION

1-A. Introduction

Triple quadrupole mass spectrometers are inherently complex instruments. The performance of these instruments is highly dependent on the adjustment of the ion optical parameters. Thus, instruments that are improperly "tuned" can produce markedly different spectra. The use of these instruments has become so widespread that a better understanding of the performance of the ion optics is necessary. In fact, there has recently been a request for the implementation of standard MS/MS spectral libraries, which will require even more attention of operating conditions. A thorough study of the ion optics has allowed a better understanding of their effects on single MS and MS/MS experiments. In addition, these experiments have led to the development of procedures for proper tuning. It is believed that the procedures that were developed will improve the sensitivity, as well as the reproducibility, for all modes of operation of the instrument.

The instrument that has been used for these characterization and optimization studies is a Finnigan MAT TSQ 70. This instrument has proven to be ideal for studies of this type, since all parameters are under microprocessor control. In fact, with older instruments, many of the experiments that have been performed would either not be possible or would have been too time-consuming to carry out. The instrument is controlled by six different single board controllers, each of which has its own microprocessor. The user interacts with the instrument with a unique procedural language known as the Instrument Control Language, or ICL. Writing procedures with the ICL is much like writing a BASIC program (i.e. the commands are simple and easy to understand). However, the scope of application of the ICL is nearly limitless, and often is only limited

by the user's imagination. Another attractive feature of this instrument is that any ion optical parameter may be varied as the mass spectrometer is scanned. This turns out to be particularly advantageous in avoiding any mass discrimination that may be present in the ion optics, as discussed below.

Shown in Figure 1-A.1 is a diagram of the analyzer assembly of the TSQ 70. As shown in the figure, the ion optics consist of three quadrupoles and eleven focussing lenses (labeled L11-L42). The first and third quadrupoles (Q1 and Q3, respectively) may be operated in the mass-selective mode or can be set to pass all ions, depending on the scan mode selected. Regardless of the scan mode used, Q2 cannot be made mass-selective like Q1 or Q3, but simply serves as an ion transmission and focussing device during single MS experiments and as the collision region for MS/MS experiments. More discussion on the characteristics of the second quadrupole is presented in section 1-D of this report.

Diagram of the Analyzer Assembly of the TSQ 70

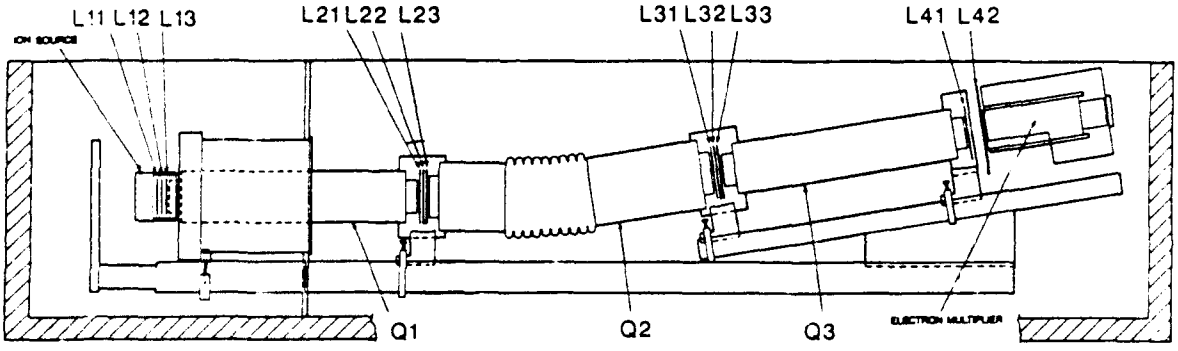

Figure 1-A.1. Diagram of the analyzer assembly of the TSQ 70 triple quadrupole mass spectrometer.

1-B. Mass-Dependent Optimization

The presence of mass dependencies in the ion optics of quadrupole mass spectrometers has long been known. However, the effects of these mass dependencies on the transmission of ions has never been easily elucidated. The use of computer-controlled instrumentation like the TSQ 70 allows for more rapid characterization and understanding of these phenomena.

Ion optics theory predicts that all ions accelerated from a specific point in space through an electrostatic lens will follow the same trajectory regardless of the masses of the ions. Thus, mass dependency does not come from the electrostatic lens per se, but is the result of non-idealities introduced from other forces. It was the object of this work to determine which lenses exhibited mass dependencies, and by observing any trends in the data to elucidate the origins of these mass dependencies. After determining which lenses are mass-dependent and optimizing the lenses accordingly, it is possible to obtain maximum sensitivity over the entire mass range.

The experiments for studying mass dependencies of ion optics are relatively simple. For most of the lens optimization studies performed, perfluorotri-N-butylamine (PFTBA) was the compound used. PFTBA is a common calibration compound that yields a wide range of masses and is conveniently leaked into the ion source. An ion transmission curve is produced by recording the intensity for selected m/z's over a range of lens voltages. A plot of ion intensity vs. lens voltage can then be made for each m/z studied. A well-behaved (ideal) lens has very similar transmission curves for different m/z's, and the lens voltage that yields the maximum transmission of ions (i.e. the optimum lens voltage) is the same for each ion of different m/z. In other words, no mass dependency is produced from an ideal lens. Figures 1-B.1 and 1-B.2 show examples of typical transmission curves for two different lenses in the normal Q1MS mode (refer to

Figure 1-A.1 for the placement of the lenses in the system). Figure 1-B.1 shows the transmission curve for a well-behaved lens (L31). In contrast, Figure 1-B.2 shows the ion transmission curves for a mass-dependent lens (L13). Note that in (b) of this figure there are discreet optimum lens voltages for each ion of different m/z; thus, setting the lens voltage at any one of these voltages will reduce the transmission of the other ions. One interesting discovery was that some of the lenses were found to be mass-dependent only in certain scan modes. For example, Figure 1-B.3 shows the mass-dependent behavior for lens L42 in the Q3MS scan mode. However, the same lens was found not to be mass-dependent in the Q1MS scan mode as shown in Figure 1-B.4. After a thorough study of the ion optics, some generalizations can be made. In the single MS scan modes (i.e. Q1MS or Q3MS), the lenses in proximity to the mass-analyzing quadrupole (i.e. the quadrupole carrying both RF and DC voltages) are mass-dependent. In particular, for Q1MS, lenses L12, L13, L21, and L22 are mass-dependent; while for Q3MS, the mass-dependent lenses are L32, L33, L41, and L42. This appears to be the case regardless of the ionization method used. For instance, positive chemical ionization (PCI) and electron capture negative CI (ECNCI) were studied and the same lenses were found to be mass-dependent. It should be noted, however, that the optimum lens voltages are dependent on the ionization method used and should be optimized accordingly.

One of the unique capabilities of the TSQ 70 is that the lens voltages may be changed with mass such that the transmission of all ions of different m/z can be optimized without compromise for a particular mass or range of masses. In order to optimize the lenses with mass, one optimizes the lens voltages at specific points along the mass range. The instrument then interpolates potentials for other masses between the set values. The result is called a tune table, which is a plot of lens voltage vs. m/z and can be created for each ion

optical parameter of the instrument. An example of such a lens table is shown in Figure 1-B.5.

One observes a significant improvement in sensitivity if mass-dependent tuning is performed. The spectrum in Figure 1-B.6 was obtained without the use of mass-dependent tuning, while the spectrum in Figure 1-B.7 was acquired after mass-dependent tuning had been performed. Both spectra are normalized to the full scale intensity of spectrum Figure 1-B.7, and both are enlarged by a factor of 10 beyond m/z 325. Note that the sensitivity is improved by a factor of two at the low mass end (e.g. m/z 69) and by a factor of four at the high mass end (e.g. m/z 502). In addition, the m/z 614 ion does not even appear in the spectrum of Figure 1-B.6, but has an intensity of about 0.5 % of the base peak in the spectrum of Figure 1-B.7.

There has been some concern that mass-dependent tuning would not yield the correct ion intensity ratios for qualitative electron ionization (EI) spectra. This is of particular concern, since EI spectra are used to compare with standard library spectra. However, it can be argued that the correct (and natural) ion abundances are obtained only when there is no mass discrimination in the ion optics. Since mass-dependent tuning effectively removes any discriminating character in the ion optics, the natural abundances of the ions are obtained. Moreover, ion intensity ratios are dependent on other parameters such as source temperature and pressure; therefore, any attempt to defocus a lens to obtain the correct ratios is not recommended.

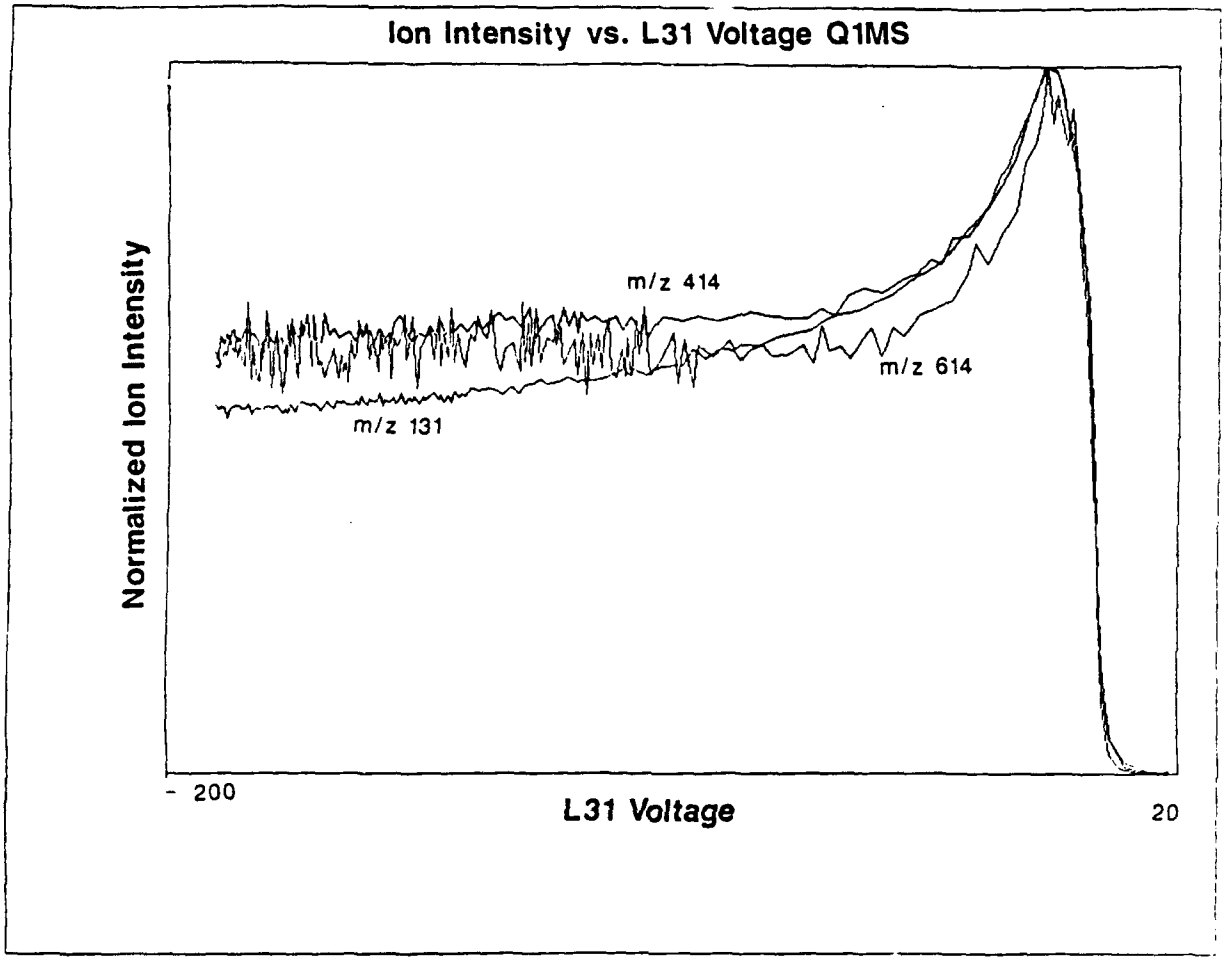

Figure 1-B.1. Typical ion transmission curves for lens L31 in the Q1MS scan mode. This lens displays ideal behavior and thus has the same optimum lens voltage for each m/z.

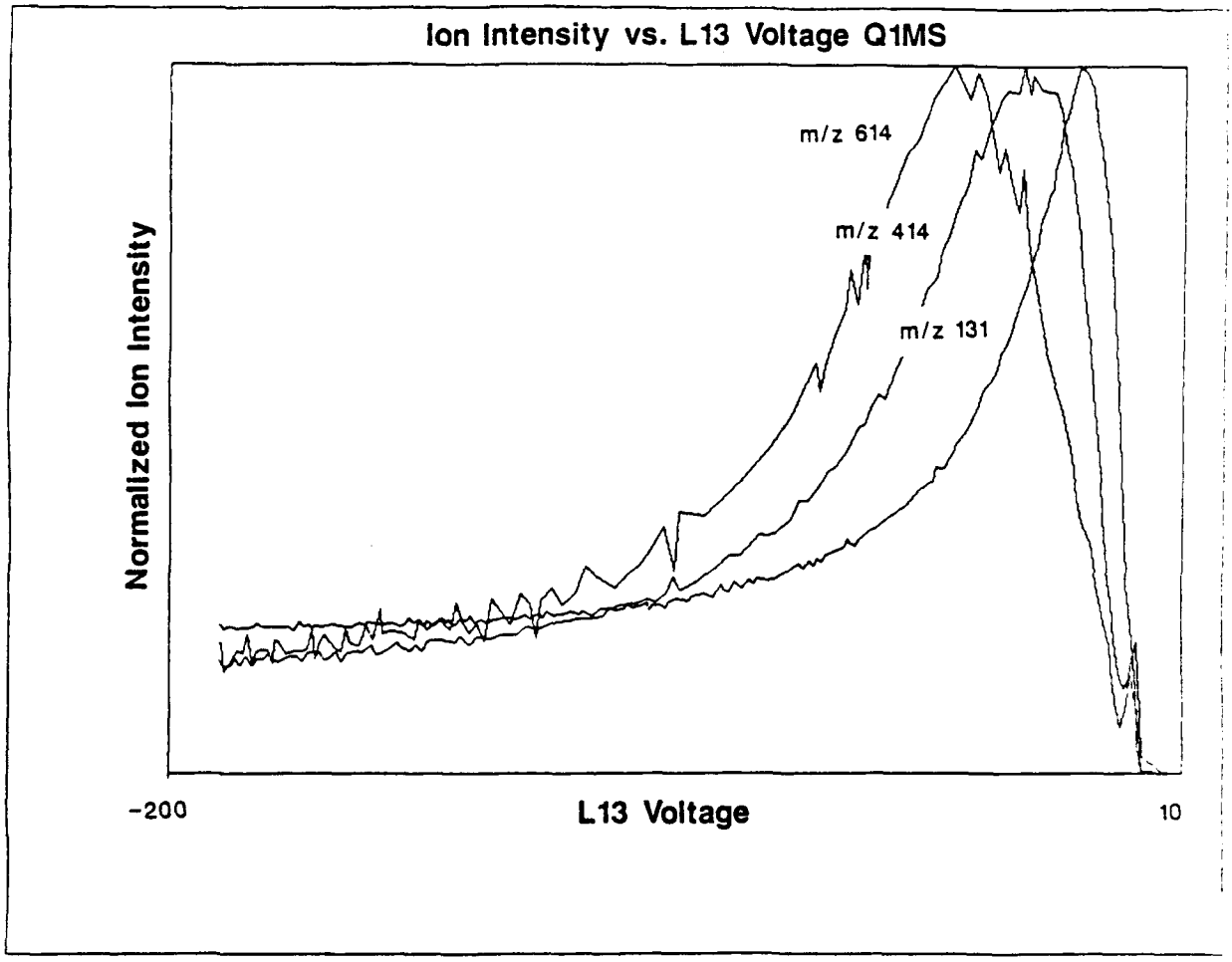

Figure 1-B.2. Transmission behavior of mass-dependent lens L13 in the Q1MS mode. Note the different optimum lens voltages for each m/z.

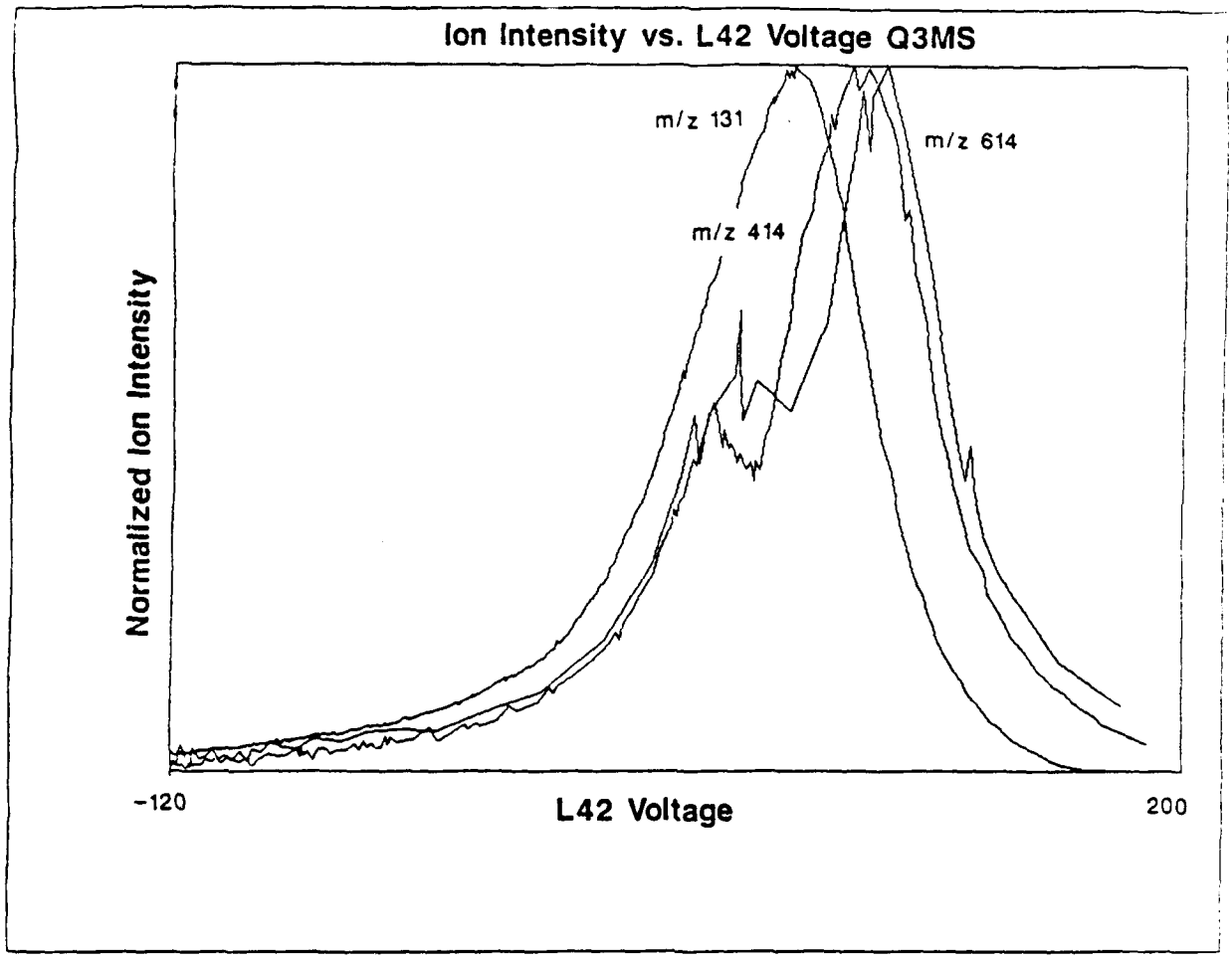

Figure 1-B.3. Ion transmission curves for lens L42 illustrating mass-dependent behavior in the Q3MS scan mode.

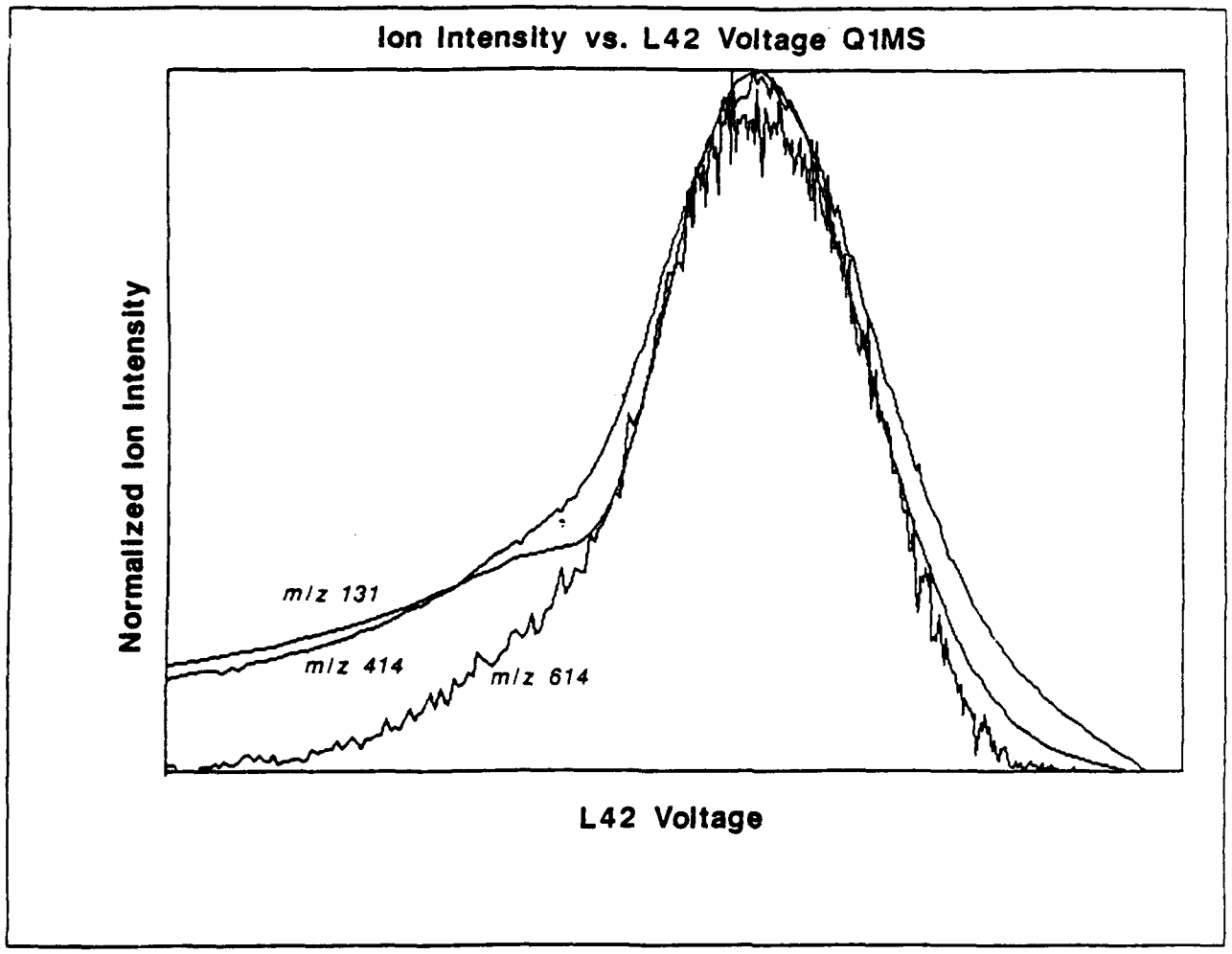

Figure 1-B.4. Ion transmission curves for lens L42 illustrating ideal behavior in the Q1MS scan mode. The lens is mass-dependent in the Q3MS mode.

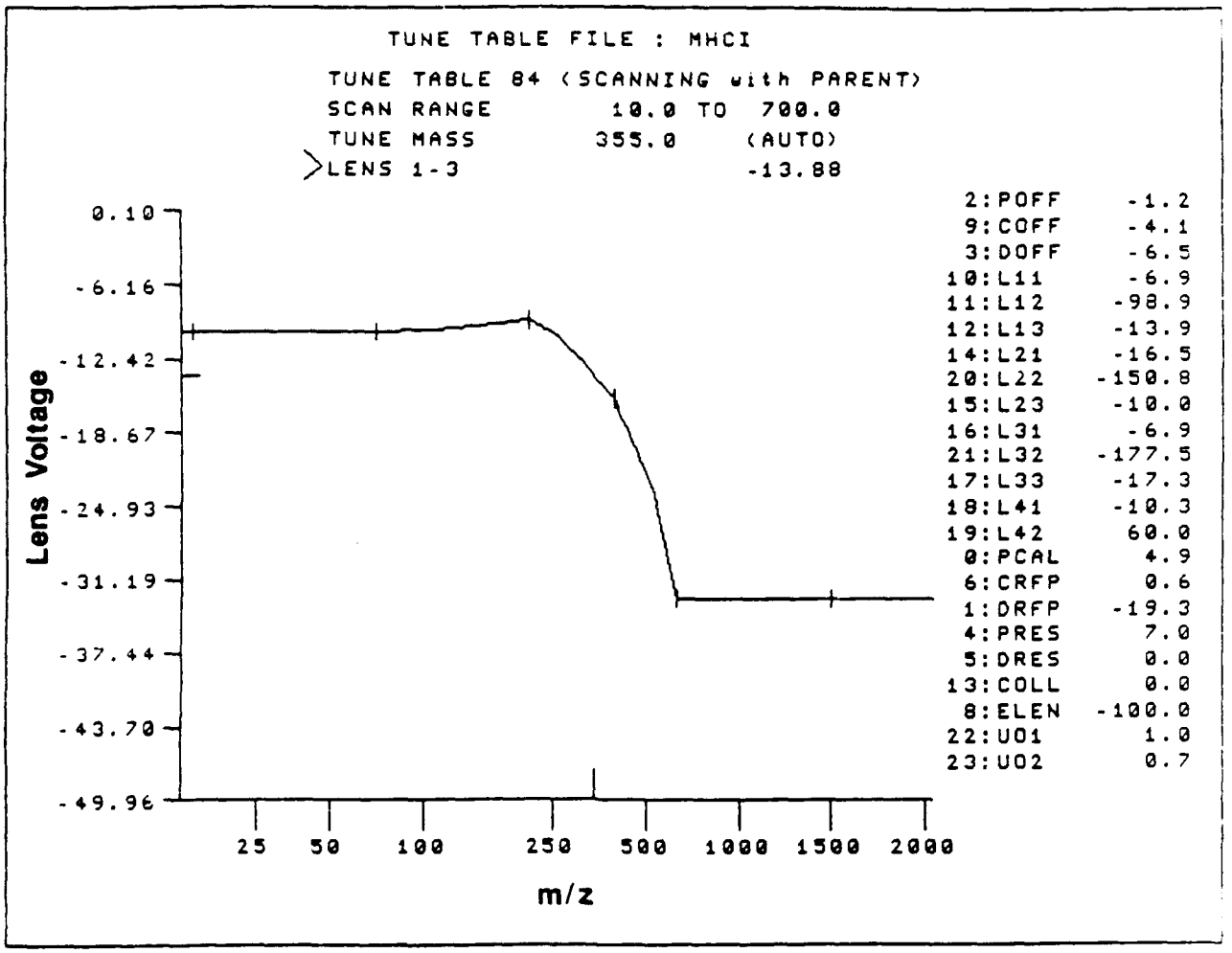

Figure 1-B.5. Example of a tune table, which allows tuning of any ion optical parameter over the entire mass range.

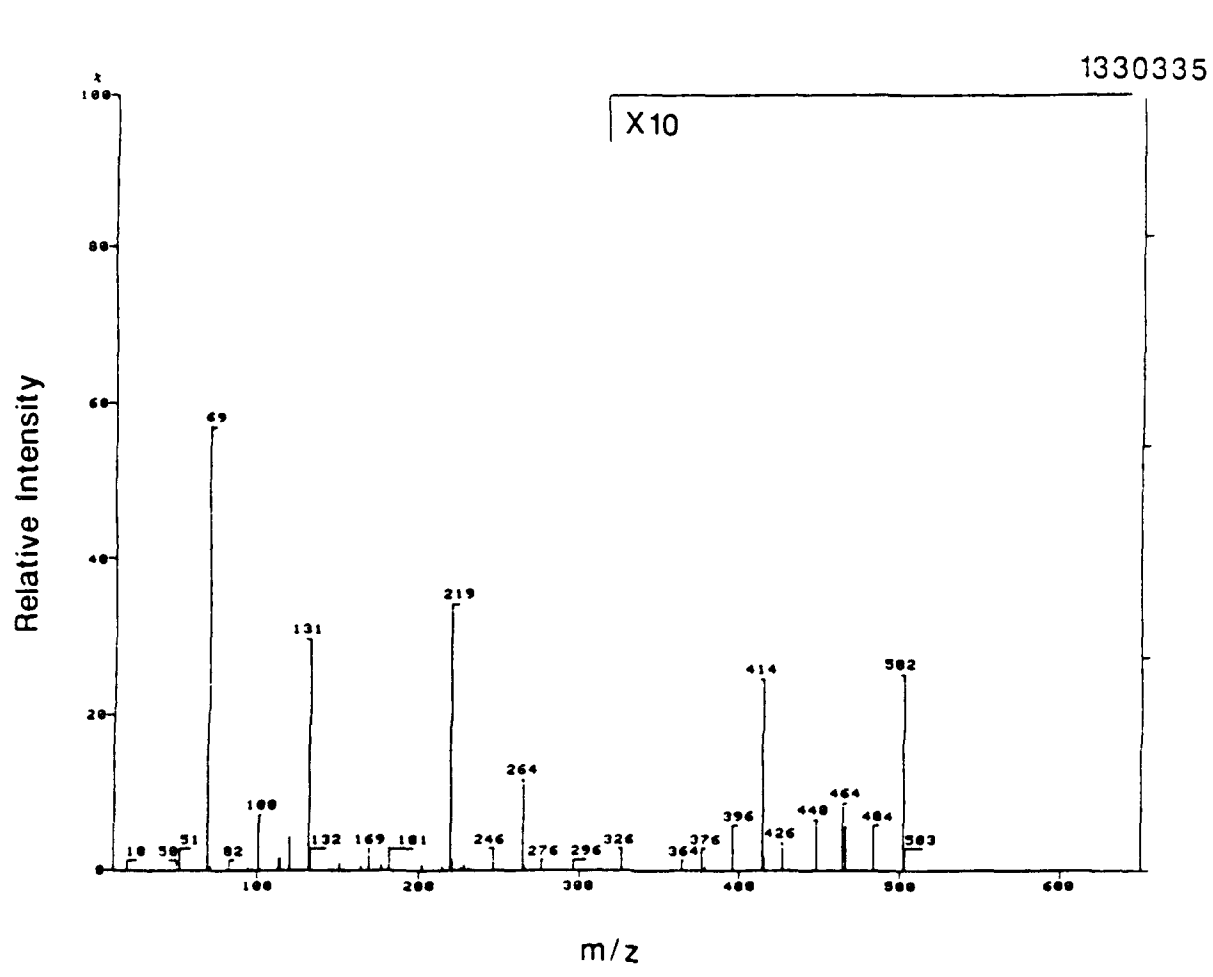

Figure 1-B.6. Mass spectrum of PFTBA obtained without mass-dependent tuning.

B

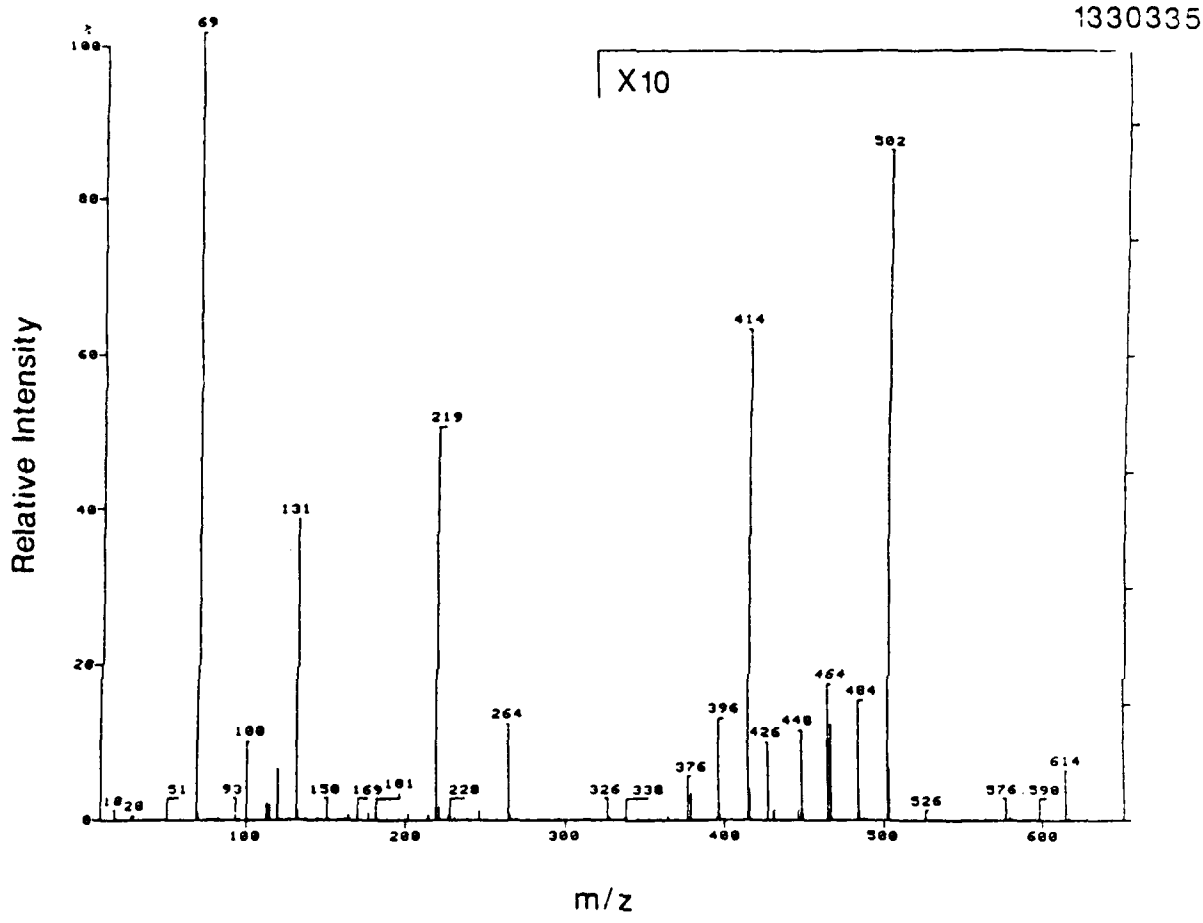

Figure 1-B.7. Mass spectrum of PFTBA obtained after mass-dependent tuning had been performed.

1-C. The Quadrupole Mass Filter

In order to obtain a better understanding of the behavior of the ion optics, some basic theory of operation of quadrupole mass filters is required. In a quadrupole mass filter, RF and DC voltages are applied in series to a set of four hyperbolic rods (one pair of rods being negatively biased with respect to the other pair). The motion of ions within quadrupoles is described mathematically by a second-order differential equation known as the Mathieu equation (1-C.1).

$$\frac{d^2u}{d\xi^2} + (a_u - 2q_u \cos 2\xi)u = 0 \qquad (1\text{-C.1})$$

The solutions of this equation define the position of an ion at any time within the device, where u is a position-dependent parameter (representing the x or y displacement of an ion) and ξ is a time-dependent variable. Ion trajectories within a quadrupole are either stable or unstable depending on the values of the Mathieu parameters 'a' and 'q'. The Mathieu parameters are given by

$$q_u = \frac{4V_{rf}e}{Mr_o^2\omega^2} \qquad (1\text{-C.2}) \qquad\qquad a_u = \frac{8V_{dc}e}{Mr_o^2\omega^2} \qquad (1\text{-C.3})$$

where V_{rf} is the zero-to-peak RF voltage of angular frequency ω, V_{dc} is the DC voltage, e is the charge, M is the mass, and r_o is the radius of the quadrupole aperture. An ion is said to have stable trajectories if its excursions in the x or y directions do not exceed the defined boundaries of the applied field. Conversely, unstable trajectories represent conditions in which the displacement of the ion increases without bound until it is eventually ejected and is not

transmitted through the device. Consequently, a stability diagram can be drawn (shown in Figure 1-C.1) where 'a' and 'q' represent the y and x axes, respectively. Ions that have Mathieu parameters within the triangular envelope of the stability diagram have stable trajectories; those outside of the area are unstable. When operating as a mass filter, RF and DC voltages are applied such that only a narrow range of masses (usually one) have stable trajectories at any one instance in time, and, thus may be transmitted to the detector. This is achieved by using a scan line that slices through the very tip of the stability diagram. The range of masses which will be stable is determined by the DC/RF ratio (i.e. the slope of the scan line). In order to obtain a scan over a range of m/z's, the RF and DC voltages are increased linearly with time (at constant DC/RF) so that ions of increasing m/z are brought within the narrow window of stability. Mass resolution is increased (with a reduction of the number of ions transmitted) by moving the scan line closer to the tip of the stability region.

The mass dependencies that were described in the previous section are a function of the fields imposed by the mass filters, and can be attributed to two major influences. The first is due to the presence of fringing fields that exist at both ends of a quadrupole mass filter. Fringing fields are capable of causing ions to become unstable as they attempt to enter the device; thus, a reduction in ion transmission results. The second factor can be attributed to the limited acceptance of the mass filter. Since the point of operation of a mass filter is near the tip of the stability diagram, the conditions of initial position and velocity have a greater effect on the transmission of ions than with an RF-only quadrupole. A more thorough discussion of the nature of RF-only quadrupoles is presented in the next section.

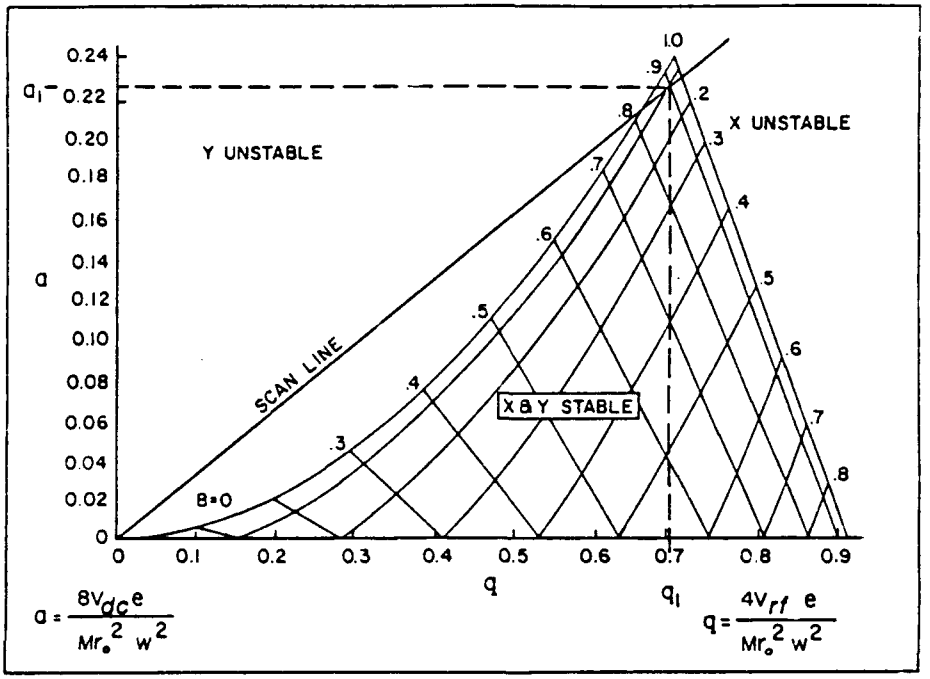

STABILITY DIAGRAM FOR BOTH X & Y

Figure 1-C.1. Stability diagram for a quadrupole mass filter.

1-D. The RF-only Quadrupole

In triple quadrupole mass spectrometry the center quadrupole operates in the RF-only mode. It is a popular misconception that an RF-only quadrupole is capable of passing all masses simultaneously. However, transmission of ions through an RF-only quadrupole is subject to the same constraints as an RF/DC quadrupole. The difference is that since the applied DC voltage is zero, a = 0 and the ion stability is determined by the x-axis of the stability diagram (i.e. the q-axis). Thus, for an ion to be stable it must have a value of 'q' between 0 and 0.908. Since there are a range of q's over which a particular mass is stable, it follows from equation (1-C.2) that there is also a range of RF voltages over which a particular mass is stable. Thus, the range of RF voltages that will lead to stable trajectories becomes smaller as the mass is decreased. This means that proper choice of the RF level is critical to avoid low mass cut-off. A condition of low mass cut-off occurs when the RF voltage has been set high enough such that ions below a certain m/z have q's greater than 0.908 and, thus, will not be transmitted. Figure 1-D.1 is a demonstration of the principles discussed above. In this experiment, ion intensities for the daughters of m/z 219 from PFTBA are plotted against Q2 RF voltage. As shown in the figure, there is an optimum RF voltage for the transmission of each ion of different m/z. Also note that the transmission curves become more narrow with decreasing m/z as discussed above. This points out a fundamental limitation of the second quadrupole. In the normal mass spectral modes, only one m/z passes through the device at any one instant in time. Thus, the RF voltage can be optimized for the transmission of ions of each different m/z. However, during MS/MS scans, Q2 is required to contain (at the same time) parent ions, as well as daughter ions of different m/z, and optimum transmission of each different ion may not be possible. Thus, there is not an optimum q-value or RF voltage for maximum

transmission of all daughter ions. Rather, the RF-voltage should be optimized for the particular experiment of interest. For example, if one is attempting to obtain good qualitative daughter spectra, then the RF voltage should be optimized for a low m/z daughter ion such that all of the resulting daughter ions could be observed. For quantitative work , where only one or a few daughter ions are monitored, the RF voltage should be optimized such that maximum sensitivity is obtained for the particular parent ion-to-daughter ion transition under study.

In the TSQ 70, the Q2 RF level is automatically set by the level chosen for the parent ion in a daughter experiment. The default setting of the Q2 RF level corresponds to a q-value of 0.2 for the parent ion. As shown in Figure 1-D.1, setting the RF level for the optimum for the parent ion m/z 219 (q = 0.21) could severely limit the transmission of daughter ions of lower mass. In addition, the lowest m/z that can be observed in the center quadrupole, $(m/z)_{cut\text{-}off}$, is determined by the m/z of the parent ion, $(m/z)_p$, and the q-value of the parent ion, q_p, as shown by equation (1-D.1).

$$(m/z)_{cut\text{-}off} = \frac{q_p(m/z)_p}{0.908} \qquad (1\text{-}D.1)$$

If the q-value of the parent is chosen to be 0.2, then equation (1-D.1) reduces to

$$(m/z)_{cut\text{-}off} = 0.22(m/z)_p \qquad (1\text{-}D.2)$$

As can be seen in Table 1-D.1, with increasing m/z of the parent ion, the lower mass limit may prevent useful daughter ions from being observed. An example

of this is seen in the methane PCI-CAD daughters of the m/z 652 fragment ion of PFTBA, as shown in Figure 1-D.2. Variation of the Q2 RF voltage during the daughter scans of Figure 1-D.2 shows there to be optimum RF voltages for the yield of each daughter ion. Note that if a daughter spectrum was acquired with the default q-value for m/z 652 of 0.2, the lower mass limit for the daughter ions would be m/z 143 (Table 1-D.1) and the daughter ions m/z 131 and m/z 69 would not be observed, as shown in Figure 1-D.3. Instead, a daughter scan obtained with the Q2 RF voltage set to yield a q-value for m/z 652 of 0.07 would include these daughter ions. Thus, more complete structural information would be available. In addition, as shown in Table 1-D.2, the maximum transmission of all daughter ions occurred for RF voltages corresponding to q-values for the parent ion, m/z 652, which were less than the default 0.2 q-value.

Table 1-D-1. Lower m/z limit of the daughter ion possible with the RF-voltage applied to Q2 to yield a q-value of 0.2 for the parent ion.

m/z Parent	Low m/z Limit of Dg Ions
69	15
31	29
219	48
264	58
414	91
502	110
614	135
652	143
2000	440
4000	880

Table 1-D-2. Q-values for the maximum transmission of daughter ions from the methane PCI-CAD (20 eV, 1.5 mtorr N_2) daughter scans of the m/z 652 ion of PFTBA (see Figure 1-D.2).

m/z	q(Dg, max)	q(Par, max)
69	0.55	0.06
131	0.49	0.11
219	0.20	0.07
414	0.17	0.11
652	0.06	0.06

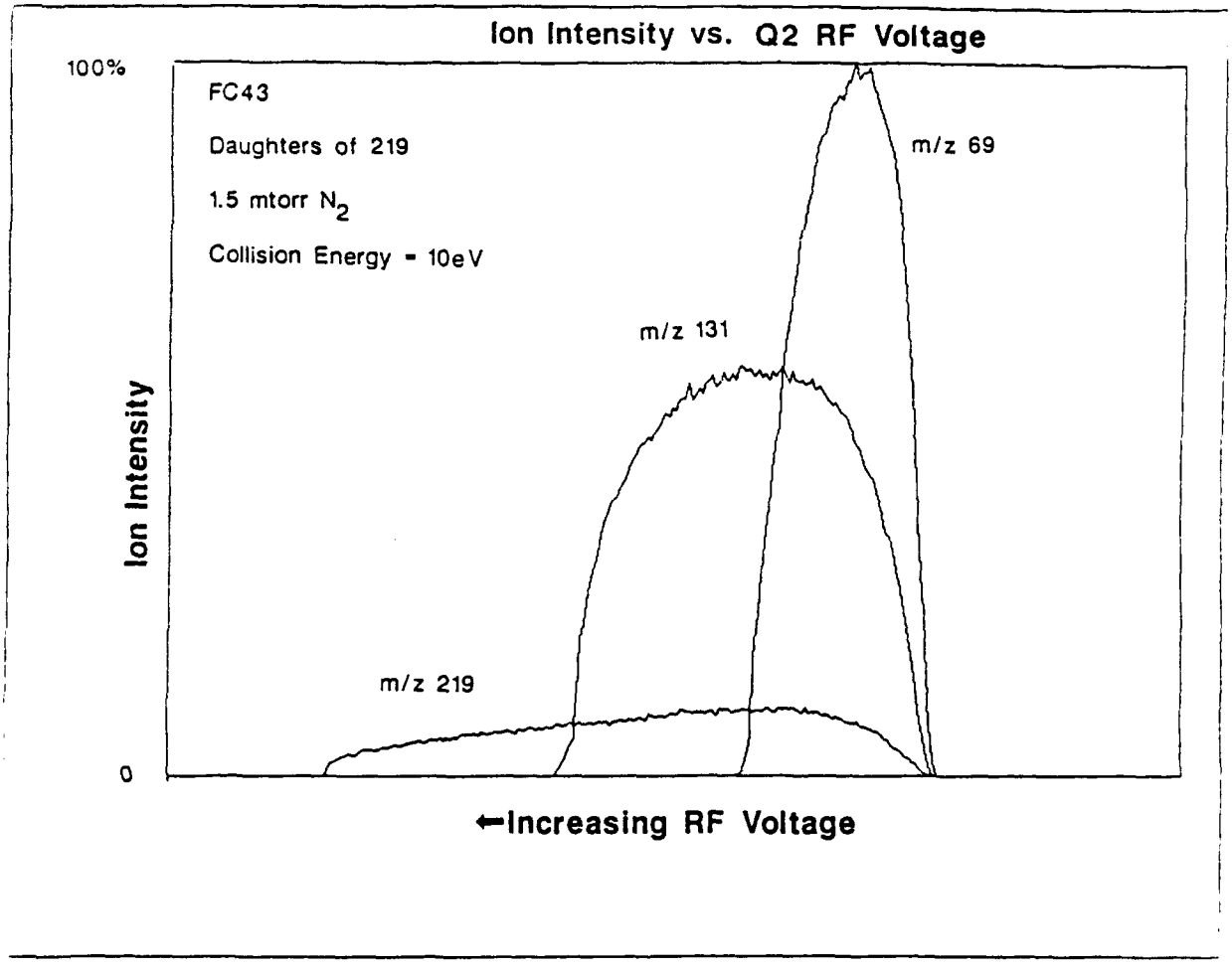

Figure 1-D.1. Transmission of different ions of PFTBA with Q2 RF voltage.

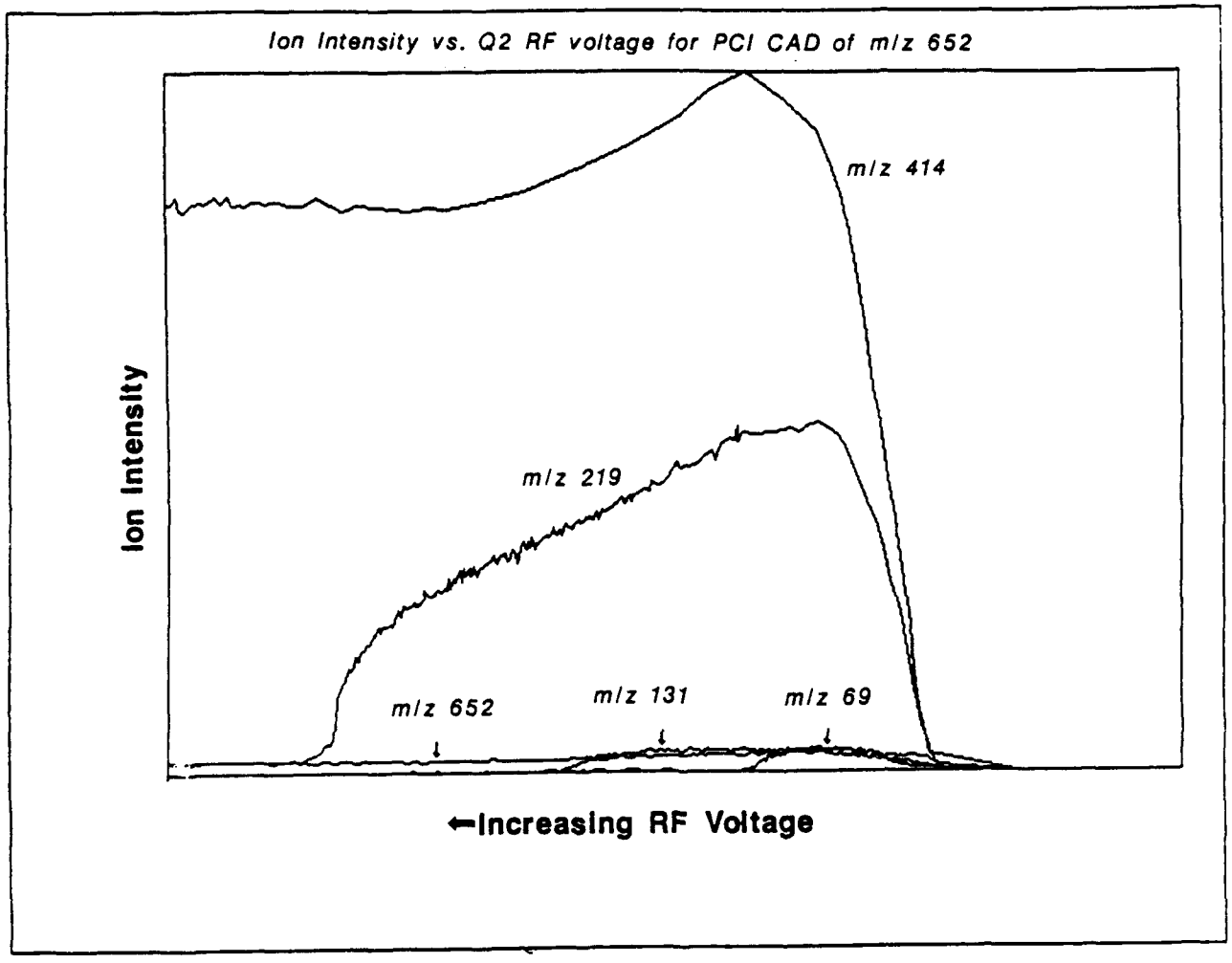

Figure 1-D.2. Ion transmission as a function of the Q2 RF voltage for the daughter ions from the CAD of m/z 652 of PFTBA.

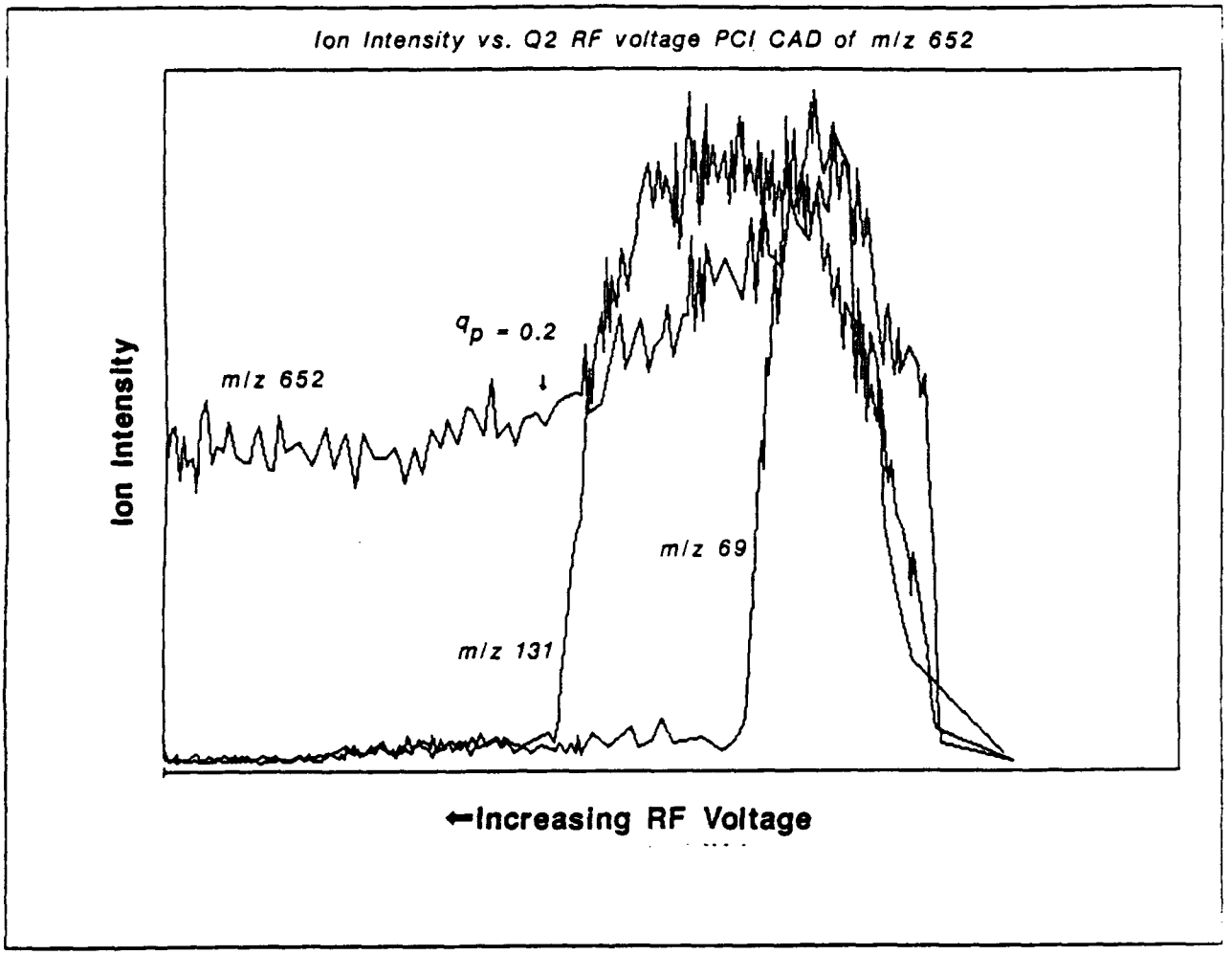

Figure 1-D.3. Same as Figure 1-D.2 except that only the parent and the two lowest m/z daughters are shown. Note with the default q-value of 0.2, the m/z 69 and m/z 131 ions would not be observed in the daughter spectrum.

1-E. Ion Transmission at High Collision Energies

Many compounds of analytical or environmental concern (e.g. polycyclic aromatic hydrocarbons) form very stable ions that are particularly difficult to fragment during MS/MS. Even at high collision energies and collision gas pressures, the yield of daughter ions from these stable parents can be very low. Therefore, proper optimization is crucial for efficient detection of the daughter ions. In addition, it has been found that operation at collision energies above ca. 30 eV requires some special tuning considerations. After tuning for the Q1MS and Q3MS scan modes, the lens voltages obtained are used in the MS/MS scan modes. For MS/MS scans, the instrument uses all ion optical parameters prior to Q2 (i.e. L11-L23) from those optimized from the Q1MS scan mode. The ion optics following Q2 are taken from those obtained from Q3MS tuning (i.e. L31-L42). Most of the lenses behave in the MS/MS modes as they do in the normal mass spectral modes; thus, no special tuning for these lenses is required. However, it has been found that lenses on either side of Q2 (L23 and L31) play a key role in the transmission of ions during MS/MS, especially when collision energies above 30 eV are used. This is shown for the case of L23 in Figure 1-E.1 for the 100 eV CAD of m/z 219 from PFTBA. The collision energy is controlled by adjusting the offset voltage on Q2. As shown in Figure 1-E.1, ion transmission is improved dramatically if the L23 voltage is made more negative than the Q2 offset voltage. In fact, as shown in the inset of Figure 1-E.1 there is a linear relationship between the optimum L23 voltage and the Q2 offset voltage. Figure 1-E.2 demonstrates the dependency of the optimum RF potential on collision energy. In this figure, Q1 was set to pass argon ions (m/z 40), Q2 contained no collision gas, and Q3 was scanned for m/z 40. Three curves were generated, each at different collision energies. As seen in the figure, the optimum RF level increases with increasing collision energy. This behavior can most likely

be attributed to the bent geometry of Q2. At higher axial energies, more RF is required to contain the ions through the bend of the quadrupole. This type of experiment demonstrates the necessity to optimize the Q2 RF voltage for the particular collision energy that is to be used. This could be an important consideration when performing energy breakdown curves, where the collision energy is varied over a wide range.

Figure 1-E.3 shows the transmission of m/z 40 from Ar^+, and demonstrates an attempt to optimize transmission of daughter ions at high collision energies. Curve A in Figure 1-E.3 was obtained using ion optical parameters that were optimum for 10 eV collisions and, as shown in the figure, ion transmission rapidly diminishes above a Q2 offset of approximately 50 V. It was found that the loss in transmission that occurs is due to two major factors. The first is due to the aforementioned dependence of optimum Q2 RF voltage on collision energy. The second is due to ion entrance and exit conditions that exist when the Q2 offset is raised above ca. 50 V. Most often, the lenses are optimized for the normal mass spectral modes at relatively low values of Q2 offset voltage (e.g. 10 V). Apparently, if MS/MS is performed at high collision energies, the ion beam becomes defocussed if the Q2 offset is changed significantly. However, ion transmission through Q2 can be significantly improved by optimizing lenses L23 and L31 (as discussed in the previous paragraph) for the collision energy being used. Trace B of Figure 1-E.3 illustrates an ion transmission curve that is improved significantly by optimizing these lenses and the Q2 RF voltage for each collision energy.

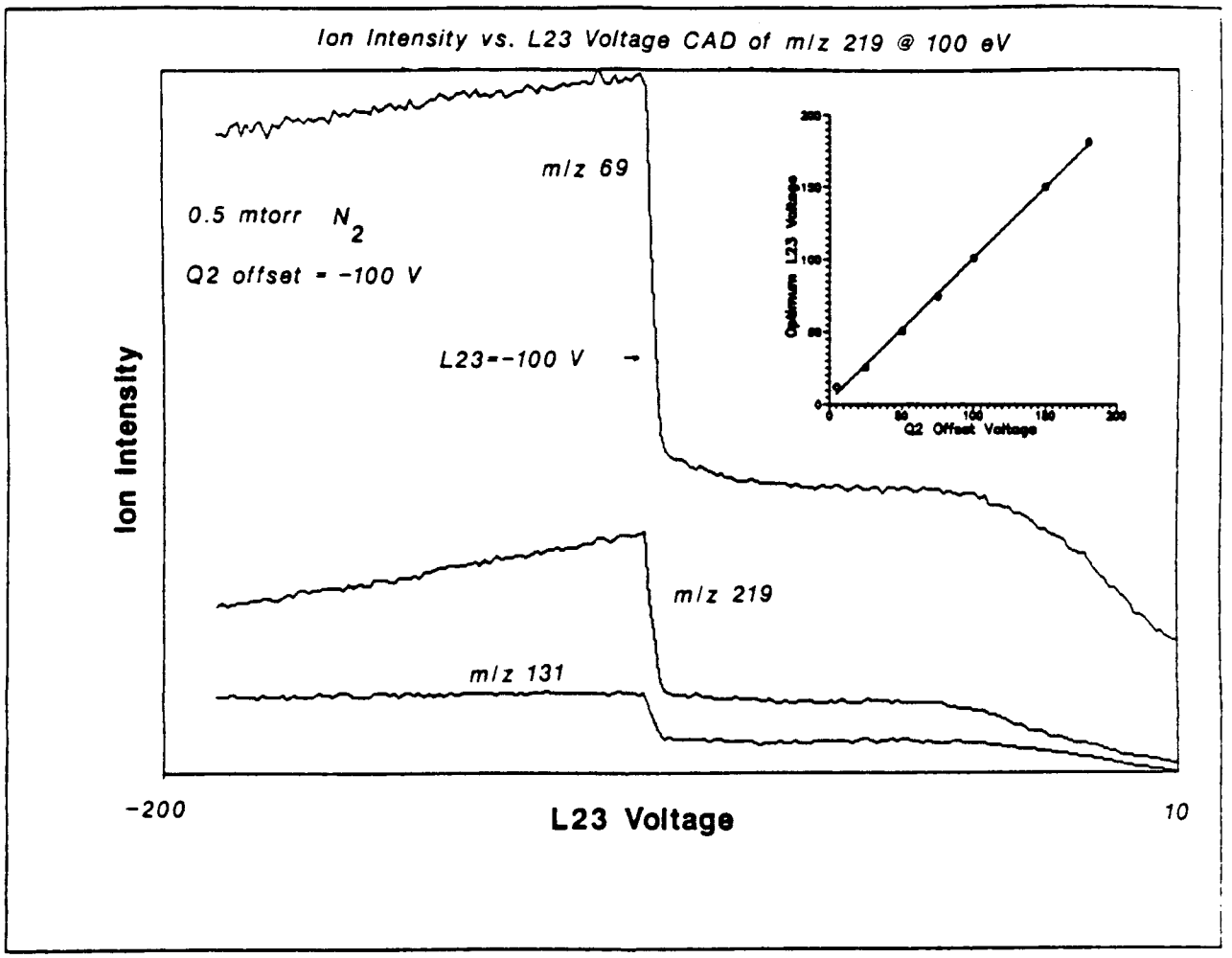

Figure 1-E.1. Ion transmission as a function of the lens L23 voltage for the 100 eV CAD of m/z 219. The inset of this figure illustrates the linear relationship between the optimum L23 voltage and the Q2 offset voltage.

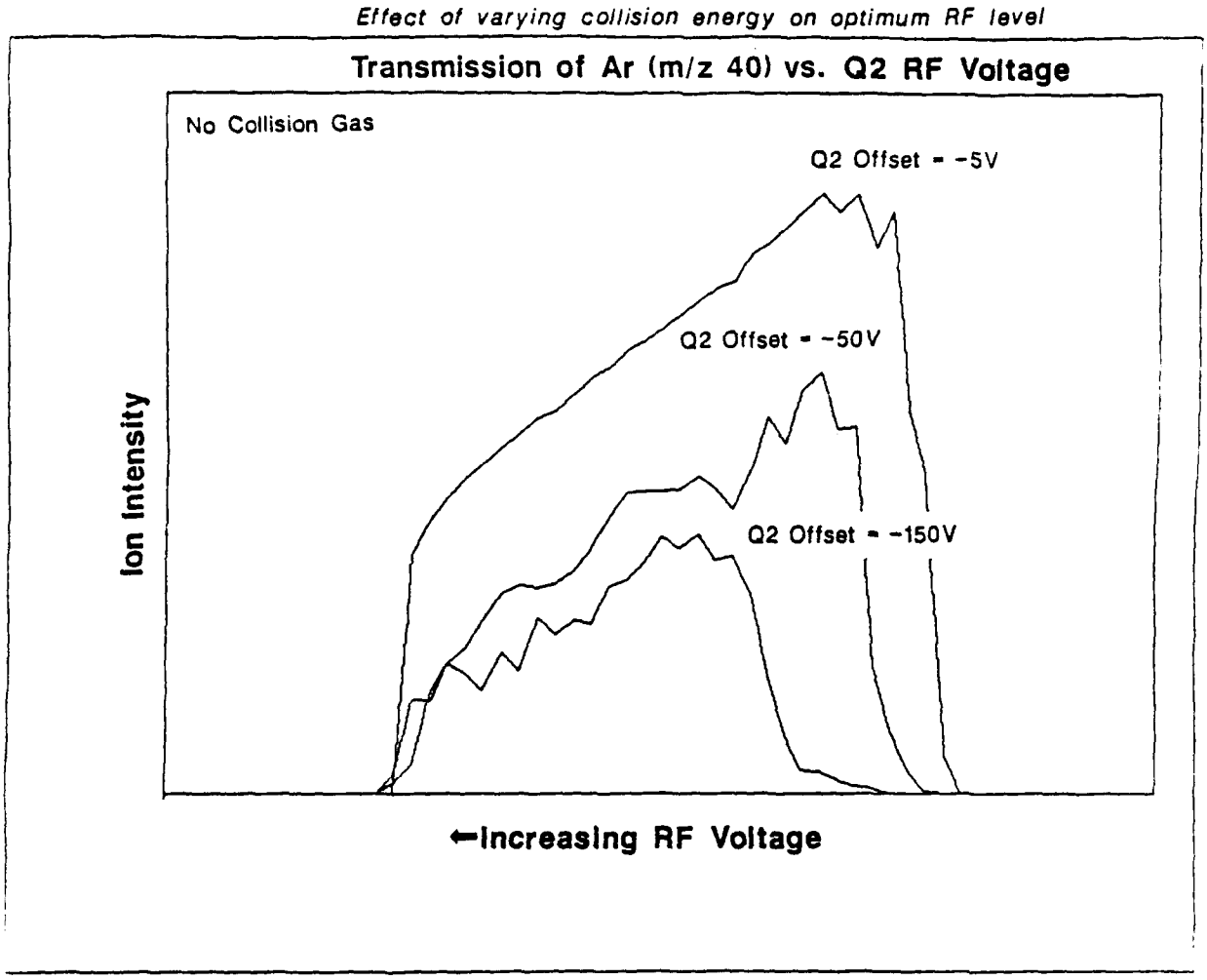

Figure 1-E.2. Ion transmission of Ar^+ (m/z 40) with Q2 RF voltage, illustrating that the optimum RF voltage is dependent on the collision energy (Q2 offset voltage) used.

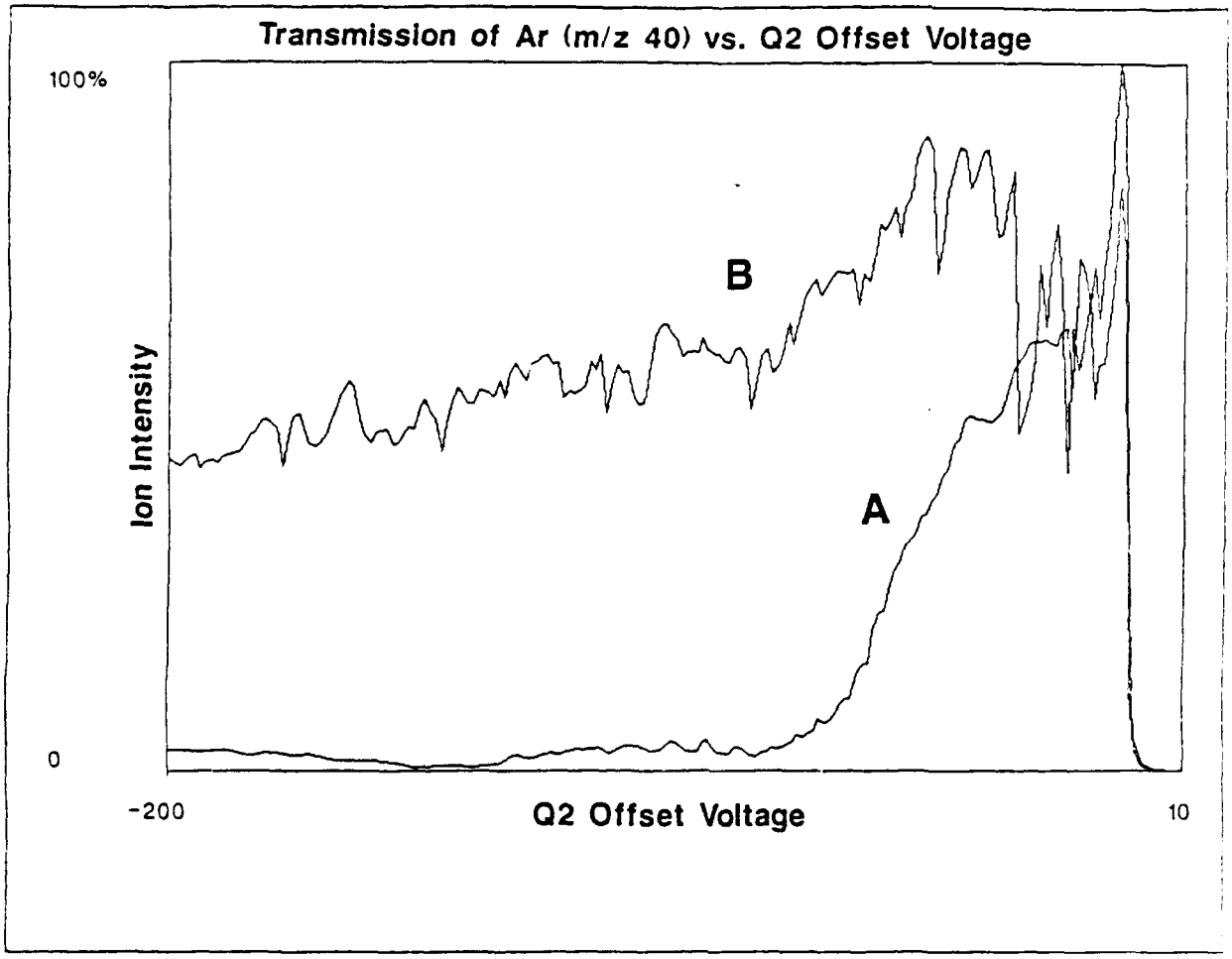

Figure 1-E.3. Ion transmission of Ar^+ with Q2 offset voltage. In **A**, the ion optical parameters used were those found to be optimum for 10 eV collisions. In **B**, lenses and the Q2 RF voltage were optimized at each collision energy.

1-F. Strategies for Automated Tuning

A more thorough understanding of the ion optics has allowed for the development of totally automated tuning procedures for single MS and MS/MS experiments. An automated Instrument Control Language (ICL) procedure performs every phase of the tuning process including adjustment of the quadrupole offsets, adjustment of the resolution, mass-dependent optimization of the ion optics, and calibration of the mass assignment. The program has been divided into subroutines such that any part of the program can be executed independent of any other part. This allows one to rapidly fine tune one or two parameters without having to execute the entire procedure over again. An example of the results of the new automated tuning routines is given in Figure 1-F.1. Figure 1-F.1(a) shows a peak at m/z 502 that is severely distorted. Shown in (b) of Figure 1-F.1 is the peak after execution of the automated tuning procedures. The programs developed thus far include optimization for EI, PCI, and ECNCI.

The main advantage of the automated strategy is the reduction in time required to complete the tuning process. For example, only about 5 minutes are required (for each analyzer) to perform the automated procedures. One new innovation of this instrument that allows for such rapid tuning is that a lens voltage digital-to-analog converter (DAC) may be varied over its full range in the same amount of time that is normally required to execute a mass spectral scan. In this mode of operation known as "DAC scan", one analyzer is set to pass a chosen m/z and the voltage on a particular lens is varied over the entire range (or scanned) in a second or less. As a result, a plot of ion intensity vs. lens voltage is obtained and the optimum voltage can be determined with great speed. Other advantages of the automated tuning are the consistency and precision inherent with the automated method. Since the procedure for the tuning is carried out in the same manner each time, day-to-day as well as operator-to-

operator reproducibility is improved. Finally, incorporation of mass-dependent tuning improves sensitivity and ion transmission over the entire mass range.

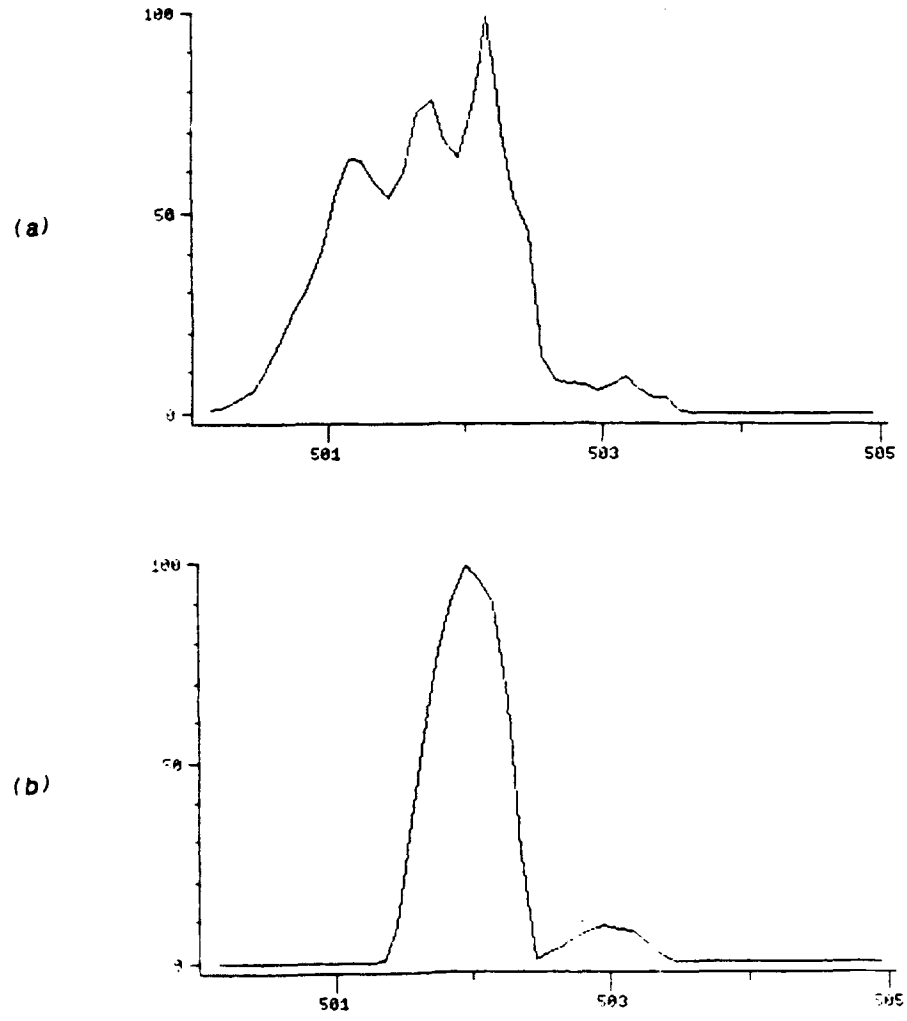

Figure 1-F.1. Peak at m/z 502 (a) before and (b) after automated tuning.

2. ALTERNATIVE SAMPLE INTRODUCTION METHODS

2-A. Theoretical and Practical Aspects of Short-Column Gas Chromatography

In the past, studies in this laboratory have demonstrated the added selectivity inherently available with tandem mass spectrometry as compared to only one stage of mass spectrometric analysis [1-3]. Because of this increased selectivity, there is less of a need for high resolution chromatographic separation of analytes in complex mixtures. The use of short (e.g. 3 meter) open tubular capillary columns in GC/MS and GC/MS/MS provides several notable advantages. Chromatographic theory predicts that optimum carrier gas velocities are higher when the column outlet is at vacuum, and with short open tubular columns higher flow velocities can be used without much loss of chromatographic efficiency. Figure 2-A.1 shows a theoretical comparison of plate heights for 30 m and 3 m columns with atmospheric and vacuum outlet pressures. The theoretical dependence of the plate height in gas chromatography is described by the Golay equation

$$H = B/\upsilon + C\upsilon \qquad (2\text{-A.1})$$

where H is the plate height, υ is the average velocity, B is a term relating to the longitudinal diffusion of the solute zone, and C is a measure of the resistance to mass transfer of the solute in the gas phase. Equation (2-A.1) can be rewritten as

$$H = 2D_g/\upsilon + K\upsilon/D_g \qquad (2\text{-A.2})$$

where D_g is the gas phase diffusion coefficient of the solute in the carrier gas and K is a constant for a given solute on a particular column. The increased optimum carrier gas velocities obtained with short columns with vacuum outlet is due to a reduction of the average column pressure and an increase in the diffusion coefficient, D_g. A better understanding of this phenomenon can be obtained by observing the effects of the outlet pressure on the calculated pressures at each point along a 3 m column, as shown in Figure 2-A.2. Figure 2-A.3 shows the theoretical dependence of the plate height on the average gas velocity for the same outlet pressures shown in Figure 2-A.2. Note that the behavior is essentially the same for 100 Torr and 1 Torr outlet pressures. Thus, any GC detector which could be operated at the reduced outlet pressures would offer significant advantages in terms of speed of analysis. Analysis times obtained with vacuum outlet pressures are reduced by a factor of 30, if a 3 m column is used instead of a 30 m column, and both are operated at their optimum gas velocities. The reduced analysis times are due to the reduction of the column length by a factor of 10, as well as the increase in the optimum gas velocity by a factor of 3 for the shorter column. In addition, the resolution lost by a using a column that is 10 times shorter is only a factor of the square root of 10.

One of the ideas that is currently being investigated is the design of a probe-type gas chromatograph. This probe type GC utilizes short columns and the same vacuum lock as a conventional solids probe. As a result, removal or changing of the GC column does not require the system to be vented. This should result in a high sample throughput with less system downtime. Other advantages of the GC probe are portability, simplicity, and lower power requirements than conventional GC ovens. Efforts in alternative sample introduction methods have focused on the development of the GC probe and other concepts that would make

it a powerful analytical tool. Areas that have been investigated include: chromatographic theory to understand the behavior of short-column vacuum outlet GC, computer-controlled exponential flow rate programming as an alternative to temperature programming, operation of GC columns at sub-ambient pressures for optimum performance, and investigation of on-column injection methods for the GC probe.

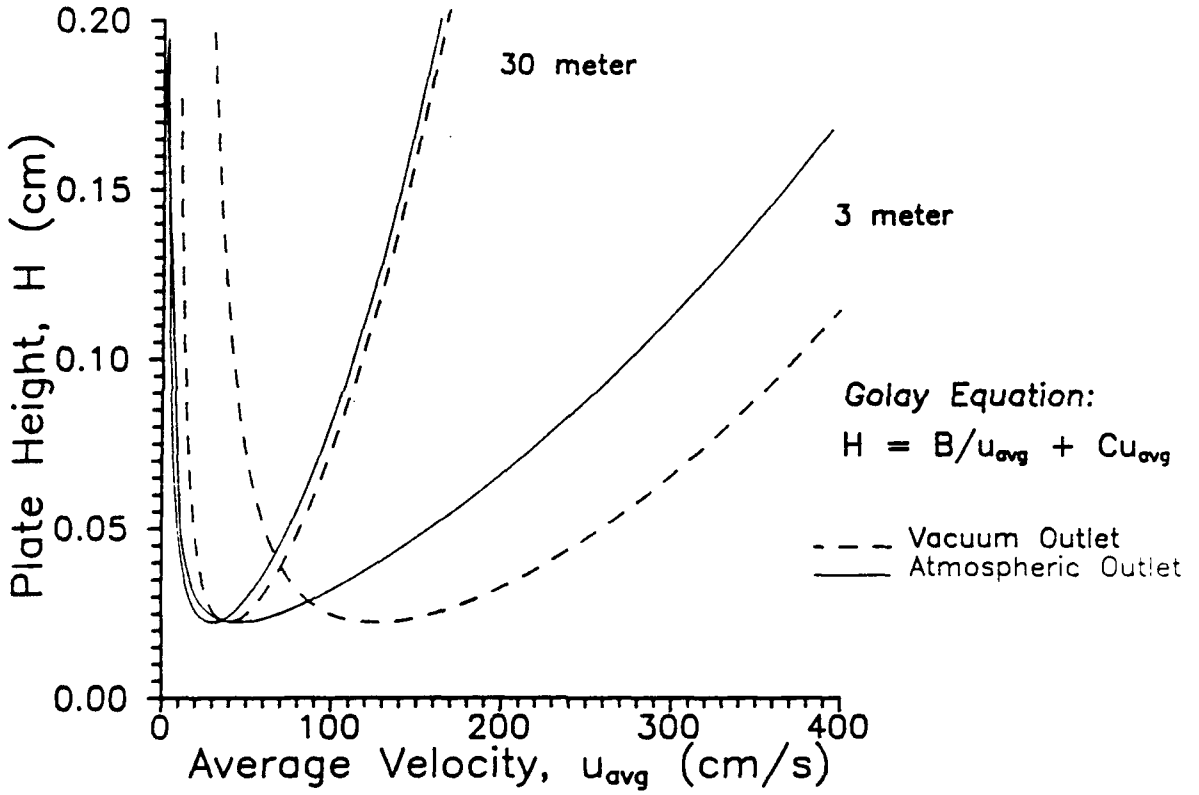

Figure 2-A.1. Theoretical dependence of the plate height on the average carrier gas velocity for 30 m and 3 m columns with vacuum and atmospheric outlet pressures.

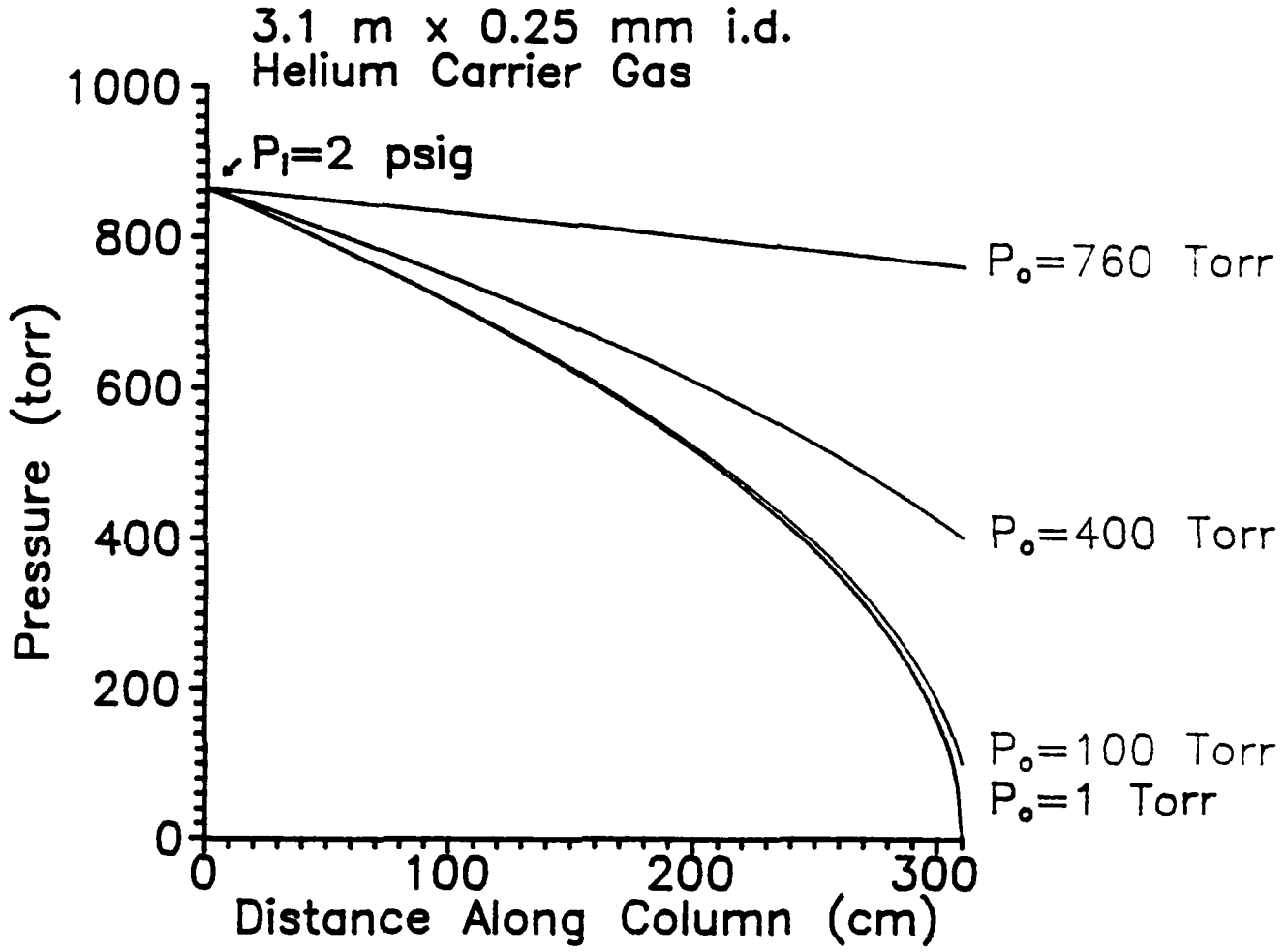

Figure 2-A.2. Effect of the outlet pressure on the pressure calculated at each point along a 3.1 m open tubular column.

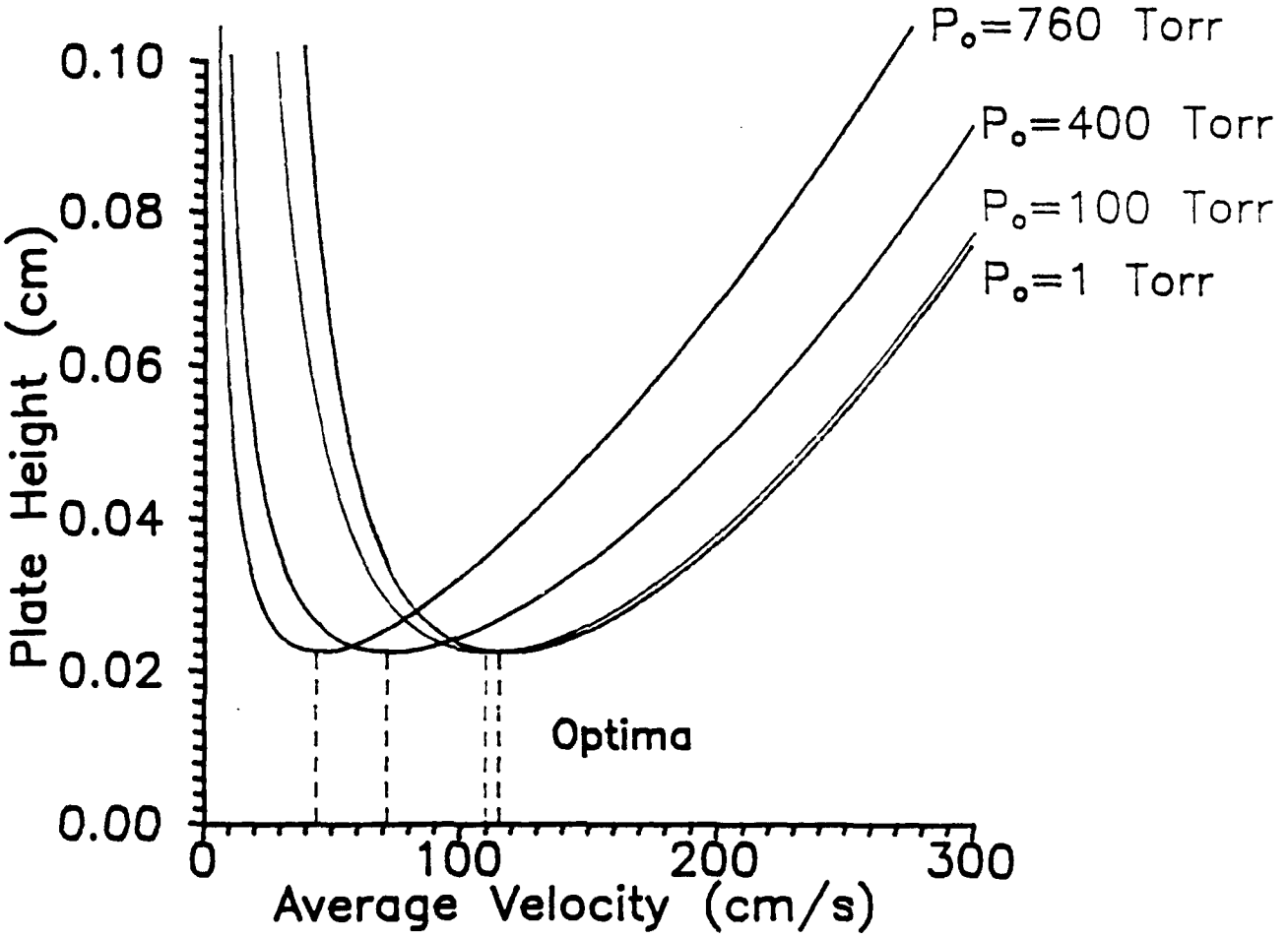

Figure 2-A.3. Plots of plate height vs. average velocity illustrating increase in optimum gas velocity associated with decreased outlet pressures.

2-B. Characterization and Computer Control of Mass Flow Controllers

For many of the experiments performed (e.g., exponential flow rate programming and sub-ambient inlet pressure GC) it was necessary to be able to control the column flow rate instead of the inlet pressure. Several methods for controlling the column flow rate have appeared in the literature [4,5,6]. Initially, flow programming was achieved by manually manipulating a needle valve in the splitter line [6]. However, due to the imprecision and inconvenience of this method more reliable methods were developed. Others have achieved flow control via feedback from a pressure transducer with a motor-controlled regulator valve [5]. This type of system first requires a calibration step to determine the dependence of input pressure and flow rate. After the flow function is determined and programmed into the computer, the pressure transducer detects any difference between the inlet pressure and the setpoint flow. If a difference is detected, a DC motor adjusts the regulator until the correct flow is achieved. The main disadvantage of this method is the slow response time, since several seconds are required for the motor to reposition the valve. The response time of the flow controller becomes even more important for short columns since the analysis times are typically only a few minutes long. For this reason it was decided that commercially available mass flow controllers would be most suitable for these applications. These types of transducers incorporate thermal mass flow sensors to determine mass flow rates of gases. Sensors placed at both ends of a laminar flow tube detect differences in heat transferred along the tube, and directly relate this difference to the flow rate of the input gas. The measured flow rate is compared to the setpoint value and is adjusted by an electromagnetically controlled automatic valve. The transducer and controller valve are contained in a single package measuring approximately ½" X 5" X 5". An external power supply/readout unit provides the appropriate power, real time

readout of the measured flow, and capability for computer interfacing. The advantages of this system are fast response (500 ms for the transducer), excellent precision (0.2% of full scale), and high accuracy (0.5% of full scale). The flow controller is interfaced to the mass spectrometer electronics via an auxiliary user output that is variable from ± 5 V DC via the instrument trackball or ICL procedure. A range of 0-5 V is used to adjust the flow controller flow rate over its full range (0-20 mL/min or 0-100 mL/min depending on the flow controller used). Figure 2-B.1 shows the relationship between the flow rate of N_2 (as measured with a common bubble flow meter used in gas chromatography) and the actual reading displayed by the transducer. Each error bar depicted in the figure represents the standard error of the mean of five measurements made at a particular flow rate. These results and those of similar experiments have demonstrated that the flow can be controlled linearly down to ca. 0.3 ml/min (1.5% of full scale).

One concern about the use of this device was its ability to regulate flow when the output was connected to the vacuum of the mass spectrometer, as it might be in short-column GC. In order to test the performance of the transducer in this configuration, the flow controller was utilized to control the input of collision gas into the collision cell of the TSQ 70. In fact, this configuration worked so well, that a flow controller dedicated for control of collision gas pressure has been installed. Operation of the flow controller is not affected by the large pressure drop; however, the mass spectrometer is only capable of handling approximately 3 ml/min in the collision cell before the pressure in the analyzer region rose too high for normal operation. The maximum allowable flow rate is much higher (ca. 30-40 mL/min) when the gas is introduced into the ion source instead of the collision cell since the ion source is pumped by a separate turbomolecular pump. The full range of the flow controller (0-20 mL/min for N_2

and 0-29.6 mL/min for He) can be used if a mechanical pump is used to divert some of the gas from the collision cell. A schematic of the system which allows computer control of the collision gas is shown in Figure 2-B.2. As shown in Figure 2-B.3, the gauge used to read the CAD gas pressure responds too slowly and does not give an accurate measure of the response time of the system. The true response time, which is less than 2 seconds, was determined by observing the signal of m/z 219 as the CAD gas pressure was changed from 0.5 - 3.0 mTorr. This type of system has particular advantages over manual control. For example, the pressure may be rapidly and precisely changed over a wide range (0.2 - 3.0 mTorr for N_2). Another advantage, which is a result of the rapid response and computer control, is the CAD gas could be optimized for each peak in a chromatogram, provided the compounds to be monitored are temporally resolved.

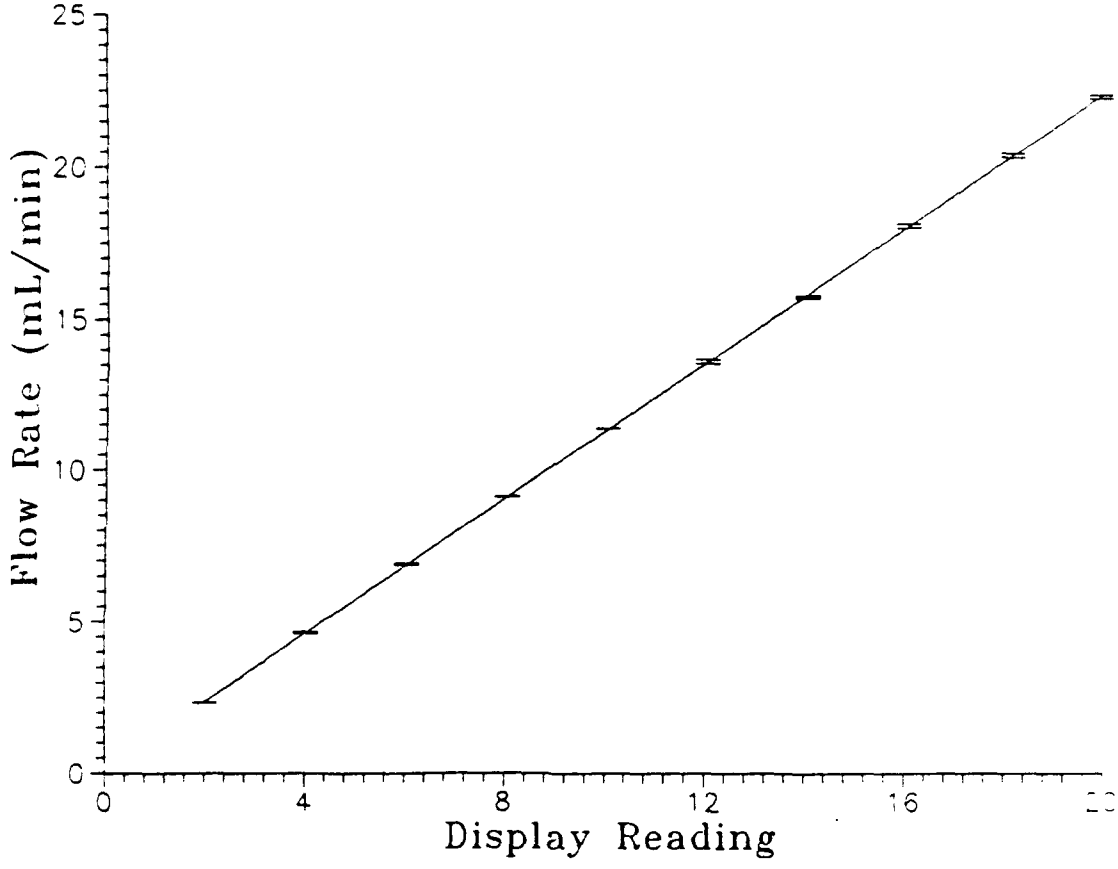

Figure 2-B.1. Measured flow rate of N_2 as a function of the display reading for a mass flow controller, demonstrating the excellent linearity and precision of the device.

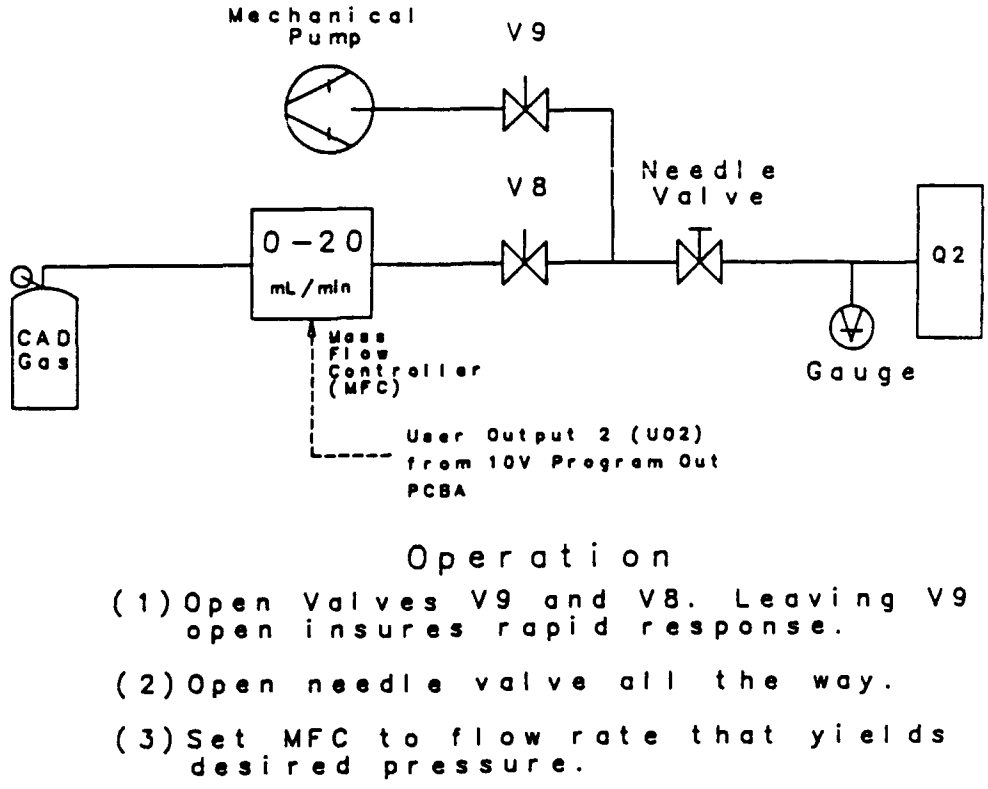

Figure 2-B.2. Schematic diagram of system that utilizes a mass flow controller for computer control of the CAD gas pressure.

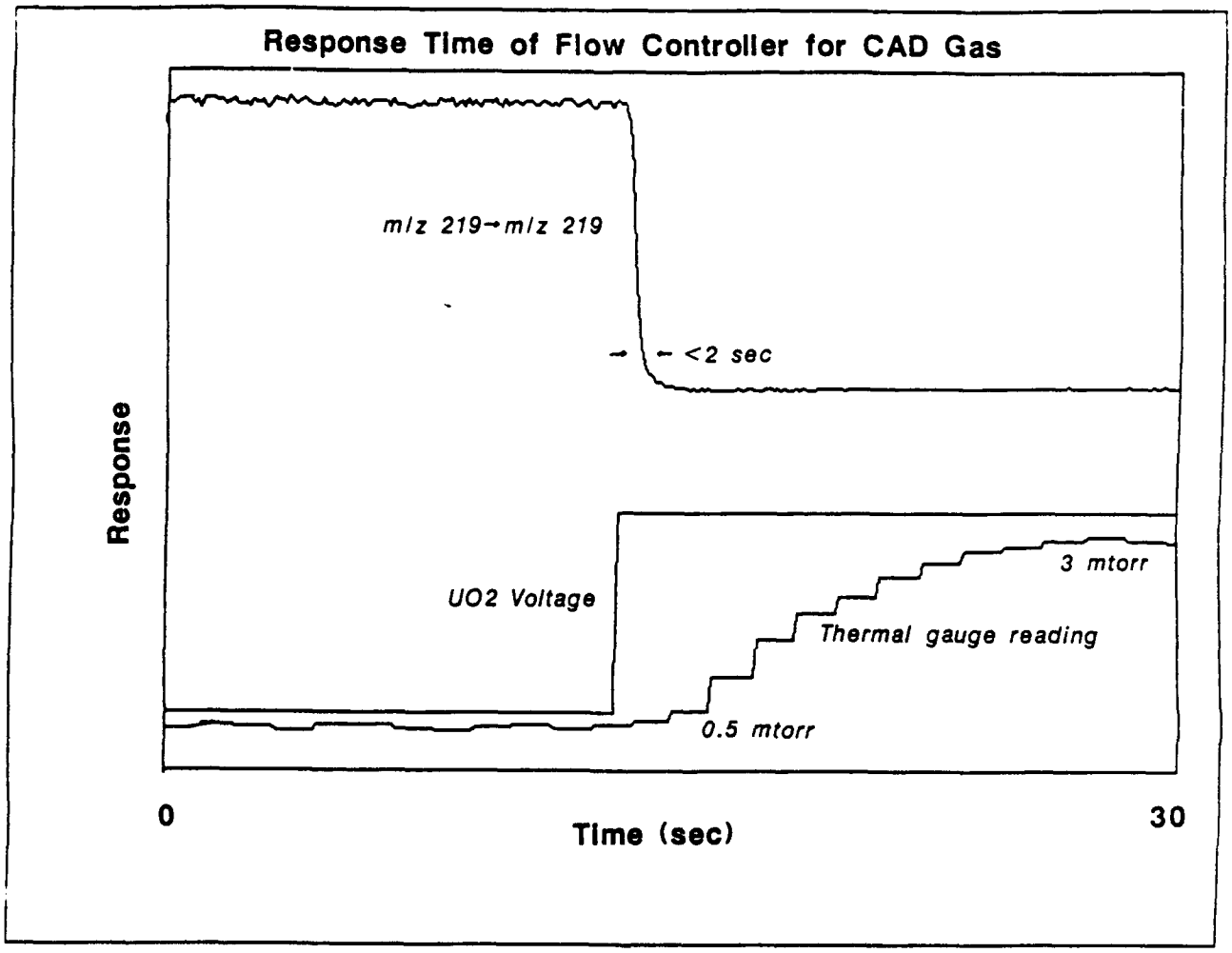

Figure 2-B.3. Response characteristics of system used for computer control of CAD gas pressure.

2-C. Exponential Flow Rate Programming

Introduction

The object of any type of chromatography is to separate a mixture of compounds. However, chromatographic mixture analysis is often complicated by the "general elution problem" [4]. This predicament results both in poor resolution in the early part of a chromatogram due to coeluting peaks and in severe peak broadening near the end of a chromatographic run. This dilemma is often solved in GC with temperature programming. In programmed temperature GC (PTGC) the column temperature is increased (usually linearly) during the course of the analysis. Since the temperature range covered can be up to 300°C, PTGC offers a wide dynamic range. However, the need to heat a GC oven (or probe) only to cool it back down requires significant amounts of electrical power, making temperature programming possibly unattractive for portable instrumentation. One alternative that has indicated potential involves programming the mobile phase flow rate. It has been demonstrated that exponential flow programming of the carrier gas flow rate under isothermal conditions results in peak distributions that are similar to those obtained with PTGC [5]. One advantage of programmed flow GC is that the sample throughput is higher since it is not necessary to wait for the column to cool for the next injection. Although resetting of the column flow rate is required, this step is essentially instantaneous due to the high permeability of open tubular columns [7]. The high permeability of short and/or wide bore open tubular columns also allows for high flow rates (> 30 mL/min) to be achieved at relatively low inlet pressures (<30 psi). The technique is particularly attractive for thermally labile compounds, since the column can be operated isothermally at relatively low temperatures. It has also been pointed out that bleed of the liquid stationary phase from the column is reduced since lower temperatures are required [7]. This could prove to be an important factor

in the reduction of chemical noise at the detector. One disadvantage of the method that is evident from GC theory, is that chromatographic efficiency is reduced if the flow rate is increased beyond the optimum. However, as shown in Figure 2-A.1 of section 2-A, optimum flow rates are higher when the column outlet is at vacuum as in GC/MS. In addition, the Golay curves are much flatter for short columns, which means that relatively high gas velocities can be used without severely degrading chromatographic resolution. Nevertheless, the maximum allowable flow rate will ultimately depend on the pumping speed available at the mass spectrometer.

Initial Experiments

Shown in Figure 2-C.1 are schematic diagrams of the pneumatics of a Varian 3400 GC in (a) the original configuration and (b) with the modifications that were made to accommodate exponential flow rate programming. In the new configuration, the three-way valve shown in (b) is rotated to switch from the normal configuration (pressure regulated) to flow-programmed operation. In both configurations, the pressure in the injection port can be monitored.

Figures 2-C.2(a) and 2-C.2(b) show typical isothermal GC/MS chromatograms of a mixture of C_{14}, C_{15}, and C_{16} n-alkanes at column flow rates of 9 mL/min and 22 mL/min, respectively. These flow rates are demonstrated since they represent the widest applicable range of flow rates for these particular conditions (3.2 m BP-1 capillary column of 0.32 mm i.d. operated isothermally at 90°C). The lowest flow rate that can be used is that which results in positive pressure at the head of the column and avoids the intake of air through the sweep or split openings. Lower flow rates can be achieved by operating the injection port at sub-ambient pressures, which will be described in a later section of this report. In this case, column flow rates were limited on the high end by the range of the

flow controller (29.6 mL/min for He) and the split flow rate. Figure 2-C.2(c) shows a chromatogram where the flow rate was programmed exponentially with time (note that the additional trace in this figure indicates the column flow rate). The flow function is controlled automatically from an Instrument Control Language (ICL) program, which allows the user to select the desired starting flow rate, program and/or delay period, and rate of the exponential. For exponential flow programming the flow rate at time t is given by

$$F_t = F_o + F_i e^{kt} \qquad (2\text{-C.1})$$

where the sum of F_o and F_i determine the starting flow rate and k is the rate of the exponential.

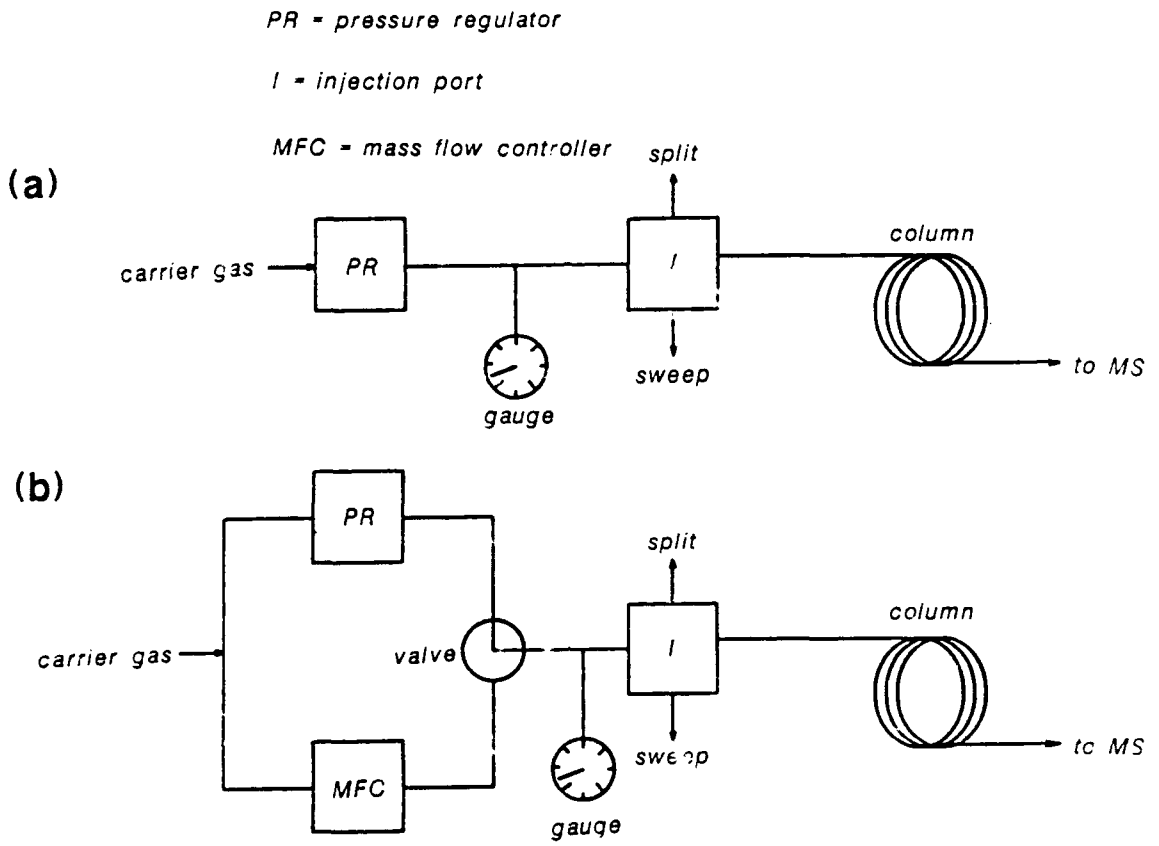

Figure 2-C.1. Schematic diagram of pneumatics of GC in **(a)** normal configuration and **(b)** configuration that allows pressure or flow regulation.

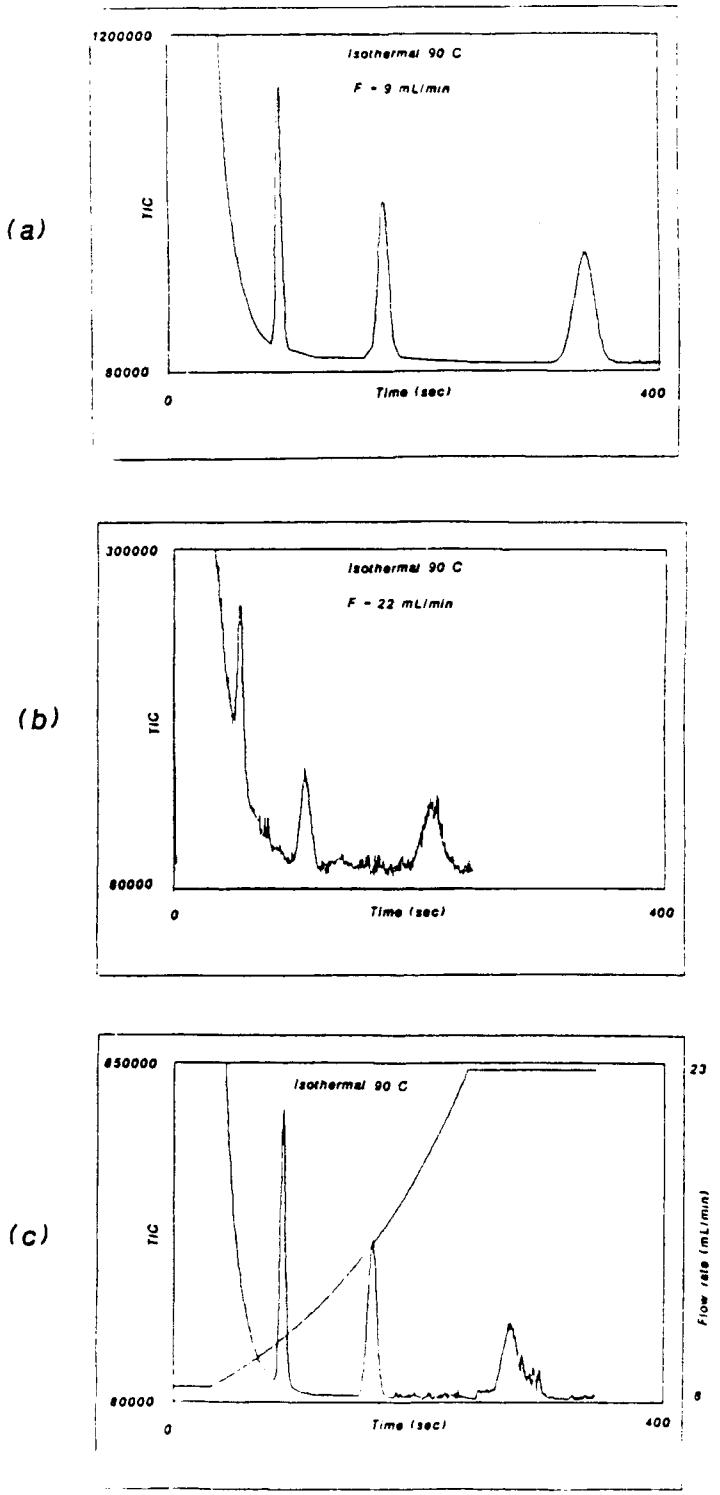

Figure 2-C.2. Total ion current chromatograms of C_{14}, C_{15}, and C_{16}, n-alkane mixture with **(a)** flow rate of 9 mL/min, **(b)** flow rate of 22 mL/min, and (c) flow rate programmed exponentially with time.

Effect of Carrier Gas Flow Rates on the Performance of the Mass Spectrometer

One problem that is evident from Figure 2-C.2 is the reduction in the signal-to-noise ratios at higher flow rates. For example, the peak area of the C_{15} component is reduced by a factor of ca. 7 when the flow rate is increased from 9 mL/min to 22 mL/min under electron ionization (EI) conditions. Initially, it was unclear whether this problem was linked to mass analysis, ion formation, or a combination of both. It is possible that the increased pressure in the mass analyzer (which causes a decrease in the mean free path of the ions) results in a reduction of the number of ions reaching the detector. Signal-to-noise ratios may also be decreased due to inefficient ion formation. Since these studies were performed with electron ionization (EI), it is possible that the high flow rates disrupt the ionization process such that the eluting components are not efficiently ionized.

It was discovered that the problem of reduced signal-to-noise ratios at high flow rates could be overcome by employing chemical ionization (CI) instead of EI. Due to the higher operating pressures (1 Torr for CI and 10^{-4} Torr for EI) and the inherent efficiency of CI, ion formation appears unaffected by the increase in flow rates. Figures 2-C.3 and 2-C.4 show a comparison of the performance of EI and methane positive CI (PCI) respectively under identical changes in column flow rates. For these experiments, the chromatograms were obtained in the splitless mode with a 3.2 m, 0.25 mm i.d., DB-5 capillary column operated isothermally at 80°C. The sample injected was 30 ng each of C_{14}, C_{15}, and C_{16} n-alkanes. Figure 2-C.3 shows the chromatograms of the major fragment ion (m/z 85) obtained with 70 eV EI. In Figure 2-C.3(a) the column flow rate is 8 mL/min and that in Figure 2-C3(b) is 20 mL/min. Both traces are plotted on the same time and intensity scale for ease of comparison. The integrated peak areas for the components at the two flow rates are given in Table 2-C.1. As

shown in the table, the peak areas within a chromatographic run are reproducible within the expected limits of error. However, when the areas of the two flow rates are compared, one can see that the areas of the peaks at the higher flow rate are approximately a factor of four less than the peak areas obtained at the lower flow rate. Similar experiments were performed using methane PCI. The major PCI ions obtained with n-alkanes are the $(M-H)^+$ ions. Figure 2-C.4 shows the chromatograms of these ions for the two flow rates. The resultant integrated peak areas for these ions are shown in Table 2-C.1. As shown in the table, the variation in the peak areas (even after the flow was increased from 8 to 20 mL/min) is insignificant and within the limits of experimental error. Also note the increased sensitivity and signal-to-noise ratios of the CI chromatograms as compared to those obtained with EI. These results indicate that the chemical ionization process is less affected by the increased He carrier gas flow rates. This may be due to the fact that sample ions created under CI conditions exist in a plasma of a large excess of reagent ions, thus the variation of He flow rates does not significantly affect sample ionization.

Table 2-C.1. Integrated Peak Areas for Comparison of EI and CI at Different flow rates

Hydrocarbon	m/z	F (mL/min)	Ionization	Peak Area
C_{14}	85	8	EI	220694
C_{15}	85	8	EI	213729
C_{16}	85	8	EI	227111
C_{14}	85	20	EI	53244
C_{15}	85	20	EI	53148
C_{16}	85	20	EI	52292
C_{14}	197	8	CI	1893613
C_{15}	211	8	CI	1827399
C_{16}	225	8	CI	1617471
C_{14}	197	20	CI	1758975
C_{15}	211	20	CI	1804526
C_{16}	225	20	CI	1679119

Once it was determined that CI was not affected by high flow rates of He carrier gas, it was believed that increasing the electron energy might help to improve the sensitivity of EI with the high flow rates of carrier gas. The electron energy is the potential difference between the filament and the source block, and represents the energy of the electrons impinging upon the sample molecules. The electron energy is usually set higher in CI than in EI (100 eV instead of 70 eV) to insure that the electron beam has sufficient energy to penetrate the source region containing ca. 1 torr of reagent gas. However, experiments have shown that an increase or decrease in electron energy and/or optimization of any of the other ion optical parameters does not improve the performance of EI under these conditions. These data indicate that CI is the ionization method that should be used if high flow rates (>10 mL/min) of carrier gas are to be used. This is not a severe limitation since CI is inherently more sensitive than EI and is, thus, usually preferred for trace analysis. In addition, since CI is a "softer" ionization method (less fragmentation than EI), molecular weight information is often more readily obtained.

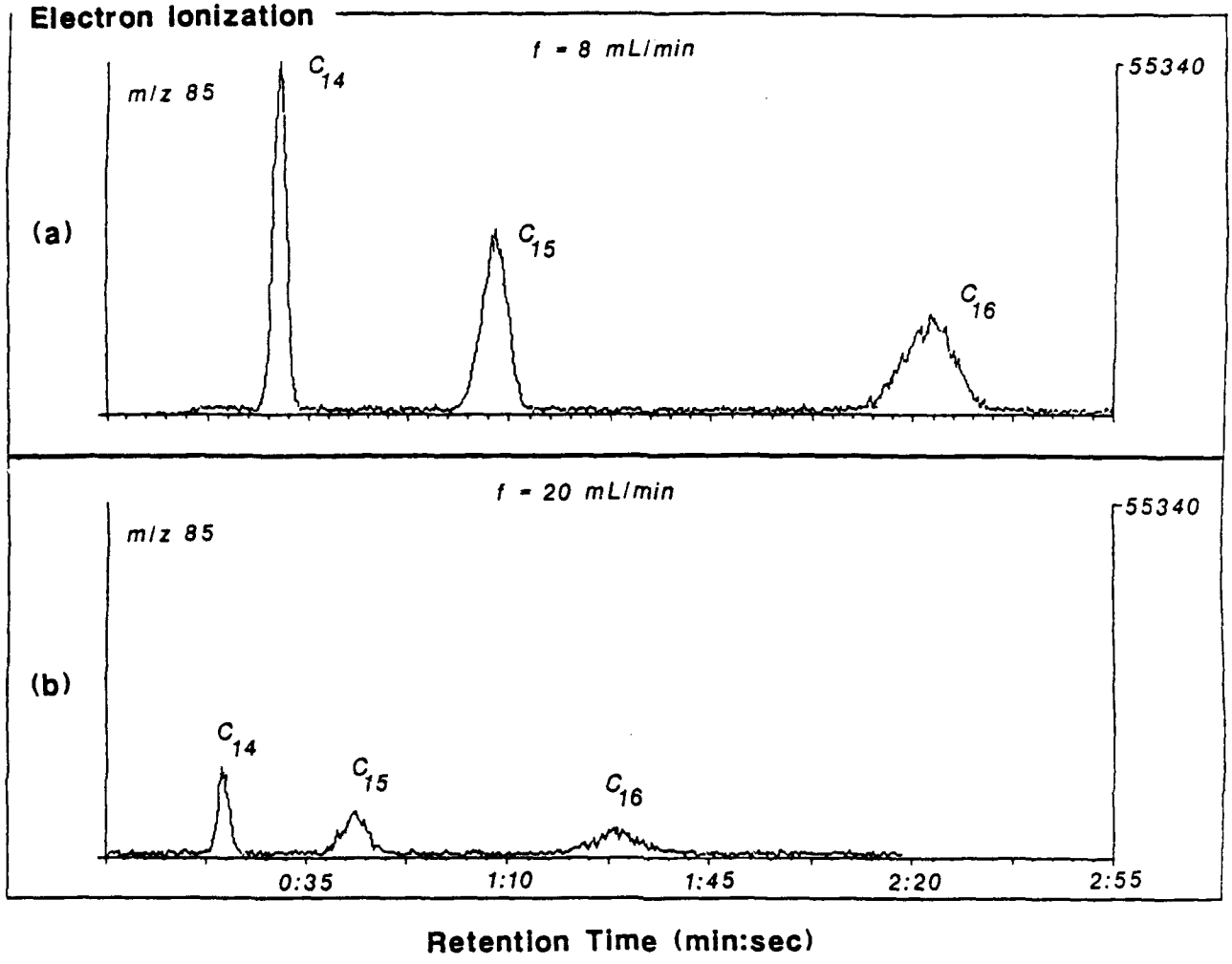

Figures 2-C.3. Mass chromatograms of m/z 85 from 70 eV EI of n-alkane mixture with **(a)** 8 mL/min and **(b)** 20 mL/min He flow rates.

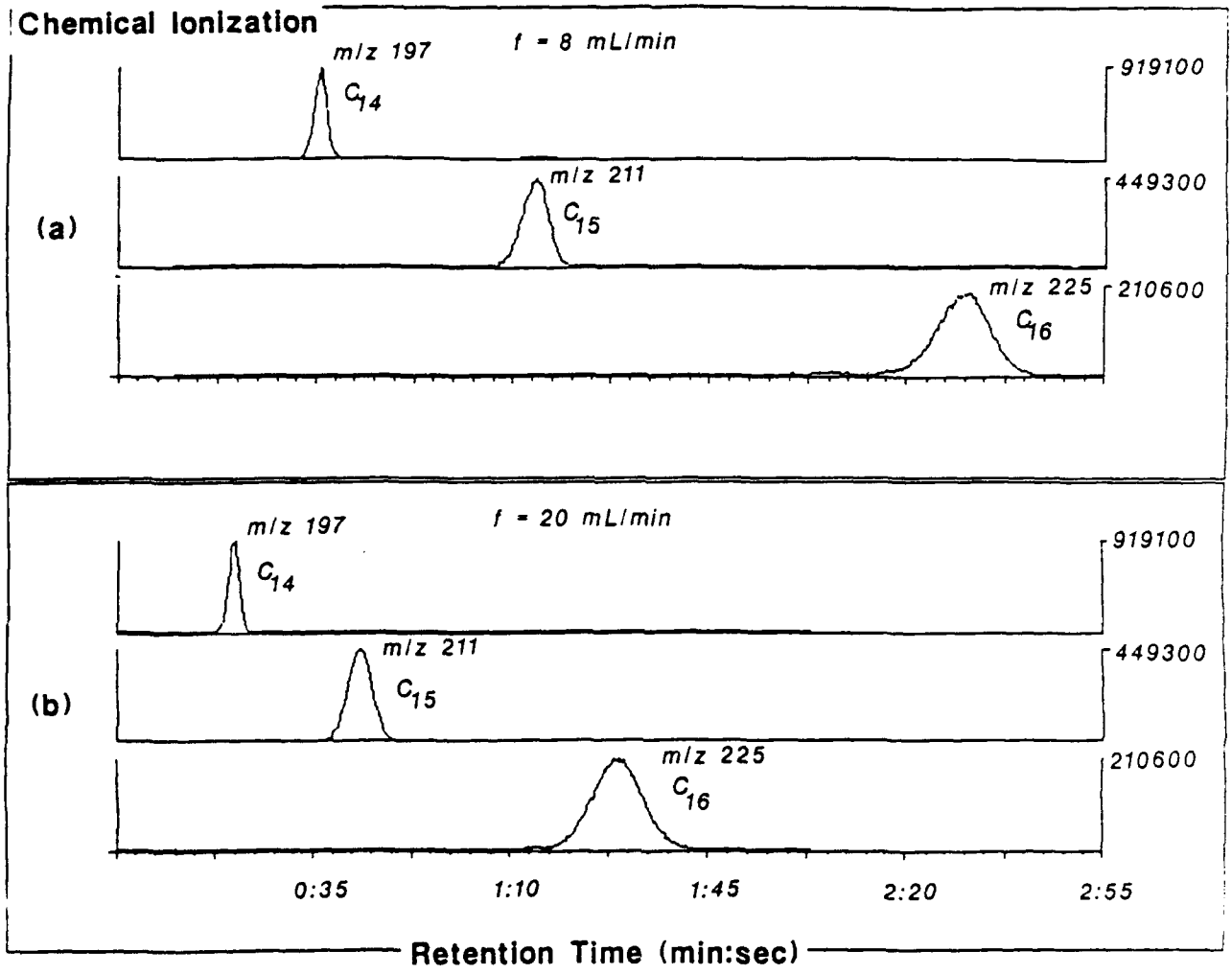

Figure 2-C.4. Mass chromatograms of major PCI ions with **(a)** 8 mL/min and 20 mL/min He flow rates.

Comparison of Temperature Programming and Flow Rate Programming

One completed study attempted to illustrate the similarities of linear temperature programming and exponential flow rate programming. In these experiments a 3 m x 0.25 mm i.d. DB-5 capillary (0.25 μm film thickness) column was used. The sample studied was an activity mixture obtained from J&W Scientific that is often used for evaluating the chromatographic performance of non-polar bonded phase columns. The sample contained 23 ng/μL of each of seven components, which are listed along with their boiling points in Figure 2-C.5. In order to obtain the widest range of flow rates in these experiments, the GC was operated in the splitless mode with the split and sweep valves closed during the entire GC run. Typically, in the splitless mode, the sample is injected and then after a short time (<30 sec) the split valve is opened to purge the remaining sample. Purging the injection port insures that sample peaks are not broadened by the excess sample vapor in the carrier gas lines and the injection port. Therefore, it was a concern that in the absence of purging, chromatographic resolution could be seriously degraded. However, it was discovered that short columns can be operated in the splitless mode without split or sweep and without loss of chromatographic resolution. This is because the high flow rates inherent with short columns cause the injection port to be rapidly flushed by the carrier gas. For example, the volume of the injection port liner used in the splitless mode is 0.24 mL and the lowest flow rate that can be used with a 3 m x 0.25 mm i.d. column with the column outlet connected to the vacuum of the mass spectrometer is ca. 5 mL/min. This means that the injection port is completely flushed in less than 3 seconds. If the sample is flushed in less than three seconds, then one would expect that the narrowest peaks in the chromatograms (in the absence of solvent focussing) would also be three seconds wide. Indeed, experimentation has shown that the width of the

peak of the earliest eluting compound (2-chlorophenol) is approximately three seconds.

In Figure 2-C.5 the flow was kept constant at 5 mL/min of He and the column was isothermal at 65°C. In Figure 2-C.6 the temperature was increased linearly, after a delay of 30 seconds, at a rate of 5°C/min. Figure 2-C.7 shows the mixture separated using exponential flow rate programming, with the rate of the exponential set so that the final flow rate was reached in 3.5 minutes. It can be seen from Figures 2-C.6 and 2-C.7 that exponential flow rate programming yields similar results to linear temperature programming. However, it is evident from this comparison that the range of boiling points spanned in a flow program will not be as large as that obtainable with temperature programming. Nevertheless, the range of boiling points is still relatively wide. For example, the components in this mixture have boiling points from 175°C (2-chlorophenol) to 271°C (pentadecane).

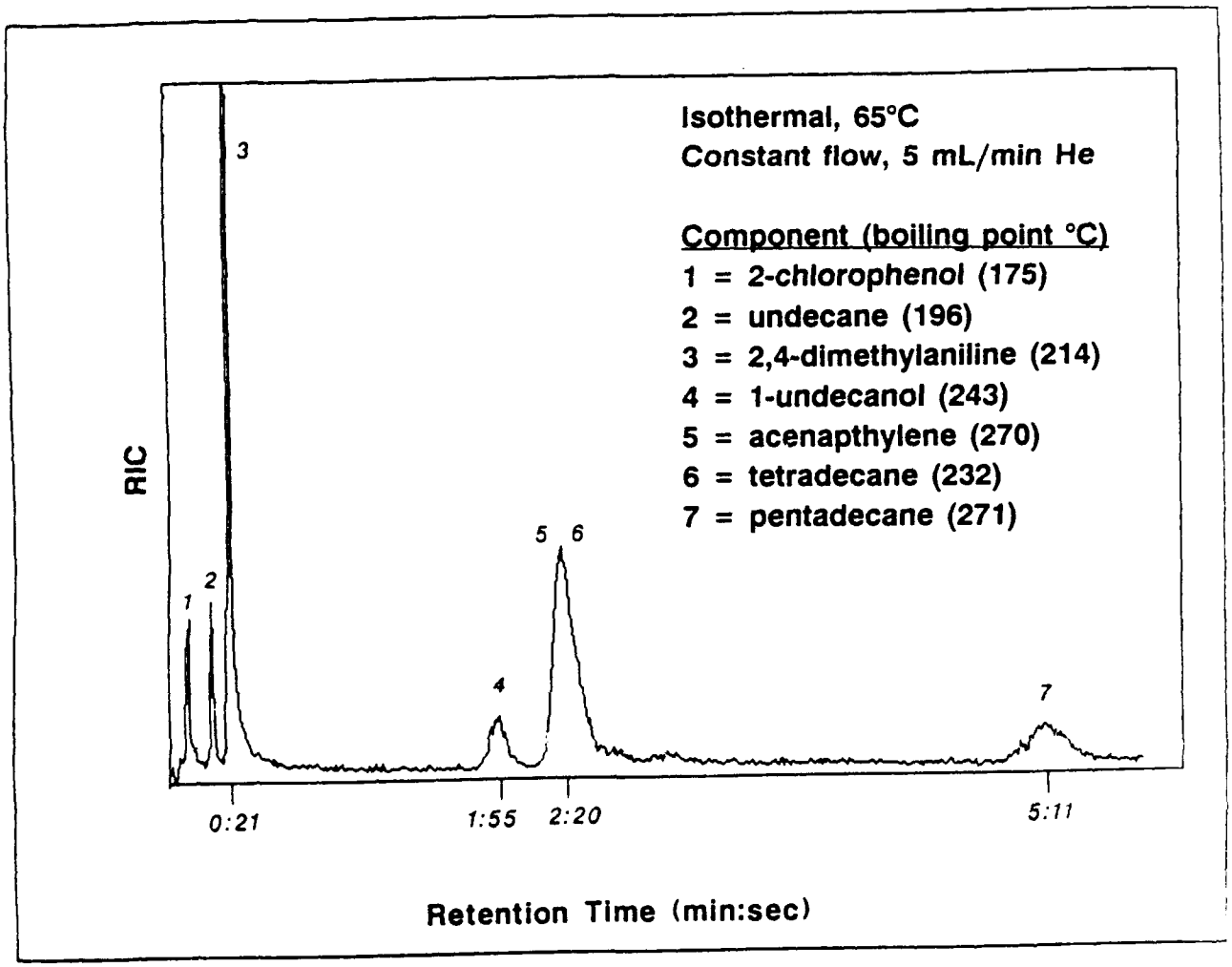

Figure 2-C.5. PCI chromatogram of seven component mixture at constant flow and temperature.

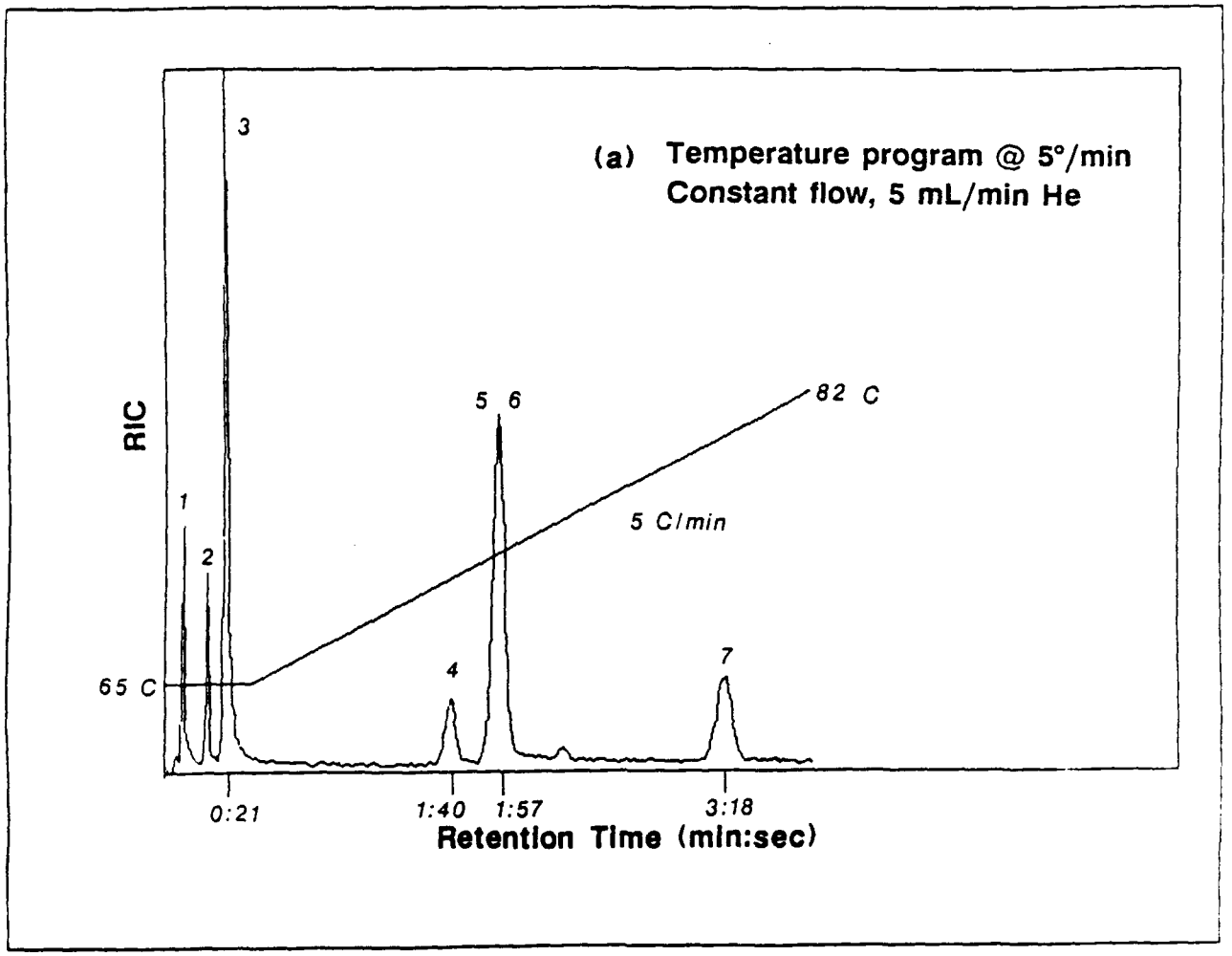

Figure 2-C.6. PCI chromatogram of seven component mixture using temperature program of 5°C/min at a constant He flow rate of 5 mL/min.

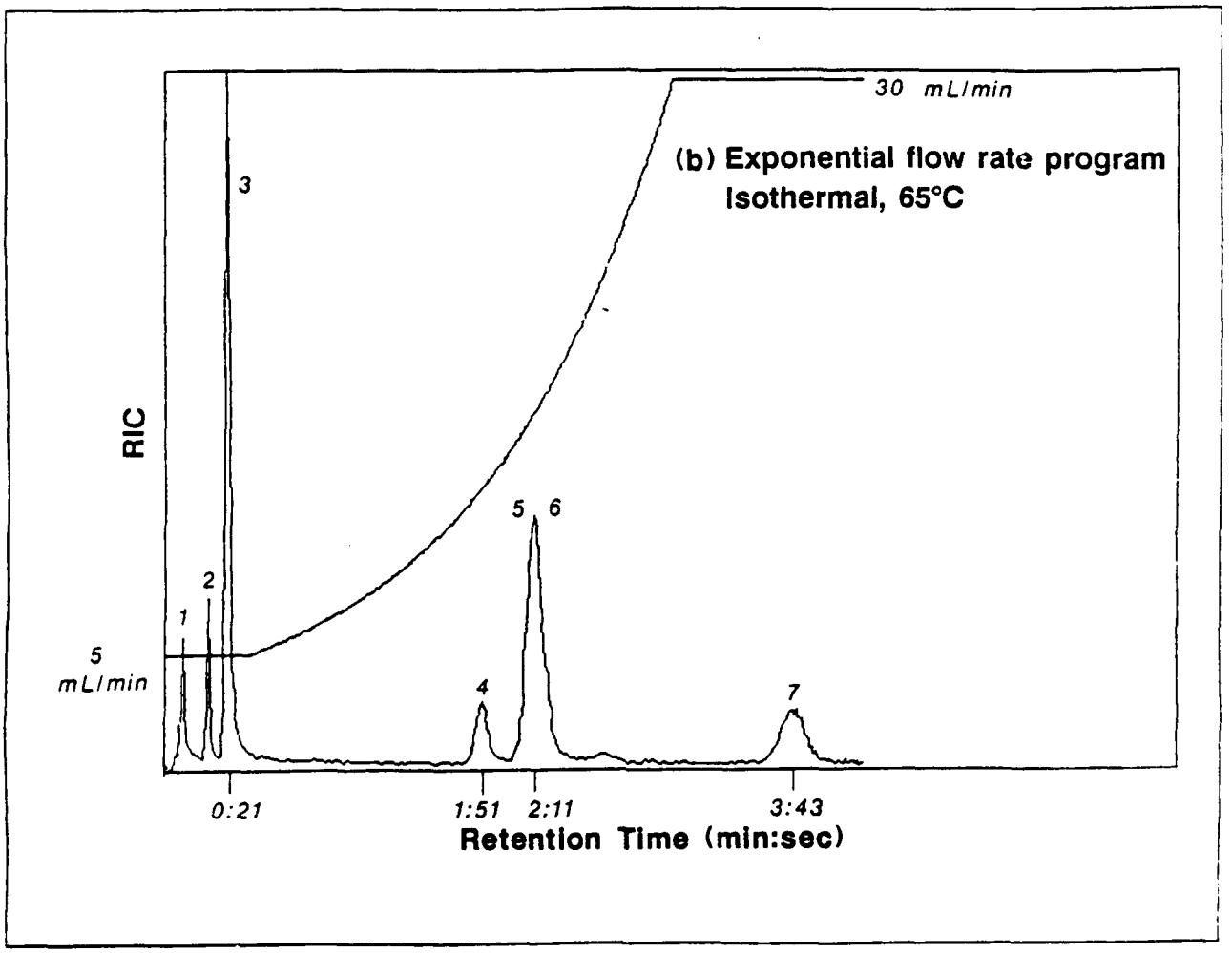

Figure 2-C.7. PCI chromatogram of seven component mixture done isothermally with exponential flow rate programming.

2-D. Thermally Labile Compounds and Component Discrimination

Short capillary columns are well suited for the analysis of thermally labile compounds. Because relatively low temperatures are required, compounds that are normally too unstable to pass through conventional length (e.g. 30 m) columns pass intact through short (e.g. 3 m) capillary columns. Compounds elute at even lower temperatures when the outlet of the column is at vacuum as in GC/MS. For example, the compounds in the activity mixture described in section 2-C have boiling points as high as 271°C, but elute from a 3 m column at 65°C. As a result short columns can often be used for the analysis of compounds that would perhaps be considered too involatile for GC separation.

One compound that provides an excellent example of the concepts discussed above is tyrosine methyl ester. Tyrosine is an important amino acid found in plant tissue. The methyl ester of this compound is a white crystalline solid with a melting point of ca. 136°C. This compound has no boiling point, but decomposes at higher temperatures. Figure 2-D.1 shows the reconstructed ion chromatogram obtained when 15 ng of tyrosine methyl ester was injected onto a 3 m column where the temperature was programmed from 75°C at a rate of 15°C/min. The interesting thing to note is that the compound elutes in less than 3 minutes at 112°C (24° below the melting point of the compound). This example clearly demonstrates the potential of these short capillary columns for the analysis of involatile and/or thermally labile compounds.

One of the most important controllable parameters in GC is the injection port temperature. For thermally labile compounds, one attempts to operate the injection port hot enough to vaporize the sample, but low enough to minimize the possibility of thermal breakdown. These concepts are illustrated in Figure 2-D.2. In this experiment, injections of the tyrosine methyl ester were performed at six different injection temperatures, and the peak area of the major ion (m/z

196 $(M+H)^+$) is shown plotted vs. injection port temperature. One can see from the figure that an optimum injection port temperature exists for this compound. At the lower temperatures much of the sample is not being vaporized, and at higher temperatures thermal degradation takes place. For a mixture of compounds, discrimination of the higher boiling components is possible if the proper injection port temperature is not used. An illustration of this is given in Figure 2-D.3, where the ratio of the peak areas of the C_{15} and the C_{11} hydrocarbons from the activity mixture are shown at different injection port temperatures. Clearly, at lower temperatures less of the C_{15} hydrocarbon is being transported from the injection port to the column. One way of minimizing the problems of thermal degradation and discrimination in the injection port is to use on-column injection as described in the following section.

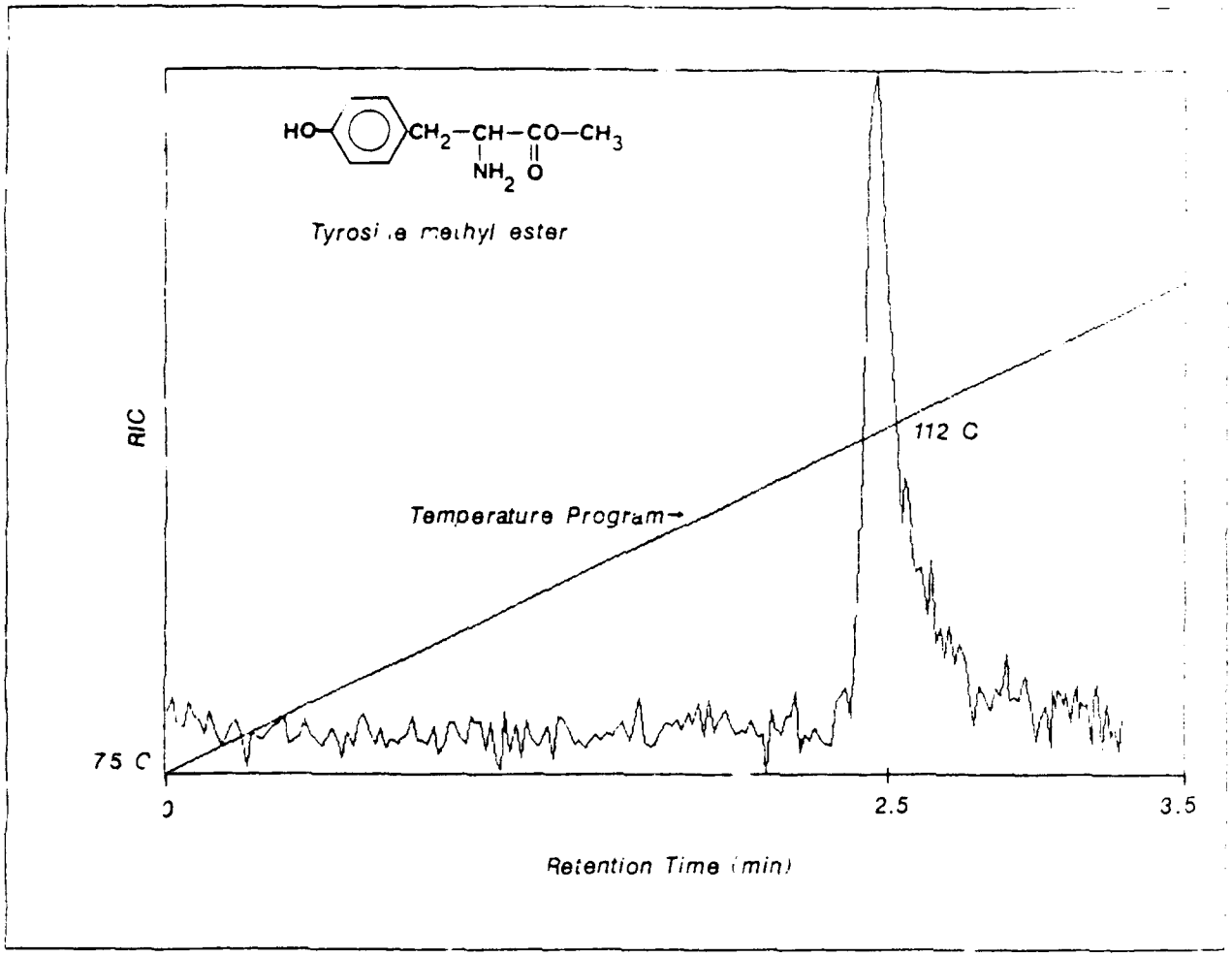

Figure 2-D.1 Reconstructed ion chromatogram for injection of 15 ng of tyrosine methyl ester.

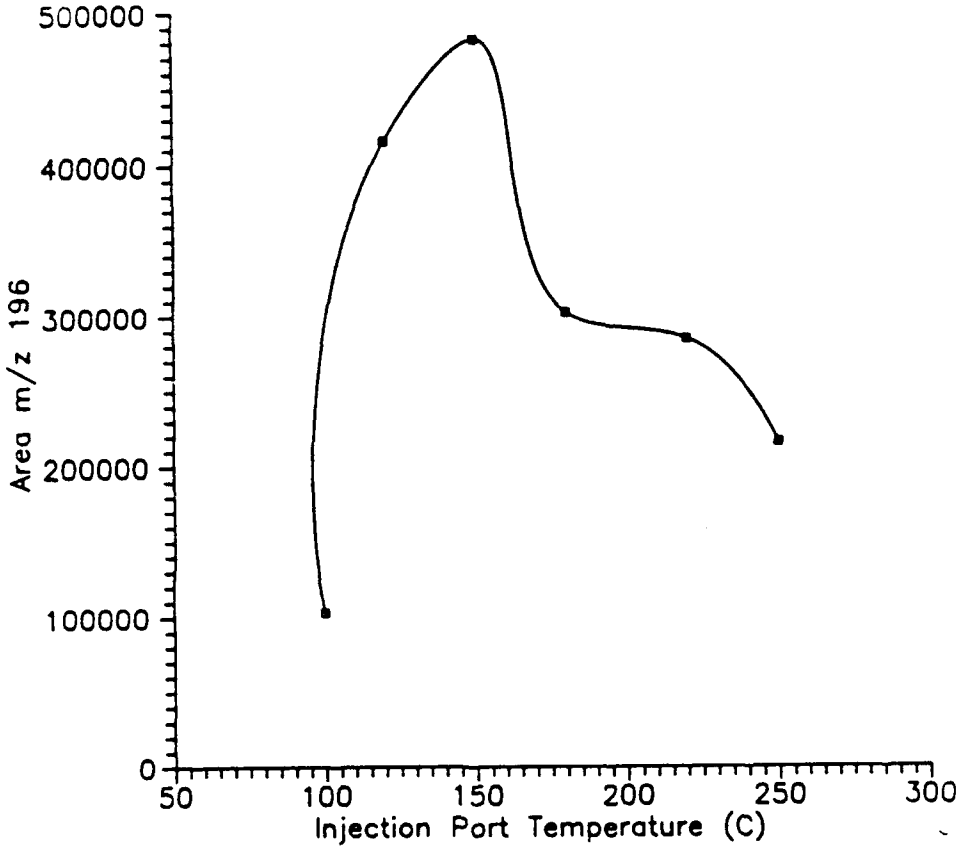

Figure 2-D.2. Effect of varying the injection port temperature, illustrating optimum temperature for thermally labile tyrosine methyl ester.

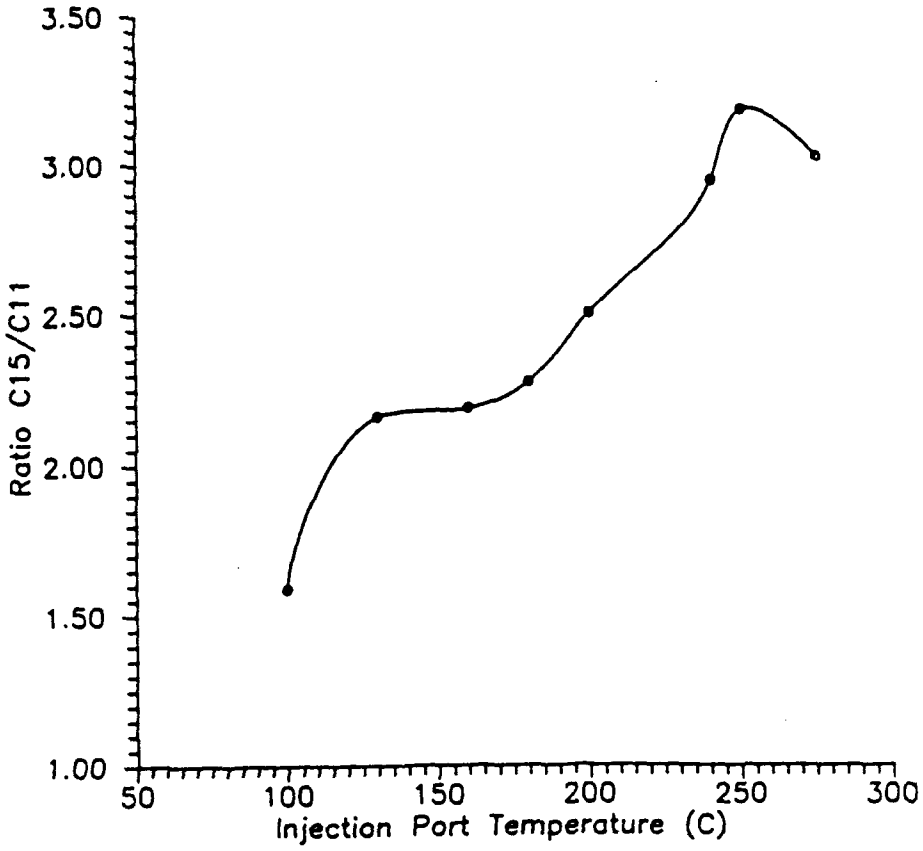

Figure 2-D.3. Effect of the injection port temperature on the discrimination of C_{15} hydrocarbon at low injection port temperatures.

2-E. Evaluation of a Simple On-Column Injection System

One of the goals for the development of the GC probe is to maintain a simple yet rugged design. Traditionally, the most complex part of a GC is the injection port, particularly those used with narrow bore (0.25 mm i.d.) open tubular capillary columns. Most injection ports for these columns utilize flash vaporization, where the sample is injected and vaporized in a glass-lined injection port. Following vaporization, the sample is transported to the column by the flow of carrier gas. As was discussed in section 2-D, discrimination of higher boiling components can occur with this type of injection system if too low an injection port temperature is used. Conversely, excessively high injection port temperatures may result in decomposition of thermally labile compounds in the injection port. Alternatively, with on-column injection, all of the sample is loaded directly onto the capillary column. On-column injection offers increased sensitivity, less component discrimination and, since lower injection port temperatures are required, it is well suited for thermally labile compounds. Nevertheless, traditional on-column injectors for narrow-bore capillary columns are fragile and mechanically complex. This is because a very narrow syringe needle (e.g. 0.2 mm o.d.) must be guided into the head of the 0.25 mm i.d. capillary column. Often the syringe needle is bent and/or the head of the column is broken off during injection. In addition, cold on-column injection with no more than 0.5 μL of sample must be used, due to the limited vaporization volume of the narrow-bore capillary.

A new, simple type of on-column injection system that avoids many of the problems discussed above has been evaluated. This injection system utilizes a short (e.g. 25 cm) length of wide-bore (0.53 mm i.d.) open tubular capillary column as a precolumn for a 0.25 mm i.d. column. The wide-bore column is inserted up through a conventional injection port liner (or wide-bore insert)

and is held firmly in place so that a standard 26-gauge GC syringe can be used to inject the sample into the precolumn, thus avoiding the use of special, fragile syringes. Connection of the wide-bore column to the narrow-bore column is accomplished by inserting the smaller column directly into the end of the larger precolumn. A standard 1/16" Swagelok union, equipped with the appropriate graphite ferrules, is used to form a low dead volume fitting between the two columns. As mentioned previously, this injection system is simple, inexpensive, and easy to assemble. Another advantage is that the short precolumn can be discarded and a new one can be inserted should it become contaminated.

The on-column injection described above was evaluated experimentally and compared with the conventional flash vaporization system. To evaluate component discrimination, a mixture containing C_{12}, C_{14}, C_{16}, and C_{18} alkylbenzenes was used. Discrimination curves for both injection systems are shown in Figure 2-E.1. The graphs represent the ratios of the C_{16}/C_{12} GC peak areas vs. injection port temperature. Each peak area ratio was normalized to the ratio obtained at 250°C (i.e. the temperature at which it was assumed little or no discrimination would occur). As shown in the figure, flash vaporization yielded as much as 15% discrimination at a temperature of 100°C, while discrimination with on-column injection was 6% in the worst case. The discrimination with either injection system is not as great as one might expect. For example, other workers in our laboratory have found that the discrimination is much greater (as much as 80% for C_{16}/C_{12} at 100°C) for the same length of column with atmospheric outlet flame ionization detection. Apparently, less discrimination is observed when the outlet of the column is connected to the vacuum of the mass spectrometer. This is most likely due to the larger pressure drop and higher carrier gas flow rates inherent with short-column GC/MS.

On-column injection also appears to be more sensitive than flash vaporization. This could be expected since all of the sample is loaded onto the column. Shown in Figure 2-E.2 are the integrated peak areas for the C_{14} alkylbenzene component for both types of injection. The error bars in the graph represent the standard deviations of three injections at each temperature. The standard deviations at each temperature are larger for the on-column injections, but the relative standard deviations are approximately the same for both types of injection (typically 6%). The peak areas are shown to increase with temperature for the on-column injections. This could be attributed to the vaporization of additional sample from the syringe needle as the temperature is increased. This does not appear to be the case with flash vaporization. However, with flash vaporization the syringe needle does not come into contact with the sides of the injection port as with on-column injection.

Two different wide-bore precolumns were evaluated. The first was a 25 cm length of column containing no stationary phase, and the other was a 25 cm length coated with a 1.5 μm film thickness of DB-5 bonded phase. The GC activity mixture (see sections above) was used to evaluate the performance of the two precolumns. Shown in Figure 2-E.3 are the chromatographic peaks obtained with the two precolumns for 2,4 dimethylaniline. Figure 2-E.3(a) is the peak obtained with the no-phase precolumn and Figure 2-E.3(b) is the peak obtained with the DB-5 precolumn. As shown in Figure 2-E.3(a) the presence of active sites on the no-phase precolumn results in tailing of the 2,4 dimethylaniline peak. However, it appears that with non-polar solutes narrower peaks are obtained with the no-phase precolumn. For example, the peak width at half height for the pentadecane peak is 3 seconds for the no-phase column and 8 seconds for the bonded phase precolumn. This can be attributed to the solute retention by the stationary phase of the DB-5 precolumn. If less solute retention is desired, then the no-

phase precolumn would be chosen for use in the GC-probe. However, the surface of the fused silica should be deactivated (i.e. silanized) in order to avoid poor peak shape for polar solutes.

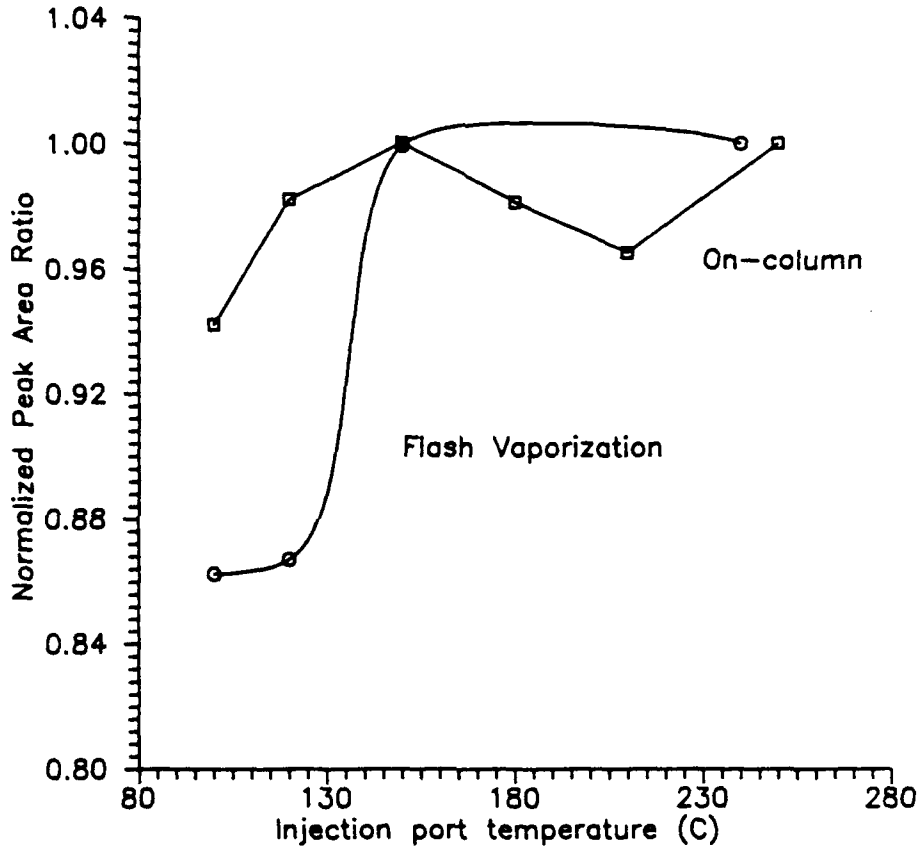

Figure 2-E.1. Normalized peak area ratio for C_{16}/C_{18} vs. injection port temperature for on-column and flash vaporization injection.

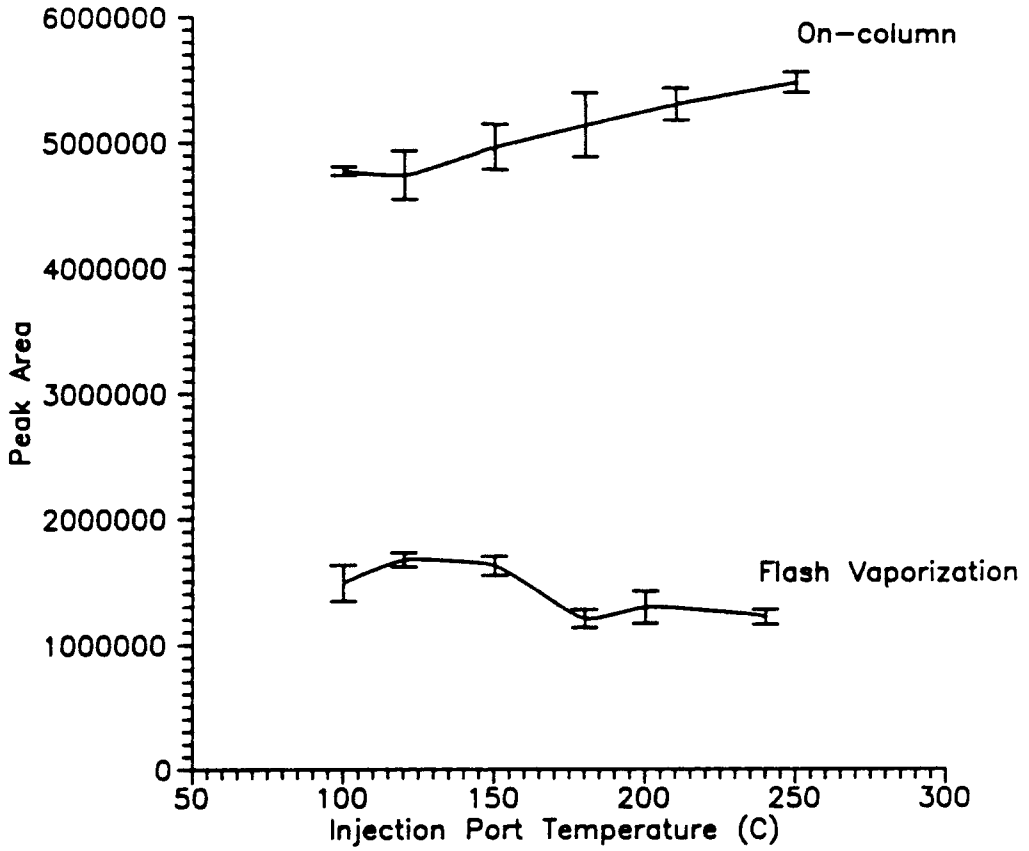

Figure 2-E.2. Peak area of C_{14} alkylbenzene vs. injection port temperature for on-column and flash vaporization injection.

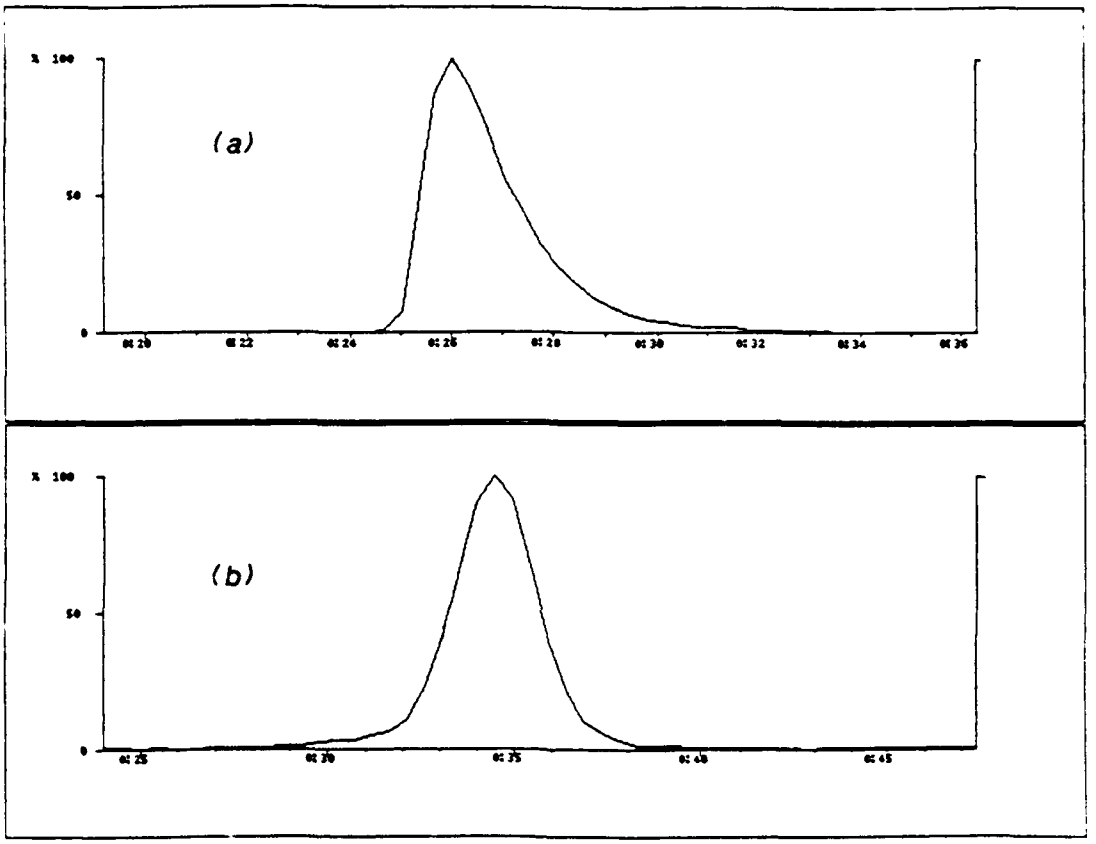

Figure 2-E.3. Chromatographic peaks obtained with 2,4 dimethylaniline with **(a)** no-phase precolumn and **(b)** 1.5 μm film thickness precolumn.

2-F. Obtaining Optimum Performance of Short Open Tubular Columns under Vacuum Outlet Conditions.

The pressure drop has a tremendous effect on the chromatographic behavior of short open tubular columns. It was previously discussed that reduced outlet pressures result in an advantageous increase in optimum gas velocities. The limitation is that short columns with vacuum outlet require sub-atmospheric inlet pressures, if optimum gas velocities are to be obtained. This is demonstrated in Figure 2-F.1, with a plot of optimum velocity vs. column length for a 0.25 mm i.d. column with both He and H_2 carrier gases. Most capillary GCs use pressure regulators, thus optimum velocities can not be obtained with short columns operated with reduced outlet pressures. Alternatively, a flow-controlled system can be used, as shown in Figure 2-F.2. This system allows the injection port to be operated at reduced pressures in the split or splitless mode for narrow bore capillaries (0.25 mm and 0.32 mm inner diameters). In particular, during splitless operation, the sample is injected at pressures slightly above atmospheric, and then the pressure is sharply reduced after a few seconds (i.e. after allowing all of the sample to be loaded onto the column). Alternatively, a short wide bore column (e.g., 3 m x 0.53 mm i.d.) can be used without overloading the mass spectrometer vacuum system and allowing direct on-column injection. The chromatograms shown in Figures 2-F.3 and 2-F.4 demonstrate the increased resolution obtained on a 3 m x 0.25 mm i.d. column by operating the injection port in the splitless mode at a reduced pressure. The chromatogram in Figure 2-F.3 was obtained at an inlet pressure of 940 Torr, and Figure 2-F.4 was obtained at an inlet pressure of 560 Torr. Note that the two components unresolved chromatographically in Figure 2-F.3 exhibit baseline resolution in Figure 2-F.4. As mentioned previously, the sensitivity under electron ionization (EI) conditions decreases dramatically with increasing flow rates of carrier gas into the ion source. Thus, this system, allowing vacuum inlet pressures (and

thus lower flow velocities) is preferred for the use of EI and short columns.

A better understanding of the influence of the pressure drop on the chromatographic behavior of open tubular columns in GC/MS has allowed for better utilization of the inherent advantages associated with short columns. The large pressure drop associated with vacuum outlet GC should not be considered a disadvantage. On the contrary, the low pressure outlet results in increased optimum gas velocities and decreased analysis times.

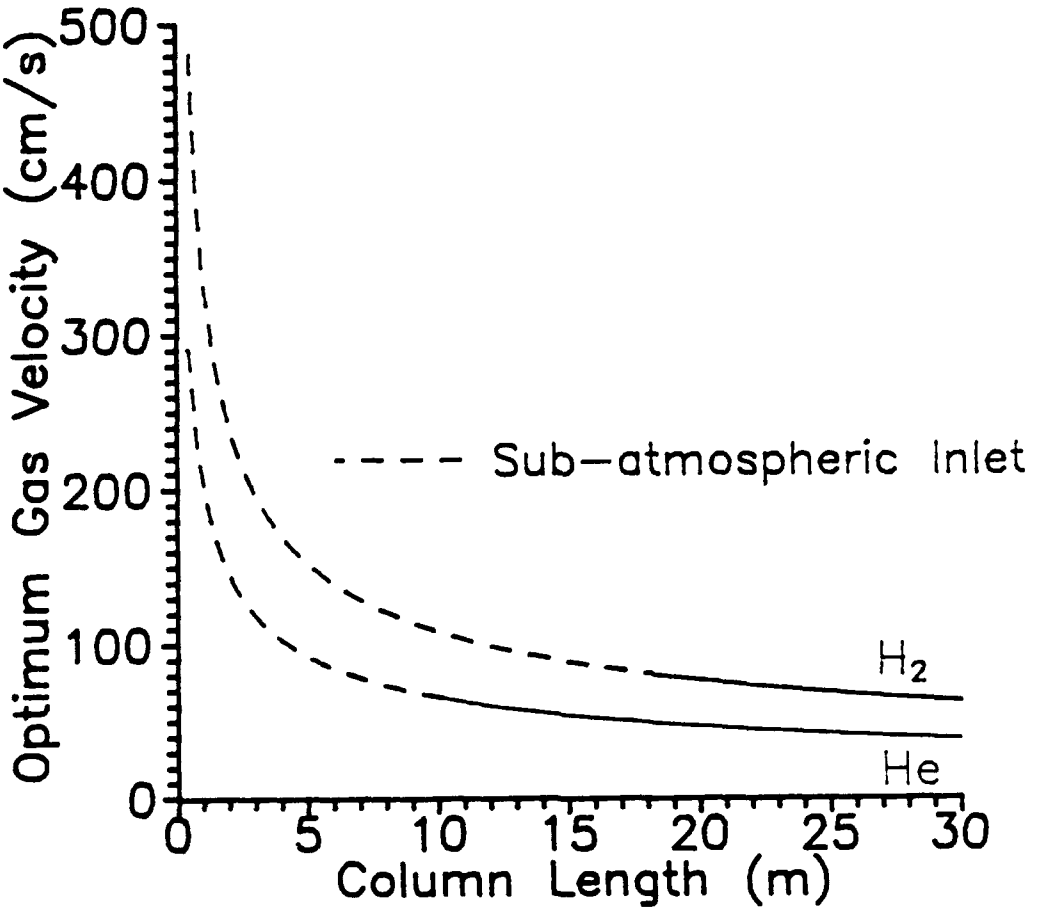

Figure 2-F.1. Plot of optimum gas velocity as a function of the column length illustrating the need for reduced inlet pressures with short columns.

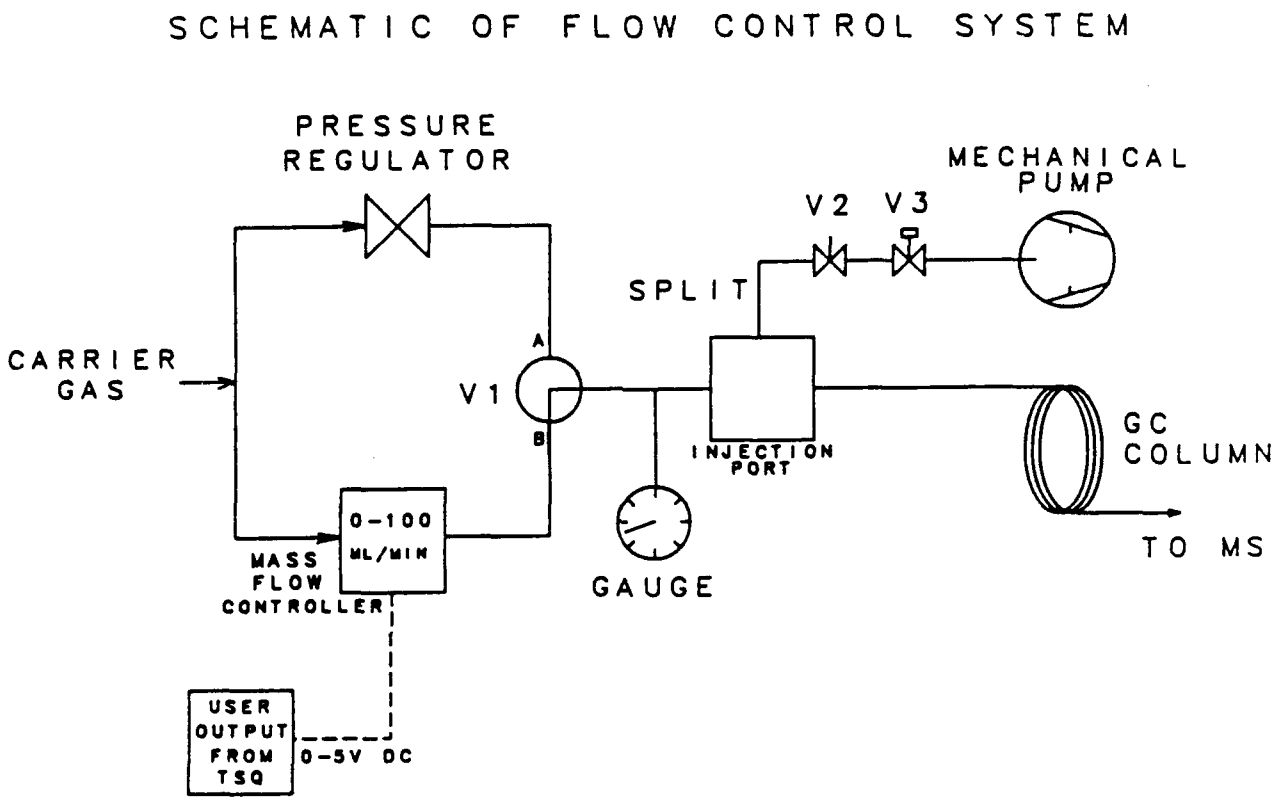

Figure 2-F.2. Schematic of flow control system designed for operation of the injection port at reduced pressures.

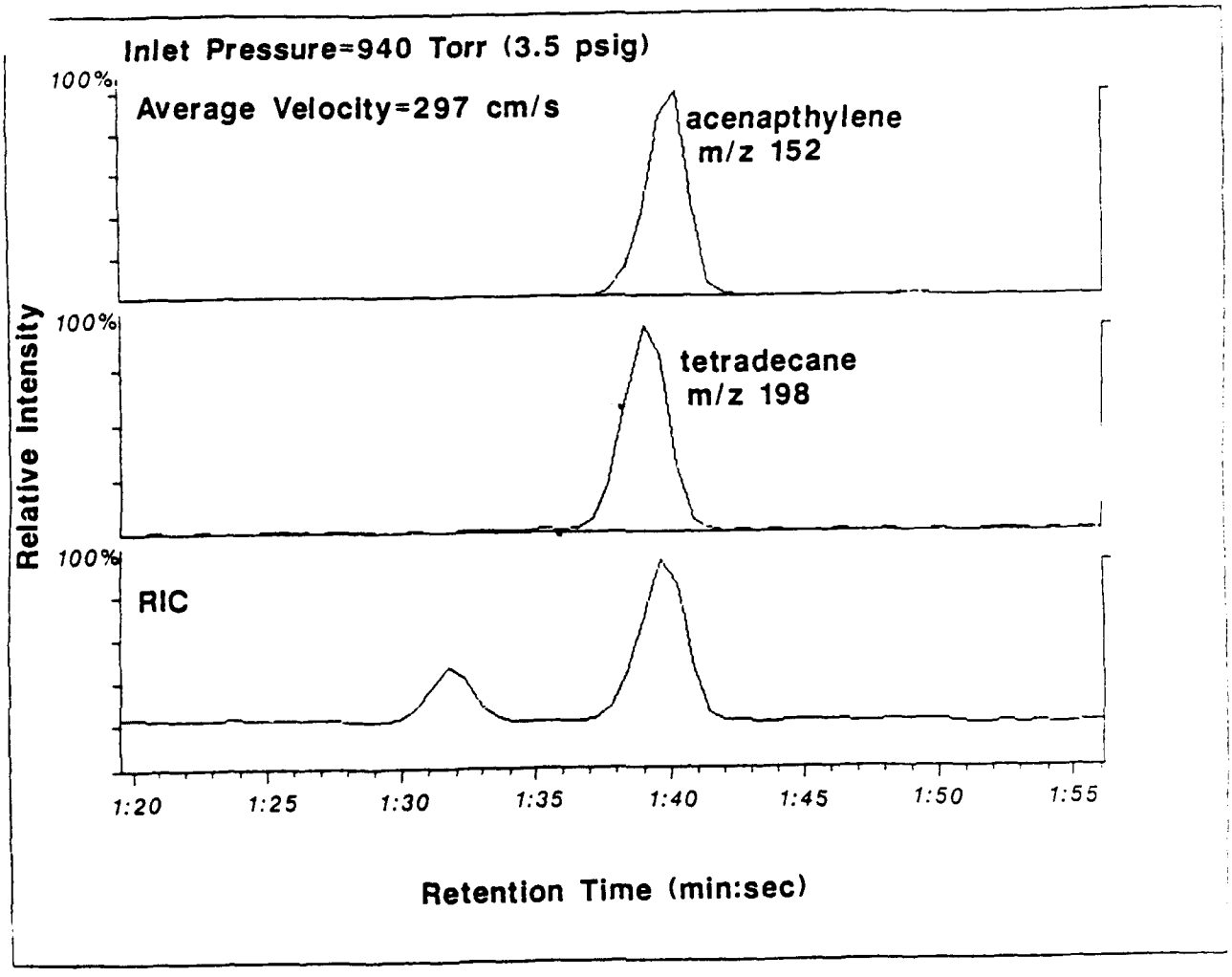

Figure 2-F.3. Chromatographic profiles of the acenapthylene and tetradecane obtained on a 3 m x 0.25 mm i.d. column with an inlet pressure of 940 Torr. The two components are not easily discerned from the RIC trace.

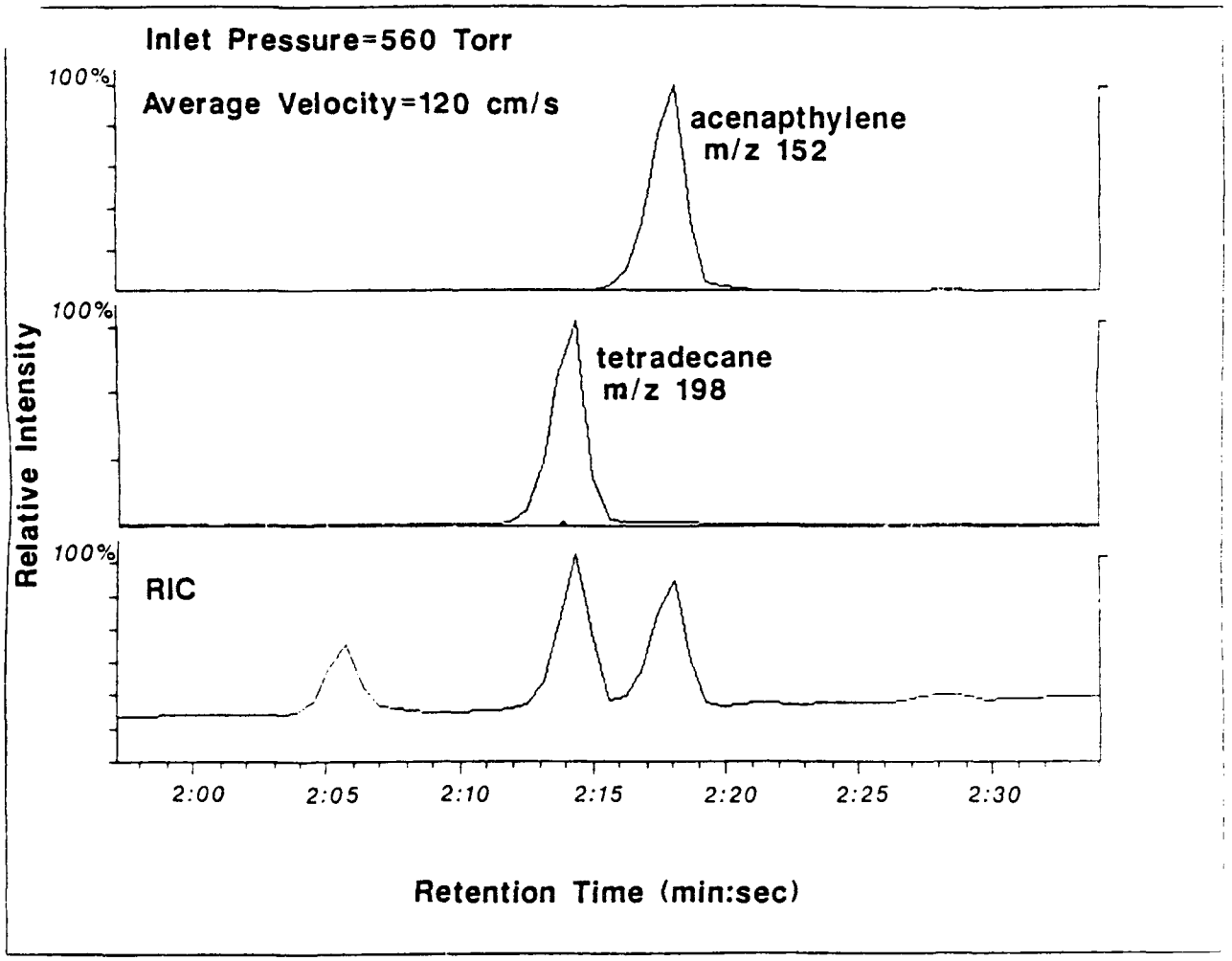

Figure 2-F.4. Same as Figure 2-F.3 except the inlet pressure was 560 Torr. Note the baseline resolution of the two components in the RIC trace.

References

(1) Johnson, J.V., Yost, R.A. Anal. Chem. **1985**, 57, 758A-768A.

(2) Trehy, M.L.; Yost, R.A.; Dorsey, J.G. Anal. Chem. **1986**, 58, 14-19.

(3) Trehy, M.L.; Yost, R.A.; McCreary, J.J. Anal. Chem. **1984**, 56, 1282-1285.

(4) Nygren, S. J. Chromatogr. **1977**, 142, 109-116.

(5) Nygren, S.; Anderson, S. Anal. Chem. **1985**, 57, 2748-2751.

(6) Nygren, S.; Mattsson, P.E. J. Chromatogr. **1976**, 123, 101-108.

(7) Zlatkis, A.; Fenimore, D.C.; Ettre, L.S.; Purcell, J.E. J. Gas Chromatogr. **1965**, 3, 75-81.

3. EVALUATION OF THE ION TRAP MASS SPECTROMETER AS A PORTABLE TANDEM MASS SPECTROMETER

3-A. Introduction to Quadrupole Ion Trap Mass Spectrometry

The Finnigan MAT ion trap mass spectrometer (ITMS) is a quadrupole ion trap consisting of a ring electrode, and two electrically connected end cap electrodes (Figure 3-A.1). Application of a radio frequency (RF) voltage to the ring electrode relative to the end caps creates a symmetrical three-dimensional quadrupole electric field within the electrode surfaces. When ions are created within or injected into this quadrupole field, they are either trapped or ejected depending upon the specific mass-to-charge ratio, m/z, of the ion and the applied field parameters (the magnitude and frequency of the RF voltage). The ITMS operates in a mass-selective instability mode. In this mode, the applied RF voltage determines the low m/z cutoff, below which ions no longer have stable trajectories and are ejected from the trap. Above this low m/z cutoff, a broad mass range of ions have stable trajectories and are trapped.

To perform normal mass spectral analysis, the end caps are grounded and the scan function of the ITMS controls the ionization time and RF levels as shown in Figure 3-A.2. During the ionization period the electron gate is biased to allow electrons to enter the trap and ionize the neutral molecules. During this period, the RF voltage applied to the ring electrode is low enough that ions over the entire mass range of interest are stored. After the electrons are "turned off", the RF voltage is scanned such that ions of consecutive m/z become unstable and are ejected from the trap and are detected by an electron multiplier, creating a mass spectrum.

Tandem mass spectrometry (MS/MS) is achieved on the ITMS by applying an auxiliary AC (tickle) voltage to the end caps. When ions are formed in the ion

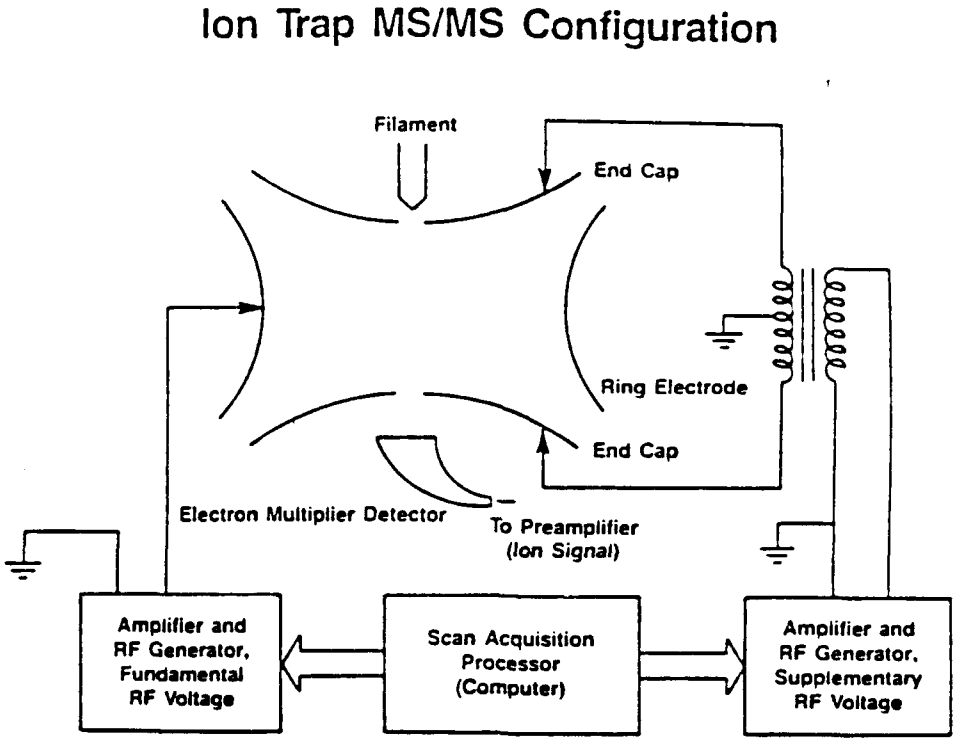

Figure 3-A.1. Schematic diagram of the Ion Trap Mass Spectrometer. Note that the end caps can be either grounded for normal mass spectrometry or an auxiliary AC voltage can be applied to them to perform tandem mass spectrometry.

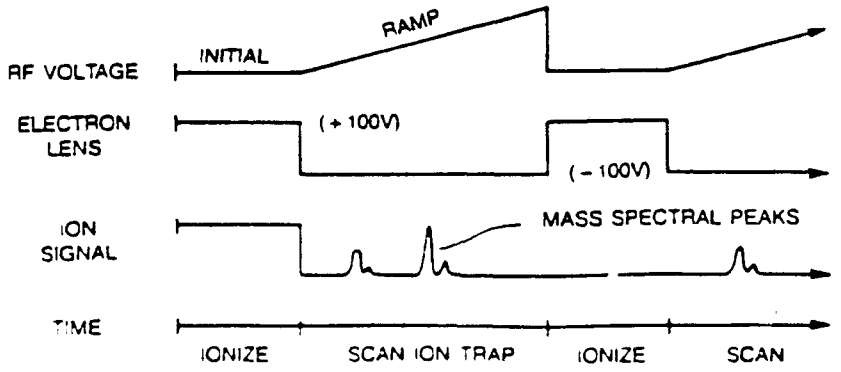

Figure 3-A.2. Normal mass spectral scan function for the ITMS showing the timing sequence for operation in the mass-selective instability mode.

trap they obtain an oscillatory motion with a secular frequency which is determined primarily by their m/z value and by the frequency and magnitude of the applied RF voltage. When the tickle voltage has the same frequency as the secular frequency of an ion, that ion begins to resonate, increasing its kinetic energy and orbit and undergoing collisions with the helium buffer gas (ca. 1 mtorr) present in the ion trap. Provided the magnitude of the tickle voltage is sufficient, the ion will undergo collisionally activated dissociation (CAD) to produce daughter ions. These daughter ions are trapped and mass-analyzed in a manner similar to the normal ITMS scan above.

Most of the applications of tandem mass spectrometry (MS/MS) to the determination of trace analytes in complex matrices have been performed with triple quadrupole (QQQ) tandem mass spectrometers. The ITMS represents a new approach to instrumentation for tandem mass spectrometry. With the ITMS, ionization of molecules, selection of parent ions, collisionally activated dissociation (CAD) of the parent ions, and mass analysis of their daughter ions all occur sequentially in the same physical space, and thus, MS/MS is tandem-in-time (Figure 3-A.3). This is in direct contrast to tandem mass spectrometry with triple quadrupole instruments, where these processes occur in discrete regions and MS/MS is tandem-in-space (Figure 3-A.3). More specifically, with the triple quadrupole an ion characteristic of the analyte (parent ion) is selected by quadrupole 1 (Q1) for CAD with a neutral gas (mtorr N_2 or Ar, typically) in Q2, and the subsequent daughter ions are mass-analyzed by Q3 (Figure 3-A.4). Because of the Q1 parent ion filter, only the ions of a specific m/z of interest are allowed to enter the CAD region.

With the ITMS being tandem-in-time, ionization, parent ion selection and CAD, and daughter ion mass analysis are implemented by a timing sequence or scan function which controls when each of these events occurs largely by

Tandem Mass Spectrometry (MS/MS)

Tandem-in-Space: Triple Quadrupole

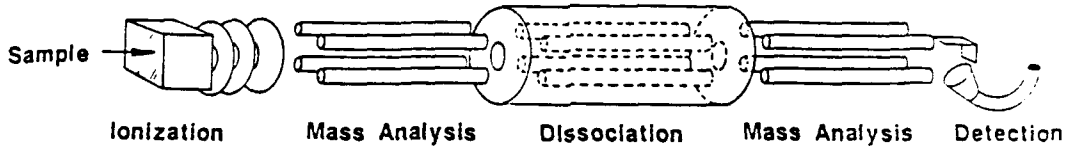

Tandem-in-Time: Quadrupole Ion Trap

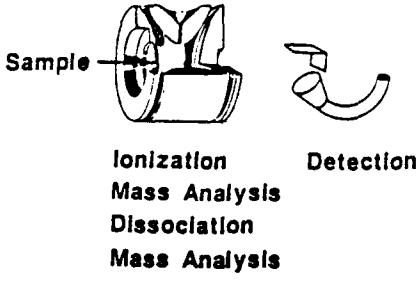

Figure 3-A.3. Two different tandem quadrupole mass spectrometers: triple quadrupole and quadrupole ion trap which are tandem-in-space and tandem-in-time, respectively.

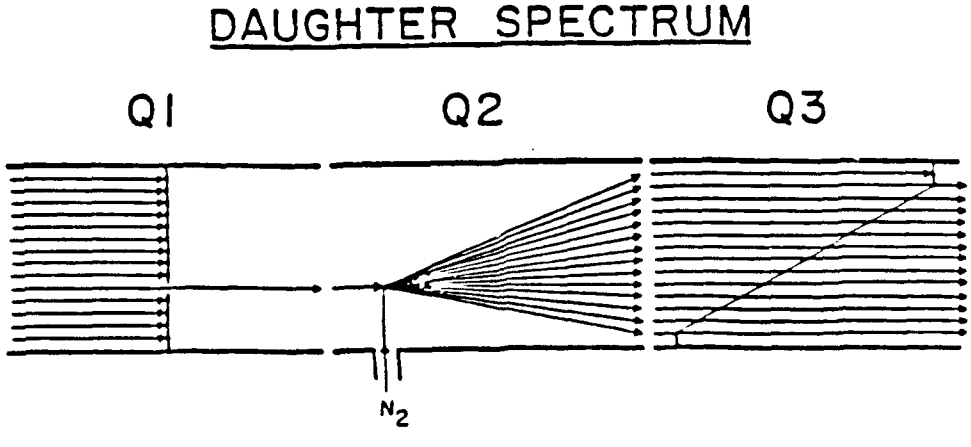

Figure 3-A.4. Schematic representation of the daughter scan mode for a triple quadrupole tandem mass spectrometer.

controlling the RF voltage level applied to the ring electrode and the auxiliary "tickle" or CAD voltage applied to the end caps (Figure 3-A.5). Initially, the RF voltage is low enough that during the ionization period, ions over a large mass range are stored (period A). Following ionization, all the ions of m/z values below that of the parent ion are swept out of the ion trap by raising the RF voltage on the ring electrode (period B). Note, however, that ions of m/z greater than that of the parent ion are still present in the trap and therefore potential interferences can occur. The RF voltage is then lowered to an appropriate level for storing the daughter ions of interest (Period C) and the auxiliary AC tickle voltage is applied at a particular frequency such that only the parent ion of interest is resonated to undergo CAD to produce daughter ions (Period D). Finally, the daughter ions are ejected from the ion trap and mass analyzed (Period E).

Here we report the results of our characterization and evaluation of the MS and MS/MS capabilities of a quadrupole ion trap tandem mass spectrometer. Our benchmarks for comparison of many of these results have been equivalent studies obtained with a triple quadrupole tandem mass spectrometer.

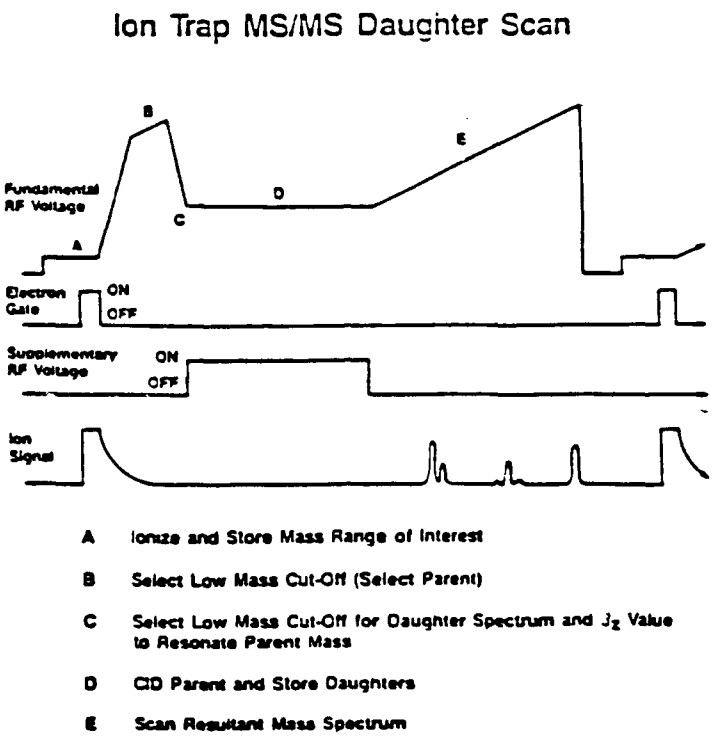

Figure 3-A.5. Timing Sequence for EI-MS/MS on the ITMS.

3-B. Evaluation of Electron Ionization and Positive Chemical Ionization

Although electron ionization (EI) was relatively easy to implement on the ITMS, it has been only recently that the capability to perform positive chemical ionization (PCI) was introduced on the ITMS. In the section below we report the results of our evaluation of the EI and PCI capabilities of the ITMS.

3-B.1. Electron Ionization

Traditionally, EI normal mass spectra are required for positive identification of a compound. The EI mass spectra of diethylethylphosphonate (DEEP) obtained on the QQQ and ITMS instruments agree well with each other and with those obtained from the literature (Figure 3-B.1). Note that with both instruments self-CI (i.e. the molecular ion, $M^{+\cdot}$, reacting with the neutral molecules, M, to form an $(M+H)^{+}$ ion) of DEEP was possible as indicated by the m/z 167 ion being of greater abundance than can be explained by the ^{13}C isotope

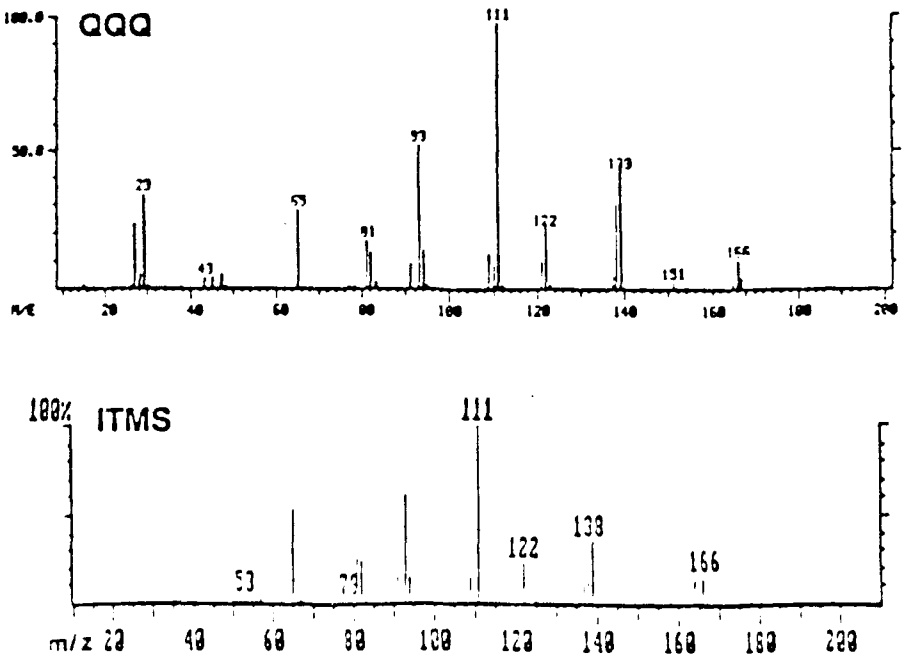

Figure 3-B.1. EI normal mass spectra of DEEP acquired on the QQQ and the ITMS. Note that the ions at m/z 135, 136, 164, and 178 in the ITMS spectrum are due to a contaminant.

peak of the molecular ion, m/z 166. The ITMS is much more susceptible to self-CI than the more traditional triple quadrupole ion source due to the longer ion residence times in the ITMS (msec versus μsecs in traditional ion sources).

Although the extensive fragmentation resulting from EI is desireable for positive identification, it often results in reduced sensitivity and selectivity in mixture analysis. In addition, the prospect of self-CI or CI from other matrix components may also present problems. Thus, most of our efforts were spent evaluating chemical ionization with the ITMS.

3-B.2. Positive Chemical Ionization

Although the abundance of fragmentation as occurs in the EI mass spectra is desired for identification, for trace analysis one desires that all of the ion current reside in a few, intense and characteristic ions: chemical ionization (CI) is traditionally used to achieve this. On the QQQ instruments, and indeed on most traditional instruments, this requires some modification of the ion source to allow pressurization (in the torr range) of that region to increase the possibility of ion-molecule reactions. With the ITMS, it is only necessary to admit some methane in the 10^{-5} torr range and vary the timing sequence and RF levels as shown in Figure 3-B.2. To achieve CI in the ITMS, the RF voltage applied to the ring electrode is set such that only low mass ions (e.g. reagent ions) are efficiently stored during the electron ionization period (Period A', when electrons are gated into the ion trap). With a reagent gas present, EI can be accomplished during this period by setting the RF voltage high enough such that no reagent ions are stored (Period A). Following the electron ionization period, the RF voltage on the ring electrode is increased during the CI reaction period to allow efficient storage of the sample ions created from ion-molecule reactions with the CI reagent ions (Period B'). Note that an equivalent period is absent for the EI scan function. Following the CI reaction

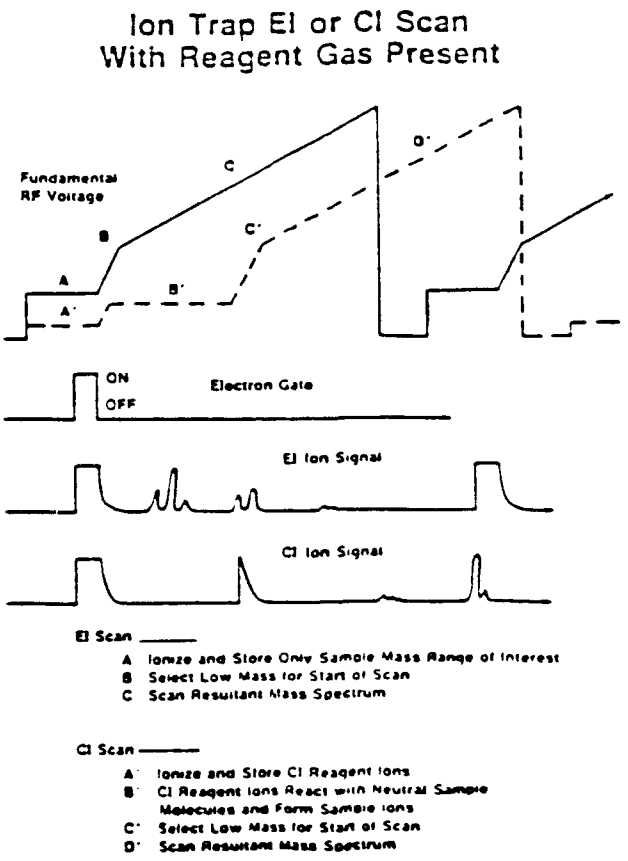

Figure 3-B.2. Comparison of the EI and CI normal MS scan functions on the ITMS.

period, mass analysis of the ions is performed by scanning the RF voltage (periods B and C for EI; periods C′ and D′ for CI). Thus, two of the major advantages of the ITMS over more traditional mass spectrometers are (1) selective storage of ions can be achieved by varying the RF voltage applied to the ring electrode and (2) the CI reaction time can be varied. As both of these attributes are under software control, they can be easily implemented.

Effect of CI Reaction Time on Methane PCI

Experimental. For these experiments that follow, DEEP was introduced into the ITMS via a fine metering valve such that a constant level (ca. 0.1 X 10^{-5} torr) was present in the ion trap. For studies of the effect of the CI reaction

time, the electron ionization time (usually 0.1 msec) and all the other time periods were held constant while the CI reaction period was varied. The RF level during ionization was kept at 5 amu while all other RF levels were kept at 12 amu. Mass spectra were acquired by scanning from m/z 12 to 400 in 2 secs with 16 microscans. Experiments were performed with indicated methane pressures of ca. 0.1×10^{-5} torr and ca. 3.4×10^{-5} torr and with a buffer gas pressure inside the ion trap of ca. 1 mtorr helium.

Results and Discussion. The results of experiments with DEEP (shown in Figure 3-B.3) demonstrate that during the CI reaction time period two other time periods can be distinguished by the reactions which are predominantly occurring during them: a **reagent ionization period** dominated by the ion-molecule reactions forming reagent ions and a **sample ionization period** dominated by the ion-molecule reactions (CI) forming the sample ions. Due to the nature of the ion trap, i.e. all reactions occur within the same physical space, there is not a distinct cutoff between these two time periods. However, due to the behavior of the sample ions, the reagent ionization and sample ionization periods will be considered separately below.

Evaluation of the Reagent Ionization Period. During the first 25 msec of the CI reaction period, the ion-molecule reactions are dominated by those which result in the formation of CI reagent ions with only relatively small changes in the sample ions. Thus, this time can be distinguished as the reagent ionization period. During this period, the methane EI ions (represented by m/z 15, CH_3^+) formed during the initial electron ionization period rapidly undergo ion-molecule reactions with methane neutral molecules to form the m/z 17 (CH_5^+) and the m/z 29 ($C_2H_5^+$) methane reagent ions according to Reactions B-1 and B-2, respectively. As no special precautions were taken to exclude water from the vacuum system, these methane reagent ions then react with residual water present

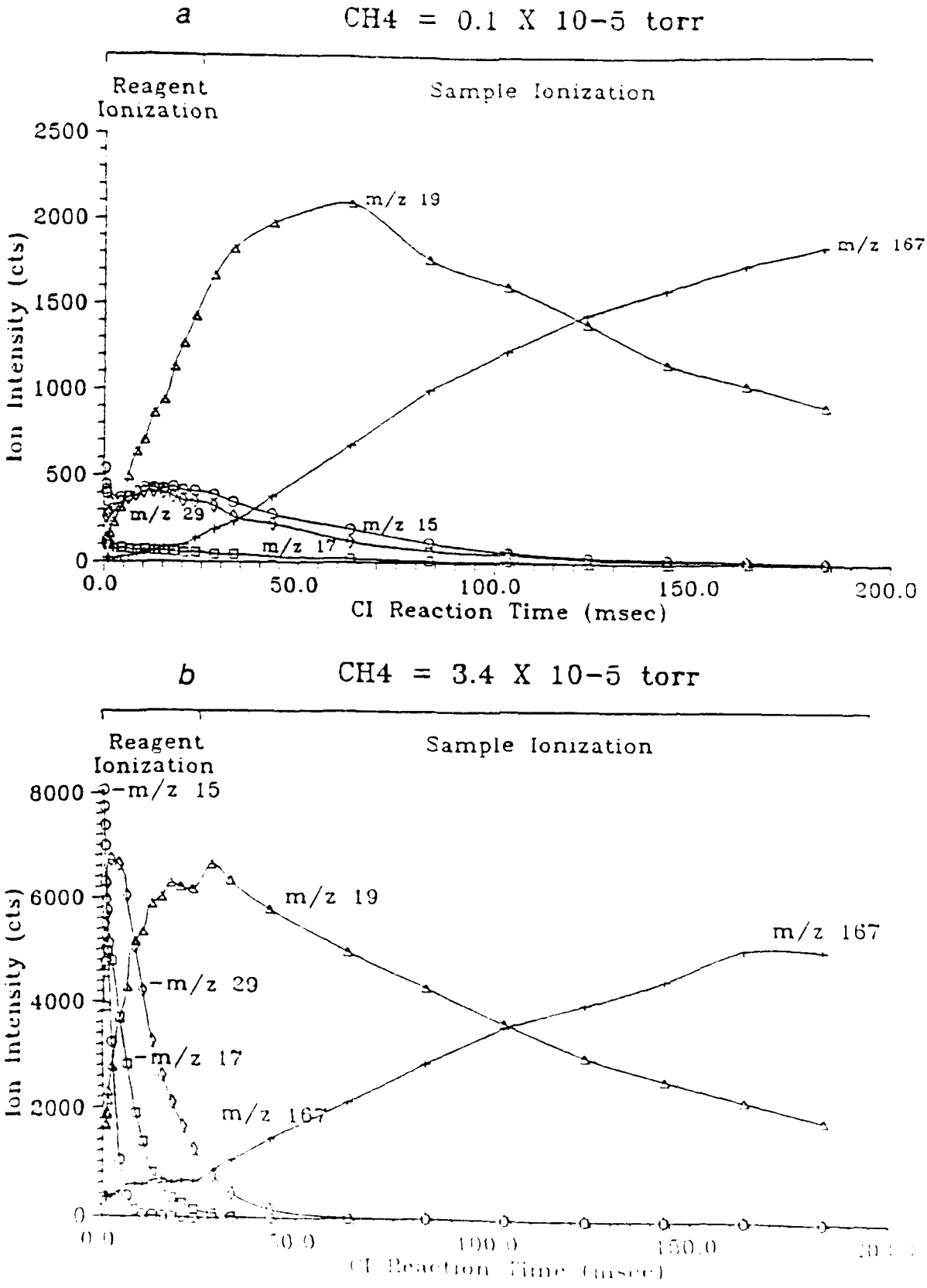

Figure 3-B.3. Variation of ion intensity with varying CI reaction time during methane PCI of DEEP at (a) 0.1 X 10^{-5} torr CH_4 and at (b) 3.4 X 10^{-5} torr CH_4. The ions shown correspond to CH_3^+ (m/z 15), CH_5^+ (m/z 17), $C_2H_5^+$ (m/z 29), H_3O^+ (m/z 19), and the $(M+H)^+$ ion of DEEP (m/z 167).

in the background and in the methane itself to produce the m/z 19 (H_3O^+) reagent ion (Reaction B-3). As the proton affinity of water is greater than that of methane, water was preferentially protonated and H_3O^+ became the dominate reagent ion. Thus, with a CI reaction time greater than approximately 15 msec, water CI is predominately occurring.

$$CH_4^{+\cdot} + CH_4 \rightarrow CH_5^+ + CH_3\cdot \quad \text{(Reaction B-1)}$$

$$CH_3^+ + CH_4 \rightarrow C_2H_5^+ + H_2 \quad \text{(Reaction B-2)}$$

$$CH_5^+ + H_2O \rightarrow H_3O^+ + CH_4 \quad \text{(Reaction B-3)}$$

As H_3O^+ is the major reagent ion under these conditions, some differences in ionization efficiencies for different compounds may be discerned in comparison to true methane CI. As the proton affinity of water (173 kcal/mole) is greater than that of methane (130.5 kcal/mole), the amount of internal energy in the protonated sample molecule (determined by the difference in the proton affinity between the sample and water) will be less and thus, less fragmentation would be expected in the water CI mass spectra as compared to true methane CI. Also, as the degree to which the proton transfer reaction occurs is governed by the relative proton affinities of the sample molecule and the conjugate base of the CI reagent ion, some classes of compounds (e.g. alkanes) may not be efficiently ionized. This may be a method to eliminate some of the potential chemical interferences. However, if true methane CI is desired, it will be necessary to use some type of water scrubbers to reduce the amount of water introduced via the gas lines and to operate in the reagent ionization time regime which is optimum for production of CH_5^+ ions.

With the reduced methane pressure (Figure 3-B.3a), these reactions to produce the CI reagent ions do not reach completion until after 100 msec. With

the higher methane pressure (Figure 3-B.3b), these reactions occur more quickly, reaching completion in ca. 45 msec. While the reagent ions are being formed, the sample is also being ionized by ion-molecule reactions to produce $(M+H)^+$ ions (m/z 167) of DEEP. With both the low and high methane pressures, the intensity of the m/z 167 ions slowly increased with the CI reaction time up to ca. 25 msec, after which the m/z 167 ion intensity increased more rapidly. The 25 msec time corresponds roughly to the time necessary to produce the maximum intensity of the H_3O^+ ions. Note that the m/z 93 and 166 ions (formed during the initial EI period) do not change with the sample reaction time, while the CI fragment ions, m/z 111 and m/z 139, and the $(M+H)^+$ ion, m/z 167, become more abundant with increasing reaction time (Figure 3-B.4). By varying the sample ionization or reaction time occurring immediately after the initial ionization period (0.5 msec), it was possible to obtain EI mass spectra at short reaction times and CI mass spectra at long reaction times for DEEP. In addition, it was possible to obtain EI mass spectra in the presence of the methane reagent gas by raising the RF voltage during the initial ionization period such that the methane ions were not stored (and thus the methane CI reagent ions were not produced). Thus, by simply changing the scan function, it should be fairly straightforward to acquire alternating EI/CI mass spectra with the ITMS, something which has not been really successfully demonstrated with traditional ion sources.

Evaluation of the Sample Ionization Period. The sample ionization period is dominated by the ionization of the sample neutral molecules to produce the desired $(M+H)^+$ ions, m/z 167. For both pressures of methane, this period starts after a CI reaction time of ca. 25 msec and continues to the maximum CI reaction time studied (183 msec). Whereas the intensity of the $(M+H)^+$ ion of DEEP increased only slowly up to 25 msec, after 25 msec the intensity of the $(M+H)^+$ ion increased rapidly with increasing reaction time while there was a

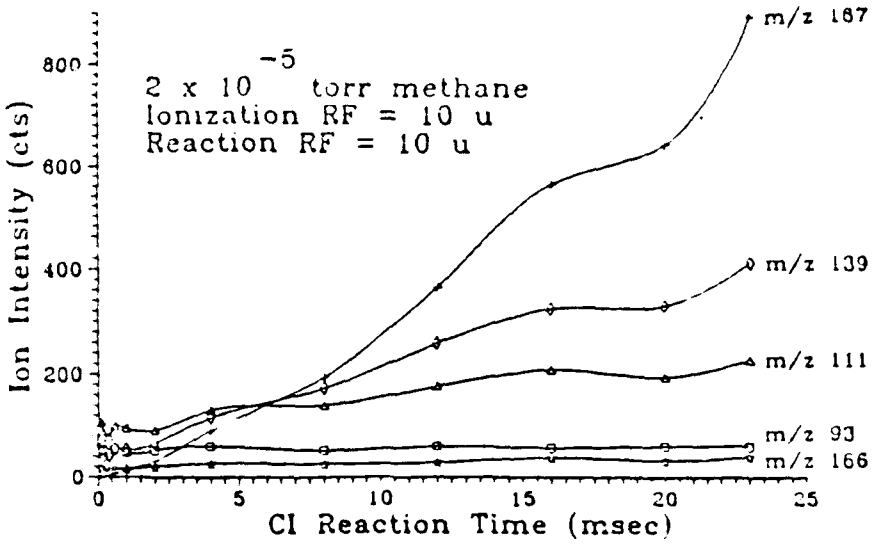

Figure 3-B.4. Effect of variation of the CI reaction time on the ion intensities of the ions of DEEP.

corresponding decrease in the H_3O^+ ion intensity, e.g. for the higher methane pressure, the intensity of the m/z 167 ion increased by a factor of 8 with an increase in time from 25 to 160 msec (factor of 6.4) of CI reaction time. Thus, for maximum CI sensitivity, a long CI reaction time would be preferred. In addition, the variation of the sample ionization time may provide a means to extend the linear dynamic range of PCI with the ITMS (see Section D-3). It should also be noted that by controlling the levels of the RF voltage during the CI reaction period, it may be possible to distinctly separate and control the formation of reagent ions and sample ions.

Comparison of the positive chemical ionization (PCI) normal mass spectra of DEEP shows that ITMS spectrum contains a greater abundance of fragment ions, m/z 111 and m/z 139, and a lower abundance of the methane $(M+29)^+$ and $(M+41)^+$ adduct ions (m/z 195 and m/z 207, respectively) than does the QQQ mass spectrum (Figure 3-B.5). Although the spectra were acquired at the same temperature (100

°C) on both instruments, the ions in the ITMS are much more affected by the temperature as they are exposed for much longer periods of time (msec) than in a traditional ion source (μsec). Thus, the greater abundances of fragment ions in the ITMS could be partially due to thermally-induced fragmentation of the $(M+H)^+$ ions and partially due to the major difference in the effective pressure of the CI gas, ca. 2 - 3 X 10^{-5} torr in the ITMS versus ca. 1 torr in the QQQ. The lower abundances of the $(M+29)^+$ and $(M+41)^+$ ions is expected as water CI tended to dominate the CI process in the ITMS, as discussed above, and the higher pressures of methane needed for their formation and stabilization are absent.

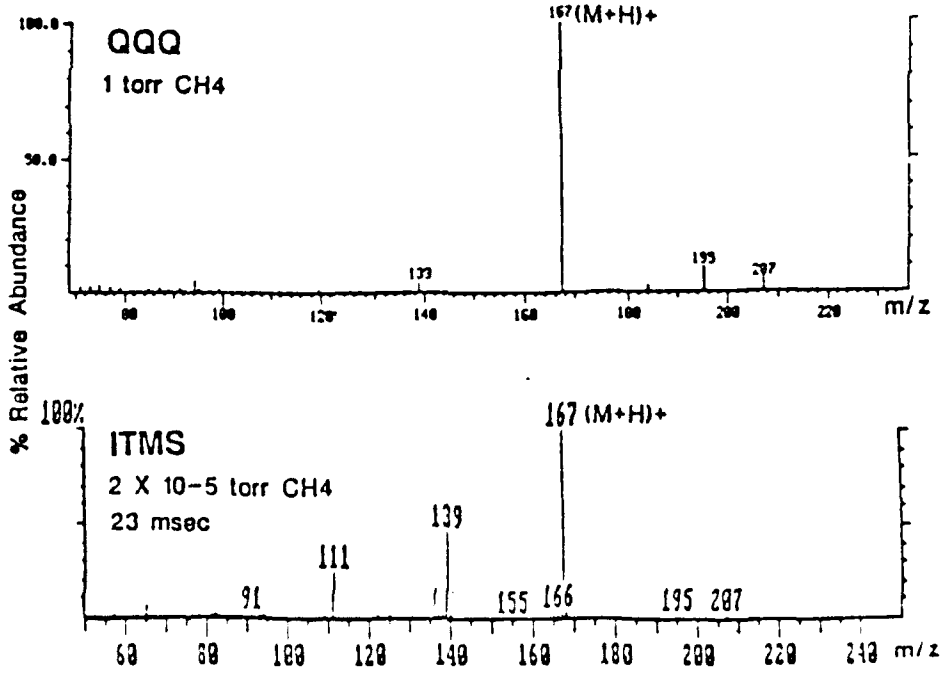

Figure 3-B.5. Methane PCI normal mass spectra of DEEP acquired on the QQQ and the ITMS. Note that the ions at m/z 136 and 166 in the ITMS spectrum are due to a contaminant.

3-C. Evaluation of Tandem Mass Spectrometry

In order to successfully perform tandem mass spectrometry in the ITMS, one must efficiently isolate and energize the parent ion and then efficiently trap and mass analyze the resulting daughter ions. In this section, our evaluations of each of these operations, as well as the studies of the parameters which affect them, are reported.

3-C.1. Isolation of the Parent Ion

The methane positive chemical ionization (PCI) normal mass spectra of diethylethylphosphonate (DEEP, MW 166) from both the triple quadrupole and ion trap are characterized by an abundant $(M+H)^+$ ion at m/z 167 (Figure 3-B.5). The PCI-CAD daughter spectra of the $(M+H)^+$ ion of DEEP are characterized by daughter ions at m/z 65, 93, 111, and 139 due to various combinations of losses of H_2O, C_2H_4, and C_2H_5OH from the parent ion (Figure 3-C.1). Prior to performing CAD of the parent ion in the ITMS, it is necessary to eject all ions

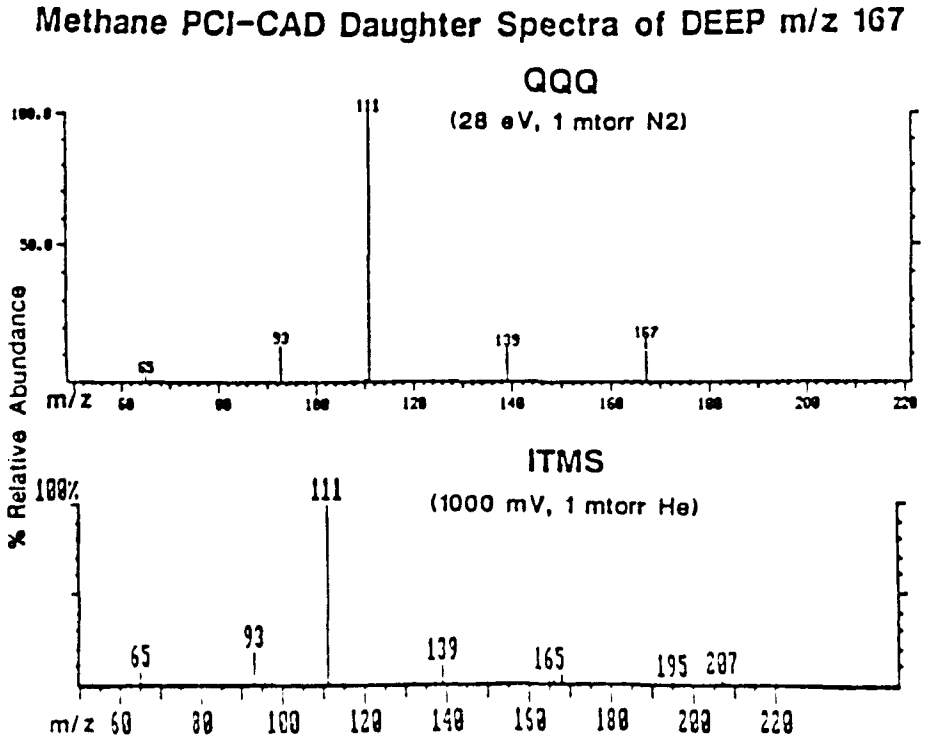

Figure 3-C.1. Methane PCI-CAD daughter spectra of the $(M+H)^+$ ion (m/z 167) of DEEP on the triple quadrupole (QQQ) and on the ion trap (ITMS) mass spectrometers.

present in the ion trap in the mass range of the expected daughter ions. By raising the RF voltage applied to the ring electrode, it was possible to eject all ions up to but not including the parent ion. However, note the presence of ions at m/z 165, 166, 195, and 207 in the ITMS daughter spectrum (only those ions up to but not including m/z 165 were ejected prior to PCI-CAD). The continued presence of these ions during the MS/MS analysis may lead to spectral interferences. In the triple quadrupole, only a single m/z ion is selected by Q1 for CAD and thus the QQQ daughter spectrum is lacking these ions and their possible interference.

3-C.2. Resolution of Parent Ion Excitation

In a quadrupole ion trap, an ion will oscillate in the RF field with a characteristic secular frequency which is determined by its m/z ratio and the applied RF field. In order to excite an ion to undergo CAD in the ITMS, an auxiliary AC voltage (tickle voltage) is applied to the end caps of the ion trap with a frequency which matches the secular frequency of the selected parent ion. Variation of the tickle frequency showed that indeed only a fairly narrow band of frequencies will excite a parent ion and there is an optimum frequency for maximum CAD efficiency (Figure 3-C.2). The width of the tickle frequency band (a measure of the resolution of parent ion excitation) increased with increasing tickle voltage. However, provided the tickle voltage was not too excessive, it was possible to excite an ion to undergo CAD with unit mass resolution (e.g. note the presence of the ions at m/z 166 and m/z 168 and the complete absence of the parent ion at m/z 167 in the ITMS daughter spectrum of Figure 3-C.1).

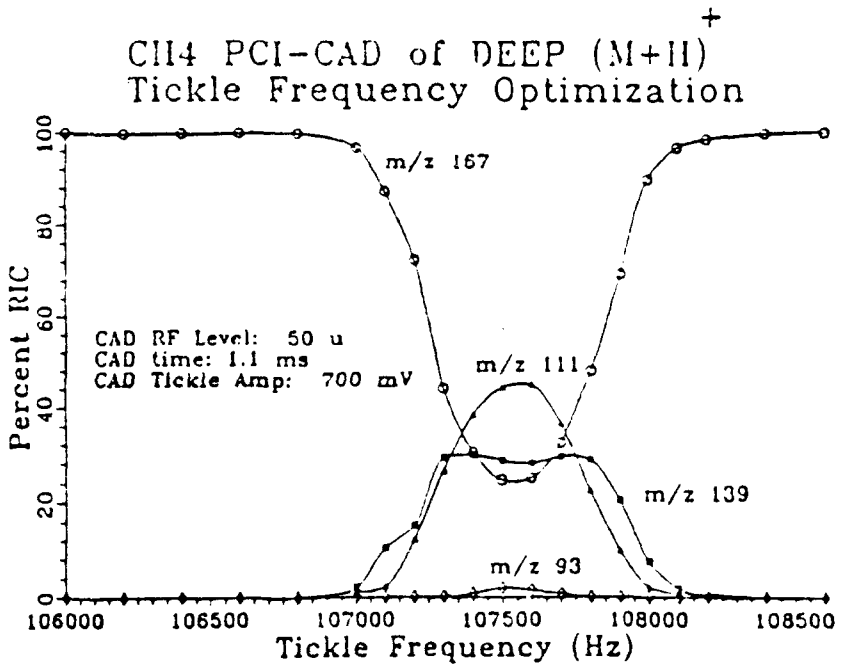

Figure 3-C.2. Optimization of the frequency of the tickle voltage to achieve maximum CAD of the $(M+H)^+$ ion (m/z 167) of DEEP.

3-C.3. Evaluation of CAD EFficiencies

The abundances of the daughter ions relative to each other are approximately the same for PCI-CAD daughter spectra of the $(M+H)^+$ ion of DEEP obtained on the triple quadrupole and ITMS (Figure 3-C.1). However, the abundances of the daughter ions relative to that of the parent ion in the daughter spectra indicate that the ITMS yielded a higher fragmentation efficiency. It was shown that as the tickle voltage or CAD energy was increased, the fragmentation efficiencies increased until reaching a maximum of 100 % and 89 % for the ITMS and TSQ45, respectively (Figure 3-C.3). The fragmentation efficiency is also affected by the mass of the collision gas. A comparison of the fragmentation efficiency for the most abundant daughter ion (m/z 111) of the m/z 167 parent ion of DEEP with a collision gas pressure of approximately 1 mtorr helium for both the QQQ and the ITMS, demonstrated that the fragmentation efficiency of the ITMS was more than 10[illegible] times more efficient than that obtained for the QQQ (Figure 3-C.4). The greater fragmentation efficiency observed with the ion

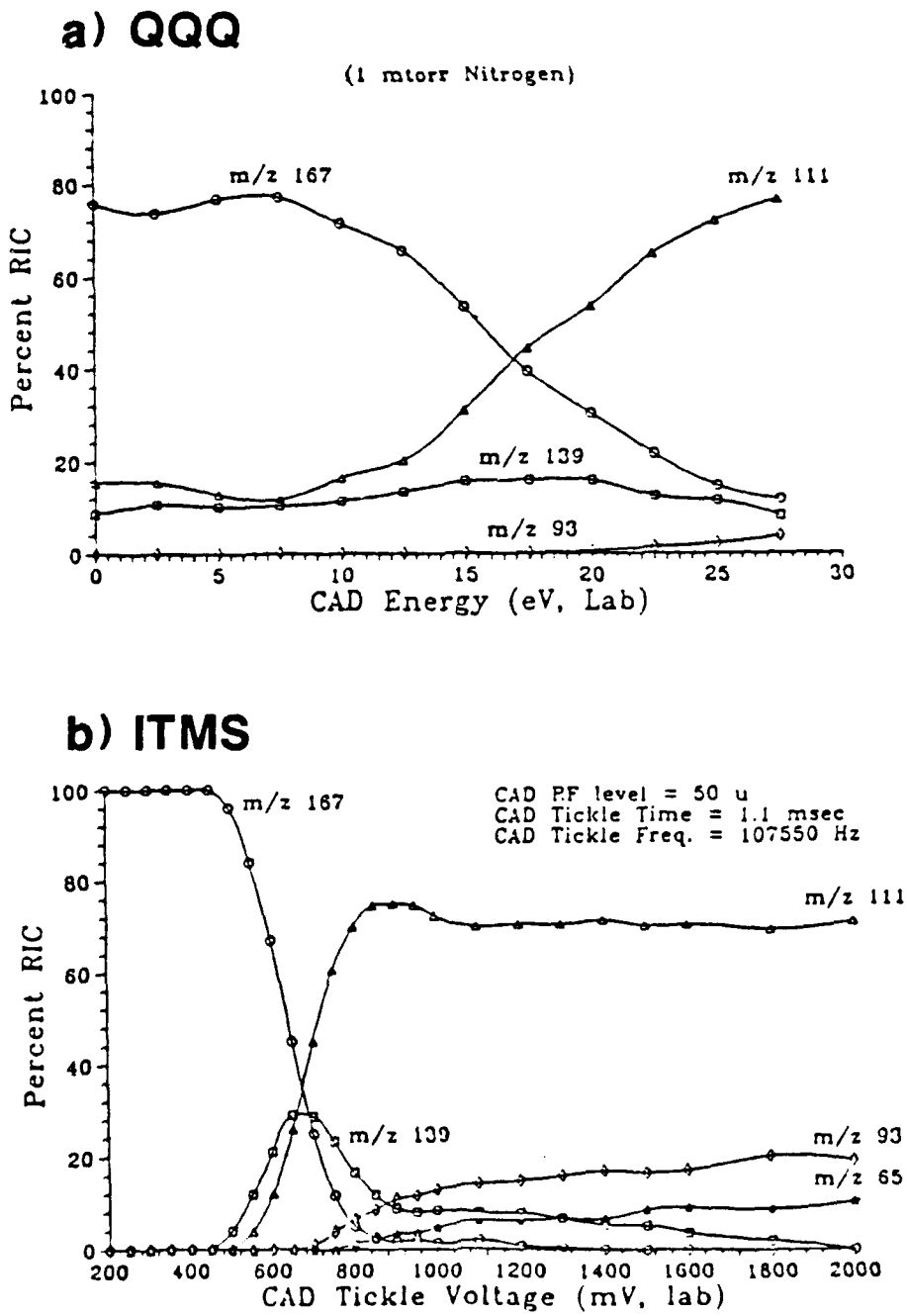

Figure 3-C.3. Methane PCI-CAD energy-resolved breakdown curves of the $(M+H)^+$ ion (m/z 167) of DEEP: (a) on QQQ (TSQ45) with 1 mtorr nitrogen and (b) on ITMS with approximately 1 mtorr helium.

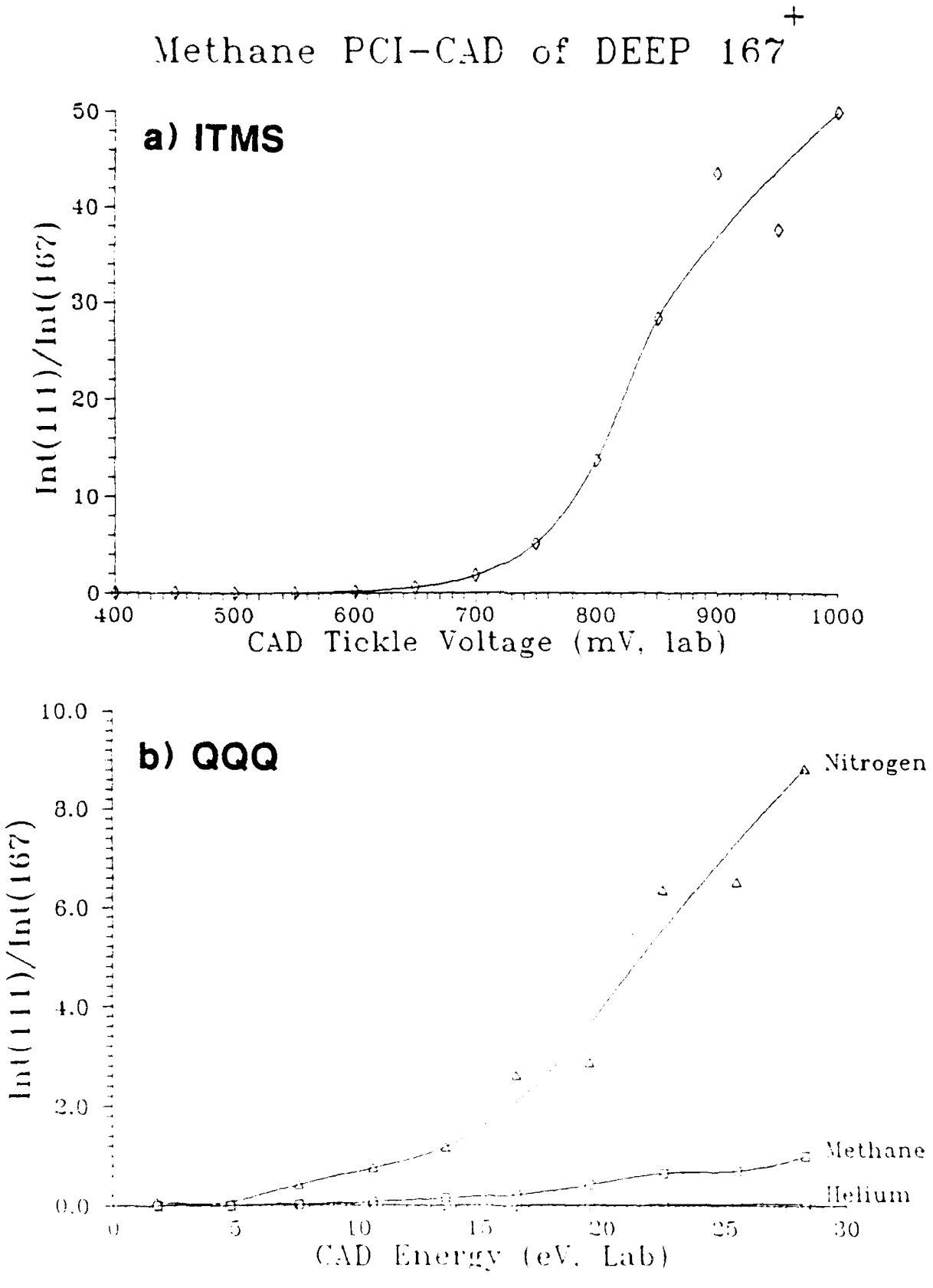

Figure 3-C.4. Efficiency of producing the major daughter ion (m/z 111) resulting from the PCI-CAD of the $(M+H)^+$ ion (m/z 167) of DEEP with an indicated CAD gas (buffer gas for ITMS) pressure of approximately 1 mtorr: (a) ITMS and (b) QQQ (TSQ 45).

trap is due largely to the time scale and nature of the CAD process. Whereas, with the QQQ, a parent ion must undergo CAD during its single pass through the collision chamber, the ITMS is able to contain the parent ion and keep energizing it to undergo multiple collisions until CAD does occur. Indeed with an increase in the CAD reaction or tickle time in the ITMS, the amount of CAD could be significantly increased (Figure 3-C.5). Both the QQQ and ITMS showed a collection efficiency of approximately 90 % provided the tickle voltage or CAD energy was not excessively high. The major loss of efficiency with the QQQ, however, is due to the requirement of unit mass resolution of the daughter ions during mass analysis by Q3 which results in a transmission efficiency for Q3 of approximately 10 %. As the ITMS lacks these ion optical elements and because of the more effective containment and trapping of the daughter ions in the ion trap, the subsequent collection and mass analysis of the daughter ions was approximately 27 time more efficient in the ITMS than in the QQQ system.

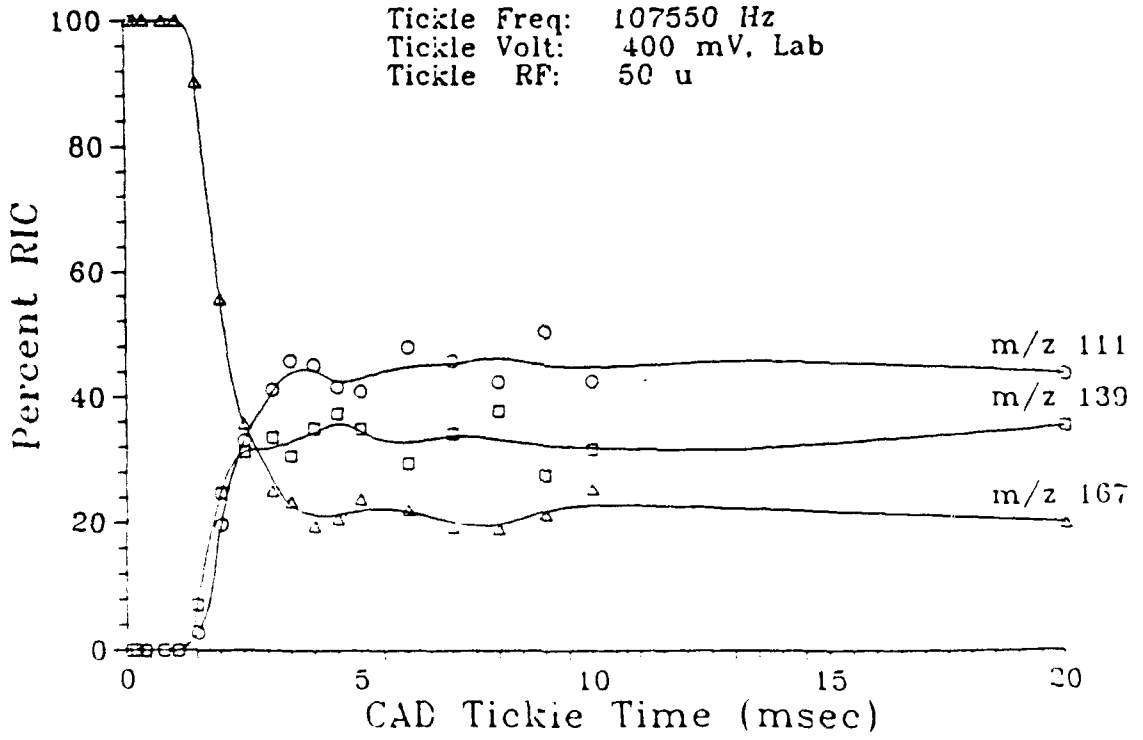

Figure 3-C.5. Effect of the length of time for which the CAD tickle voltage is applied on the relative abundances of the daughter ions and parent ion for the PCI-CAD of the $(M+H)^+$ ion (m/z 167) of DEEP.

3-C.4. Relationships between the CAD Parameters: Tickle Frequency, Tickle Voltage, and CAD Reaction Time

With the ITMS, in order to excite a parent ion to undergo CAD, an auxiliary AC or tickle voltage is applied to the endcap electrodes. Provided the frequency of the CAD tickle voltage matches the secular frequency of the parent ion within the ion trap's RF field, the parent ion will begin to resonate, increasing the size of its orbit and thus its kinetic energy, until CAD begins to occur. As there is no observable CAD occurring when the tickle voltage is not applied, when it is applied there must be a finite tickle time, dependent upon the tickle voltage, necessary in order for the parent ion to reach sufficient kinetic energy for CAD to occur. Indeed, three different periods could be distinguished when the CAD reaction time was varied for a set tickle voltage: a period during which no CAD occurred, a period following the onset of CAD where the abundances of daughter ions increased rapidly over a relatively short time, and then a period where the amount of CAD remained fairly constant (Figure 3-C.5). The first period and second period agree well with the model. Indeed, it was shown that there is an inverse relationship between the magnitude of the tickle voltage and the CAD reaction time for which it was applied, i.e. increasing the tickle voltage reduced the amount of CAD reaction time required for onset of CAD (Figure 3-C.6). Based upon the simplistic model, once the onset of CAD occurred, all of the parent ions would undergo CAD instead of leveling off as demonstrated by the third period. It may be that ion-molecule reactions between the $(M+H)^+$ ions and neutral M molecules to create new $(M+H)^+$ ions may become important during this period. Some evidence was shown for this by the increase in abundance of two adduct ions (resulting from ion-molecule reactions) with increasing CAD reaction time (Figure 3-C.7).

In addition, the importance of operating at the optimum tickle frequency was demonstrated. As the efficiency of coupling the tickle voltage to increasing

the kinetic energy of the parent ion decreased rapidly at frequencies away from the optimum, the degree of CAD (or the tickle voltage or CAD reaction time required to achieve a certain level of CAD) also decreased dramatically.

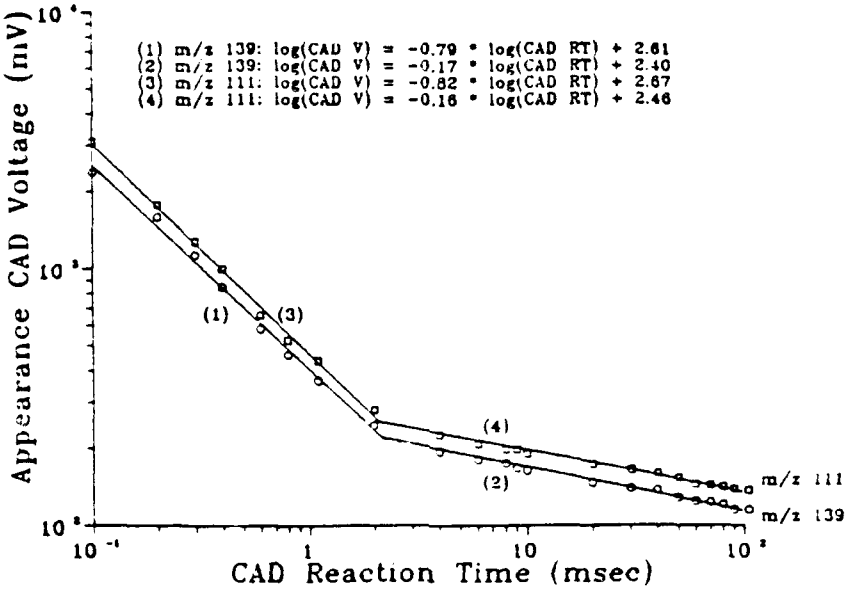

Figure 3-C.6. Variation of the CAD tickle voltage necessary for the "appearance" of the PCI-CAD daughter ion m/z 111 and m/z 139 of the $(M+H)^+$ ion (m/z 167) of DEEP.

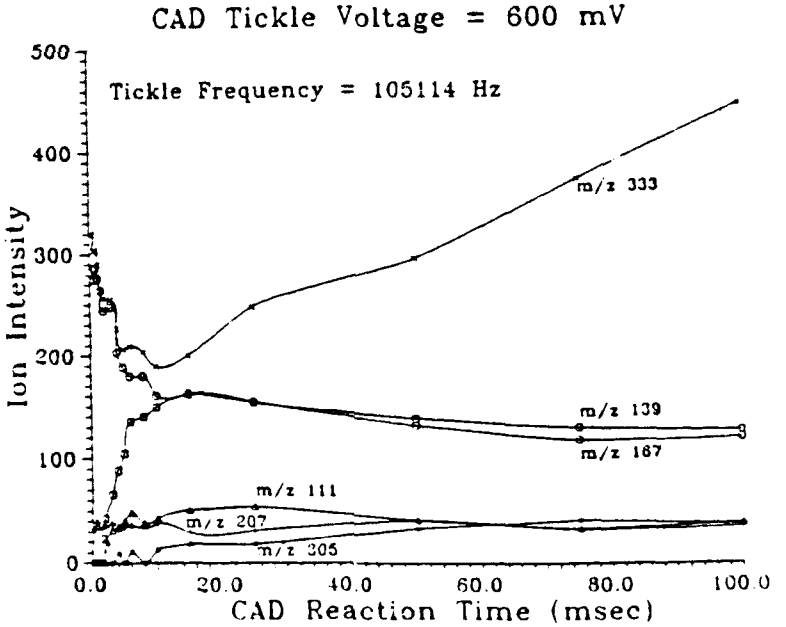

Figure 3-C.7. Effect of variation of the CAD reaction time on the absolute ion intensities of the major ions observed in the PCI-CAD daughter spectra of the $(M+H)^+$ ion (m/z 167) of DEEP. The m/z 305 and 333 ions are presumably adduct ions resulting from ion-molecule reactions between the m/z 139 and m/z 167 ions, respectively, and neutral DEEP molecules. Note that the relatively constant intensity of the m/z 207 ion (the $(M+29)^+$ ion resulting from methane PCI of DEEP) indicates that the level of DEEP in the ion trap was relatively constant.

3-C.5. Mass Resolution of Daughter Ions

When not limited by space charge effects, it is possible to obtain unit mass resolution across the entire mass range of the daughter spectra on the ITMS and on the QQQ. However, the ITMS is more sensitive to space charge effects which result from the presence of too many ions of mass greater than or equal to the parent ion. These space charge effects broaden the peak profile and cause an apparent shift to a higher m/z; these then lead to mass assignment problems with the centroiding algorithms of the ITMS (Figure 3-C.8). In this example, the space charging was caused by the sample itself. In the case where large amounts of other compounds are present, the ions of the interferents which are below the m/z of the parent ion should not lead to space charge effects as they are swept out of the ion trap prior to CAD. However, any interferent ions

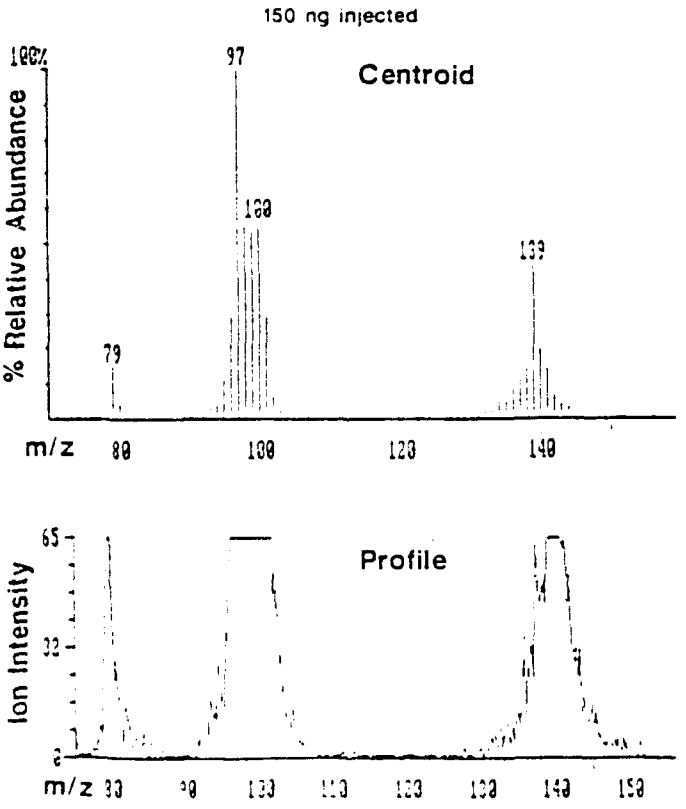

Figure 3-C.8. Centroid and profile daughter spectra of the $(M+H)^+$ ion (m/z 181) of diisopropylmethylphosphonate (DIMP) obtained at the top of its GC peak for 150 ng injected.

equal to or greater than the parent ion will still remain in the ion trap and may affect the resolution of the daughter ions. Although space charging can occur also with QQQ instruments, its magnitude is much lower due to Q1 mass filtering only a single m/z for CAD in Q2. The use of direct current (DC) voltage in conjuction with RF voltage on the ITMS will result in the isolation of a single parent ion and should reduce the magnitude of the space charging problem significantly. Further experiments are planned to assess the extent to which space charging by other compounds affects the daughter ion mass resolution in the ITMS with and without DC voltages.

3-C.6. Effect of Space Charge on the CAD Tickle Frequency and CAD Energy Deposition

In addition to the broadening of the ion profile and an apparent shift to a higher m/z, space charge effects also result in reduced CAD efficiency (Figure 3-C.9). Indeed, with extreme space charging, no CAD of the parent ion occurs. With a variation of the tickle frequency for ions exhibiting extreme space charge, it was determined that space charging causes the secular frequency of the parent ion to change to a lower frequency (expected due to an apparent shift to a higher m/z) (Figure 3-C.10). Whereas, the width of the ion profile at 1/2 height increased by 700 % (from 0.5 u to 3.5 u) with space charging, the width of the tickle frequency band at 1/2 height only increased by 10 %. Thus, even though the ion intensity profile was significantly broadened, it was possible to accomplish CAD with essentially unit mass resolution of the parent ion. With a better understanding of how space-charging affects the daughter and parent ions, it may be possible to devise scan functions (e.g. neutral loss) to compensate for these effects; research in this direction is continuing in our laboratory.

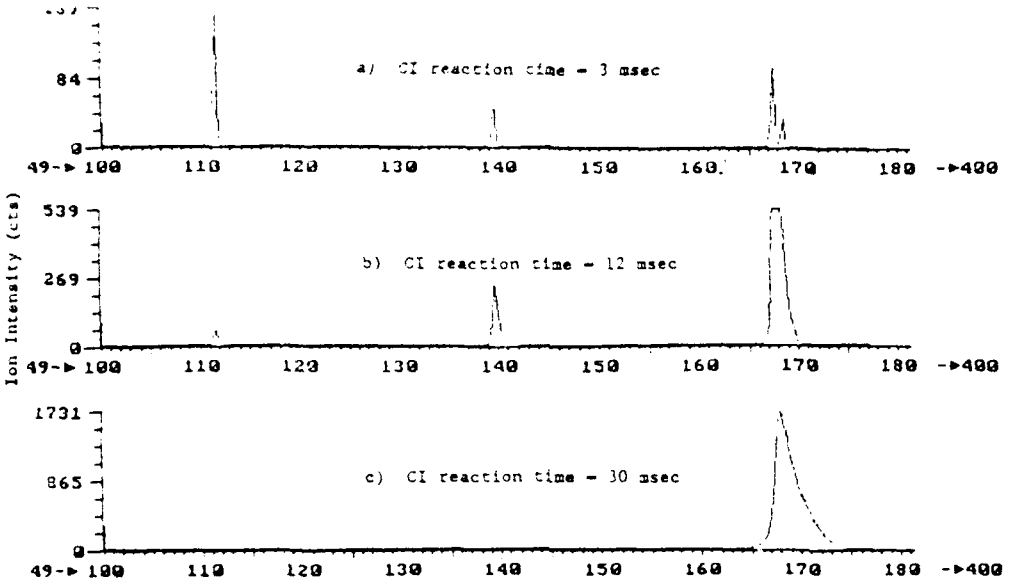

Figure 3-C.9. Ion peak profiles for the m/z 111, 139, and 167 ions resulting from the methane PCI-CAD of the $(M+H)^+$ ion (m/z 167) of DEEP at 105400 Hz. Note that with an increase in the CI reaction time (and thus an increase in the number of ions in the ion trap) from (a) 3 msec to (b) 12 msec to (c) 30 msec that space charging developed.

Figure 3-C.10. *Variation of the* %RIC with the CAD tickle frequency for the PCI-CAD of the $(M+H)^+$ ion (m/z 167) of DEEP with a tickle voltage of 600 mV and (a) with no space charging present (corresponds to Figure 3-C.9a) and (b) with severe space-charging present (corresponds to Figure 3-C.9c). Note that the RIC = Σ(intensities of m/z 65, 93, 111, 139, and 167). The m/z's shown on the top indicate the frequencies calculated by the ITMS algorithms based upon quadrupole ion trap theory.

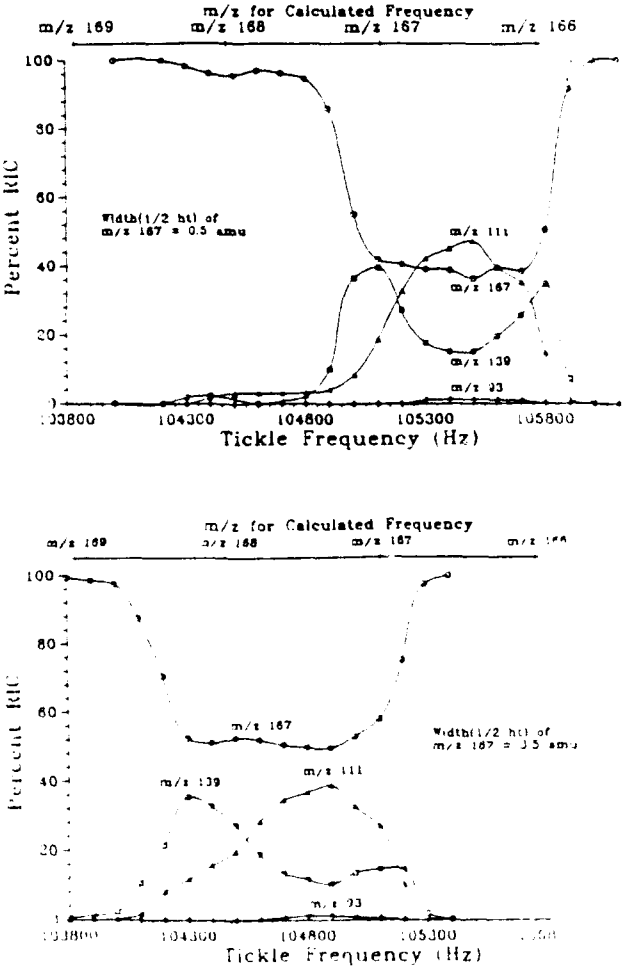

3-D. Evaluation of Sensitivity, Linear Dynamic Range and Limits of Detection

3-D.1. Evaluation of EI Normal MS Sensitivity and Linear Dynamic Range with Variable Ionization Time

The dynamic range of any device which converts analytes into charged particles (e.g., flame ionization detectors or mass spectrometers) will be limited by the onset of space charge. These space-charge effects lead to saturation of instrument response when the density of charged particles (ions) rises so high that ion-ion repulsions become significant. These effects are especially evident in devices which trap or store ions. In the ion trap, these effects are manifested when too large an analyte concentration leads to loss of mass resolution and degradation of mass spectral quality [e.g., self-chemical ionization to form $(M+1)^+$ ions].

The Finnigan MAT ion trap detector (ITD), as well as the ion trap mass spectrometer (ITMS), has a new Automatic Gain Control (AGC) which provides automatic variation of ionization time. This approach maximizes sensitivity for low levels of analyte, and prevents saturation of the ion trap at high levels of analyte. This AGC software has been evaluated and the results are impressive with full scan EI mass spectra are easily obtained at low picogram levels injected, while linear response is maintained up to low microgram levels.

Whereas the operation of the ion trap has traditionally used a fixed (1 msec) ionization time, the new approach automatically selects an ionization time from 0.078 ms to 25 ms (a range of 320) for each microscan, depending on the amount of analyte in the trap. For low levels (e.g., for baseline or small GC peaks) a maximum ionization time of 25 ms is selected, offering an improvement of approximately 25 times in sensitivity. As the amount of analyte increases, the ionization time is automatically decreased in order to prevent overfilling the trap with ions. The ion signals in each microscan are automatically scaled to correct for the variation in ionization time. The new scan function

compared with the normal scan function in Figure 3-D.1. A short "prescan", consisting of a 0.2 ms ionization provides an estimate of the number of ions formed in the trap. This value is then used to calculate the optimum ionization time for the actual mass scan which follows.

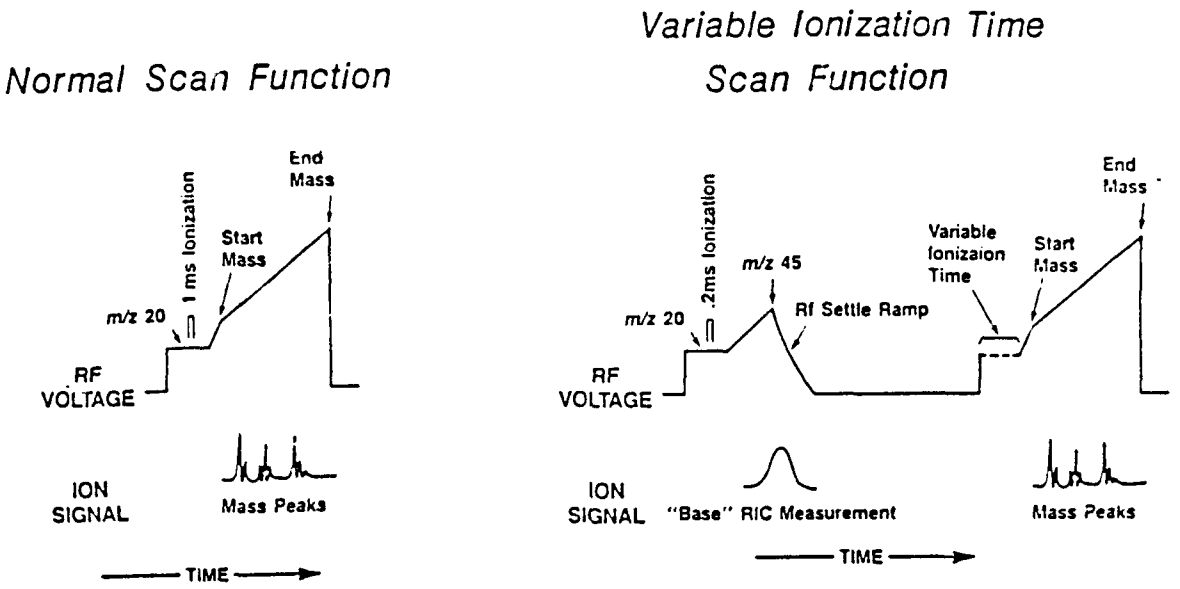

Figure 3-D.1. A new EI MS scan function with a variable ionization time compared with the normal EI MS scan function with a constant ionization time.

In order to evaluate this new approach, solutions of JP-10 jet fuel (tricyclodecane), methyl salicylate, n-decanol, dipropylene-glycol monomethyl ether, and bis-methoxy-ethyl ether were analyzed by GC/EI-MS (full scan) with the Finnigan ITD. Samples were analyzed with a 15 m x 0.32 mm ID, 0.25 μm film thickness, DB-5 fused silica open tubular column (programmed form 30 °C to 130 °C at 20 °C/min, 4.4 psig inlet pressure, 1 μL on-column injections), scanning from m/z 40 to 160. Standard solutions ranged upwards from 150 fg/μL. The chromatograms for a solvent blank and 15 pg of tricyclodecane are compared in Figure 3-D.2. The tricyclodecane peak at a retention time of 4:20 is clear at the 15 pg level in the reconstructed ion chromatogram (RIC), as well as in the

ion (m/z 67). The background-subtracted mass spectrum for the 15 pg GC peaks is shown in Figure 3-D.3a. This spectrum compares favorably with that obtained for 150 ng (10,000 time more analyte), shown in Figure 3-D.3b.

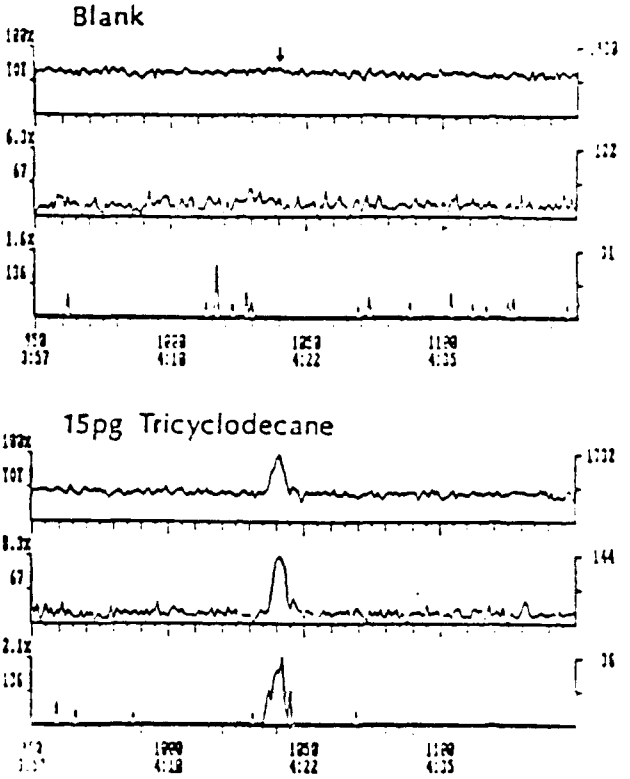

Figure 3-D.2. The GC/EI-MS chromatograms for a solvent blank and 15 pg of tricyclodecane.

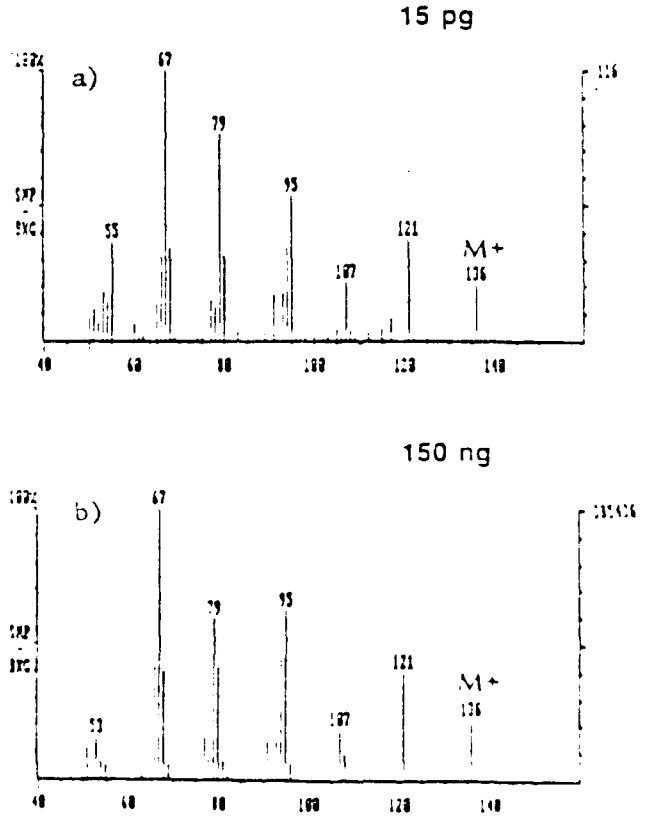

Figure 3-D.3. The background-subtracted mass spectra for (a) the 15 pg GC peak and (b) the 150 ng GC peak of tricyclodecane.

The clearest indication of the performance of this new approach is the linear dynamic range indicated in the calibration curves for tricyclodecane shown in Figure 3-D.4. Over 6 decades of concentration, the calibration curves for the RIC, m/z 67, and m/z 136 ($M^{+\cdot}$) show excellent agreement and linearity (slope of the log-log plots = 1.0). Similar results were observed for the other compounds studied.

In conclusion, this new operational mode provides the ITD with sensitivity and dynamic range which equal if not exceed those of any other GC/MS system. The use of relatively long ionization times offers high full-scan sensitivity for trace-level components in the low picogram range, while the automatic variation of ionization time provides linear response into the low microgram range, well above the upper limit of open-tubular-column GC capability.

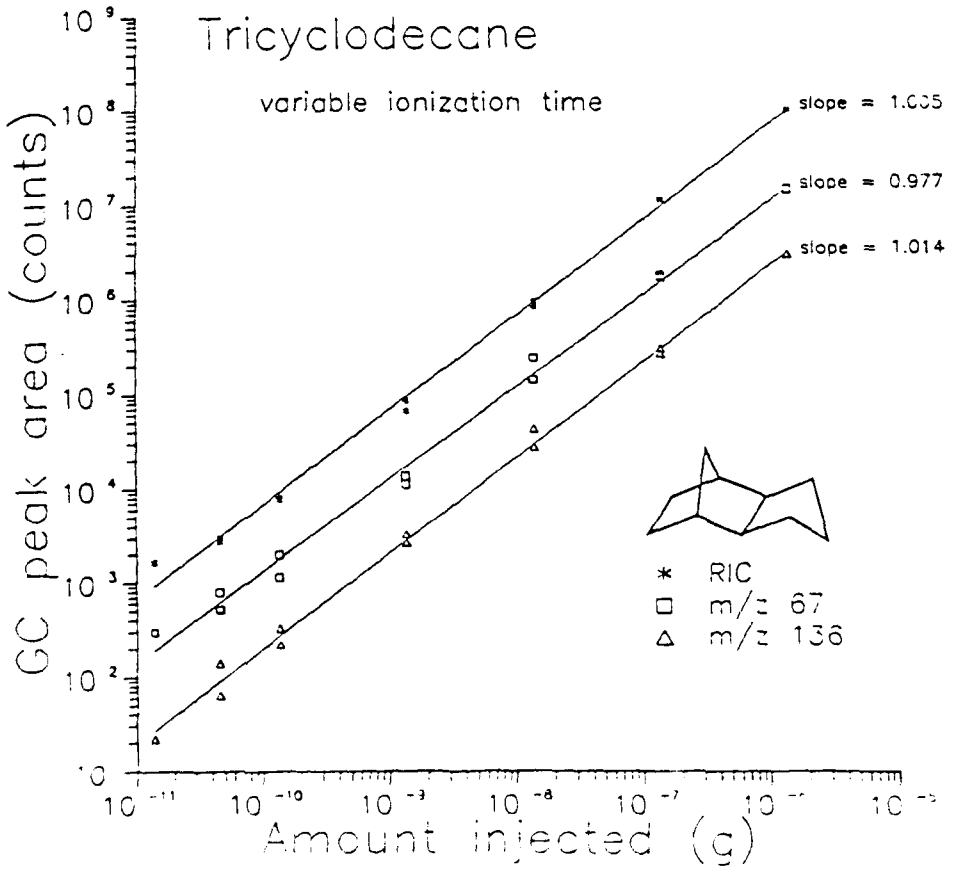

Figure 3-D.4. The GC/EI-MS calibration curves for tricyclodecane.

3-D.2. Variation of the Ionization Time for Extension of the Linear Dynamic Range with Methane PCI

We have just seen that GC/EI-MS with variable ionization time can yield a linear dynamic range covering 5 orders of magnitude from ca. 10 pg to 1 μg of tricyclodecane injected. However, as will be seen below, GC/MS/MS of diethyl-ethylphosphonate (DEEP) with methane positive chemical ionization (PCI) but with a **constant** ionization time (13 msec) exhibited a linear dynamic range of only 3 orders of magnitude from ca. 2 pg to 2 ng injected. The linear dynamic range in both cases was limited at the higher amounts by space charge effects due to excessive numbers of ions in the trap. To extend the linear dynamic range for higher amounts of analyte, the number of ions produced by the analyte would have to be reduced.

The PCI scan function of the ITMS differs from the EI scan function in having a time period for reaction of the EI-generated reagent ions with the neutral molecules (period B' of Figure 3-D.5). To change the number of analyte

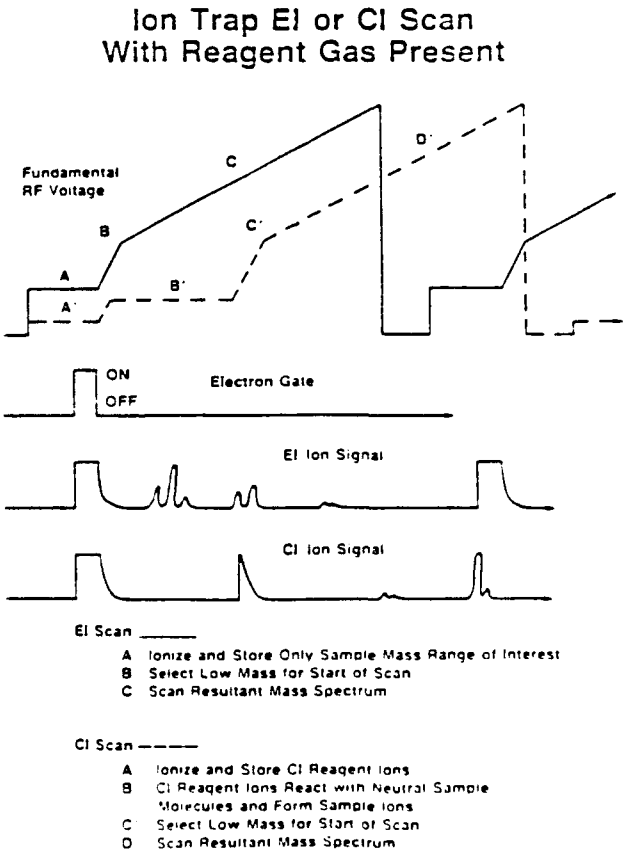

Figure 3-D.5. Comparison of the EI- and PCI-MS scan functions on the ITMS.

ions with the PCI scan function of the ITMS, two different time periods can be varied: (a) the actual electron ionization time (period A': when electrons are introduced into the ion trap to ionize the reagent gas and these initially formed ions react with the reagent gas to create CI reagent ions) and (b) the CI reaction period (period B': when the CI reagent ions react with neutral sample molecules to form sample ions). Here we evaluate the variation of the actual ionization time (period A') to extend the linear dynamic range of methane PCI-MS in the ITMS.

DEEP was introduced into the ITMS such that a constant level of DEEP was present in the ion trap and the ionization time was varied from 0.1 to 12.5 msec during the methane (ca. 7 X 10^{-5} torr) PCI normal MS scan function. The intensity the m/z 167 (the $(M+H)^+$ ion) ion of DEEP increased linearly with the ionization time between 0.1 and 1 msec (the dashed line of Figure 3-D.6).

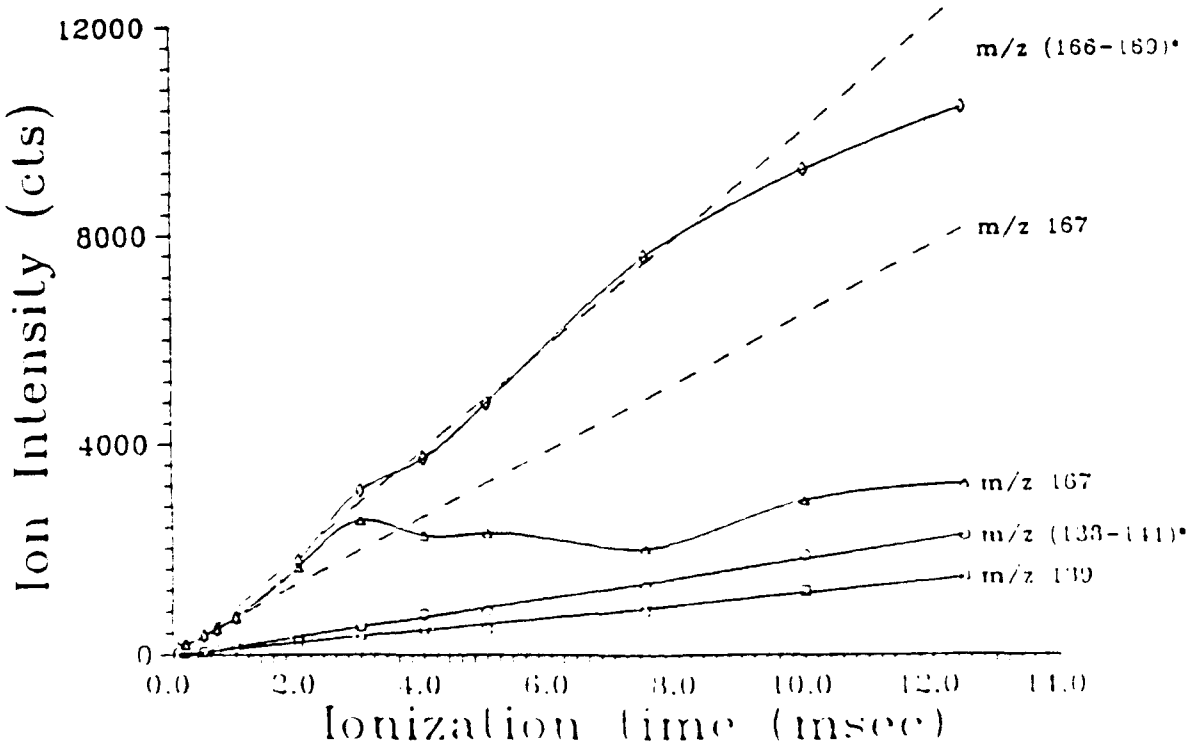

Figure 3-D.6. Effect of ionization time (0.1 to 12.5 msec) on the intensities of the methane PCI m/z 167 [$(M+H)^+$ ion] and m/z 139 ions of DEEP. *Note the m/z (166-167) and m/z (138-141) are integrated areas from these ions in the centroid spectra corrected for the ^{13}C contribution.

However, unlike for EI, when the ionization time was doubled with PCI, there was not a doubling of the analyte ions. Whereas with EI a change in the ionization time directly changes the number of ions of the analyte, with PCI the ionization time largely affects directly the reagent ion population which then changes the analyte ion population during the subsequent chemical ionization reactions. Increasing the ionization time past 1 msec resulted in an increased efficiency of chemical ionization as evidenced by the positive deviation of the intensity of the m/z 167 ion (the solid lines in Figure 3-D.6). This positive deviation may be due to the dependence of the efficiency of PCI upon the number of reagent ions present. Space charge effects begin to become significant for ionization times greater than 3 msec. These space charge effects lead to peak broadening and problems with the mass assignment algorithms (Figure 3-D.7). However, by integrating all the ions in the centroided spectra about the ions of interest

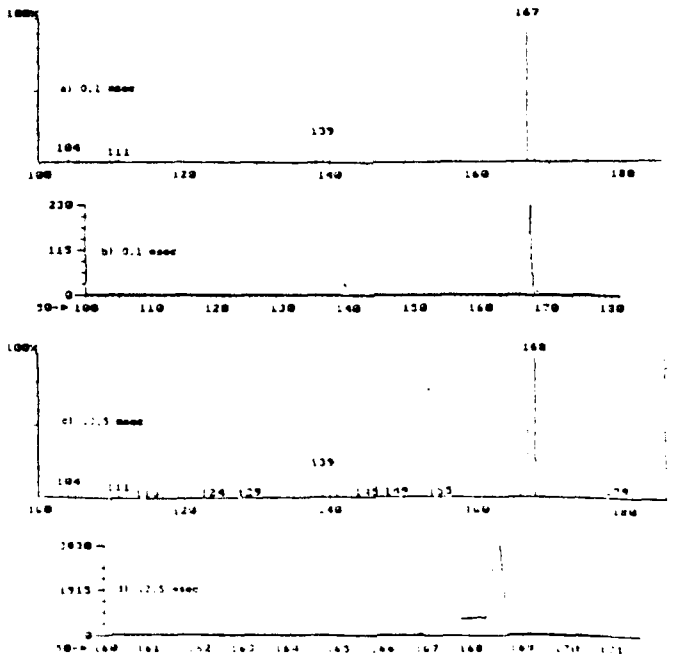

Figure 3-D.7. Centroided mass spectra (a and c) and profile mass spectra (b and d) for the PCI of DEEP with ionization times of 1 msec (a and b) and 12.5 msec (c and d).

(e.g. integrate m/z 166 to m/z 169 for m/z 167) and correcting for the ^{13}C contributions, one sees that, indeed, the total number of $(M+H)^+$ ions increase in a fairly linear fashion up to ca. 7.5 msec. Beyond 7.5 msec space charging becomes severe enough to cause inefficient trapping of ions (the negative deviation from the m/z (166-169) trace of Figure 3-D.6). It may be that some of the space charge effects are due to the large abundance of reagent ions which are present in the trap. Changes in the RF-levels and time periods of the CI scan function may lead to some improvement in this regard.

Note that unlike the intensity of the m/z 167 ion, the intensity of the m/z 139 ion increased linearly over the entire ionization time regime examined (Figure 3-D.6). The m/z 139 ion is a major fragment ion of DEEP produced during EI and perhaps PCI, as well. As its intensity increased linearly with ionization time, we attribute the majority of its formation to occur during the actual ionization period.

Based upon these preliminary results it may be possible to increase the linear dynamic range for PCI by at least an order of magnitude by varying the ionization time. However, PCI, due to its greater complexity as compared to EI, may not be as amenable to automatic control of the ionization time to increase the linear dynamic range as has been demonstrated for EI. Further experiments are planned to help us to better understand the capabilities and limitations of PCI in the ion trap and enable us to develop approaches to improve it.

3-D.3. Variation of the CI Reaction Time for Extension of the Linear Dynamic Range of Methane PCI

In Section 3-B.2, the effect of the CI reaction time (Period B' in Figure 3-D.5) on the methane PCI of DEEP was discussed. Briefly, two time periods could be distinguished by the reactions which were predominantly occurring during them: a reagent ionization period and a sample ionization period. The reagent ionization period (0.1 msec to approximately 25 msec) was dominated by the reactions which lead to the reagent ions themselves. Although the sample was also ionized during this period, there was only a relatively minor increase in the abundance of ions with an increase in CI reaction time. Thus, variation of the CI reaction time over this period would not have much effect on the abundance of sample ions. The sample ionization period (from approximately 25 msec to 185 msec) was characterized by CI reactions which led to the formation of $(M+H)^+$ ions of the sample. Whereas the intensity of the $(M+H)^+$ ion of DEEP increased only slowly up to 25 msec, after 25 msec the intensity of the $(M+H)^+$ ion increased rapidly with increasing reaction time (e.g. with an indicated methane pressure of 3.4×10^{-5} torr, the intensity of the m/z 167 ion increased by a factor of 8 with an increase in time from 25 to 160 msec (a factor of 6.4) of CI reaction time). Thus, the variation of the CI reaction time between 25 msec and 185 msec may offer a method to vary the abundance of the sample ions as was done for the EI AGC method discussed above. However, this preliminary data indicates that the increase in ion abundances is not as linear as would be desired. Further research is required before implementation of such a method would be feasible.

3-D.4. Quantitative Comparison of MS/MS on the ITMS and QQQ

In previous sections, the ITMS was shown to have efficiencies of fragmentation, collection, and mass analysis higher than those for a triple quadrupole instrument (QQQ). Therefore, it was expected that the ITMS would also have a higher MS/MS sensitivity than the QQQ. The quantitative comparison of the two MS/MS instruments was evaluated for the GC/MS/MS methane PCI-CAD of the $(M+H)^+$ ions of diisopropylmethylphosphonate (DIMP, MW 180) for the ITMS with full daughter scan and for the TSQ70 with selected reaction monitoring (SRM) and full daughter scan on the same day with the conditions given in Table 3-D.1.

Table 3-D.1. Experimental Conditions for GC/MS/MS Determination of DIMP Standards on a Triple Quadrupole (QQQ) and a Quadrupole Ion Trap (ITMS)

		<u>Mass Spectrometry</u>
Methane PCI	QQQ:	100 eV, 100 °C, 2 torr indicated
	ITMS:	100 °C, 3 X 10^{-5} torr indicated
		13 msec electron ionization time
		175 msec CI reaction time
CAD	QQQ:	1 mtorr argon, 30 eV
	ITMS:	ca. 1 mtorr helium, 800 mV
		15 msec CAD reaction time
		CAD RF of 50 amu
Daughter Ion Analysis	QQQ:	full scan: 50 → 225, 1 sec
		SRM of $181^+ \rightarrow 97^+$, 0.1 sec
	ITMS:	full scan: 50 → 225, 1 sec; 7 μscans
		<u>Gas Chromatography</u>
Column	QQQ:	30 m SE-54 FSOT
	ITMS:	28 m DB-5 FSOT
Inj. Port Temp.		250 °C
GC/MS Interface Temp.		250 °C
Column Temp. Program		50 °C (1 min, split and sweep closed)
		50 to 165 °C @ 30 °C/min
Sample Size		1.5 μL, splitless (methanol solvent)

Calibration curves obtained from the GC/MS/MS determination of DIMP in methanol standards are shown in Figure 3-D.8 for the ITMS with full scan (50 to 225 u in 1 sec, 7 μscans) and for the TSQ70 with selected reaction monitoring (SRM, $181^{+} \rightarrow 97^{+}$, 0.1 sec) and full scan (50 to 225 u in 1 sec). The limits of detection are approximately 2-6 pg of DIMP injected onto the GC column for both the QQQ SRM and for the ITMS. Whereas the TSQ70 was only able to obtain good, qualitative daughter spectra (without background subtraction) on approximately 1.5 ng DIMP injected (Figure 3-D.9), the ITMS was able to obtain very good daughter spectra on only 15 pg (Figure 3-D.10). Although the triple quadrupole yielded a linear dynamic range of 4 orders of magnitude with SRM, the QQQ full scan and ITMS full scan only exhibited a linear dynamic range of 3 orders of magnitude (it should be noted that the automatic gain control was not used in these studies). The linear dynamic range is limited at the upper range in the ITMS by space charge effects which result in broadened ion peaks, mass assignment problems, and apparent shifts in the secular frequencies of the parent ions (Figure 3-D.11). Integration of all the "ions" from m/z 90 to m/z 105 for the ITMS increase the linear dynamic range somewhat, but is not a desirable alternative. More attractive alternatives to overcoming this limitation are available, including variable ionization time, variable sample ionization time, and mass-selectively filling of the ion trap. Experiments are planned to further evaluate each of these alternatives.

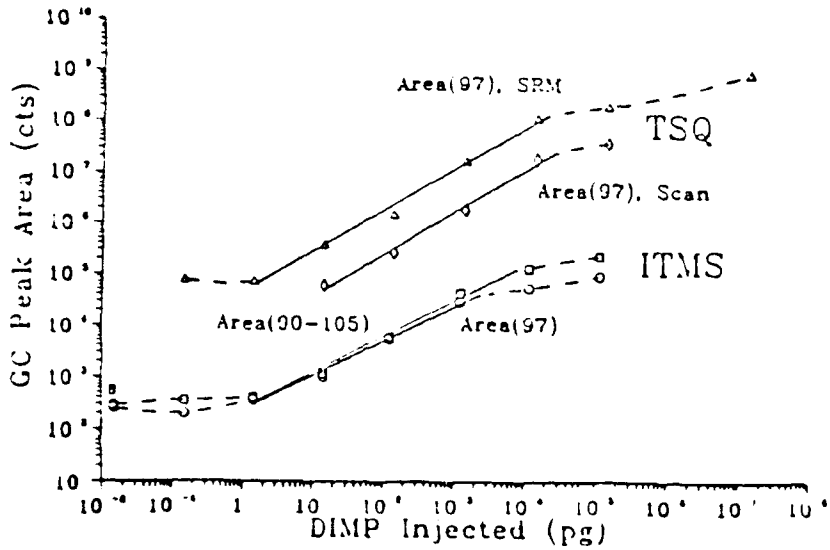

Figure 3-D.8. Calibration curves obtained for the GC/methane PCI-CAD of the $(M+H)^+$ ion (m/z 181) of DIMP.

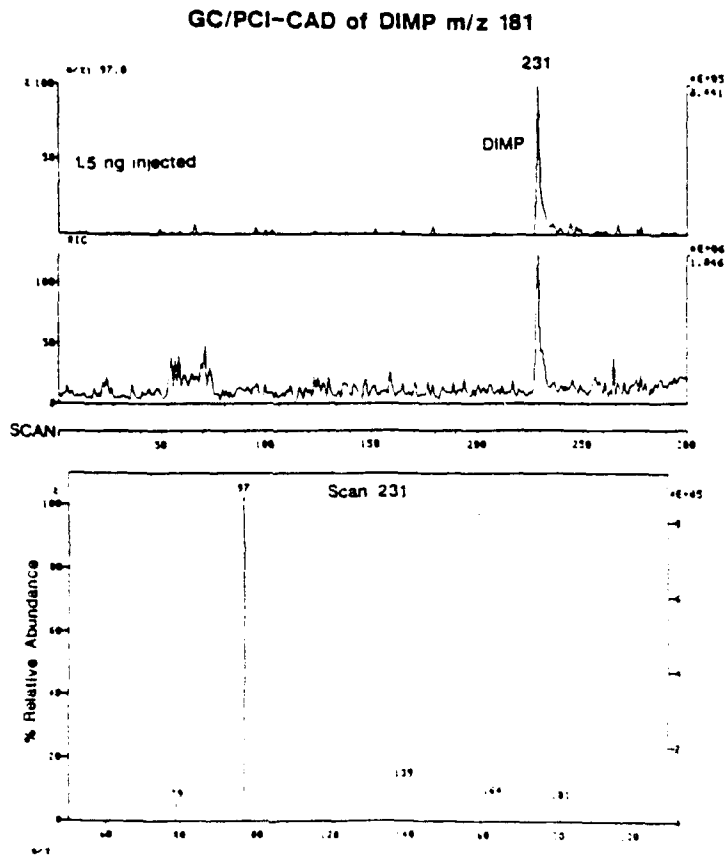

Figure 3-D.9. GC/PCI-CAD with full daughter scan determination of 1.5 ng of DIMP on the Finnigan TSQ70: (a) trace of m/z [illegible], (b) trace of RIC, and (c) daughter mass spectrum of $(M+H)^+$ of DIMP.

Figure 3-D.10. GC/PCI-CAD with full daughter scan determination of 15 pg of DIMP on the Finnigan MAT ITMS: (a) trace of m/z 97, (b) trace of RIC, and (c) daughter mass spectrum of the $(M+H)^+$ ion of DIMP. Note the presence of numerous ions above m/z 170 which are not present in the daughter spectrum obtained with the QQQ (Figure 3-D.9c); these ions were not ejected prior to obtaining the daughter spectra of m/z 181.

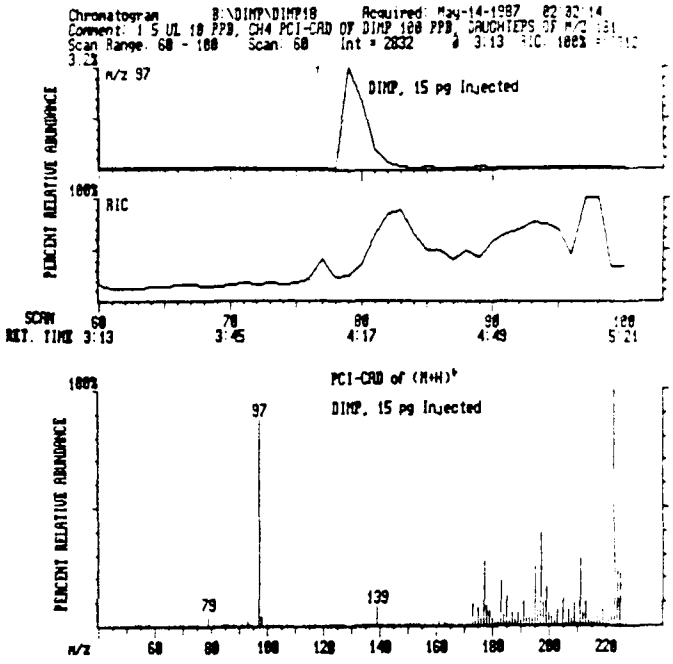

Figure 3-D.11. Centroid and profile daughter spectra of the $(M+H)^+$ ion (m/z 181) of DIMP obtained at the top of its GC peak for 150 ng injected. Note the broadening of the ion peak due to space charging. This leads to mass assignment problems in the centroiding algorithms.

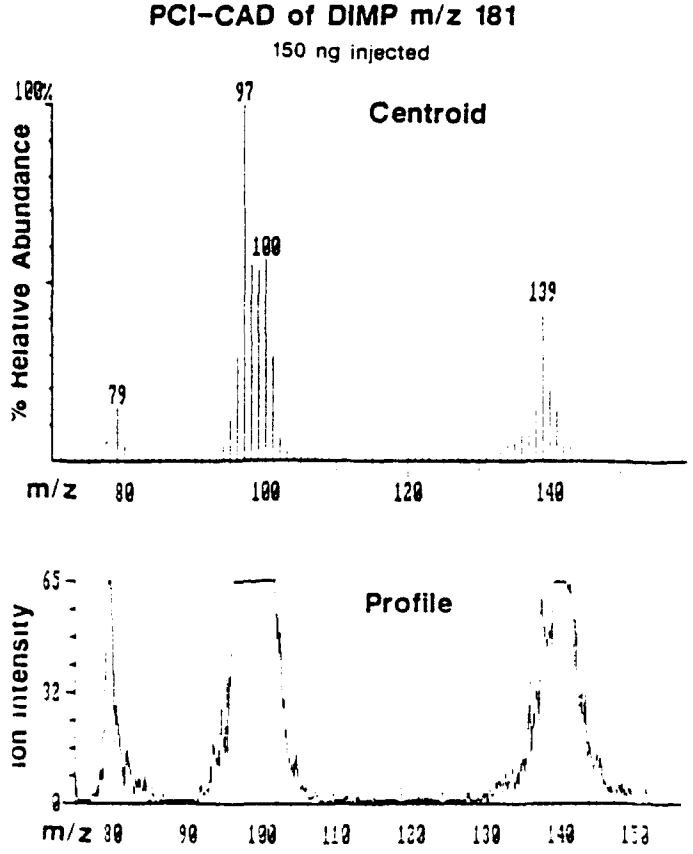

3-F. The ITMS as a Portable Tandem Mass Spectrometer for Environmental Monitoring

The task of monitoring for chemicals in the environment has been a major challenge for many years. The need to detect the presence of a large number of anticipated compounds at extremely low levels demands an extremely sensitive and versatile analytical system. However, in addition to monitoring for expected compounds, monitoring must also be performed for unexpected chemical pollutants. The need to detect and identify compounds whose presence was unanticipated necessitates a system capable of providing structural elucidation. Finally, the ability to discriminate against a wide range of possible interferents in the field imposes stringent requirements for selectivity. Tandem mass spectrometry is the most promising approach to meeting these needs. Such an analytical system can provide the sensitivity, selectivity, speed, and small size to detect, identify, and quantitate trace levels of chemical pollutants which may be encountered in environmental monitoring.

F-1. Analytical Requirements

The major analytical requirements for the monitoring of environmental pollutants are the same as those for any system for trace analysis: **sensitivity**, **selectivity**, and **speed**. In the case of monitoring for trace pollutants, high sensitivity is required for high detection probability; high selectivity is required for a low false positive rate, as well as interference rejection; and high speed permits fast response. It is informative to consider these characteristics in detail. In order to obtain a detectable signal for a trace amount of analyte, an analytical technique must have high **sensitivity**, defined by the slope of a calibration curve. Although sensitivity may be a useful figure of merit for "pure" analytes, it can become meaningless for the determination of analytes in increasingly complex mixtures. In the analysis of real-world

samples, interferences can arise from other chemical constituents of the mixture or the background and can be referred to as "chemical noise". The effectiveness of a trace analytical technique, therefore, may be determined not so much by its sensitivity, but by its ability to discern the signal of the analyte from the chemical noise, its **selectivity**. Thus, a more descriptive figure of merit for a trace analytical technique is the limit of detection, defined as the amount of analyte which will give a signal (S) which can be distinguished from the chemical noise (N) with the desired confidence (typically S/N = 3). The limit of detection thus takes into account both the sensitivity and selectivity (inversely related to the level of chemical noise) of an analytical technique. Finally, small **size** is a key requirement for an analytical system which needs to be quickly deployed and highly mobile.

F-2. Tandem Instrumental Methods

A powerful approach to increase the selectivity is the use of two or more analytical techniques in tandem. It has been shown that, as the number of stages of analysis is increased, the absolute levels of both signal and noise decrease; however, if the additional stages increase the selectivity of the technique, the chemical noise will decrease more rapidly than the signal (Figure 3-F.1). If the chemical noise dominates over the electrical noise (as is almost always the case in mass spectrometry), an overall improvement in the S/N ratio will result. As long as there is still a detectable signal above the electrical noise level, therefore, an increase in the number of tandem analytical stages will result in improved limits of detection.

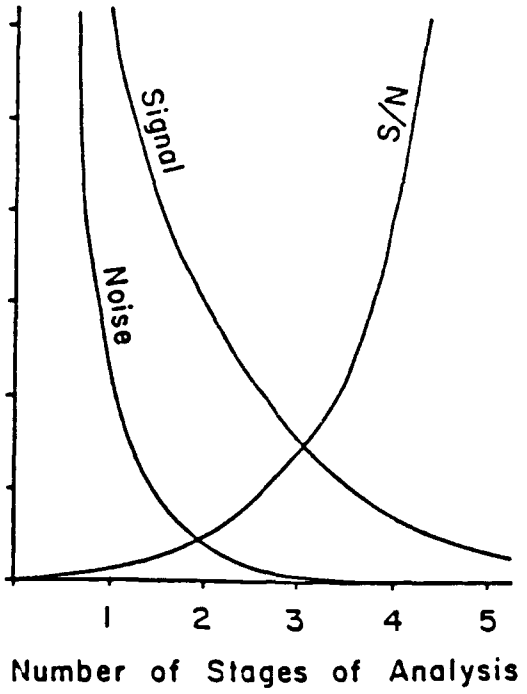

Figure 3-F.1. Effect on the signal (S), chemical noise (N), and the S/N ratio of increasing the number of stages of analysis used in tandem.

F-3. Tandem Mass Spectrometry (MS/MS)

Tandem mass spectrometry (MS/MS) is a relatively new method for rapid trace analysis of complex mixtures. Research in our laboratory with triple quadrupole tandem mass spectrometers has demonstrated the capabilities for the detection of targeted compounds at part-per-billion levels and below, in both environmental and physiological matrices. In MS/MS, the use of two stages of mass analysis provides an enormous increase in analytical selectivity. For a mixture component to interfere with the detection of the analyte, it must be ionized to form an ion (parent ion) of the same mass as the analyte, which then must undergo collisionally activated dissociation (CAD) to form a fragment ion (daughter ion) of the same mass as the daughter ion of the analyte.

The most common MS/MS operating modes of tandem mass spectrometers are daughter scan, parent scan, neutral loss scan, and selected reaction monitoring. The specific operational mode chosen for a particular analysis will depend on

the information desired. To screen for targeted compounds, selected reaction monitoring (SRM) is employed, in which the first mass analyzer is set (sequentially) to pass the parent ion of each compound while the second mass analyzer is set to pass a daughter ion characteristic of that compound. To screen for targeted classes of compounds, parent scans or neutral loss scans can be employed. To screen for all compounds which fragment upon CAD to form a characteristic daughter ion, a parent spectrum is obtained, in which the first mass analyzer is scanned over a specific mass range, while the second mass analyzer is set to pass the characteristic daughter ion. To screen for all compounds which fragment to lose a characteristic neutral upon CAD, a neutral loss spectrum is obtained, in which both mass analyzers are scanned, with a constant difference in mass. To confirm the identity of a compound indicated from one of these screening modes, the daughter scan mode can be used, setting the first mass analyzer to pass the suspect parent ion while scanning the second mass analyzer. The resulting daughter spectrum can be interpreted or compared with the library spectrum of an authentic standard for confirmation.

For monitoring environmental pollutants, a critical concept is the role of two operating modes: continuous monitoring for the presence of any targeted (or other) pollutants, followed by confirmation (identification and semiquantitative determination) of any positives. In MS/MS, this would involve rapid screening for targeted compounds (by SRM) and/or targeted compound classes (by neutral loss or parent scans); positives would be confirmed by obtaining complete daughter scans of suspect ions. The rapid selection, under computer control, of operational modes is clearly a key requirement of an MS/MS instrument for such an application.

F-4. ITMS Matching the Analytical Requirements: A Summary of the ITMS Research

A brief summary of the ITMS research will show that ITMS matches the analytical requirements of a sensitive and selective trace analytical instrument for the monitoring of environmental pollutants. A major advantage of the ITMS over more conventional mass spectrometers is its versatility. This is due to its capability to control via computer in real-time the various operational modes without any hardware changes. Thus, switching from electron ionization (EI) to positive chemical ionization (PCI) or from normal mass spectrometry to tandem mass spectrometry is easily implemented. The capability of selecting between EI and conventional methane (CH_5^+) PCI or H_3O^+ PCI was demonstrated (Section 3-B). Thus, the particular ionization which yields the highest selectivity and sensitivity for a particular analyte can be chosen. Although not demonstrated in this report, other workers at Oak Ridge National Laboratory and at Purdue University have demonstrated the capability of obtaining negative chemical ionization mass spectra. One major disadvantage of the ion trap had been the lack of compatibility of many of the ionizations which have been successfully implemented on more traditional mass spectrometers, such as fast atom bombardment, thermospray, and atmospheric pressure ionization. Fast atom bombardment and thermospray would be especially useful due to their ability to ionize relatively non-volatile compounds. This lack of compatibility of these ionizations has been due to the necessity to have the ionization process occur external to the ion trap and then inject the ions into the ion trap. The major difficulty has been the successful trapping of these injected ions. Recently, however, other workers at Purdue University have demonstrated the possibility of trapping ions which have been injected into the ion trap from an external ionization source. The results of their ongoing research and the research which we have started in laboratory in this area may enable the use of alternate

ionization methods (e.g. thermospray or fast atom bombardment) to extend the use of ITMS to the analysis of more non-volatile samples. These capabilities can be added to the ITMS with only minor modifications and additions to the electronics and software and not to the ion trap itself.

The most important capability of the ion trap, however, is its MS/MS capabilities (demonstrated in Sections 3-C and 3-D). Comparison of the ITMS to the more conventional triple quadrupole tandem mass spectrometer, demonstrated that the ITMS has high (80-90%) CAD efficiencies with an overall MS/MS efficiency approximately 30 times higher than that of the triple quadrupole. In addition, the quantitative studies showed that the ITMS was able to obtain complete daughter spectra on low pg amounts of analyte, 100 times lower than the amounts required for comparable spectra of the triple quadrupole (Section 3-D). Two very useful MS/MS scans which are used for screening for compound classes are the neutral loss and parent scans. These two scans are easily implemented on triple quadrupole instruments. However, the equivalent scan modes have yet to be demonstrated on the ITMS; currently, it is necessary to due successive daughter scan experiments and then extract the parent or neutral loss relationship from the data. We are currently investigating some new scan functions which may allow us to obtain "true" parent and neutral loss scans.

As a tandem-in-time tandem mass spectrometer, the ITMS offers the capability of performing more than two stages of mass analysis (i.e. MS/MS/MS/....). Although not demonstrated in this report, we and other have successfully demonstrated this capability. This is achieved via software control of the ion trap parameters as opposed to the tremendous hardware modification and additions which would be required to add just one additional stage of mass analysis for a conventional tandem-in-space tandem mass spectrometer (e.g. a triple quadrupole

instrument). This capability will greatly enhance the selectivity and structure elucidation capability of the ITMS.

The major limitation of the ITMS may be due to its limited dynamic range at higher concentration levels where space charge effects limit the performance of the ITMS (Section 3-C.6). With automatic control of the ionization time, the linear dynamic range could be extended over six orders of magnitude (from low pg to low μg) with EI-MS (Section 3-D.1). Similarly, control of the ionization and CI reaction time was demonstrated to offer the potential to extend the linear dynamic range by an order of magnitude for PCI (Sections 3-D.2 and 3-D.3, respectively). However, these results were obtained on "pure" components (i.e. a single compound or a mixture with the components separated via GC prior to their introduction into the ion trap) and not on the complex mixtures (e.g. raw urine) which are routinely and successfully analyzed without sample preparation on triple quadrupole instruments. The simultaneous ionization of the numerous components with the direct analysis of such mixtures is expected to greatly accentuate the space charging problem. However, we have recently added the capability to use direct current (DC) voltages in conjunction with RF voltages on the ion trap to isolate ions of a single m/z. This should substantially reduce the space charge problems as some initial research has indicated. As space charging is the result of the ionization process and not the CAD process, the use of DC and variable ionization and reaction times should allow extension of the linear dynamic range with MS/MS as well. We are continuing research in these areas.

The ion trap MS/MS instrument also offers a number of features which make it appealing for development as a miniature mass spectrometer for monitoring of CB agents. These features offer advantages in terms of miniaturization, modularity, analytical capability, and ease of computer integration. The

potential for miniaturization of a quadrupole ion trap tandem mass spectrometer is dramatically illustrated by the small size (6 cu. ft., 130 lbs) of the ion trap detector (ITD) for gas chromatography which is commercially available from Finnigan MAT. The addition of capabilities for MS/MS requires little if any increase in size. The tandem-in-time nature of the ion trap means that MS/MS does not require additional analyzers, unlike other MS/MS implementations. Furthermore, there is no requirement (even with chemical ionization [CI]) for two stages of (differential) pumping as is needed in conventional MS/MS instruments between the ion source and/or the collision cell and the mass analyzers. Indeed, there is no need for separate supplies of CI reagent gas and collision gas. A simple 90% helium/10% methane (or water) mixture can serve as buffer gas, reagent gas, and collision gas. It should be noted that a 5 lb lecture bottle of this gas mixture would last approximately a month at the normal operating pressures of the ITMS. Finally, there are no extra power supplies required for additional mass analyzers, collision cells, or ion lenses, because these components are not necessary, thereby reducing size, weight, and power requirements.

The use of the tandem-in-time MS/MS implementation offers maximum modularity and upgradability. Adding new features such as CI or MS/MS to the basic ion trap MS system requires only software and possibly electronics modifications, not changes of ion optics or vacuum system hardware. Similarly, such modifications do not significantly increase the size, weight, or power requirements of the system. Finally, the inherent simplicity of the hardware design and the resultant ease of automated control point toward straightforward modification for upgraded capabilities.

Our research presented in this report has indicated MS/MS capabilities of the ion trap which are extremely promising for rapid, sensitive, and selective

trace detection. In particular, evaluation of the sensitivity and dynamic range of the ion trap in the MS mode (using automatic control of the ionization time) and of the efficiency of the MS/MS mode suggest that the ion trap may well be the most sensitive MS/MS instrument ever. Finally, quadrupole ion trap tandem mass spectrometry offers ease of computer integration for automated control, testing, and decision-making. Optimization of instrumental sensitivity and resolution involves only electronic, not mechanical, adjustments. Alternating between operational modes (ionization type, ion polarity, MS/MS scan mode) can therefore be accomplished rapidly as the analytical results dictate. Similarly, testing of the instrumental performance (mass calibration, resolution, sensitivity) can be automated. MS/MS with the quadrupole ion trap offers an ideal opportunity for instrumental optimization, evolution of analytical protocols, and decision-making by artificial intelligence.

4. ATMOSPHERIC PRESSURE IONIZATION

Our research efforts in the design, development, and characterization of an atmospheric pressure ionization/tandem mass spectrometer (API/MS/MS) for direct atmospheric analysis are summarized below. A more detailed description is provided in the Appendix, which is drawn from the Ph.D. dissertation of one of the students supported on this project.

4-A. API Source Design and Development

One of the original purposes of this work was to design and develop a new atmospheric pressure ionization (API) source for a turbomolecularly-pumped triple stage quadrupole (TSQ) tandem mass spectrometer (MS/MS). This API source could be used to study API and direct atmospheric monitoring by mass spectrometry. To accomplish this, the work initially evaluated an API source which Finnigan developed as a GC-detector but never marketed. This API source was characterized on a Finnigan 4500 single quadrupole mass spectrometer. Even as a GC-detector, the Finnigan-developed source suffered from memory effects (because of a small source region) and severe clustering of ions with molecules in the supersonic jet expansion of the post-orifice region. Because of these effects, direct atmospheric monitoring with this source was essentially impossible.

Therefore, a new API source was designed, which would be compatible with a commercial turbomolecularly-pumped mass spectrometer, and which would reduce or eliminate the problems of clustering and memory effects. This source was at first developed to be compatible and interchangeable with the Finnigan 4500 mass spectrometer used to evaluate the Finnigan-developed API source; however, because of its design, this API source suffered from vacuum integrity problems. Even with these problems, ions were obtained with reduced, but not eliminated,

clustering. Because of this clustering effect, this source was not viable for use as a direct atmospheric monitor.

This API source was redesigned to be compatible and interchangeable with a state-of-the-art triple stage quadrupole (TSQ) tandem mass spectrometer (MS/MS), the Finnigan TSQ 70. The modifications included moving all junctions between parts of the source canister outside of the vacuum chamber of the mass spectrometer, thus reducing some of the vacuum integrity problems. A new interfacing flange was designed to mate the source with the mass spectrometer. This flange contained the diaphragm seat, which now became the only interface between the atmospheric pressure source region and the vacuum of the mass spectrometer, and allowed the orifice to be electrically floated. Replaceable diaphragms were obtained with laser-drilled orifices, and a diaphragm with a 70 μm diameter orifice was installed in the interface place. This interface flange maintained vacuum integrity to near theoretical levels calculated from fluid-flow theory.

Unfortunately, moving all source components outside of the vacuum chamber resulted in a greater distance between the orifice and the first quadrupole. An ion optical modeling program (SIMION) was employed to model the region between the orifice and the first quadrupole. Although the model, which the program utilized, did not take into consideration the inelastic collisions of ions in the supersonic jet expansion in the post-orifice region, it proved invaluable in the actual design of two lenses. These lenses increased the fraction of ions which were transmitted to the quadrupoles.

This new version of the API source employed a small tube near the orifice to provide a gas jet in the discharge region. This gas jet served to keep particulate matter away from the orifice (to prevent orifice clogging) and

reduced the amount of water vapor which entered the post-orifice region (to reduce clustering).

A new current-regulated power supply, which was adjustable between 0.5 and 4.5 μA with a discharge voltage between 3 and 4.8 kV, was developed that generated a stable corona discharge. Along with this power supply, a ±500 V low output impedance power supply was developed to electrically float the orifice. The ability to electrically float the orifice allowed for an increased sensitivity and a strong declustering capability by creating a potential difference between the orifice and the first conical lens. The combination of these effects provided the ability to minimize clustering with or without the gas jet. The gas jet still served, however, to prevent orifice clogging.

Direct atmospheric monitoring was accomplished for various common laboratory solvents by sampling vapors from the caps of the solvent bottles. The orifice and lens potentials could be tuned such that the molecular or pseudo-molecular ion was the predominant ion in the mass spectrum for each solvent (methanol being the only exception).

The API/MS/MS instrument was applied to differentiating a pair of solvents with the same molecular weight which generated pseudo-molecular ions of the same m/z value. MS/MS was used to fragment each of the pseudo-molecular ions and generate daughter spectra which were easily distinguishable.

Electrical floating of the orifice caused a larger spread in the kinetic energy of the ions generated. Clustering and fragmentation occurred simultaneously, which in true mixture analysis would make the interpretation of mass spectra more difficult. While the API source was shown to detect compounds directly in the atmosphere at the ppm concentration range (≈15 μg of methoxy benzaldehyde), the potential of the sensitivity of the API source remains to be evaluated.

4-B. Suggestions for Future Work

For the future development of this source, several components should be modified or replaced. Sciex has shown that varying the needle-to-orifice distance can affect the relative intensities of the ions produced. This may be useful for providing additional selectivity for the ionization process. Although the new corona discharge power supply has served to generate a stable corona discharge, the needle-to-orifice separation has been limited. For a given current, a larger needle-to-orifice distance requires a larger voltage from the power supply. The current power supply is limited to 5 kV. This has limited the needle-to-orifice separation to a few millimeters, and therefore it is proposed that a new discharge power supply be constructed based on a 10 kV power supply.

The vacuum system has proved inefficient in handling the large gas loads provided by the API source. When a normal gas load is put on the system, the forepump pressure (the pressure at the entrance to the mechanical pumps) is a few mTorr. With the API source installed, this pressure increases to approximately 400 mtorr. On the TSQ 70, one mechanical pump serves as the backing-pump for both turbomolecular vacuum pumps. For future work, the turbomolecular pump for the analyzer region should be provided with an independent backing-pump. This may allow for pressures closer to the theoretical value for the analyzer region and may allow the size of the orifice to be increased, increasing the sensitivity of the instrument.

The API source canister for this work was designed to allow flexibility in its configuration. Since the one-orifice system has been shown to perform adequately, a new, second-generation source canister should be built that has a larger diameter source region, is shorter, and provides micrometer control over the needle position. The walls of the original canister are approximately 0.5"

thick stainless steel. This makes the source heavy and cumbersome. Therefore, the canister should be built out of a lighter material such as aluminum, or the wall thickness should be reduced where possible.

To achieve total computer control of the API/MS/MS instrument, digital-to-analog (DAC) converters should be implemented to control the corona discharge current, the ±500 V orifice potential, and the potentials for the additional lenses that the API lens system has added to the mass spectrometer.

To sample gases, the sample must currently be brought near the entrance to the glass sampling tube. A larger capacity gas sampling fan should provide the ability to sample from greater distances.

Finally, the applications of API/MS/MS with this instrument should be extended. While this instrument has been applied to simple mixtures, it has not be applied to any "real" samples. With improvements listed above, the sensitivity of the instrument should be significantly increased. Also, this instrument has yet to be applied to samples which are more amenable to negative ionization.

The research presented in this report has demonstrated the ability to develop a functional API source for a commercial, turbomolecularly-pumped tandem mass spectrometer. The future research proposed here should prove this combination to be a viable method for the direct atmospheric monitoring of trace compounds.

(The reverse of this page is blank.)

APPENDIX

THE CHARACTERIZATION OF ATMOSPHERIC PRESSURE IONIZATION/TANDEM MASS SPECTROMETRY FOR DIRECT ATMOSPHERIC ANALYSIS

Drawn from a Ph.D. Dissertation
by
Kenneth Paul Matuszak
University of Florida
1988

Final Report

PORTABLE TANDEM MASS SPECTROMETRIC ANALYZER

From:

University of Florida
Department of Chemistry
Principal Investigator - Richard A. Yost
Gainesville, FL 32611

To:

Contract No. F08635-83-C-0136 Task Order no. 85-2
Air Force Engineering and Services Center
Environics Division
Technical Monitor - Howard Mayfield
HQ-AFESC/RDVS
Tyndall AFB, FL 32403-6001

TABLE OF CONTENTS

Abstract of Dissertation Presented to the Graduate School of the University of Florida in Partial Fulfillment of the Requirements for the Degree of Doctor of Philosophy

The Characterization of Atmospheric Pressure Ionization/Tandem Mass Spectrometry for Direct Atmospheric Analysis

by

Kenneth Paul Matuszak

April, 1988

Chairman: Richard A. Yost
Major Department: Chemistry

Atmospheric pressure ionization (API) has been shown to be very useful when combined with tandem mass spectrometry in performing direct atmospheric monitoring of trace compounds. The design and development of a new API source that has been developed to be compatible with a commercial tandem mass spectrometer (MS/MS) is presented. This API/MS/MS instrument has been used to study (1) direct atmospheric sampling by mass spectrometry, (2) the production of ions in the atmosphere, (3) the effects of supersonic expansion on the clustering of these ions with neutral species, (4) the effectiveness of declustering of these ions by collisional means, and (5) the ability to qualitatively identify atmospheric gases. These studies will serve to lay the groundwork for the development of an instrument capable of performing trace analysis while performing direct atmospheric monitoring.

This API source utilizes a corona discharge for the primary ionization of

the atmospheric molecules and an orifice system to selectively leak the ions into the mass analysis region. It has been constructed so that it is interchangeable with a standard electron ionization (EI)/chemical ionization (CI) source on a Finnigan-MAT TSQ 70 triple quadrupole tandem mass spectrometer. In developing this source, a program to model the ion optics (SIMION) has been used to aid in the design of the post-orifice lens configuration.

The design of this source is such that memory effects have been essentially eliminated and the clustering of ions with molecules in the post-orifice region has been significantly reduced. Samples that have been studied include a variety of laboratory solvents. These solvents have been injected into streams of pure nitrogen carrier gas and have been analyzed under direct atmospheric conditions by bringing the caps of the solvent bottles near the sampling region of the API source.

Recommendations are made for overcoming the limitations of the present API source design and lens system. These include the consideration of supersonic jet expansion theory to redesign the post-orifice lens system and additional modifications to the discharge needle system.

CHAPTER 1

INTRODUCTION

The purpose of this work is twofold: first to design, construct, and develop, a new atmospheric pressure ionization (API) source for a turbomolecularly-pumped triple stage quadrupole (TSQ) tandem mass spectrometer (MS/MS), and second, to characterize and apply this new source to study (1) direct atmospheric sampling by mass spectrometry, (2) the production of ions in the atmosphere, (3) the effects of supersonic expansion on the clustering of these ions with neutral species, (4) the effectiveness of declustering of these ions by collisional means, and (5) the ability to qualitatively identify atmospheric gases. These studies will serve to lay the groundwork for the development of an instrument capable of performing trace analysis while performing direct atmospheric monitoring. Such an instrument could be used as an airport "sniffer" for drugs and explosives, or as an on-line vapor detector in the microchip, incineration, or chemical production industries. The major use of such an instrument, however, is anticipated as an environmental monitor for chemical waste spills and chemical dump sites or other forms of environmental contamination.

Analytical Scenario

Because this API source is interchangeable with the standard electron ionization (EI)/chemical ionization (CI) source for a

commercial tandem mass spectrometer, one such use would be as a preliminary pollution detection device, that is, to use this instrument to perform direct atmospheric analysis, sampling at various locations, and determining possible contamination of the air at each area of analysis. Thus, the instrument in that configuration would be able to perform preliminary identification of the pollutants present, as well as quantitation to determine the extent of the contamination. Once a site of contamination was found, the API source could be interchanged with the standard EI/CI source and the instrument in this configuration could be used to analyze soil and water samples in the surrounding area with ionization techniques which are already established and standardized for these two forms of sample matter. In this way, the extent of contamination could be mapped out in the full environmental scheme of air, water, and soil.

Overview of API/MS

Background and History of API/MS

To perform the analysis of atmospheric gases by mass spectrometry there are two basic approaches. Because a mass spectrometer operates under high vacuum, in the case of a quadrupole instrument at 10^{-5} to 10^{-7} torr, the pressure of the atmospheric sample must be vastly reduced. The first approach (Figure 1.1) is to bleed the atmospheric sample through an orifice or membrane and use high-vacuum pumps to reduce the pressure to that typically used in the ionization region for normal mass spectrometry. Unfortunately, while doing this, most of the

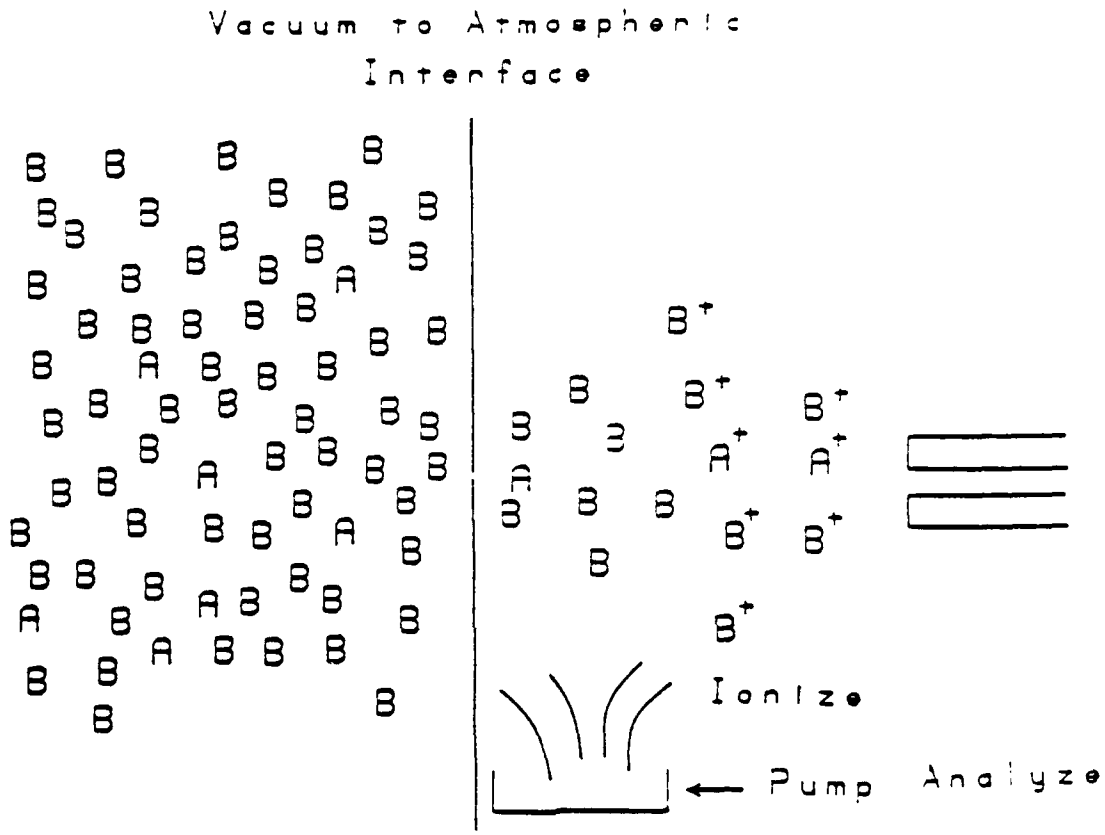

Figure 1.1

An atmospheric sampling methodology in which gas is reduced to normal mass spectrometric pressures and then ionized.

analyte is pumped away with the excess gas. For trace analysis this is obviously undesirable.

The second method (Figure 1.2) is to somehow ionize the analyte at atmospheric pressure and focus the ions through a small orifice into the mass analysis region by means of electrostatic fields, while pumping away the excess gas.

API is a unique ionization technique for mass spectrometry. Ionization occurs outside of the mass analysis (high vacuum) region of the mass spectrometer and the ions are permitted to enter the high vacuum region, usually via a sub-millimeter orifice in a thin diaphragm.

Molecules in an atmospheric pressure gas can be ionized by passing high energy electrons through the gas allowing, the gas molecules to collide with these electrons. This ionization process can produce both positive and negative ions. Positive ions are formed when an electron (e^-) collides with a gaseous molecule (G) and causes a second electron to be ejected, as in Equation 1.1.

$$G + e^- \rightarrow G^+ + 2e^- \qquad (1.1)$$

Negative ions are generated when a low energy (near thermal) electron is absorbed by a molecule of the gas, as in Equation 1.2. This is called electron capture ionization.

$$G + e_{th}^- \rightarrow G^- \qquad (1.2)$$

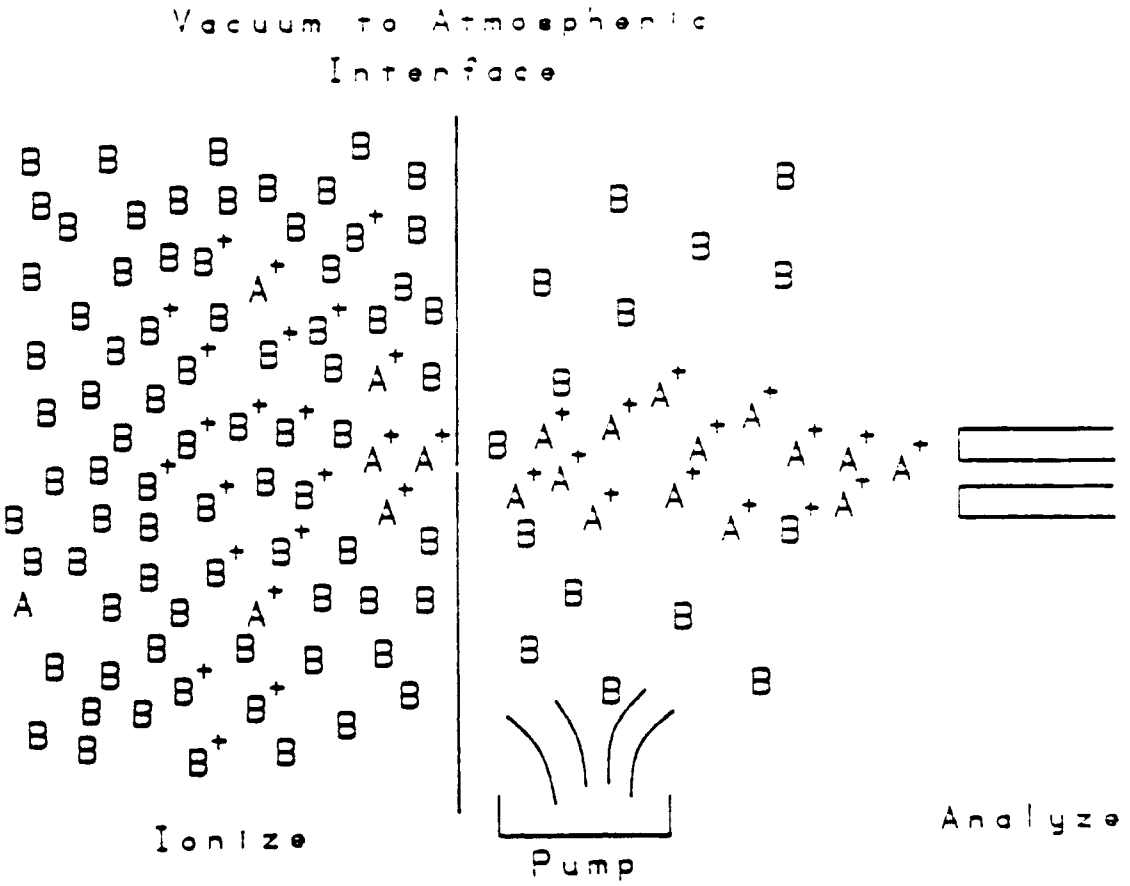

Figure 1.2

An atmospheric sampling methodology in which sample is ionized, sample ions are focused by electrostatic fields into mass analyzer, and gas is pumped away.

These ions can further react with background molecular species to form background reagent ions. In the case of direct atmospheric analysis, positive ions are formed when N_2 and H_2O molecules in the air react with the high energy electrons (Equations 1.3 and 1.4).

$$N_2 + e^- \rightarrow N_2^+ + 2e^- \quad (1.3)$$

$$H_2O + e^- \rightarrow H_2O^+ + 2e^- \quad (1.4)$$

These ions can further react by charge exchange and proton transfer reactions through collisions with other background molecules (Equations 1.5 and 1.6) to form reagent ions.

$$N_2^+ + H_2O \rightarrow N_2 + H_2O^+ \quad (1.5)$$

$$H_2O^+ + H_2O \rightarrow H_3O^+ + HO \quad (1.6)$$

Sample molecules (M) can react with these reagent ions by proton transfer or charge exchange to form molecular (M^+) or pseudo-molecular ($M+H^+$) ions (Equations 1.7 and 1.8).

$$M + H_2O^+ \rightarrow M^+ + H_2O \quad (1.7)$$

$$M + H_3O^+ \rightarrow M+H^+ + H_2O \quad (1.8)$$

Ion clusters can also be formed when ions associate with neutral species before the orifice or in the supersonic expansion in the post-orifice region. Low molecular weight molecules readily form clusters with ionized species. Thus sample and hydronium ions may cluster with either sample or water molecules (Equations 1.9-1.12).

$$M^+ + M \rightarrow M_2^+ \quad (1.9)$$

$$M^+ + H_2O \rightarrow M{+}H_2O^+ \quad (1.10)$$

$$M{+}H^+ + H_2O \rightarrow M{+}H_3O^+ \quad (1.11)$$

$$H_3O^+ + H_2O \rightarrow H(H_2O)_2^+ \quad (1.12)$$

In the preliminary studies with a commercially developed [1] but never marketed API source in an attempt to perform direct atmospheric monitoring, as many as 20 water molecules have been observed to cluster with a hydronium ion (Equation 1.13) to form a distribution of water cluster ions (Figure 1.3).

$$H_3O^+ + nH_2O \rightarrow H(H_2O)_{n+1}^+ \quad \text{where } n = 1\text{-}20 \quad (1.13)$$

At atmospheric pressure, molecules will undergo multiple collisions and those with the highest proton affinity (for positive ions) or highest electron affinity (for negative ions) will quickly become ionized by means of charge or proton transfer with the ions from the bulk gas. Because this is a collisional energy transfer, API is a low energy process and therefore little fragmentation of the molecular analyte ion will occur. Also, due to the multiple collisions, chemical and thermal equilibria will be established in the gas and thus there should be nearly a 100% ionization efficiency for analyte molecules that possess these characteristics. These factors should lead to a very high sensitivity. High selectivity is also obtained for certain classes of compounds because of this non-democratic process.

Sampling of Ions Formed at Atmospheric Pressure

Some of the earliest cases of performing mass spectrometric analyses upon ions formed at atmospheric pressure were performed by

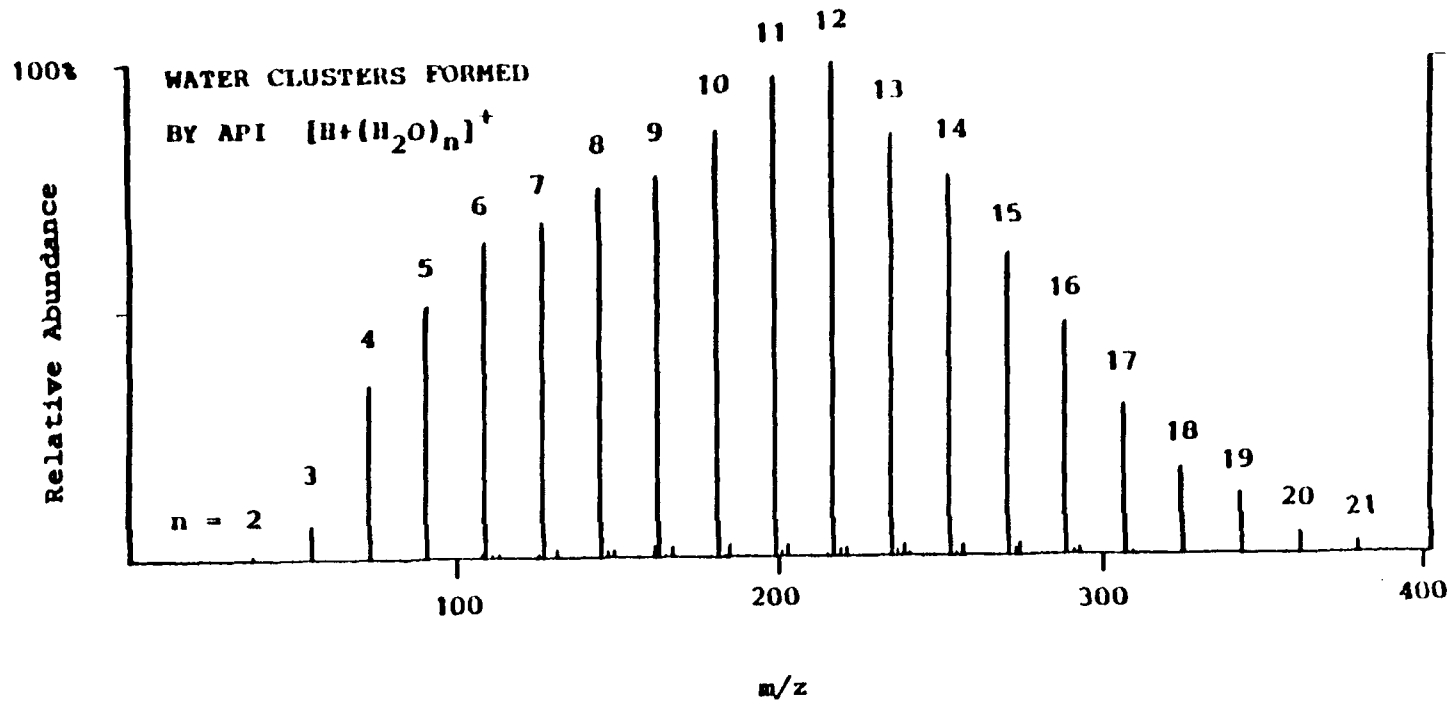

Figure 1.3

Mass spectrum of water cluster ions produced while performing direct atmospheric monitoring with Finnigan-MAT API source.

Knewstubb and Sudgen [2-5]. They used a 50 μm sampling orifice in a thin platinum foil attached to a water-cooled block, sampling ions produced in an atmospheric flame, to study the combustion chemistry of flames. Their system utilized three stages of differential pumping to reduce the pressure from atmospheric down to less than 10^{-6} torr in the analyzer region of their magnetic deflection mass spectrometer.

Kebarle and co-workers [6-8] used α-particle radiation to study the chemistry of the ionization processes for "spectroscopically pure" gases near atmospheric pressure. Their system utilized a 75 μm orifice to sample ions from these pure gases into a differentially pumped magnetic deflection mass spectrometer at pressures less than 10^{-6} torr, a similar instrument to that used by Knewstubb and Sudgen. They found that the spectra from the gases were dominated by ions from trace impurities in the gases, especially from water. Kebarle [9] used these findings to study the kinetics of the ionization process and the production of water cluster ions, of the form $(H_2O)_nH^+$, formed in the post-orifice adiabatic expansion from the atmospheric pressure source to the high vacuum of the mass spectrometer.

At about the same time, Shahin [10] developed a system for the mass spectrometric study of corona discharges in air at atmospheric pressures. Ion products were sampled using a 15 μm aperture into a differentially pumped region. This analyzer region (a quadrupole mass analyzer) was maintained at about 1×10^{-5} torr. The major positive ions that he observed were $(H_2O)_nH^+$ and $(H_2O)_nNO^+$ clusters in wet nitrogen. He also found that $(H_2O)_nH^+$ could be dissociated to H_3O^+ by collisional means in the post-orifice region by increasing the pressure and accelerating the ions through that region.

Analytical API/MS

Two excellent articles [11-12] review in detail the history of API/MS and the currently available API/MS technology. Because API is a "soft" ionization technique, the major positive ions formed and detected with mass spectrometry are the molecular ($(M)^+$), pseudo-molecular ($(M+H)^+$), and cluster ($(M_X)^+$, $(M_X+H)^+$, or $[M(H_2O)_X+H]^+$) ions. In the API source chemical and thermal equilibria are established owing to the large number of collisions occurring at atmospheric pressure. This leads to a nearly 100% ionization efficiency for compounds with either high proton or electron affinities [11]. The absolute ionization efficiency for a normal EI source is approximately 1 ion for every 10^4 molecules and a CI source may be 10 or 100 times greater than this [11]. Therefore an API source has a great potential as a very sensitive ionization source.

Many researchers have taken advantage of this and used API sources in conjunction with gas chromatography (GC), liquid chromatography (LC), and supercritical fluid chromatography (SFC). In a series of articles [13-15], Horning, et al., reported the development of an API/MS system for analysis of GC effluents. In 1973 they demonstrated the detection of 20 ng of nicotine, 20 ng of cocaine, 30 ng of methadone, and 500 ng of caffeine in 1 μL of chloroform by GC/API/MS using negative ions. Also analyzed were barbiturates, extracted from urine, in the 3-5 μg/mL concentration range. Mitchum et al. [16-17] used an Extranuclear API/MS instrument to detect 60 pg of 2,3,7,8-tetrachlorodibenzo-p-dioxin (TCDD) and 2,4,5-trichlorophenoxyacetic acid (20 ppm in 3 μL of whole blood and 30 ppb in urine and feces samples) with capillary column GC as the sample introduction method.

Tsuchiya and Taira [18], Carroll et al. [19], Scott et al. [20], and Arpino et al. [21] have all developed LC/API/MS systems and applied them to a variety of sample types.

Because of the design of the sources described above, cleanliness of the source and instrument was extremely important. Source regions for these instruments were characteristically very small (<1 cm^3) and this lead to contamination and memory effects. These sources also suffered from orifice clogging and clustering problems and these two problems would have been even more evident if these sources had been used as direct atmospheric monitors.

While performing direct atmospheric analyses, the low energy API method is likely to produce ions of the same mass-to-charge (m/z) values from components of the same molecular weight. In order to distinguish two such compounds it is therefore necessary to look at fragments of these compounds. However, if fragmentation is caused without first isolating the ion of interest, it would be impossible to tell which ions were fragments or merely ions formed from other compounds. Thus, to perform direct atmospheric analysis with an API source, a separation step is needed before mass analysis.

API/Tandem Mass Spectrometry

Much work has been performed showing that a mass spectrometer can be used as a mass separation technique followed by a second mass spectrometer for sample analysis [22]. Presently, only three examples have been reported of API sources being installed on tandem mass spectrometers, all triple stage quadrupole instruments. Caldecourt, Zackett, and Tou [23] constructed their own mass spectrometer and API source to analyze vapors from manufacturing processes. Extrel

Corporation [24] has reported installing its commercially available API source on a tandem mass spectrometer but as of this writing that system is not commercially available.

Sciex Inc. [25] has developed a API/MS/MS system with liquid helium cryogenic pumping. This API system has seen the most analytical usage of any system to date, although conventional mass spectrometric ionization techniques cannot be used with this mass spectrometer. This instrument has been shown by Bruins et al. to be applicable to LC [26-27] by means of an "ion spray" interface for the analysis of sulfonated azo dyes and to SFC [28] for the analysis of anabolic steroids at the 20-30 ppb concentration level. Snyder et al. have used the Sciex API/MS/MS instrument with a pyrolysis probe to analyze various pharmaceuticals in commercial polymer matrices [29]. The mobile Sciex TAGA 6000 has been applied to dioxin analysis [30] and for the detection of explosives and drugs in airports [31].

While the Sciex instrument has seen a wide spectrum of use, most of the analyses performed with it can be more easily performed with conventional, standardized methods utilizing EI/CI ionization. Its true advantage is its API source. However, because of the liquid helium cryopumping vacuum system, this instrument cannot be operated near any appreciable levels of hydrogen or helium gas, as the vacuum system has essentially no pumping speed for those gases.

One other tandem mass spectrometer system for direct atmospheric analysis that needs to be addressed is that built by Glish et al. at Oak Ridge National Laboratories [32]. This instrument uses an atmospheric sampling ionization (ASI) source in which glow discharge ionization occurs at sub-atmospheric pressures (0.1 to 1 torr), and a

tandem quadrupole/time-of-flight mass spectrometer for analysis. This source has been used to analyze the head space vapor of drinking water with 150 ppm trichloroethylene, and the head space vapor over trinitrotoluene (saturated head space vapor concentration for trinitrotoluene is approximately 6 ppb).

Overview of Thesis Organization

This thesis is divided into 5 chapters. This introductory chapter provides background material on atmospheric pressure ionization (API) and its marriage with mass spectrometry (MS) to help the reader understand the research described in succeeding chapters.

Chapter 2 describes the design of the API source which has been constructed for this work and its interfacing to two different mass spectrometers. Problems and characteristics of other early API sources are described to emphasize some of the features of this source.

The third chapter describes experimental results obtained during the development of the API/MS/MS instrument and the use of these results to guide the development of the API source to its final form. Included in this chapter are descriptions of computerized ion optic modeling which was used to help in source development and as an aid in gaining an understanding into some of the results that were obtained.

A description of the analytical performance of the API/MS/MS instrument as a direct atmospheric monitor can be found in Chapter 4.

The final chapter includes conclusions drawn from this work as to the potential for this API/MS/MS instrument to analytically perform

direct atmospheric analyses and proposes future work that should help attain that goal.

CHAPTER 2

DESIGN OF THE API SOURCE

In designing a new ion source of any type for a mass spectrometer, the design of the mass spectrometer and its component parts must be taken into consideration. The API source for this work was developed and modified to work with two different mass spectrometers.

Overall System Design

Even though the API source for this work was eventually modified to be compatible with a Finnigan-MAT TSQ 70 triple-stage quadrupole tandem mass spectrometer, at the inception of this work that instrument was itself, still in the design stages. Initial source design work was therefore performed on a Finnigan-MAT 4500 single quadrupole mass spectrometer with the goal of obtaining a functional API source that could later be adapted to the specifications of the mass spectrometer at hand.

Early attempts at developing API sources for performing direct atmospheric analyses suffered from many problems, not the least of which were severe memory effects from previously analyzed samples, clogging of the orifice, and clustering of the sample ions with neutral molecules of the bulk gas [11]. Stringent cleaning procedures were

required to clean these sources, including electropolishing of stainless steel surfaces, boiling in deionized water, washing with acetone or methanol, and baking at temperatures greater than 350 C. Indeed, an API source developed (but never marketed) by Finnigan [1] that generated the water cluster spectrum in Chapter 1 (Figure 1.3), demonstrated many of these problems. Figure 2.1 is a schematic drawing of this source, which is similar in design to many of the early API sources. The characteristics of this source include a small ion source region (approximately 0.25 cm^3 in volume), a discharge needle as the high energy electron supply, adjustable needle-to-orifice distance, sample inlet and outlet made out of 1/16" stainless steel tubing, and a single orifice interface between the atmospheric and vacuum regions. During operation the source was heated to ca. 200 C, in order to reduce memory effects. As can be surmised from viewing Figure 1.3, this source had little use as a direct atmospheric monitor because of the severe clustering problems. To be fair, this source was developed as a GC-detector and not an atmospheric monitor, but even as a GC-detector it suffered from memory effects (because of the small source region).

The goals of the development aspect of this work were to develop an API source that would be able to perform real-time atmospheric monitoring, minimize memory and interference effects, minimize the amount of clustering, and achieve a high sensitivity for compounds of interest.

Both the Finnigan-MAT [1] 4500 quadrupole and TSQ 70 triple quadrupole mass spectrometers utilize differential pumping (two 330 L/s turbomolecular pumps) to evacuate the separate ion source and analyzer

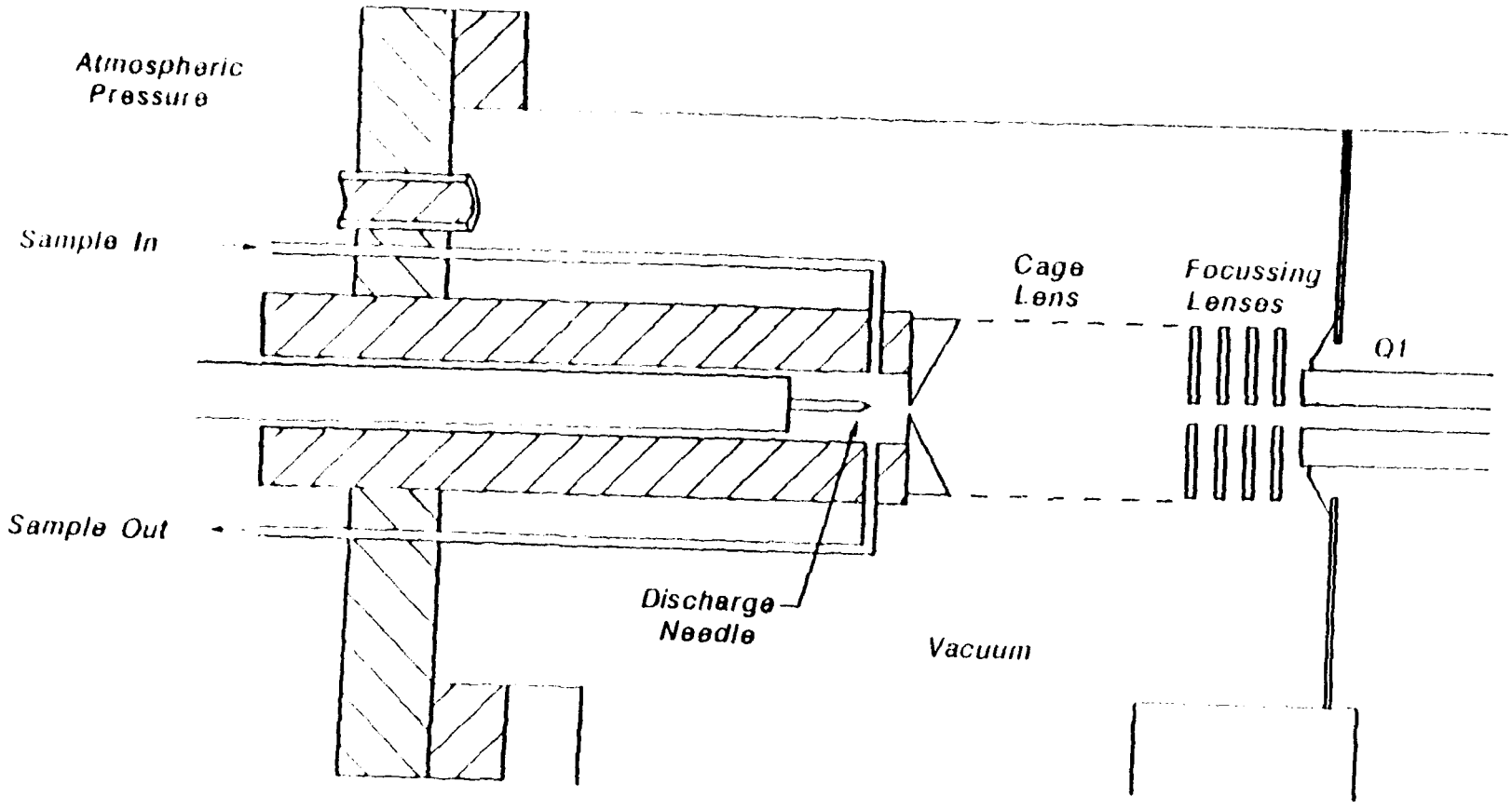

Figure 2.1

Schematic representation of experimental API source developed by Finnigan for a Finnigan 4500 quadrupole mass spectrometer.

regions. Because these instruments are pumped differentially, a much lower vacuum pumping speed is required (to maintain the analyzer regions at a sufficiently low pressure so that the performance of the analyzer is not degraded) than for a mass spectrometer which is pumped by normal means. These pumping speeds are significantly lower than those used by previously developed API/MS/MS instruments. Sciex has reported extremely high pumping speeds (as high as 60,000 L/s) [25] for its cryogenically pumped instrument. These pumping speeds allow for a much larger orifice diameter (>100 μm) than previously developed instruments (<20 μm) [33]. Sciex also claims that the large pumping speeds allow for a very quick, large drop in the pressure after the orifice to avoid the gas dynamics problem of shock waves at the end of the supersonic expansion of the gas in this region [34]. However, the differential pumping of the Finnigan instruments also allows for larger orifice diameters, on the order of 70 μm for this design. And since each of the two Finnigan instruments has easily interchangeable ion sources and lens assemblies, the potential for developing an interchangeable API source for these instruments was good.

Initial Source Design

Initial source design efforts began by developing an API source that was compatible with a Finnigan-MAT 4500 single quadrupole mass spectrometer while waiting for the new TSQ 70 tandem mass spectrometer. In order to make the API source compatible and interchangeable with the Finnigan EI/CI ion source assembly, it was built into a standard 6"

stainless steel conflat flange. The Finnigan EI/CI ion source assembly was mounted onto a similar flange, with associated electrical and gas feedthroughs also mounted in this flange.

In order to reduce the interference and sample memory effects, it was necessary to start with a much larger internal volume for the ionization region (Figure 2.2(a)) than used by the Finnigan API source. To minimize the number of lenses needed for focussing the ions from the orifice to the quadrupole entrance, it was desirable to have the orifice as close as possible to the pre-quadrupole focussing lenses. Because the distance between the face of the flange on the front of the instrument and the entrance to the quadrupoles was greater than 6", the API source canister was designed to be inserted through this flange, held in place by an o-ring. This limited the outside diameter of the flange to less than 3.7", which defined the inside diameter to be approximately 2.6", a significant increase over the 0.5" diameter source region of the old Finnigan API source.

The next step in designing a source for direct atmospheric monitoring was to develop a system to efficiently draw sample air into the source, past the discharge region, and then out of the source again. This was accomplished by drawing sample air through concentric glass tubes (Figure 2.2(b)), past the discharge region, and out a side port attached to the source canister, by means of a common laboratory blower fan that was modified to draw in sample air (≈100 mL/min) instead of blowing it out. The inner of the two concentric glass tubes can be removed for cleaning when necessary.

Figure 2.2

Development of an API source for direct atmospheric monitoring with (a) a large source region, (b) inlet system of concentric glass tubes, (c) corona discharge ionizer, (d) orifice system and associated electrostatic lenses.

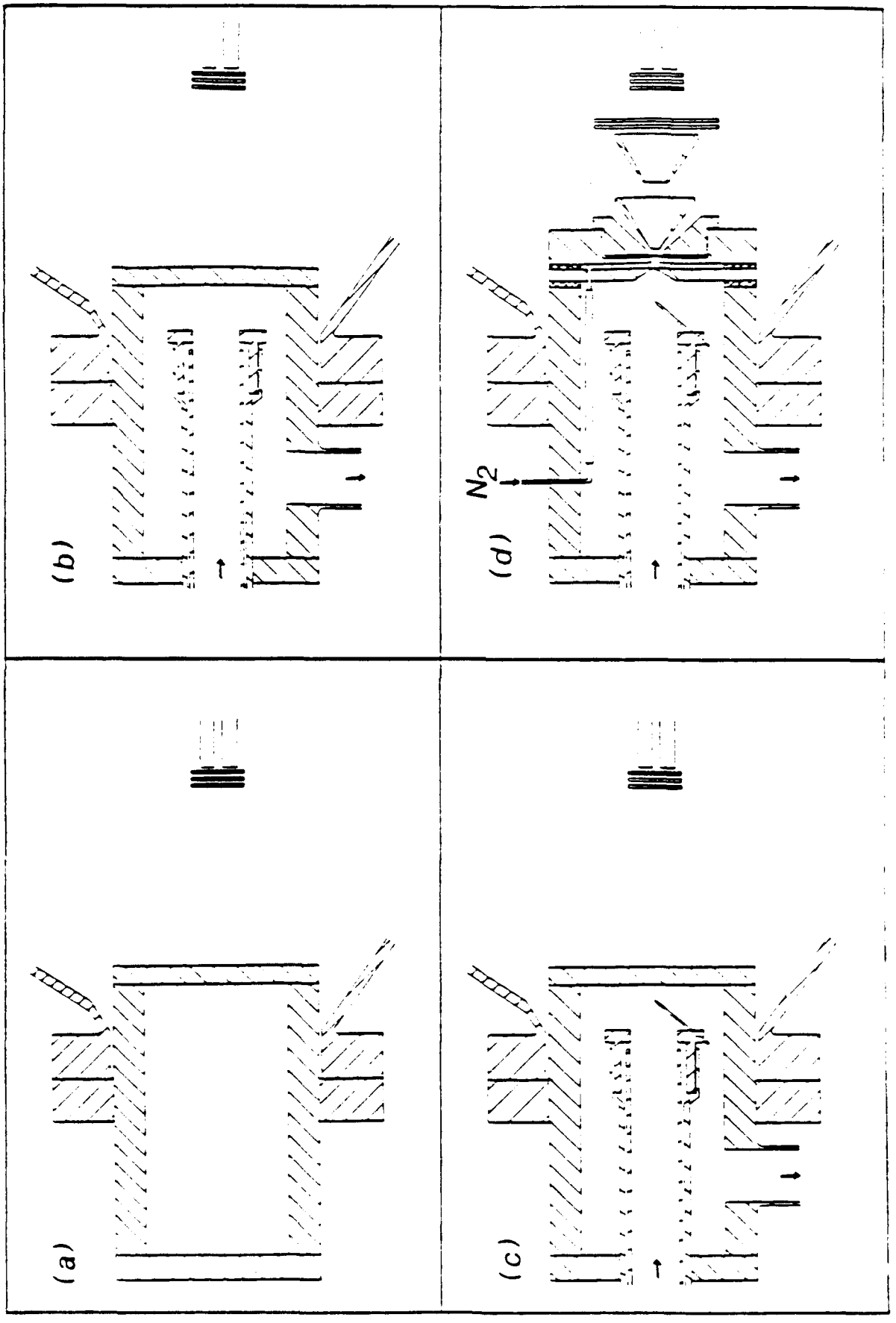
(a)
(b)
(c)
(d)
N2

For a source of high energy electrons, the two most common methods in API have been a ^{63}Ni foil β^- emitter and a corona discharge. The radioactive foil has the advantages of using no external power and of continually emitting a steady flux of electrons. However, the electrons it emits have a wide energy distribution (the most probable energy being ca. 20 keV), and this energy distribution has a significant tail at high energies [11]. As a result, the spatial distribution of reactant ions is not well defined and the path length of the electrons and ions vary over a wide range [11].

The alternative source of high energy electrons in API is a corona discharge from the tip of a metal needle (often a common sewing needle) to a planar surface (usually the plate containing the diaphragm). This discharge provides a more well defined spatial distribution of electrons as well as a much higher electron flux. One other advantage is the ability to select the needle-to-orifice distance, which may be used to alter the relative intensity and distribution of ions produced in the source. However, it should be pointed out that, in order to obtain a true corona discharge, a current-regulated, high voltage (up to 10 kV), current limited (<20 μA) power supply is required. Later in this chapter, the design of such a power supply is discussed (there are presently no such supplies commercially available); however, all preliminary work was performed using a Bertan 205A-05R voltage-regulated power supply which provided 0 to ±5000 V [35]. Because this was a voltage-regulated supply, the discharge was unstable, and this contributed to not only clogging of the orifice and short needle

lifetimes (because of sputtering of the needle tip), but an ion signal which was extremely noisy.

To provide a supply of electrons for this source, a discharge needle was mounted in a teflon ring which threaded into the outer glass tube (Figure 2.2(c)). By attaching the needle to the tube in this way, rough control of the needle position and needle-to-orifice distance could be accomplished by rotating the glass tube or by sliding it in or out of the back plate of the source canister.

Finally, Figure 2.2(d) shows a proposed two-orifice and lens system to focus the ions to the quadrupoles. Because clustering was such a problem in the early sources, and because it is not clear what portion of the clustering was occurring in the thermodynamic cooling of the post-orifice supersonic jet expansion, it is therefore desirable to prevent water and sample molecules from entering into this region. Sciex uses a similar system [33,34] and pressurizes the region between the two apertures with a relatively inert gas such as carbon dioxide or nitrogen to act as an "ion window" which is transparent to ions (because of potential fields which pull the ions through this gas), but is restrictive to non-ionized species of the sample gas which might clog the orifice or cluster with the ions in the post orifice region. In ion mobility/mass spectrometry, it is common to have a backstream of a neutral nonreactive gas such as nitrogen or helium to prevent particulate matter from reaching the orifice [36], so this idea is not entirely unique to the Sciex instrument. Thus, it was felt that such a stream of dry nitrogen gas might serve both purposes for this instrument, that is, to keep particulate matter away from the orifice

and to keep all neutrals, except nitrogen molecules and small amounts of impurities from the nitrogen supply, from entering the post-orifice region.

Therefore, to provide this backstream of nitrogen gas, a two-orifice system was designed that could be pressurized with nitrogen gas. The gas would flow out into the atmospheric region of the source and also into the vacuum region of the mass spectrometer. The first orifice was a 500 μm aperture drilled into a stainless steel plate. This plate served to contain the nitrogen gas and possibly provide some focussing for the ions by electrically "floating" it relative to the ground. The major interface between the atmospheric pressure source region and the vacuum region of the mass analyzer was a thin, replaceable, stainless steel diaphragm with a laser-drilled orifice (20-100 μm diameter) obtained from Precision Aperture [37].

Two skimmer cone lenses were designed to focus ions and to divert excess gas away from the axis of the mass analysis system so that the gas could be more easily pumped by the turbomolecular pump in the normal ion source region. The region after the orifice and before the first conical lens (hereafter referred to as the post-orifice region) is at relatively high pressure. Shahin in 1965 [10] noted the ability to perform some declustering of the background water clusters by accelerating the ions through this region. Fite in 1971 [38] and Levy in 1984 [39] noted the effect of multiple collisions in a supersonic jet on thermodynamic cooling of molecules. Sciex applied similar knowledge to develop an ion lens and gas skimming system to focus ions in a supersonic jet expansion with little increase in their kinetic

energy spread [34]. This can be done by creating a potential difference between the diaphragm and the first conical lens. If this potential difference is sufficiently large, it can add enough kinetic energy to the ion clusters that have formed to cause collisional declustering with neutral molecules in the supersonic expansion. This ability should help reduce clustering in the mass spectra.

Potentials for additional lenses not in the Finnigan system were provided by a power supply designed and constructed by Mark Hail, a fellow research group member. The voltages for these lenses are adjustable by means of ten-turn potentiometers from 0 to ±225 V and are monitored by a 3-1/2 digit LED display.

API Source Configuration for Finnigan 4500

Unfortunately, discharging to the first orifice was not possible with that lens floated because the lens power supply described above did not provide a low output impedance. When a discharge is created between the needle and another surface, the current will seek to follow the lowest path of resistance to ground. Thus the power supply for this floated orifice would need a very low output impedance. If the power supply does not have a low output impedance, a destructive situation can occur in which the current passes through the electronic circuitry of the mass spectrometer seeking a path to ground, and this may result in the damage of circuit components. Since such a power supply was not immediately available, the source design was simplified (Figure 2.3) to include just one electrically grounded orifice

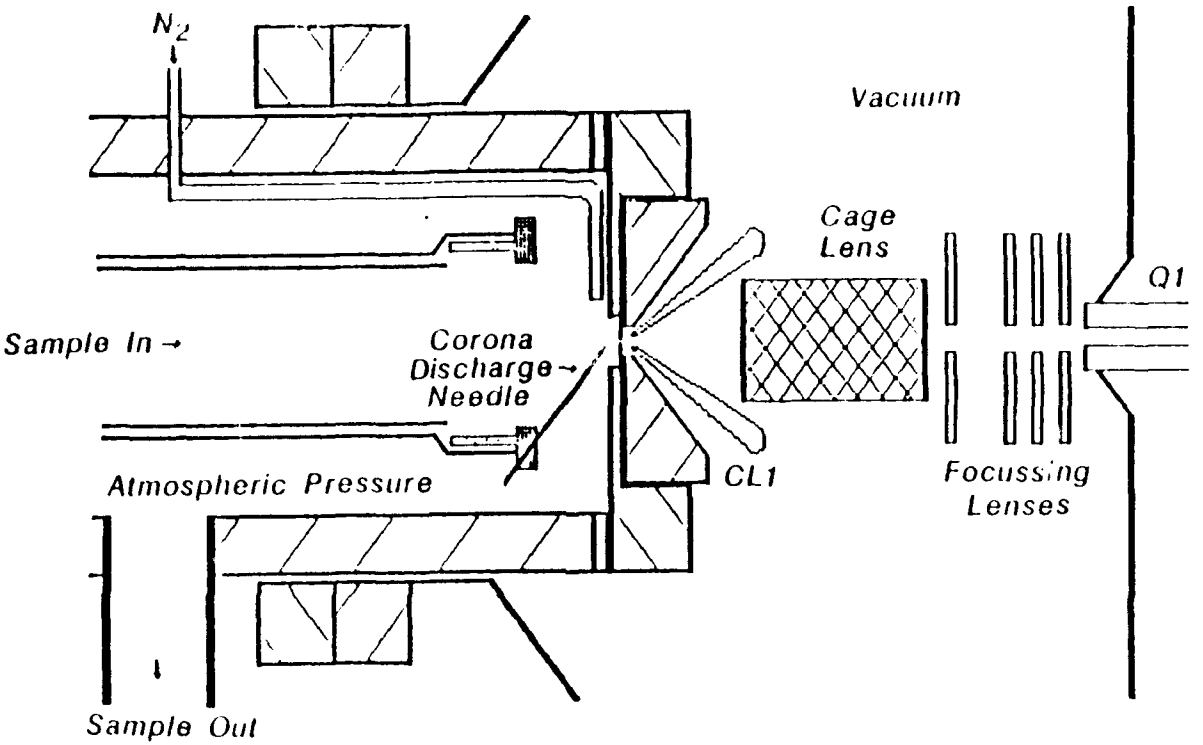

Figure 2.3

API source configuration developed for Finnigan 4500 quadrupole mass spectrometer.

(circumventing the need for the additional power supply). In early studies, a cage electrode was inserted in place of the second conical lens to mimic the lens system of the old Finnigan API source. To solve the problem of orifice clogging and cluster formation a flow of nitrogen gas was directed in a stream from a tube placed near the orifice parallel to the plane of the diaphragm. This design significantly reduced the frequency of orifice clogging when performing direct atmospheric monitoring.

API Source Configuration for Finnigan TSQ 70

To interface this source to the TSQ 70 system, several modifications were made. Figure 2.4 shows a schematic of the current API source design. This configuration again incorporates the less complicated one-orifice system. However, in this design, the seat for the diaphragm has been machined directly into a standard iso-K flange which is a standard vacuum flange for the instrument. This flange is divided into two sections with the inner section (which contains the diaphragm seat) having electrical and vacuum isolation from the outer ring. The outer ring clamps directly onto the TSQ 70 vacuum manifold and makes interchanging sources relatively easy. The first conical lens (CL1 in Figure 2.4) is mounted on the flange with the diaphragm seat. The second conical lens (CL2), a lens directly behind it (the back lens), a cylindrical lens, and three pre-quadrupole focussing lenses are all attached to a grounded mounting plate which replaces the

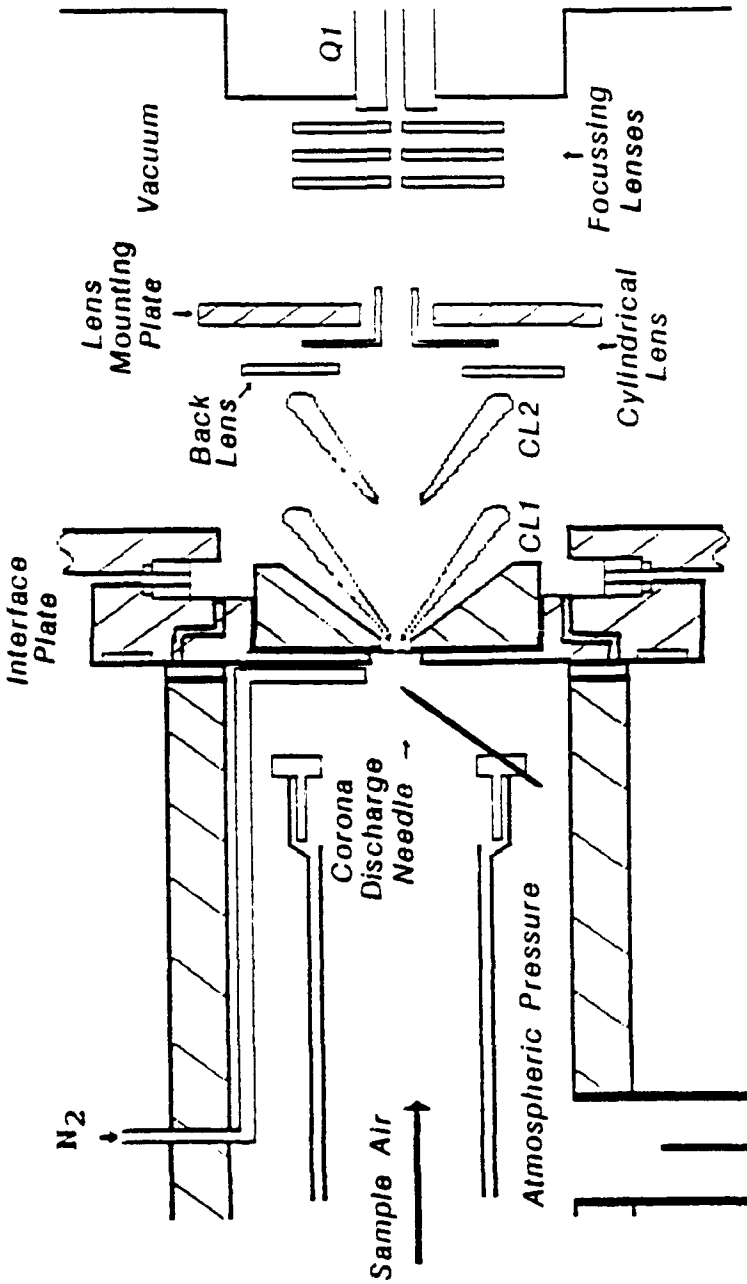

Figure 2.4

API source configuration developed for Finnigan TSQ 70 tandem mass spectrometer.

normal EI/CI source mounting plate and associated lenses. These lens assemblies can be switched by loosening two allen screws.

The API source canister and the associated lens system have been designed to be totally interchangeable with the related Finnigan components. Indeed, the instrument can be changed over from its normal EI/CI operating configuration to an API/MS/MS system, evacuated, and running in about 30 minutes. This increases the potential for the system to be later developed for possible field work.

The most recent addition to the source configuration was the development of a current-regulated, high voltage, low current, corona discharge power supply. This supply is capable of producing "true" (stable and invisible) corona discharges up to ±5000 V and with currents in the range of 0.5 to 5 μA. Figure 2.5 is a schematic for this power supply with the appropriate components labeled. The system is centered around an EMCO [40] 2 to 6 kV adjustable high voltage dc-dc converter. The current from the discharge is monitored and used in a feedback loop to regulate the input voltage into the dc-dc converter. Current and voltage are adjusted with two ten-turn potentiometers. The required voltage to generate a particular current depends upon different environmental factors such as the composition of the gas near the discharge needle, the flow rate of gas past the needle, and the needle-to-orifice distance. If the environment changes, the voltage changes so as to keep the current constant. However, if the dc-dc converter reaches its voltage limit, the system will become unregulated. In this case, the circuitry has been designed so that a

Figure 2.5

Electrical schematic of new current-regulated, high voltage, corona discharge power supply.

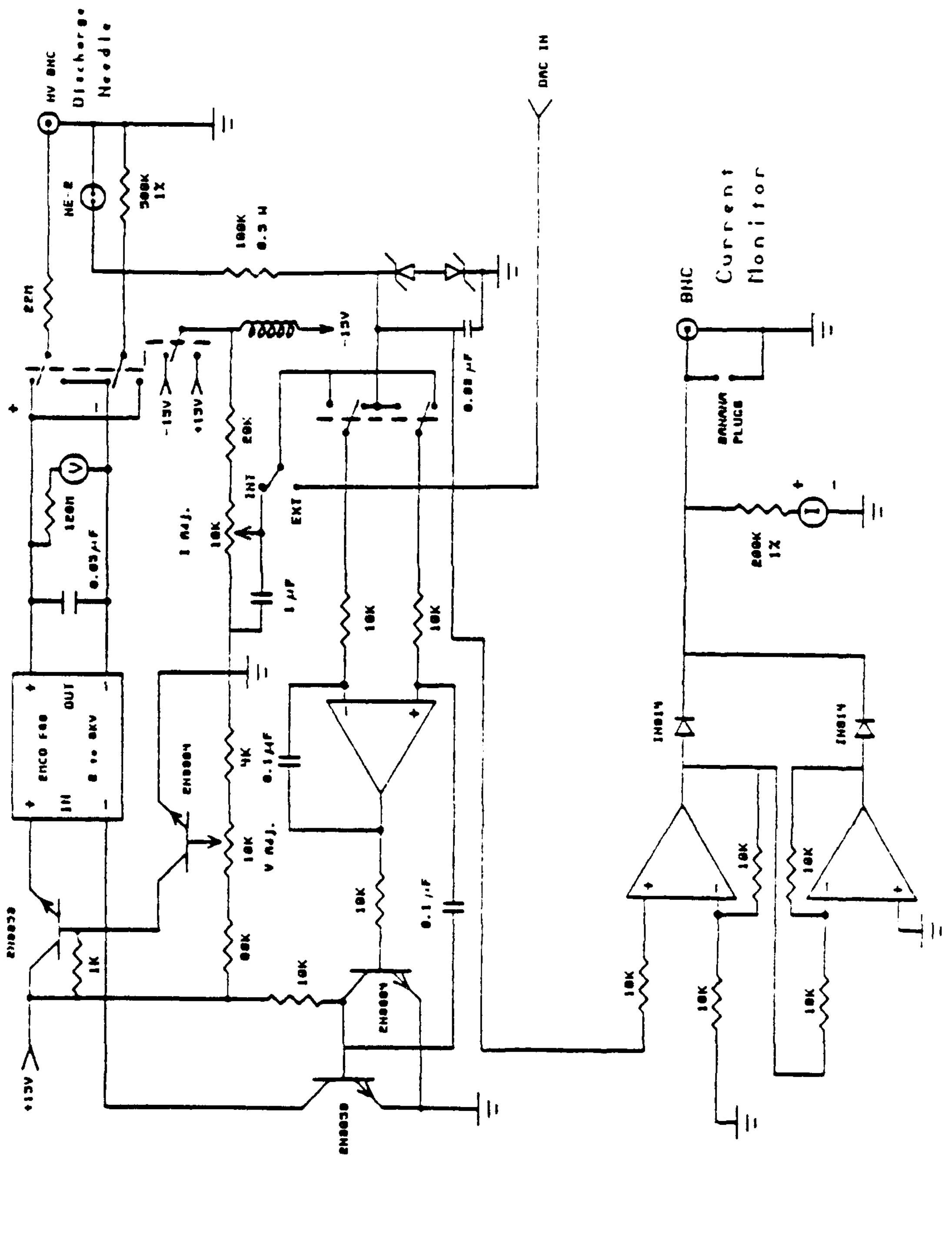
HV BNC
Discharge Needle
NE-2
500K 1X
100K 0.5 W
22M
120M
0.05 μF
EMCO F60
IN
OUT
0 to 6KV
2N3904
2N3053
1K
+15V
-15V
10K V ADJ.
4K
0.1 μF
8K
10K
20K
10K I ADJ.
INT
EXT
1 μF
DAC IN
0.08 μF
BNC
Current Monitor
BANANA PLUGS
200K 1X
1N914

large drop in current will occur to prevent an erratic and possibly dangerous discharge from ensuing.

Figure 2.6 is a schematic of the power supply for electrically floating the orifice from 0 to ±500 V based on an EMCO E05 dc-dc converter. This is a low output impedance power supply that is adjustable by means of a ten-turn potentiometer.

All parts of this source (except the normal Finnigan pre-quadrupole focussing lenses) including the power supplies for the corona discharge and the orifice potential were designed in this laboratory and constructed in the University of Florida Chemistry Department machine, electronics, and glass shops.

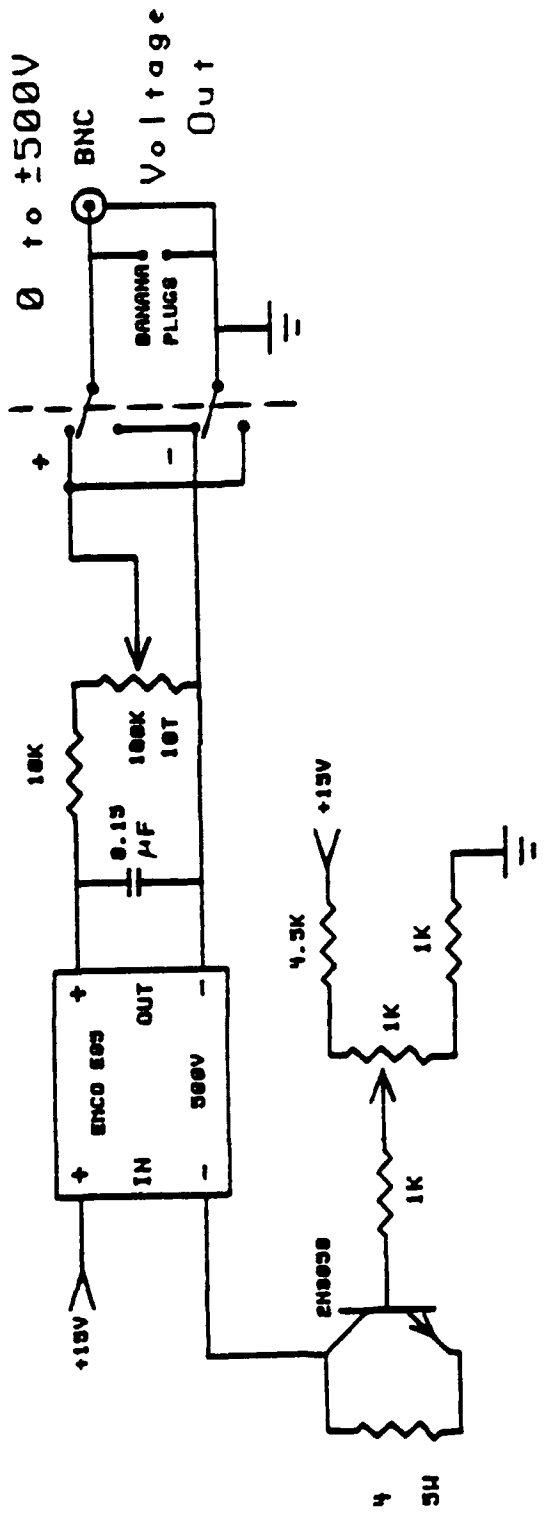

Figure 2.6

Electrical schematic of low impedance ±500V orifice power supply.

CHAPTER 3

EXPERIMENTAL RESULTS AND SOURCE DEVELOPMENT

Results with API Source Configuration for Finnigan 4500 Mass Spectrometer

As was stated in Chapter 2, the API source canister was designed to slide through a modified 6" conflat flange and into the vacuum region of the Finnigan 4500 single quadrupole mass spectrometer. While this design allowed the API source to be compatible with the Finnigan instrument, it caused several problems. The API source was designed to be modular in construction so that design changes could be made to selected parts of the assembly without the need to re-machine the entire API source for each modification made. Unfortunately, at each junction between individual parts of the source canister, there existed the potential for gas leaks from the atmospheric pressure source region, through the junctions in the assembly, into the vacuum region of the mass spectrometer. The source was designed so that the orifice plate was electrically isolated from the source canister (in the initial design, a second orifice flange was to be inserted between, and electrically isolated from, these two flanges). This concept was to be used later in electrically floating this flange. Electrical isolation was accomplished by means of placing am anodized aluminum, ring-shaped spacer between these two components. Vacuum integrity was maintained by two o-rings, one on either side of the aluminum spacer. The

assembly was to be held together with nylon screws. Because of the large force of atmospheric pressure pushing on the orifice flange, the nylon screws could not induce a sufficient counter pressure to maintain vacuum integrity. The nylon screws were replaced by metal screws to obtain vacuum integrity to some degree (although the metal screws did not allow for electrical isolation), and a pressure in the analyzer region of 1.2×10^{-5} torr was eventually obtained for a 20 μm diameter orifice. To calculate the expected pump-down pressure for an aperture of this size, fluid dynamics can be applied to treat each stage of differential pumping separately.

The conductance (C_{visc}) of a 20 μm diameter orifice at atmospheric pressure can be obtained from equation (1) below [41].

$$C_{visc} = 76.6 \times \delta^{0.712} \times (1-\delta^{0.258})^{0.5} \times \frac{A}{1-\delta}, \text{ in } Ls^{-1} \quad (1)$$

where $\delta = (P_2/P_1) < 1$ (where P_1 and P_2 are the respective pressures on either side of the orifice) and A is the surface area of the orifice (in cm^2). If $p_2 << p_1$, then C_{visc} approaches the limiting value for air in equation 2.

$$C_{visc} = 20 \times A, \text{ in } Ls^{-1}. \quad (2)$$

A 20 μm diameter orifice has a surface area of

$$S = \pi r^2 = \pi \times (1.0 \times 10^{-3} \text{ cm})^2 = 3.1 \times 10^{-6} \text{ cm}^2. \quad (3)$$

Thus, for this system,

$$C_{visc} = 20 \times (3.1 \times 10^{-6}\ cm^2) = 6.3 \times 10^{-5}\ Ls^{-1}. \qquad (4)$$

The gas throughput, q_{pv}, can be defined as in Equation (5).

$$q_{pv} = C_{visc} \times (P_1 - P_2),\ \text{in torr}\cdot Ls^{-1} \qquad (5)$$

Substituting for C_{visc}, $P_1 = 760$ torr, and making the approximation that $P_1 - P_2 = P_1$, the gas throughput is found to be 4.8×10^{-2} torr$\cdot Ls^{-1}$. With q_{pv} as defined above and s as the pumping speed of the first turbomolecular pump (330 Ls^{-1}), P, the expected pump-down pressure for the first region of differential pumping, can be found from equation 6.

$$P = q_{pv}/s = (4.8 \times 10^{-2}\ \text{torr}\cdot Ls^{-1})/330\ Ls^{-1} = 1.5 \times 10^{-4}\ \text{torr}. \qquad (6)$$

Applying this calculation again, now with $P_1 = 1.5 \times 10^{-4}$ torr, and with an aperture radius (for the aperture between the first and second vacuum chambers), r, of approximately 0.15 cm, the expected pressure in the second region of differential pumping is 6.0×10^{-7} torr. Although, in the calculations above, the nominal pumping speeds for the turbomolecular pumps were used and the effective pumping speeds are somewhat less (because of restrictions), the failure to get the analyzer pressure below 10^{-5} torr seems to indicate that the o-ring design was inefficient in its ability to maintain vacuum integrity.

Nevertheless, even though the vacuum integrity of the source was poor, these pressures were sufficient to perform mass spectrometry. The first ions generated with this source, in a one-orifice (at ground potential) system with no nitrogen jet, were cluster ions of the form $H(H_2O)_n^+$ (n = 5 (m/z 91) to n = 21 (m/z 109)), $(CH_3)_2COH(H_2O)_n^+$ [n = 3 (m/z 113) to n = 8 (m/z 203)], $[(CH_3)_2COH]_2(H_2O)_n^+$ [n = 2 (m/z 153) to n = 4 (m/z 189)], generated by inducing a flow of laboratory air past the discharge region (Figure 3.1). The acetone ions are from residual solvent left after source cleaning, which vaporizes off source walls and diffuses to the discharge region because of the lack of a nitrogen jet. These ions were of very low intensity, and the lack of cluster ions with higher m/z values probably results from a lens tuning effect.

Without the nitrogen gas or an electrically floated orifice, this source configuration had only limited abilities for declustering. Figure 3.2 shows the resulting mass spectra (all normalized to the same intensity) when the potential difference between the grounded orifice and the first conical lens was changed from 2 to 8 V. While the effect is not dramatic, the slight decrease in the cluster ions with higher m/z values relative to those with lower m/z values is apparent.

However, even when analyzing vapor samples injected into a nitrogen stream (no direct atmospheric monitoring), clustering was still a problem. Figure 3.3 (a) - (c) shows mass spectra obtained for representative compounds which undergo charge exchange ionization in the API source, carbon disulfide (MW 76), benzene (MW 78), and toluene (MW 92), respectively. Carbon disulfide forms almost exclusively the

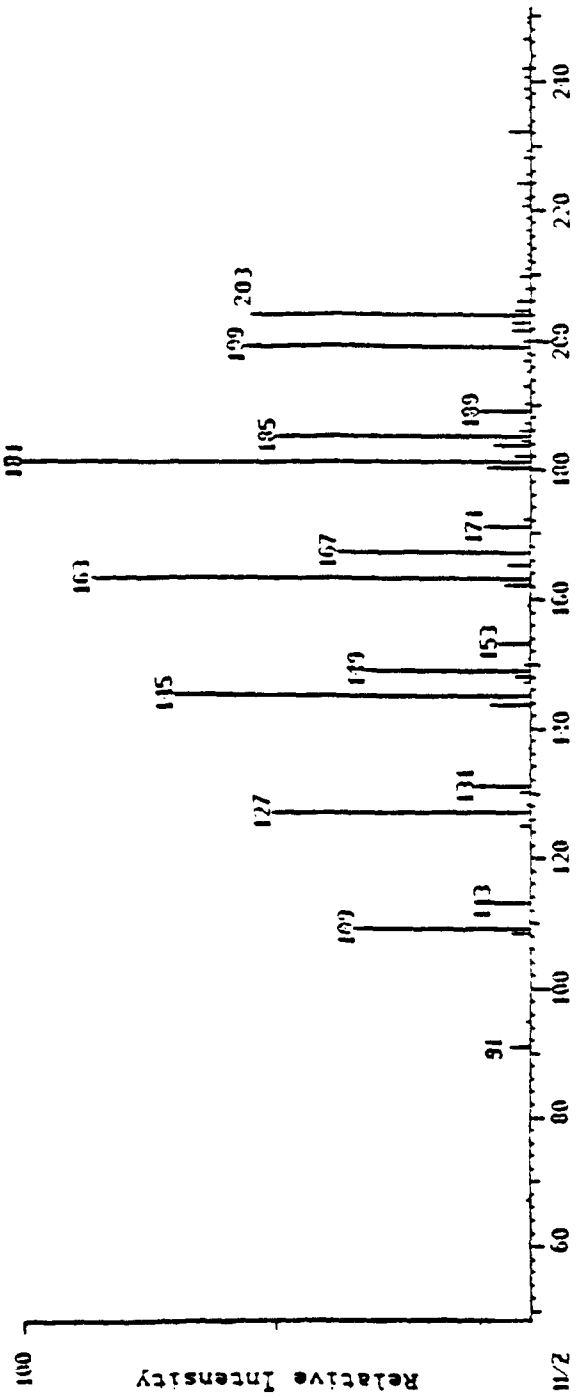

Figure 3.1

Mass spectrum of the first API ions generated with the new API source.

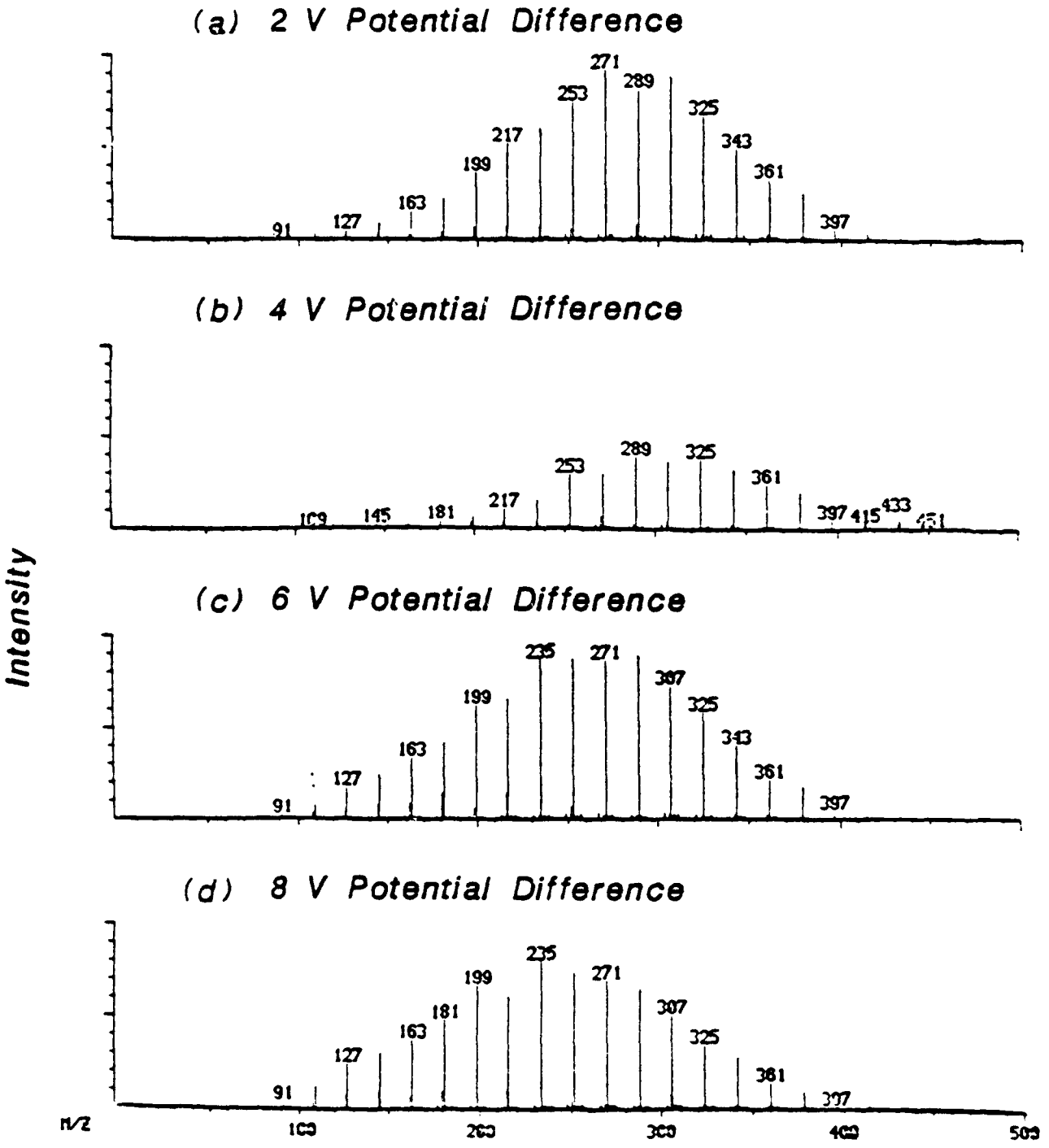

Figure 3.2

Declustering in post-orifice region with grounded orifice, no declustering gas, and with the potential of the first conical lens at (a) -2 V, (b) -4 V, (c) -6 V, and (d) -8 V.

Figure 3.3

API/MS of compounds that undergo charge exchange ionization in a pure nitrogen stream (a) carbon disulfide, (b) benzene, and (c) toluene.

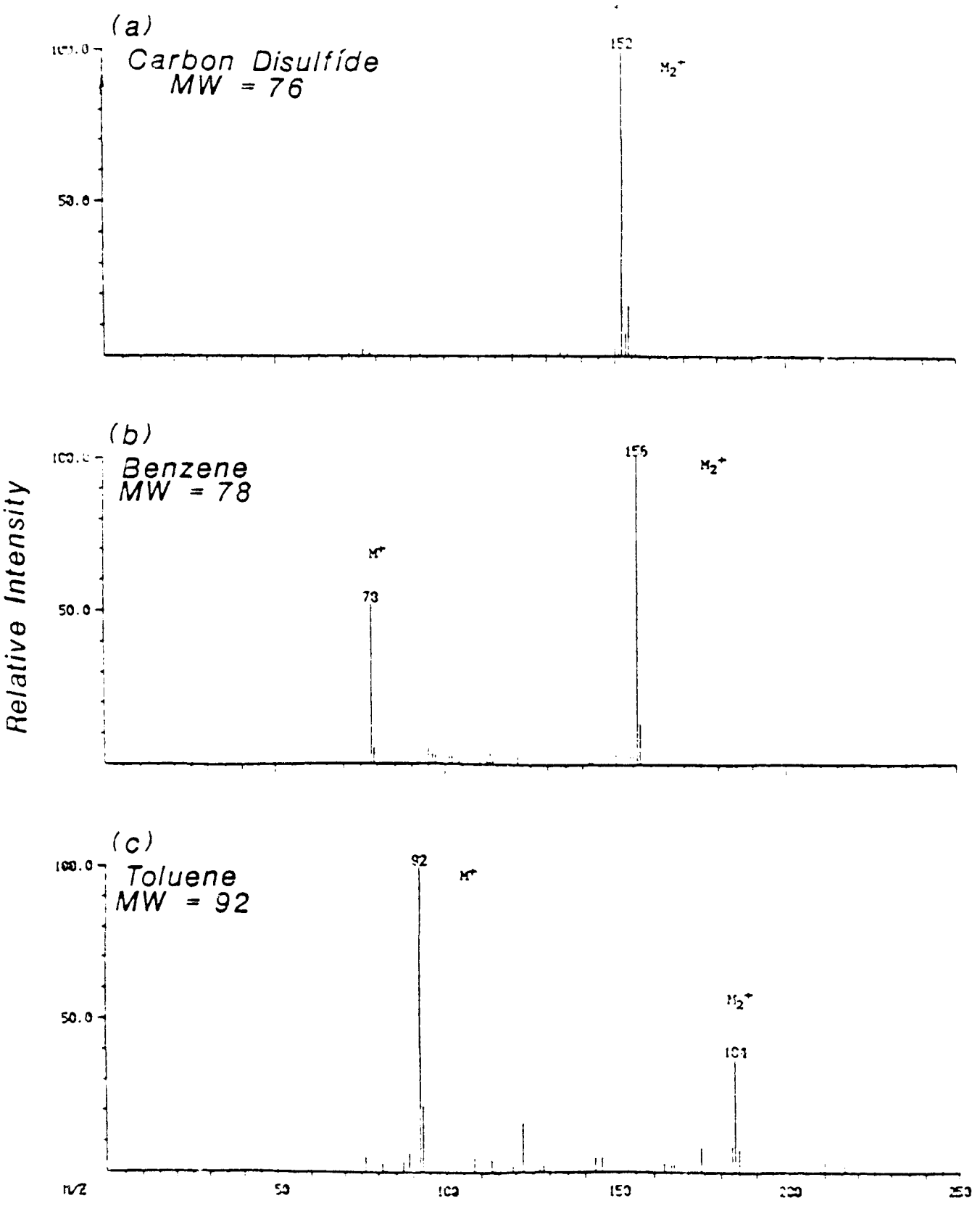
(a)
Carbon Disulfide
MW = 76
152
M_2^+
50.0
(b)
Benzene
MW = 78
156
M_2^+
M^+
78
50.0
Relative Intensity
(c)
Toluene
MW = 92
92
M^+
M_2^+
184
50.0
m/z
50
100
150
200
250

M_2^+ cluster ion. Benzene and toluene form both the M^+ molecular and the M_2^+ cluster ions. Figure 3.4 (a) - (c) shows mass spectra obtained for representative compounds which undergo proton transfer ionization in the API source, acetone (MW 58), ethyl acetate (MW 88), and methanol (MW 32), respectively. Acetone and ethyl acetate form both the $(M+H)^+$ pseudo-molecular and the $(M_2+H)^+$ cluster ions. The ions formed from methanol display severe clustering and are of the form $[M+H(H_2O)_n]^+$ (n = 2 - 5), $[M_2+H(H_2O)_n]^+$ (n = 0 - 2), $[M_3+H(H_2O)_n]^+$ (n = 0 and 1), and $(M_4+H)^+$.

Adaptation of the API Source to the Finnigan TSQ 70 Mass Spectrometer

TSQ 70 Characteristics

This mass spectrometer has some unique characteristics, most of which have proven beneficial to performing source development on it. This instrument is almost totally under microprocessor control. All valves, pumps, heaters, and most importantly lenses and quadrupoles can be controlled by "firmware" (program code stored on erasable, programable read-only memory (EPROM) chips) which accesses 5 single board minicomputers located on the instrument. This allows sophisticated tuning and optimization to be performed with relative ease. The instrument is differentially pumped by two 330 Ls^{-1} turbomolecular pumps, which can reach a vacuum suitable for mass spectrometry in less than 15 minutes (with no additional gas loads on the system) The vacuum manifold is shaped as a rectangular box, with a thick, glass lid, which presses down on two o-rings (one each for the

Figure 3.4

API/MS of compounds that undergo proton transfer ionization in a pure nitrogen stream (a) acetone, (b) ethyl acetate, and (c) methanol.

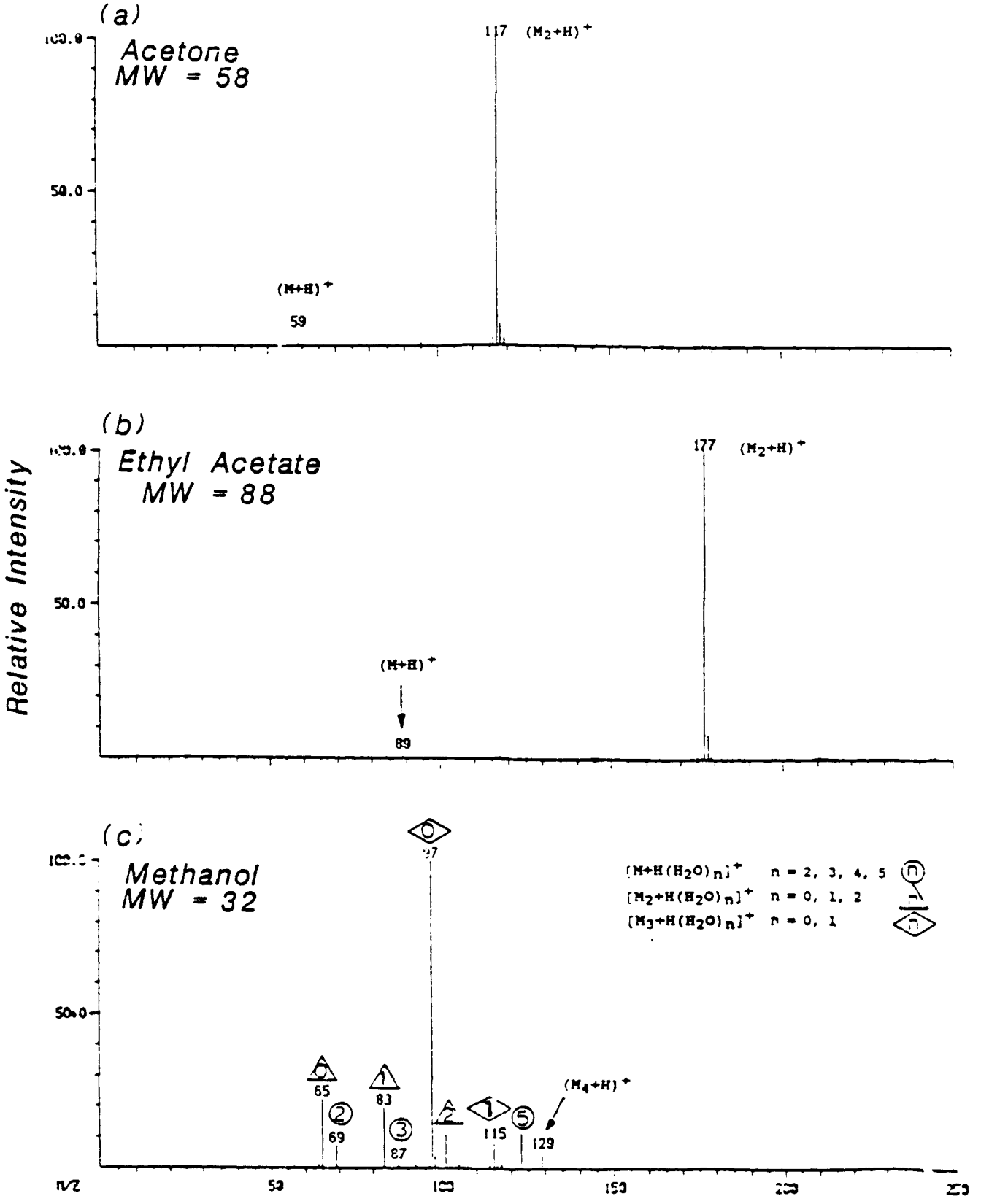
(a)
Acetone
MW = 58
117 (M2+H)+
50.0
(M+H)+
59
(b)
Ethyl Acetate
MW = 88
177 (M2+H)+
50.0
(M+H)+
89
Relative Intensity
(c)
Methanol
MW = 32
97
[M+H(H2O)n]+ n = 2, 3, 4, 5
[M2+H(H2O)n]+ n = 0, 1, 2
[M3+H(H2O)n]+ n = 0, 1
50.0
65
69
83
87
115
129
(M4+H)+
m/z
50
100
150
200

differentially pumped ion source and analyzer sections) to maintain a suitable vacuum. Vacuum flanges on the instrument are standard 6" diameter iso-K flanges which clamp onto the manifold using an o-ring between the flange and the manifold to maintain vacuum integrity. All lenses and quadrupoles are mounted on an optical rail for easy maintenance (and in this case easy modification) and are each held in place by only one or two screws. The normal EI/CI ion source and lens assembly mounts to this optical rail in the first differentially pumped chamber of the mass spectrometer, and is removable by loosening two allen screws.

Source Modifications and Ion Optical Modeling

In order to interface the source canister to the TSQ 70 vacuum manifold, a new adapter flange was needed to replace the conflat flange compatible with the Finnigan 4500. Since all the vacuum ports on the TSQ 70 vacuum manifold used iso-K type flanges, it was necessary to base the adapter flange on this standard. With the freedom to design a new flange, it was also decided to alter the design of the source to reduce the problems with vacuum integrity. This modified source design moves all the junctions between source parts outside of the vacuum manifold of the mass spectrometer by machining the diaphragm seat directly into the iso-K flange. Thus, the only possible locations for a gas leak are the knife-edge seal on the orifice and the o-ring between the iso-K flange and the vacuum manifold (which is in the normal instrument configuration). The rest of the canister attaches to the adapter flange by four bolts and can be easily removed without breaking vacuum. When the orifice gets clogged, a jet of high pressure

gas (such as that from a can of common laboratory freon, or from compressed nitrogen, or air) can be used to clear the blockage. Later, the flange was re-designed so that in the final configuration it was divided into two concentric sections, the inner section (containing the diaphragm seat) being electrically isolated from the outer section.

To test the vacuum integrity of this source, a diaphragm containing a 70 μm diameter orifice was installed. Using the equations found earlier in this chapter, the theoretical pump-down pressures, for the first and second differentially pumped-regions of the mass spectrometer are calculated to be 1.8 x 10-^{3} torr and 7.2 x 10^{-6} torr, respectively. The actual pump-down pressures were found to be 2.0 x 10^{-3} and 3.0 x 10^{-5}. Therefore it appears that this interface serves to maintain vacuum integrity.

An ion optical modeling program, SIMION [42], that has been modified to run on a PC/AT microcomputer [43], was used to model the lens system for the API/MS/MS instrument configuration. This approach has proven advantageous in the design and development of the lens system for interfacing the API source to the mass spectrometer. Two examples of the use of this program are given below, although it should be pointed out that this program does not take into consideration the multiple inelastic collisions that the ions incur in the relatively high pressure post-orifice region. Therefore the actual lens voltages used for maximum ion transmission can be very different from the values that give the best transmission in the collision-force model used by the SIMION program. Despite this, the model is very useful for the

physical design of the lenses themselves, rather than predicting the actual lens potentials.

To simplify the system and facilitate testing, the source has been used in the one-orifice configuration. One characteristic of the TSQ 70 mass spectrometer which turned out to be a disadvantage to the adaptation of the API source to the mass spectrometer was the electrically grounded source mounting plate. Since the API source has been installed on the front of the mass spectrometer, this grounded plate resides between the API source and the mass analyzer. This plate holds the normal EI/CI ion source assembly, including the pre-quadrupole lenses. Since the positioning of these pre-quadrupole lenses is critical, it was desired to use this same mounting plate with a modified lens block which held only the pre-quadrupole lenses and had the excess metal removed. Unfortunately, there is only a 3/4" aperture in this mounting plate through which the API generated ions are to be focussed.

Figure 3.5 (a) shows the SIMION representation of the lens system for the API source interfaced to the TSQ 70 mass spectrometer. Figure 3.5 (b) shows the equipotential lines on each of the lenses and the lens mounting block. Because the TSQ 70 lens mounting plate is electrically grounded, relatively low energy positive ions which enter even slightly off-axis are repulsed by the associated field. Figure 3.5 (c) shows the ion trajectories for an ion with a m/z value of 181, an initial energy of 0.2 eV, and with initial angles of 0, 10, and 20 degrees off the center axis. Figure 3.6 (a) shows the addition of a cylindrical lens to penetrate the field produced by the grounded source

Figure 3.5

Ion optic modeling of lens configuration for API source on TSQ 70 mass spectrometer showing (a) the representation of this lens system with the SIMION program, (b) with potential contours (at values 10% more positive than lens voltages), and (c) with representative ion trajectories.

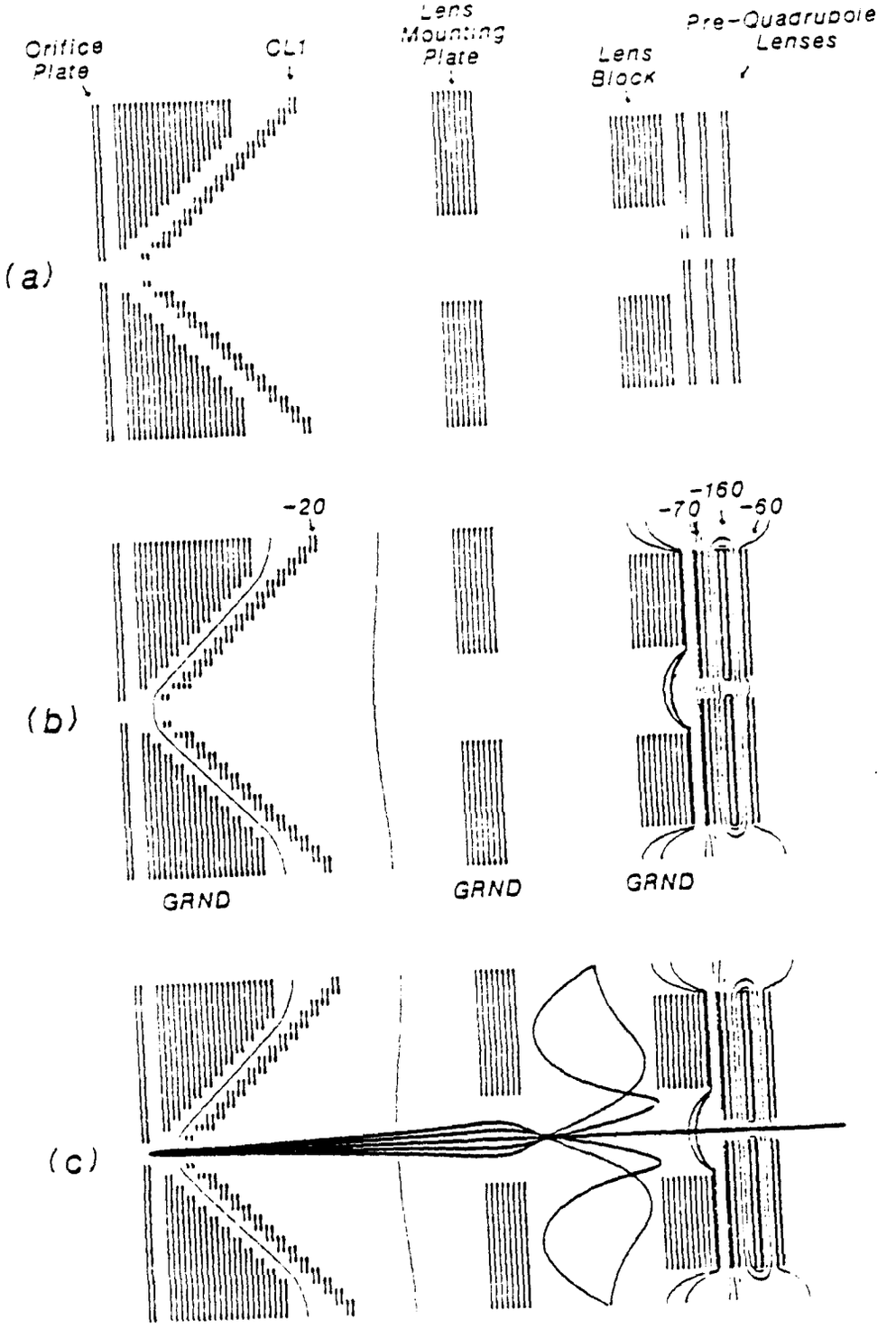
Orifice Plate
CL1
Lens Mounting Plate
Lens Block
Pre-Quadrupole Lenses
(a)
-20
-160
-70
-60
(b)
GRND
GRND
GRND
(c)

Figure 3.6

Ion optic modeling of lens configuration for API source on TSQ 70 mass spectrometer with the addition of a cylindrical lens showing (a) the representation of this lens system with the SIMION program, (b) with equipotential contours (for potentials of 10% more positive than the lens potential), (c) with representative ion trajectories for -5 V, and (d) with representative ion trajectories for -30V.

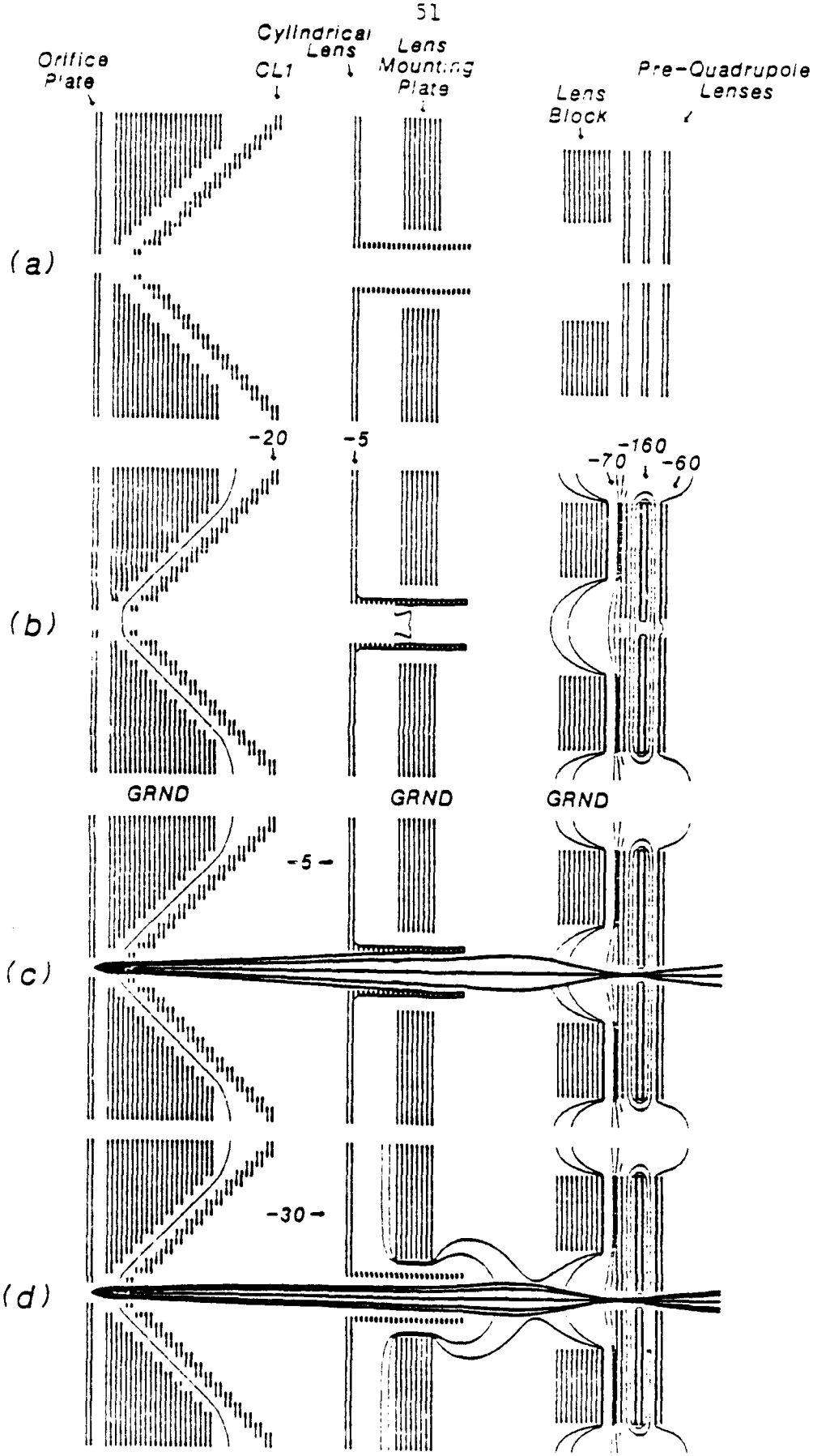
Orifice Plate
Cylindrical Lens CL1
Lens Mounting Plate
Lens Block
Pre-Quadrupole Lenses
(a)
-20
-5
-160
-70
-60
(b)
GRND
GRND
GRND
-5
(c)
-30
(d)

mounting plate. Figure 3.6 (b) shows the equipotential contours for a cylindrical lens potential of -5 V. This improves the transmission of ions with m/z 181, initial ion energy of 0.2 eV, and initial angles of 0, 10, and 20 degrees off the center axis. With this potential, ions ≤10 degrees off the center axis are focussed through the lens system. In Figure 3.6 (d) the potential on the cylindrical has been increased to -30 V. By plotting the trajectories for ions with the same initial conditions as above, it can be seen that ions with initial angles of ≤20 degrees off the center axis are focussed through the lens system to the quadrupoles.

To aid in the focussing of ions and the pumping of the excess gas, a second conical lens (CL2) was added to the design. In order to implement this lens as a focussing lens element, a plate lens with a cylindrical hole is required directly behind the 2nd conical lens. The SIMION program was used to model the effect of the aperture size of a lens (the back lens), immediately behind CL2, on the focussing of ions (now with a higher energy (≈ 5 - 10 eV) after being accelerated through the first conical lens) through CL2 and into the cylindrical lens. Figure 3.7 (a) is the SIMION representation of a portion of the lens assembly consisting of CL2, and the back, and cylindrical lenses with potentials of -5 V, -50, and -150 V, respectively. Figure 3.7 (b)-(d) shows the effect of small (0.25" diameter), medium (0.50" diameter), and large (0.75" diameter) apertures on ion trajectories for ions with initial angles of 25, 20, 15, 10, and 5 degrees off the center axis. For a small aperture (b), ions with initial angles ≤10 degrees off axis are focussed through the cylindrical lens. For medium

Figure 3.7

Ion optic modeling of the effect of the aperture size of the back lens on ions passing through a conical lens showing (a) the SIMION representation of those lenses and the associated potential contours (10% more positive than the associated lens), and ion trajectories with (b) a small aperture, (c) a medium aperture, and (d) a large aperture.

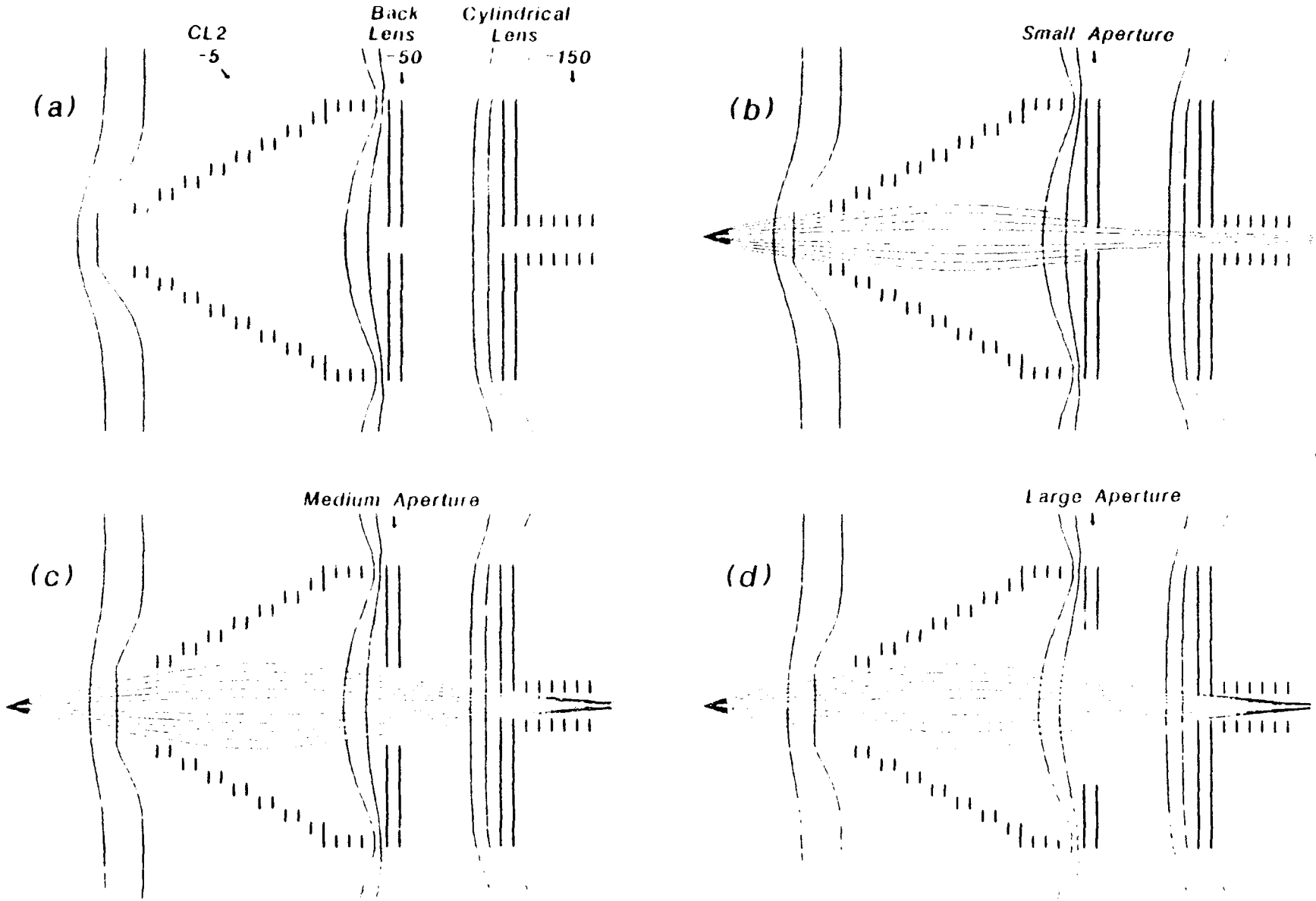
(a)
CL2
-5
Back
Lens
-50
Cylindrical
Lens
-150
(b)
Small Aperture
(c)
Medium Aperture
(d)
Large Aperture

(c) and large (d) apertures this value improves to 20 and 25 degrees, respectively. However, if this back lens is removed completely (not shown), the potential field of the cylindrical lens is not capable to cause sufficient convergence of the ions to allow transmission through the pre-quadrupole lenses.

The re-design of the source with a new adapter flange and the use of the SIMION program to model the lens system proved advantageous in developing an operable API source. By moving all junctions between source canister parts outside of the vacuum system, it became practical to use a 70 μm diameter orifice. Ion optical modeling saved much effort and time developing two new lenses for the system, a cylindrical lens to penetrate the potential field generated by the grounded source mounting plate and the optimum aperture size for the lens immediately following CL2.

Gas Flows

Using the equations presented earlier in this chapter, the conductance (C_{visc}) of a 70 μm diameter orifice is calculated to be 7.7×10^{-4} Ls^{-1} or 46.2 $mL \cdot min^{-1}$. To measure the rate of gas flow through the orifice a common laboratory bubble meter was hooked up to the exhaust port of the mechanical backing pump for the turbomolecular pumps. Since one mechanical pump serves as the backing pump for both turbomolecular pumps, any gas that enters the system must exit through this port. With the orifice (70 μm diameter) plugged, the flow rate, F_o, was $<<$ 1 $mL \cdot min^{-1}$. When the orifice was unplugged, this flow rate increased to 45.3 $mL \cdot min^{-1}$. This would indicate a flow rate through the orifice of 45.3 $mL \cdot min^{-1}$, which agrees within the experimental

error (the actual size of the orifice is 70 μm ±10%) for the calculated conductance.

For the measurement of the flow rate through the glass tube used for direct atmospheric sampling, the bubble meter was modified such that air was drawn through the bubble meter by attaching, with flexible tubing, the top of the bubble meter to the glass sampling tube. Both the orifice and the sampling fan served to draw air through the sampling tube. Because the flow rates through the orifice and through the sampling fan are fixed, any additional gas loads would reduce the flow through the sampling tube. With no flow of gas for the nitrogen jet, the sampling flow rate was found to be 77.4 $mL \cdot min^{-1}$. With the nitrogen gas jet on, the flow was found to be 74.8 $mL \cdot min^{-1}$. Therefore, the flow rate of the nitrogen jet (flowing out of a 1/16" tube) was 2.6 $mL \cdot min^{-1}$. This is the common configuration for the instrument while performing direct atmospheric analysis.

Discharge Power Supply

As was stated in the second chapter, the discharge power supply which was used for most of this work was a Bertan 205A-05R voltage-regulated power supply. The discharge from which ions were detected (with this power supply), was visible (violet in color), unstable to varying degrees, had a current >20 μA, and produced an ion signal which was extremely noisy. At times this discharge would become very unstable and erratic and would change to a bright white color. Since the power supply regulated the voltage, any change in resistance in the path of the discharge (such as those caused by changes in the gas flow rate or composition) would cause a change in the current and thus a

change in the ion intensity. Tuning was performed by scanning at a much slower rate (>1 s/scan) than is normally required for quadrupole mass spectrometry and still was, at best, difficult.

A true corona discharge is invisible, stable, and of much lower current than the discharge obtained above [34]. The second chapter discusses the power supply that was designed and built to generate such a discharge. The corona discharge obtained with this current-regulated power supply meets the aforementioned requirements, with a stable, selectable current of 0.5 to 4.5 μA. The voltage required to produce the corona discharge is dependent on the current desired, the flow rate and composition of gases in the discharge region, and the needle-to-orifice distance, but usually was on the order of 3 to 4.8 kV. With this stable discharge, the ion signal was significantly less noisy, and therefore, tuning could be performed with automated tuning procedures and at a much faster rate.

Orifice Potential

With the present design it is possible to have the orifice electrically grounded or floated by a ±500 V, low-impedance power supply (see Chapter 2). Initial experiments were performed with the orifice placed at instrument ground by connecting its electrical lead directly to the instrument manifold. Later, to improve sensitivity, the orifice was electrically floated at up to +150 V.

Experimental Physical Parameters of API Source and Mass Spectrometer

Initial Ion Energy and Energy Spread

An experiment was set up such that the intensity of the ions generated by the API source was monitored as the voltage on the second conical lens (CL2) was varied, while keeping the orifice at ground potential (0.0 V) and the first conical lens (CL1) at -4.4 V relative to ground.

Figure 3.8, a "stopping-potential curve", is a plot of the ion intensity (scale on left-hand y axis) vs. the potential of lens CL2 (with a potential of CL1 = -4.4 V), together with the first derivative of this curve (intensity scale on right-hand y axis). The first derivative provides (a) the potential that will stop an ion with the average kinetic energy (i.e. the peak of the first derivative curve) and (b) the kinetic energy spread of the ions (i.e. the peak width at half height). A simple numerical method was employed to find the first derivative, in which the difference of consecutive y axis values relative to the difference of consecutive x axis values ($\Delta y/\Delta x$) was plotted vs. the average of their corresponding pair of x axis values. The difference curve that was generated yielded values of -3.8 V and 0.8 eV for the potential required to stop an ion with the average ion kinetic energy and the ion kinetic energy spread, respectively.

Since the orifice is at 0.0 V (ground potential), the first conical lens is at -4.4 V, and positive ions were analyzed, the ions should be accelerated by 4.4 eV between those two components. If this were true, it should take a potential of 0.0 V on the second conical lens to

Figure 3.8

A stopping potential curve for the 2nd conical lens with a electrically grounded orifice and the superimposed associated differential curve showing the potential required to stop an ion with the average energy and the energy spread of the ions.

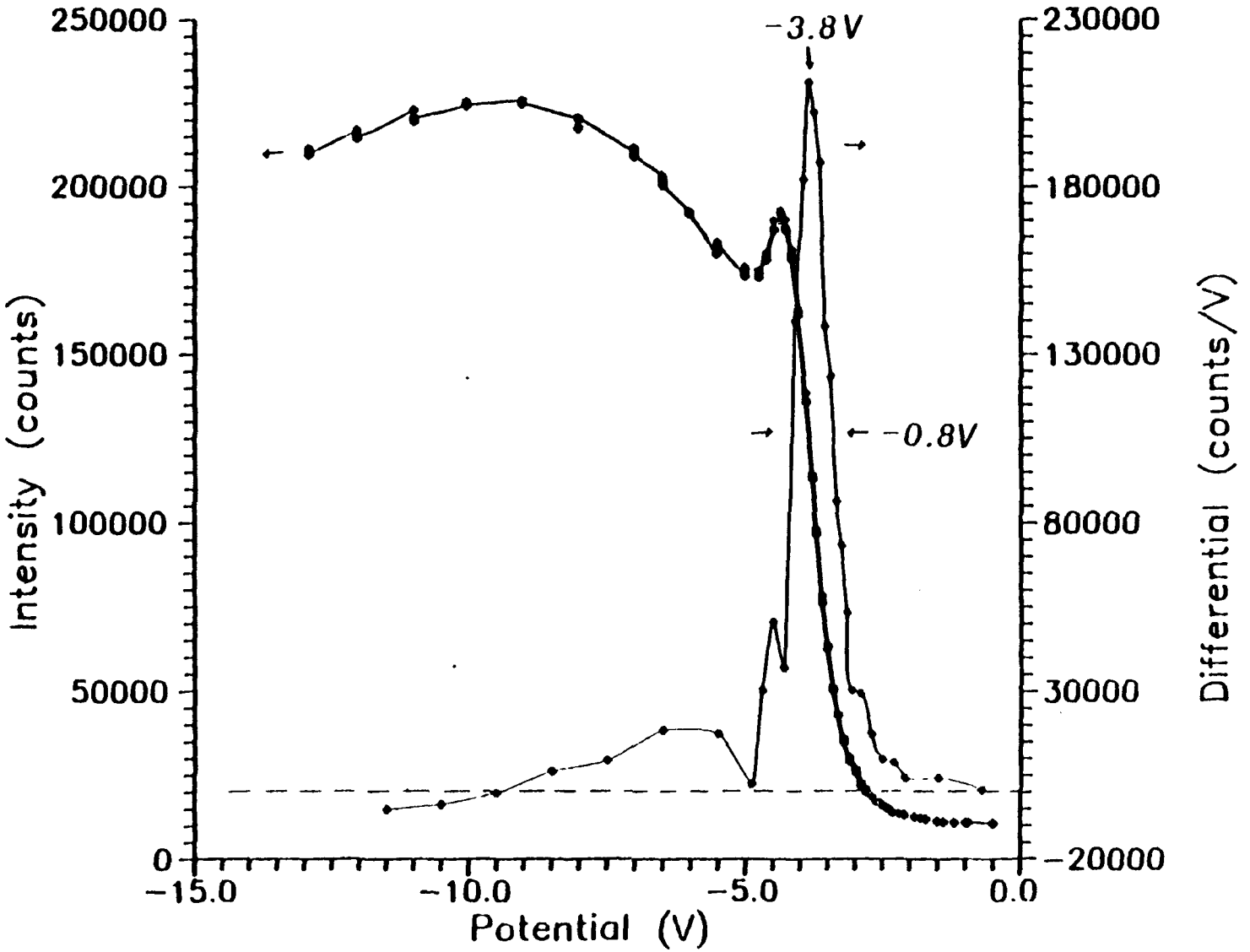
250000
200000
150000
100000
50000
0
230000
180000
130000
80000
30000
-20000
-3.8V
-0.8V
Intensity (counts)
Differential (counts/V)
-15.0
-10.0
-5.0
0.0
Potential (V)

"stop" the ions (i.e. decelerate the ions by 4.4 eV, to 0.0 eV of energy). A simplistic model for this system is displayed in Figure 3.9 (a). The ion, transversing the potential field, can be thought of as a ball rolling down a slope. If the ball is released down the slope from a resting position, it will be accelerated (i.e. gain in kinetic energy) due to gravity by falling some height, h, and therefore it will take a height equal to h to decelerate the ball (reduce its kinetic energy) until it stops again. The experimental results seem to indicate a situation more like Figure 3.9 (b), in which the ball is stopped by a slope that is only a fraction of the initial height; that is, it takes a smaller decelerating energy than expected to stop the ball. Barring other factors, if the ball were released from the same initial height as in Figure 3.9 (a) it should not be stopped on the opposite slope but should continue on out of the system (Figure 3.9 (c)). Likewise, barring other factors, the ion would be expected to pass through the decelerating field provided by CL2 instead of being stopped. The experimentally determined voltage needed to stop the ions was found to be -3.8 V (a deceleration of 0.6 eV from the CL1 to CL2 lenses); therefore, the ions must have been accelerated by only 0.6 eV on their way to the first conical lens. This could occur if the ions were generated at a potential field 0.6 V more positive than that of the first conical lens (i.e., at -3.8 V with respect to ground). This is analogous to the ball starting at a very low height. However, it is known that the ion is formed on the atmospheric side of the orifice (i.e. the ball is starting all the way up the slope). A second possible reason is that the ion's ability to increase its kinetic

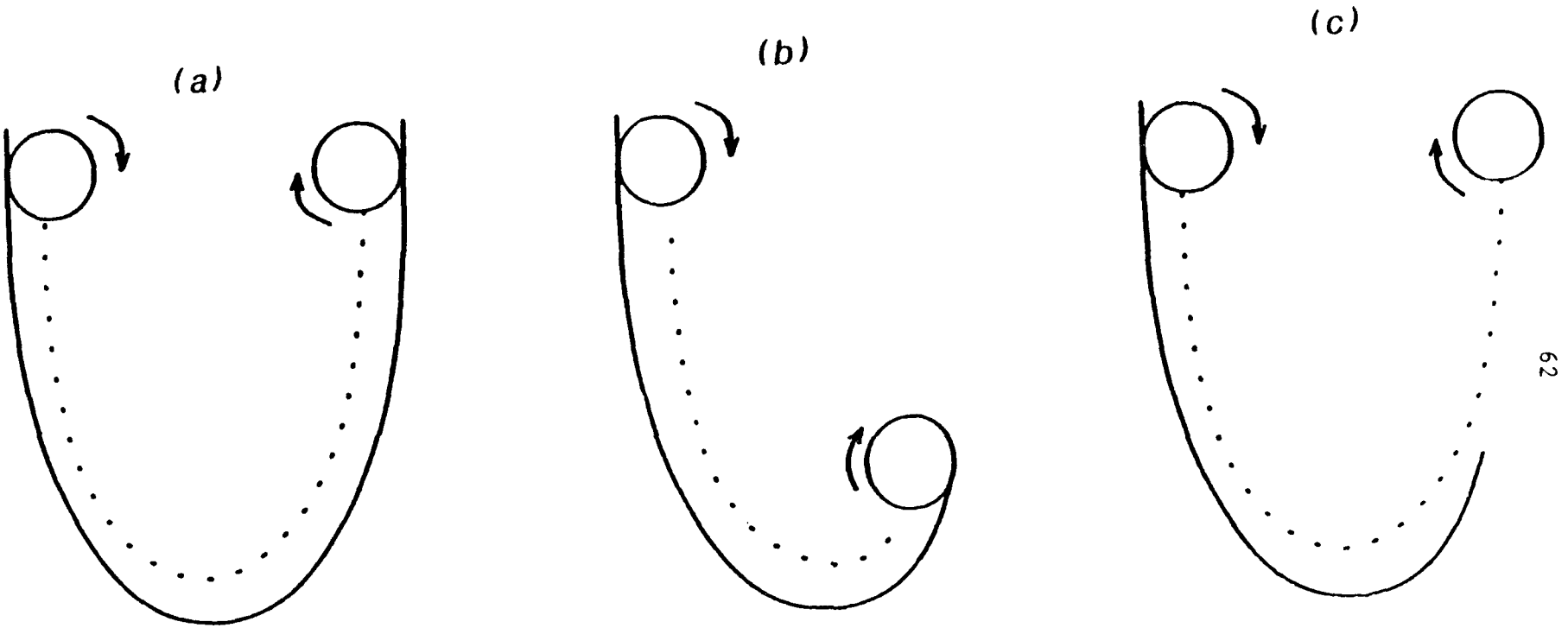

Figure 3.9

Schematic of a simplistic model to explain results of initial ion energy study. Response of ball (a) in a frictionless system, (b) experimentally observed, and (c) the expected response with the conditions in (b).

energy was being retarded. If the ball was rolling down a surface where the friction was large, the ball's acceleration would be slowed by the friction; that is, the friction would retard the ball from increasing its kinetic energy. In the post-orifice region, a supersonic jet expansion occurs as the ions and molecules go from the atmospheric side of the orifice to the vacuum side of the orifice. Since near the orifice the ions and molecules are still at a relatively high pressure (several mtorr), the bulk gas molecules undergo a lthermodynamic cooling of their translational energy through multiple collisions with each other in the supersonic jet expansion [39]. As the ions exit the orifice, they are translationally cooled along with the bulk gas molecules. The inelastic collisions the ions have with the translationally cool molecules also allows the rotational and vibrational motion of the ions to be transferred to the translationally cool molecules. Thus, the ions do not experience the full accelerating potential field because of collisional energy exchange with the more abundant neutral molecules which remain unaffected by the potential field. Further downstream in the jet, the number of collisions between the ions and the molecules decreases and this collisional cooling no longer occurs.

Figure 3.10 is stopping-potential curve (plotted on the left-hand y axis and its associated differential (plotted on the right-hand y axis) determined for CL2 with an electrically floated orifice with a potential of +120 V and with a potential for CL1 of +81.9 V. The potential of CL2 required to decelerate the average ion to rest orifice is approximately 89 V and the energy spread of the ions is

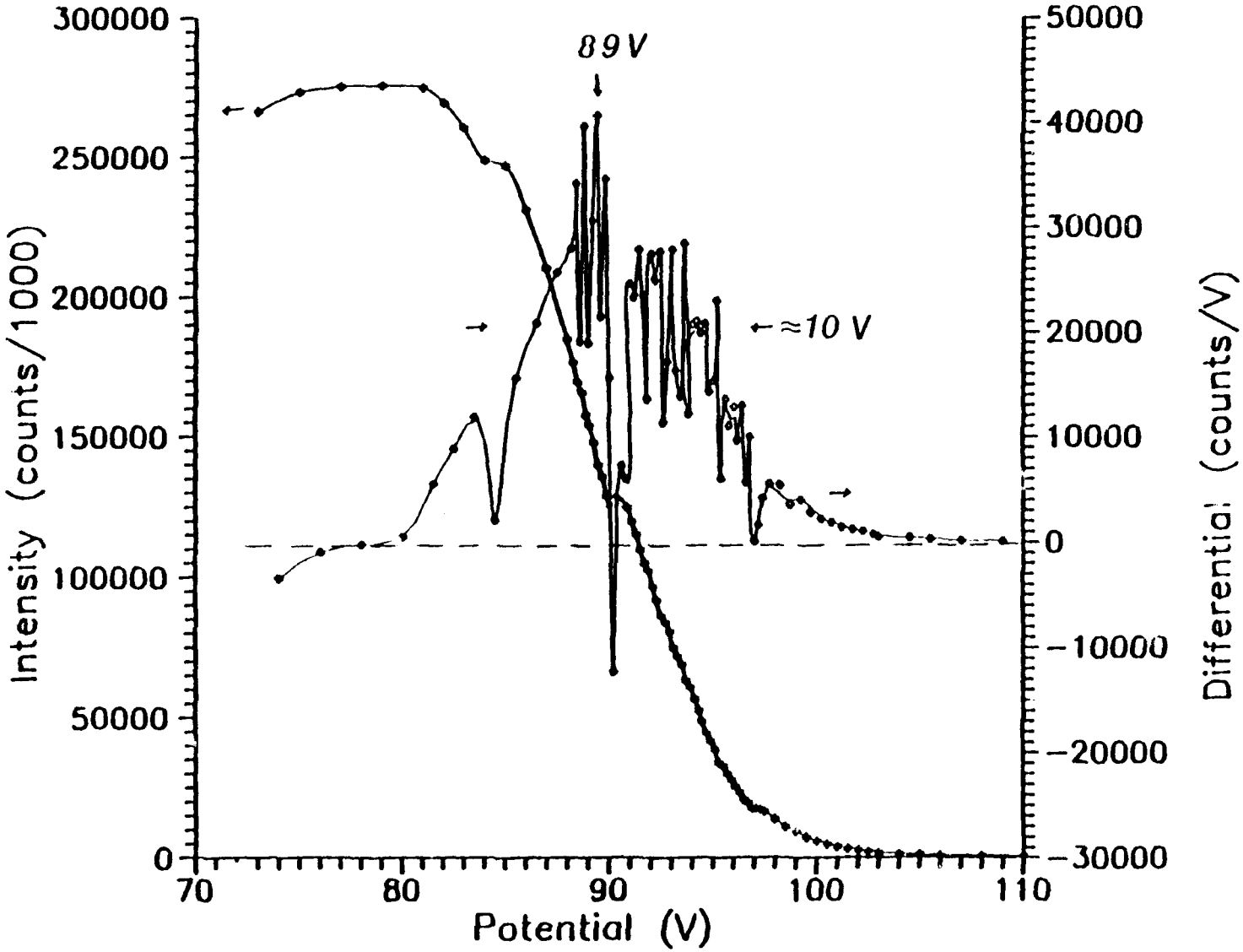

Figure 3.10

A stopping potential curve for the 2nd conical lens with a electrically floated orifice (-120 V) and the superimposed associated differential curve showing the potential required to stop an ion with the average energy and the energy spread of the ions.

approximately 10 eV. Because it required only 7.1 V to decelerate the average ion to rest, the ion therefore could only have been accelerated by 7.1 eV from the orifice to CL1 despite the 38.1 V potential difference between these components. At these higher voltages, however, there is a much greater spread in the ion energies.

Needle-to-orifice Positioning

For a discharge provided by a voltage-regulated power supply, the position of the needle was critical to the production of even a semi-stable discharge and to the number of ions which were detected by the mass spectrometer. Figure 3.11 (a) (all dimensions in inches) is a schematic representation of the needle position relative to the orifice and the orifice plate for which the greatest intensity of ions were obtained. Characteristically, the discharge was formed across the face of the orifice to the opposing sharp edge of the orifice plate. When the needle was moved across the face of the orifice towards the center axis of the orifice (Figure 3.11 (b)), the ion intensity decreased rapidly to zero. A semi-stable discharge was also obtained by moving the needle in towards the orifice (Figure 3.11 (c)); however, no ions were detected by the mass spectrometer for this needle-to-orifice position. Since the needle is at a large positive potential (≈ 4000 V), positive ions will be repelled from it and accelerated towards whatever surface is serving as the counter electrode. When the needle is in the position in Figure 3.11 (a), ions that are created in the region between the needle tip and the center axis of the orifice can be directed through the orifice by the potential field. However, when the tip of the needle is towards the center of the orifice, ions will be

Figure 3.11

Schematic representation (not to scale, 1/8" = 1") of needle position relative to orifice. Position which generates (a) a discharge across face of orifice and from which ions are detected, (b) a discharge similar to (a) but shorter in length and for which no ions are detected, and (c) a discharge to the orifice.

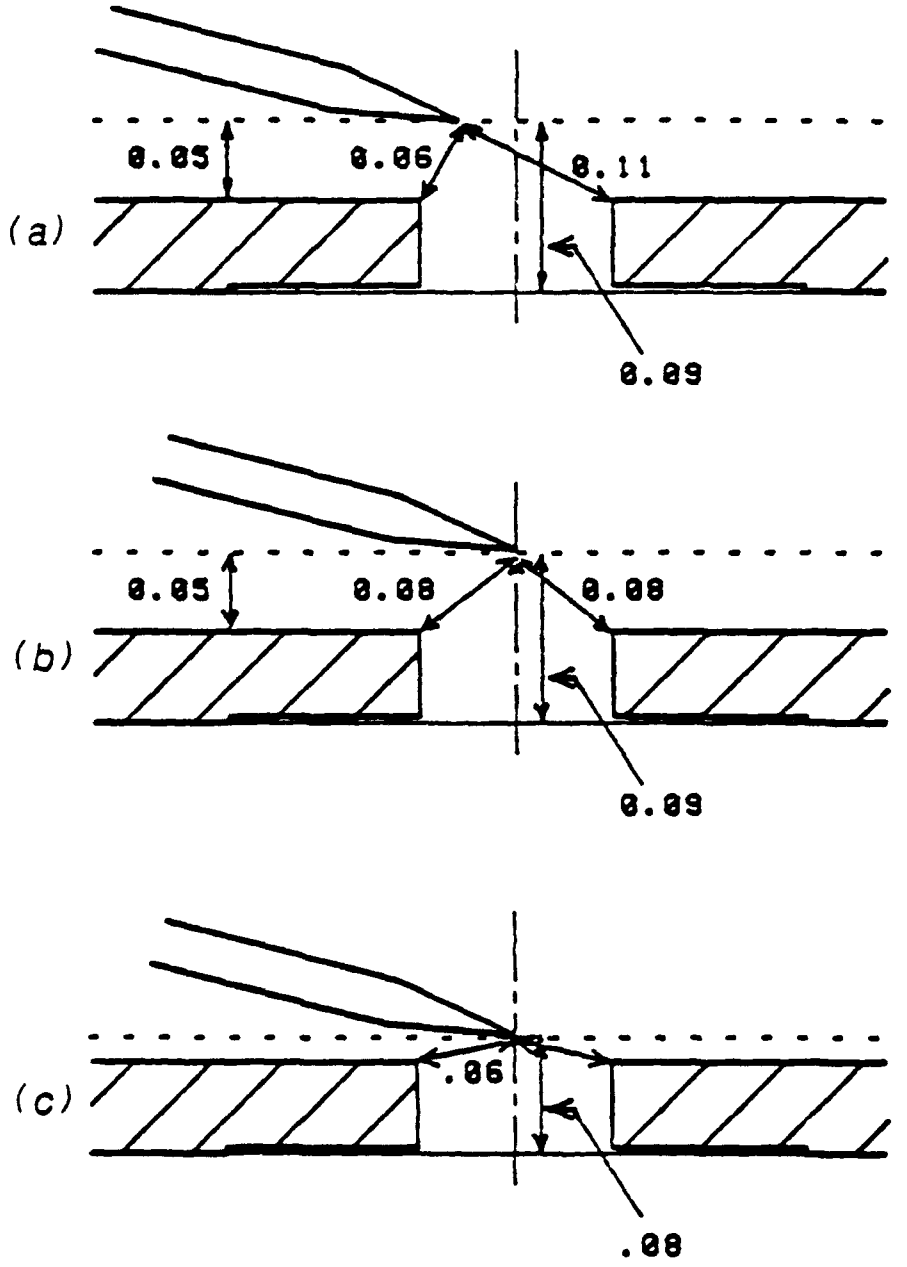
(a)
0.05
0.06
0.11
0.09
(b)
0.05
0.08
0.08
0.09
(c)
.06
.08

repelled into the diaphragm or into the source mounting plate and will not be directed through the orifice. Likewise, if the needle is moved in towards the orifice and discharges to the orifice, the potential field of the lens system will not be strong enough to direct ions through the orifice because the field generated by the discharge needle will be very strong in this region due to the close proximity of the needle to the grounded surface. For an electrically floated orifice, the position of the needle and the needle-to-orifice position are not as critical as in the case above for the production of a stable discharge and for the detection of ions. Factors that affect the discharge voltage required to produce a selected current include the gas flow rate and composition in the discharge region, the potential on the orifice, and the needle-to-orifice positions. Because of the limited output voltage (5 kV) of the dc-dc converter, the needle-to-orifice distance required to maintain a discharge is limited to only a few millimeters. However, within this range, this discharge was easily obtainable and always stable (unless the needle was shorted to the surface of the orifice plate).

Effect of Various Parameters on the Ethyl Acetate Ion Family

While the potential field from electrically floating the orifice to a positive potential causes a greater transmission of ions through the orifice, it also increases the energy spread of the ions. The ions with a very small amount of kinetic energy (<2 eV) can cluster in the post-orifice region. Ions with a large amount of kinetic energy (>7-10 eV) can undergo fragmentation through collision-induced dissociation (CID) with the bulk gas. Ions with an energy between these values can

be declustered to form molecular (M^+) or pseudo-molecular ($M+H^+$) ions [34].

When ethyl acetate (M = $CH_3CO_2CH_2CH_3$) is ionized in the API source, ions with m/z values of 177 (M_2+H^+), 125 [$M+H(H_2O)_2^+$], 107 ($M+H_3O^+$), 89 ($M+H^+$), 61 ($M+H^+ - C_2H_4$), and 29 ($C_2H_5^+$) are detected. Because of the kinetic energy spread, both cluster ions (m/z 177, 125, and 107) and fragment ions (m/z 61 and 29) are present with the pseudo-molecular ion (m/z 89). It is desirable to limit the production of both cluster and fragment ions to increase the amount of the pseudo-molecular ion that is detected. Therefore, the orifice potential and the potential of the first conical lens were varied and the intensities of members of the "ion family" of ethyl acetate (m/z 177, 107, 89, 61, and 29) were plotted vs. these values. Figure 3.12 shows the intensities of these ions plotted (m/z 125 and 61 not shown) vs. the orifice potential, while holding the potential of CL1 at +40 V. At approximately 100 V (a 60 V potential difference in the supersonic jet expansion region) the greatest intensity of m/z 89 relative to the intensities of the other ions is achieved. At lower values of the orifice potential (lower potential difference between the orifice and CL1) clustering increases, and at higher values (higher potential difference) fragmentation increases.

These same ions are plotted vs. the potential of the first conical lens, while holding the orifice at 100 V in Figure 3.13. The greatest intensity of m/z 89 relative to the intensities of the other ions occurred at ca. 36 V (approximately 2 to 1). Below this value the intensity drops off rapidly for all the ions. Above this value, all

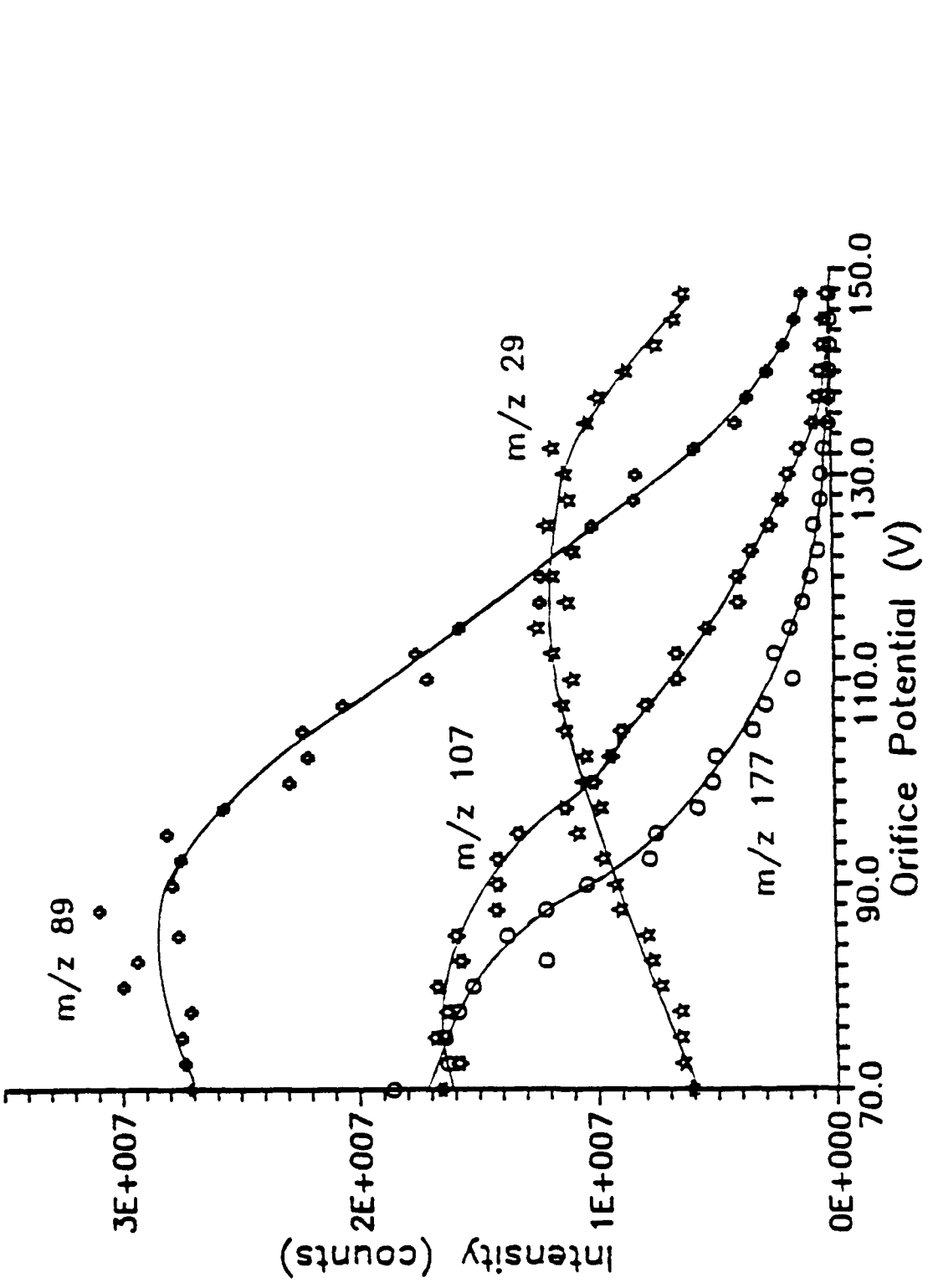

Figure 3.12

The intensities of members of the ion family of ethyl acetate (clusters, fragments, and the pseudo molecular ion) vs. the potential of the orifice with the potential of Cll = 140 V.

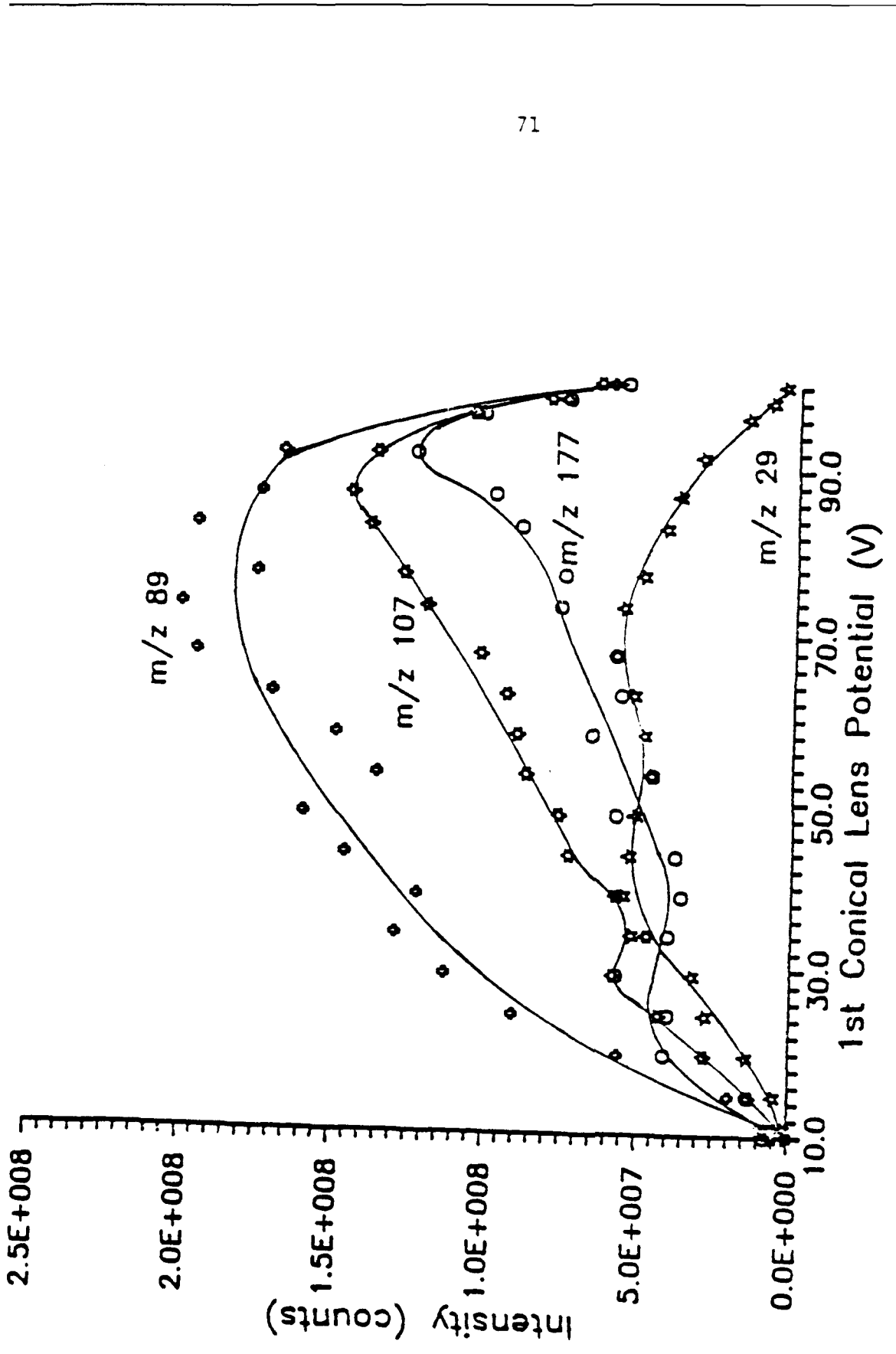

Figure 3.13

The intensities of members of the ion family of ethyl acetate (clusters, fragments, and the pseudo molecular ion) vs. the potential of CL1 with the potential of the orifice = 120 V.

the ions increase steadily in intensity until a potential of about 70 V for the conical lens, at which time the intensity of the fragment ion, m/z 29, drops off. The other ions increase in intensity until approximately 85 V when the intensities for all the ions begins to decrease. It is apparent that, with the floated orifice, both clusters and fragments will be observed because of the kinetic energy spread; however, this seems to be a worthwhile tradeoff due to the increase in intensity that the floated orifice provides.

The intensities of members of the ion family of ethyl acetate (m/z 177, 107, 89, 29) were plotted relative to the discharge current (Figure 3.14) to determine what effect the current had upon the two processes of clustering and fragmentation, as well as on the intensities of all the ions. From these data, it appears that the highest intensities of the ions and the highest ratio of the pseudo-molecular ion intensity to that of the cluster and fragment ions occur in two regions, from 0.5 to 1.2 μA and from 2 to 3 μA. The lowest discharge current that can be set is 0.5 μA, because below this value it becomes very difficult to regulate the current. Between 1.2 and 2 μA the intensity of the protonated dimer increases significantly, while the intensities of the other ions decrease. Above about 3 μA the intensities of all the ions decrease rapidly. Currently, the effect of current on the relative intensities of these ions is not yet understood.

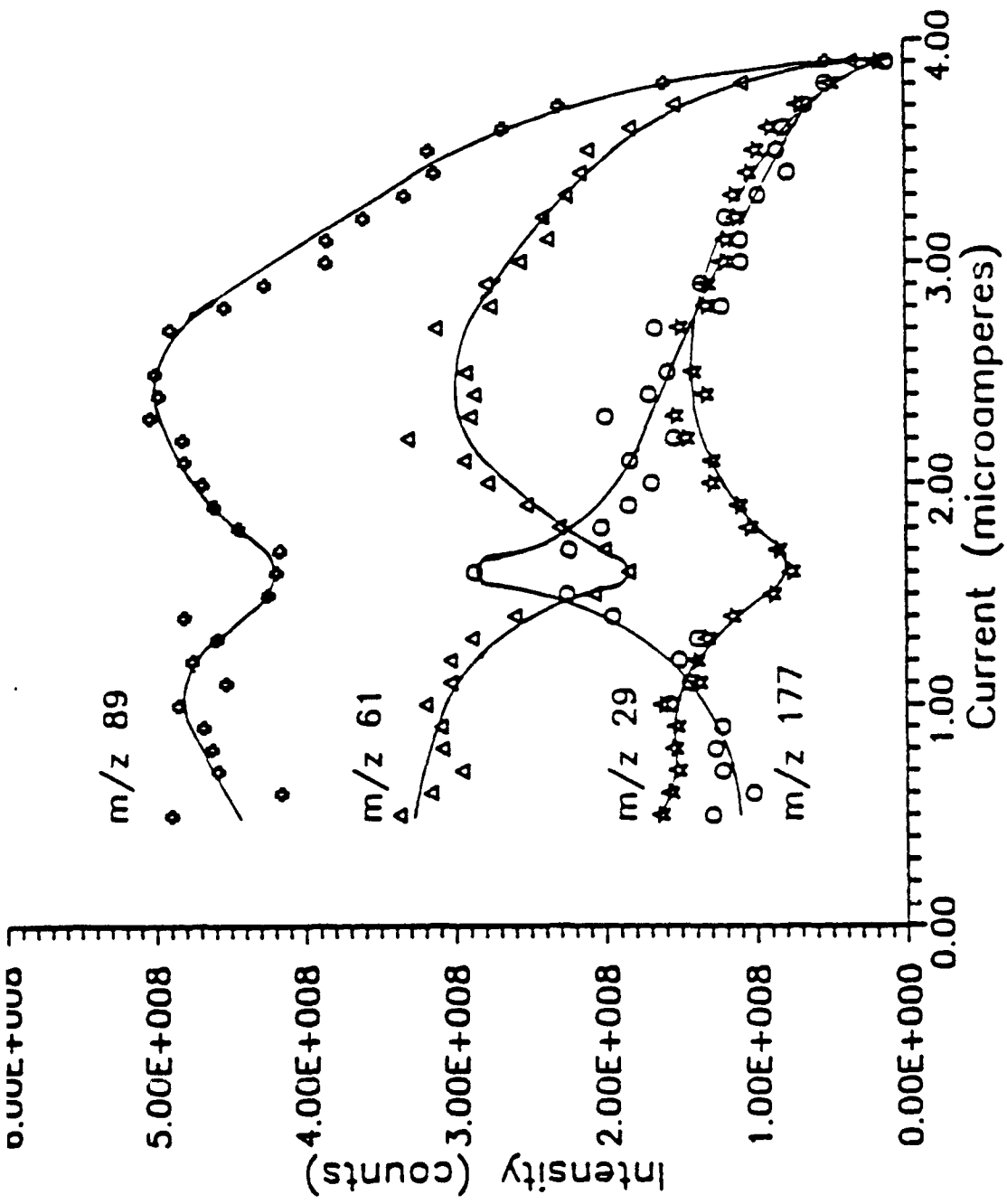

Figure 3.14

The intensities of members of the ion family of ethyl acetate (clusters, fragments, and the pseudo molecular ion) vs. the discharge current.

Clustering/Declustering

The clustering of ions with molecules in the supersonic expansion of the post-orifice region has been one of the major problems in the development of an API source for direct atmospheric monitoring. Indeed, the only source that successfully overcomes this problem has been built by Sciex [25]. This problem can be minimized in one of three ways. The first is to start with a sample that contains no water vapor, such as the effluent from a GC. Unfortunately, in direct atmospheric monitoring removing the water vapor is nearly impossible.

A second method to reduce clustering is to prevent water molecules and other neutral impurities from entering the post-orifice region. Sciex accomplishes this by drawing the ions that are formed through a pre-orifice region (enclosed by an aperture plate, to which the discharge is struck, and the orifice plate) which has been pressurized (slightly > 1 atm) with a pure, relatively inert, cryopumpable gas such as carbon dioxide (for liquid nitrogen or liquid helium cryogenic pumping) or nitrogen (for liquid helium cryogenic pumping). Sciex has referred to this region as a "gas curtain" or "ion window" [33]. In this instrument, with a less complicated one-orifice system, a gas "jet" has been produced by introducing a gas through the aperture of a 1/16" tube positioned near the orifice. With an electrically grounded orifice, this gas jet has an appreciable effect on the amount of clustering that occurs. Figure 3.15 shows mass spectra of the water cluster ions obtained (with a grounded orifice) for direct atmospheric monitoring with (a) the nitrogen on and (b) the nitrogen off. With the

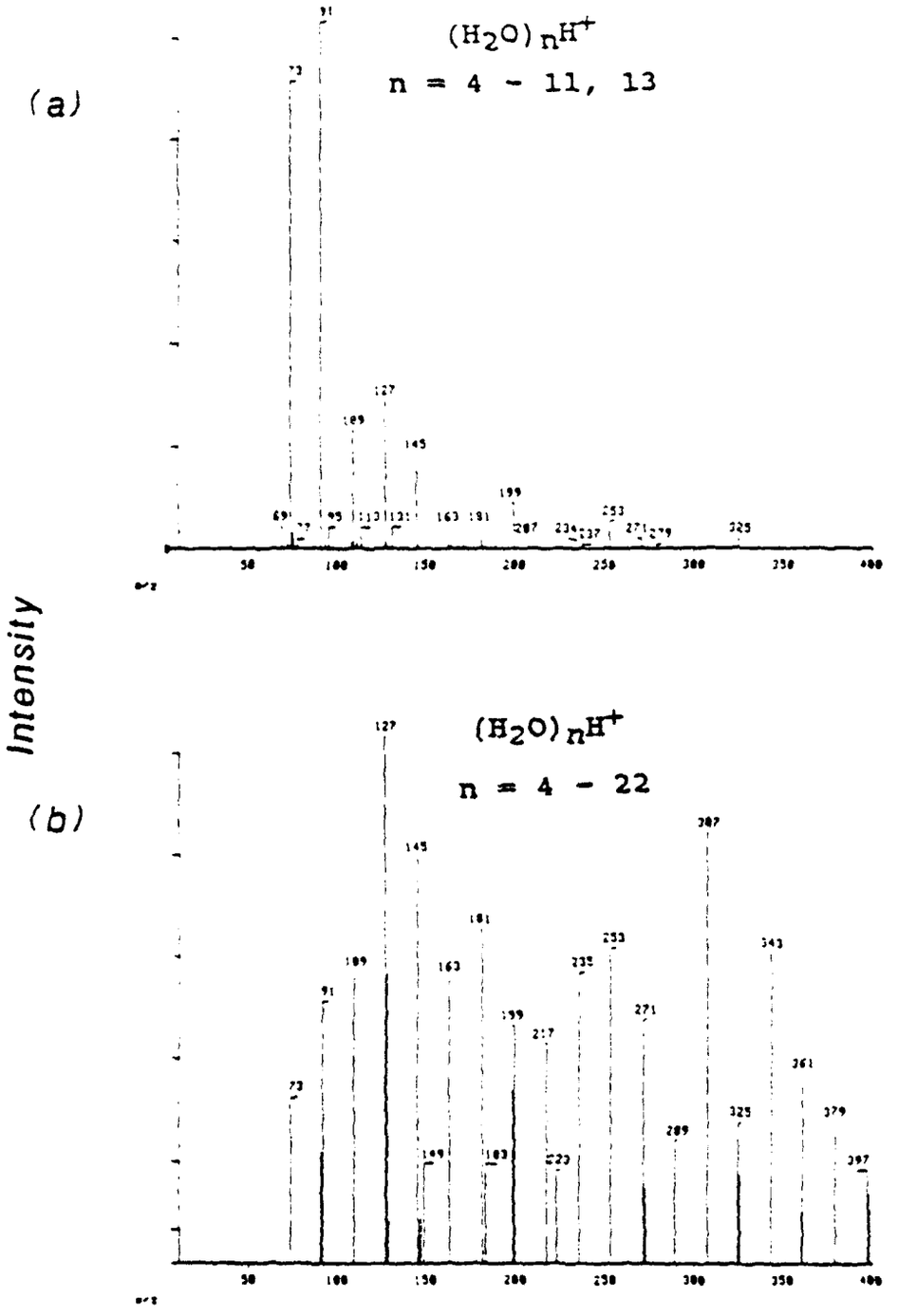

Figure 3.15

Mass spectra of background water cluster ions generated from direct atmospheric monitoring of laboratory air with nitrogen jet (a) on and (b) off.

nitrogen on, the intensities of the large cluster ions are reduced, while the intensities of the small cluster ions are increased by ≈2 orders of magnitude relative to their intensities with the nitrogen jet off.

The third method to reduce clustering is to perform collision-induced declustering in the post-orifice region. Sciex has performed this by applying a potential field in this region to impart enough kinetic energy to allow CID of the cluster ions to occur [34]. In theinstrument developed in this lab, this same effect can be observed. Figure 3.16 shows mass spectra obtained (orifice potential = +100 V and a dry compressed air jet flow rate of approximately 1 $mL \cdot min^{-1}$) for (a) a potential difference between the orifice and the first conical lens of 17 V and (b) a potential difference of 66 V (both mass spectra plotted on the same intensity scale). While the cluster ions with large m/z values are reduced, the cluster ion with small m/z values are increased (by a factor of ≈2 for m/z 37 and ≈7 for m/z 19). Furthermore, with a floated orifice (at a potential difference high enough to cause CID declustering), the gas jet appears to have no effect. Figure 3.17 (a) and (b) show the mass spectra attained with a floated orifice (potential difference = 50 V) and a nitrogen jet on and off, respectively. This same effect is observed for sample cluster ions. Figure 3.18 shows that having the gas jet (a) on or (b) off has little or no effect on the spectra obtained when ethyl acetate is analyzed by direct atmospheric monitoring by this source with a floated orifice (potential difference = 50 V). While with a floated orifice the gas jet has little effect on clustering, it may still be worthwhile

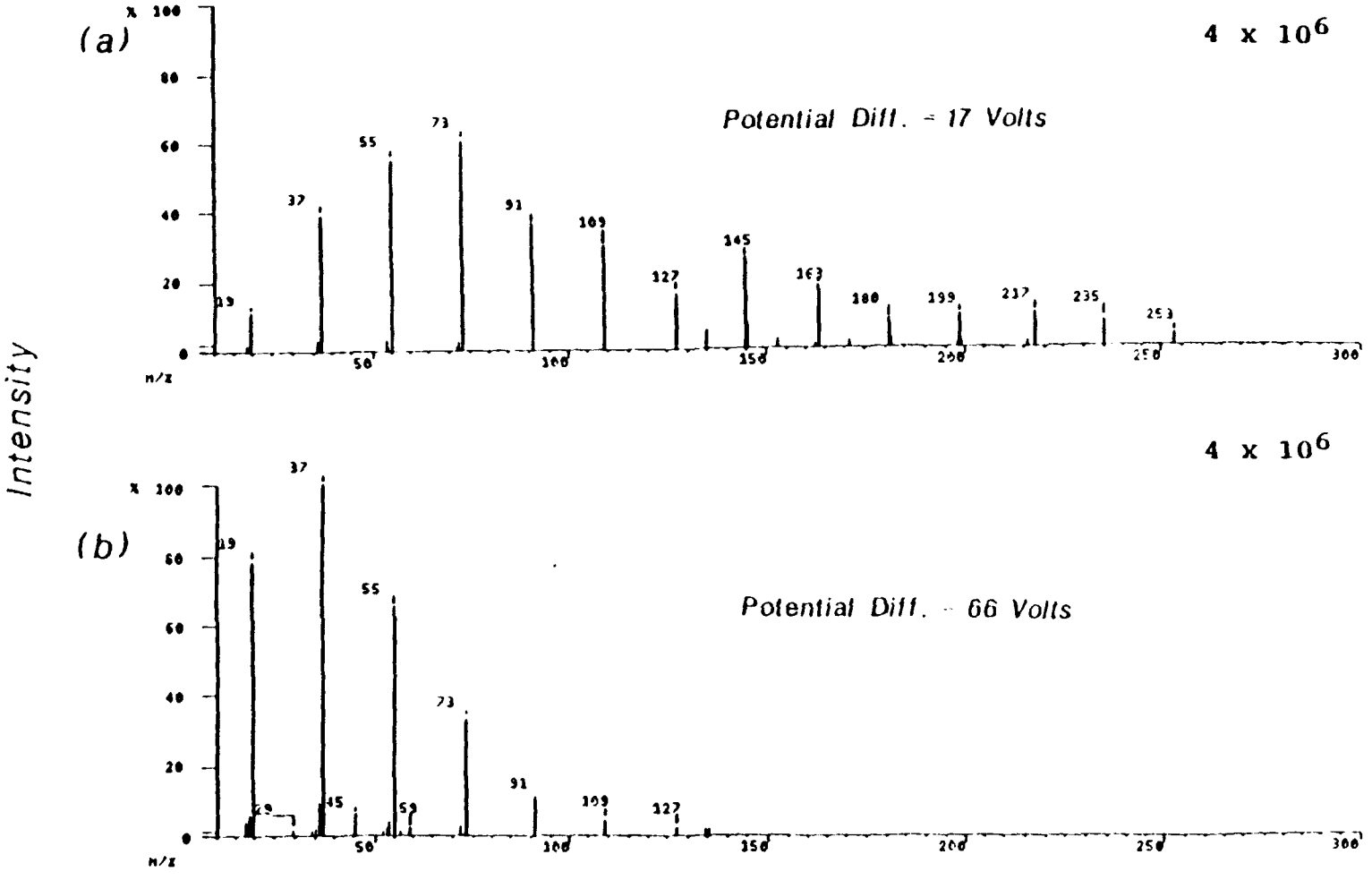

Figure 3.16

Mass spectra of background water cluster ions generated from direct atmospheric monitoring of laboratory air with the orifice potential at +100 V and a potential difference in the post-orifice region of (a) 17 V and (b) 66 V.

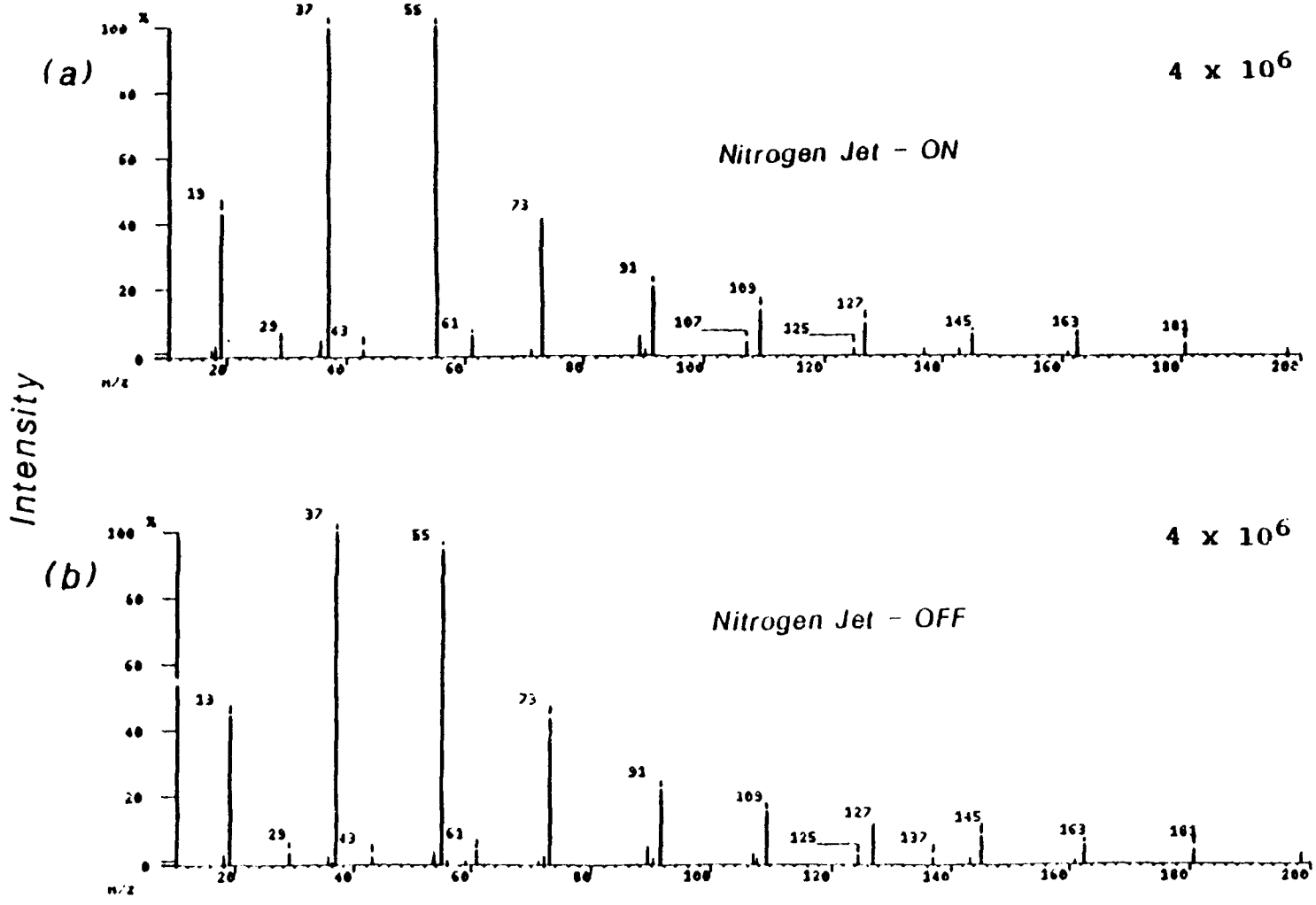

Figure 3.17

Mass spectra of background water cluster ions generated from direct atmospheric monitoring of laboratory air with a potential difference in the post-orifice region of 50 V and with the gas jet (a) on and (b) off.

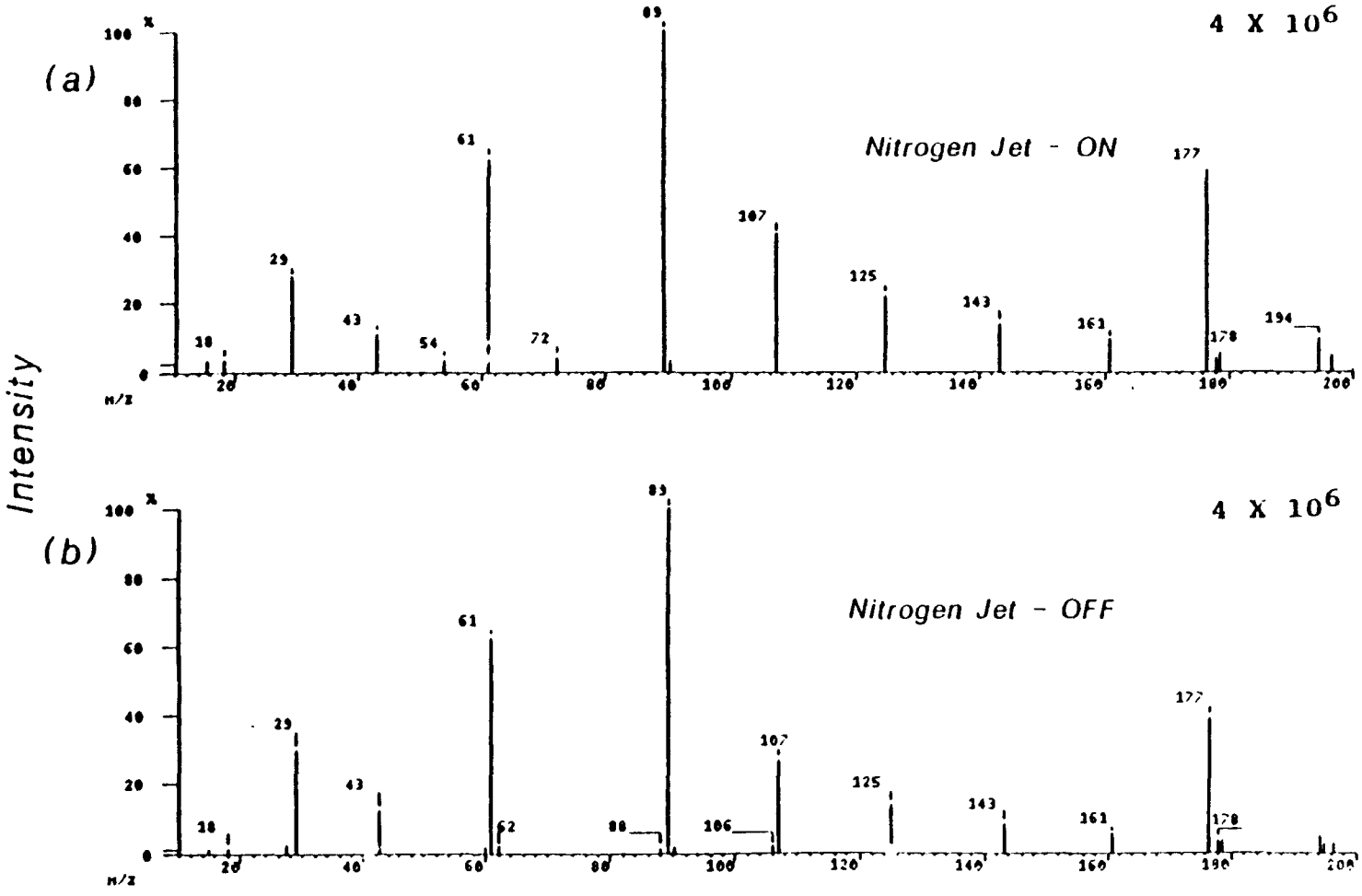

Figure 3.18

Mass spectra for direct atmospheric monitoring of ethyl acetate with the gas jet (a) on and (b) off.

to employ the gas jet to prevent orifice clogging and to reduce memory effects.

Experimental Methods for Direct Atmospheric Monitoring

Mass Calibration of API/MS/MS Instrument

In order to employ any mass spectrometer for mass analysis, the instrument must have a way to accurately assign m/z values to the signals it is obtaining. This process is called mass calibration. The tuning of a mass spectrometer usually refers to the adjustment of lens and quadrupole offset voltages so that the maximum ion intensity is obtained. In the case of a quadrupole mass spectrometer, a calibration compound which produces ions of known m/z values is analyzed (for EI/CI this is typically perflurotributylamine (FC43)). A calibration table is then generated which relates the scanning voltage of the quadrupole to the correct m/z value. These values can be compared to the voltages needed to pass ions, of otherwise unknown mass, from other samples to calculate their m/z values. Although mass calibration for this instrument does not change while switching between EI and CI, the installation of this source requires a new lens system which results in the need to re-calibrate and re-tune for API. Since background ions are abundant in API/MS, water cluster ions (no API ions were detected for FC43) are used to calibrate the instrument and perform lens tuning, after which sample gases may be analyzed. As can be ascertained from the spectra shown in this thesis, this method for tuning and mass

calibration proved efficient at the unit mass resolution of the quadrupole mass analyzers.

Sampling Methodology

All vapors analyzed by direct atmospheric monitoring were generated by drawing air across the caps from bottles of liquid compounds. For studies which required a steady concentration of sample for long periods of time (such as calibration and tuning), a few drops of compound were placed in the bottle cap and the cap was placed in front of the 1" diameter glass sampling tube of the API source. Although the vapor pressure of the liquid samples can be estimated, the amount of sample introduced is not accurately known, and absolute determination of the API/MS/MS instrumental sensitivity or LOD is therefore not possible.

CHAPTER 4

ANALYTICAL PERFORMANCE

To evaluate the performance of an analytical instrument, several factors may be considered; however, not all factors are necessarily important for all types instruments. For an instrument which performs direct atmospheric analysis, these factors include the ability of the instrument to identify the sample it is analyzing, the ability of the instrument to detect trace amounts of the sample, the ability of the instrument to distinguish between compounds in the same sample, memory and interference effects in the analysis, ease of use of the instrument, and the time required for sample analysis (including equilibration time between samples).

Characterization of an API/MS/MS Instrument

Analyses of Pure Compounds

With the source configuration for the Finnigan 4500 quadrupole mass spectrometer, clustering proved such a large problem that direct atmospheric monitoring was nearly impossible. Indeed, even solvent vapors injected into a pure nitrogen stream displayed cluster ions as the predominant ions detected (Figures 3.3 and 3.4). In the source design for the TSQ 70 with a nitrogen jet, the instrument can be tuned to significantly minimize the clustering, even while performing direct atmospheric analyses. Figure 4.1 (a) - (c) shows mass spectra obtained

Figure 4.1

Direct atmospheric monitoring/API/MS of compounds that undergo charge exchange ionization (a) carbon disulfide, (b) benzene, and (c) toluene.

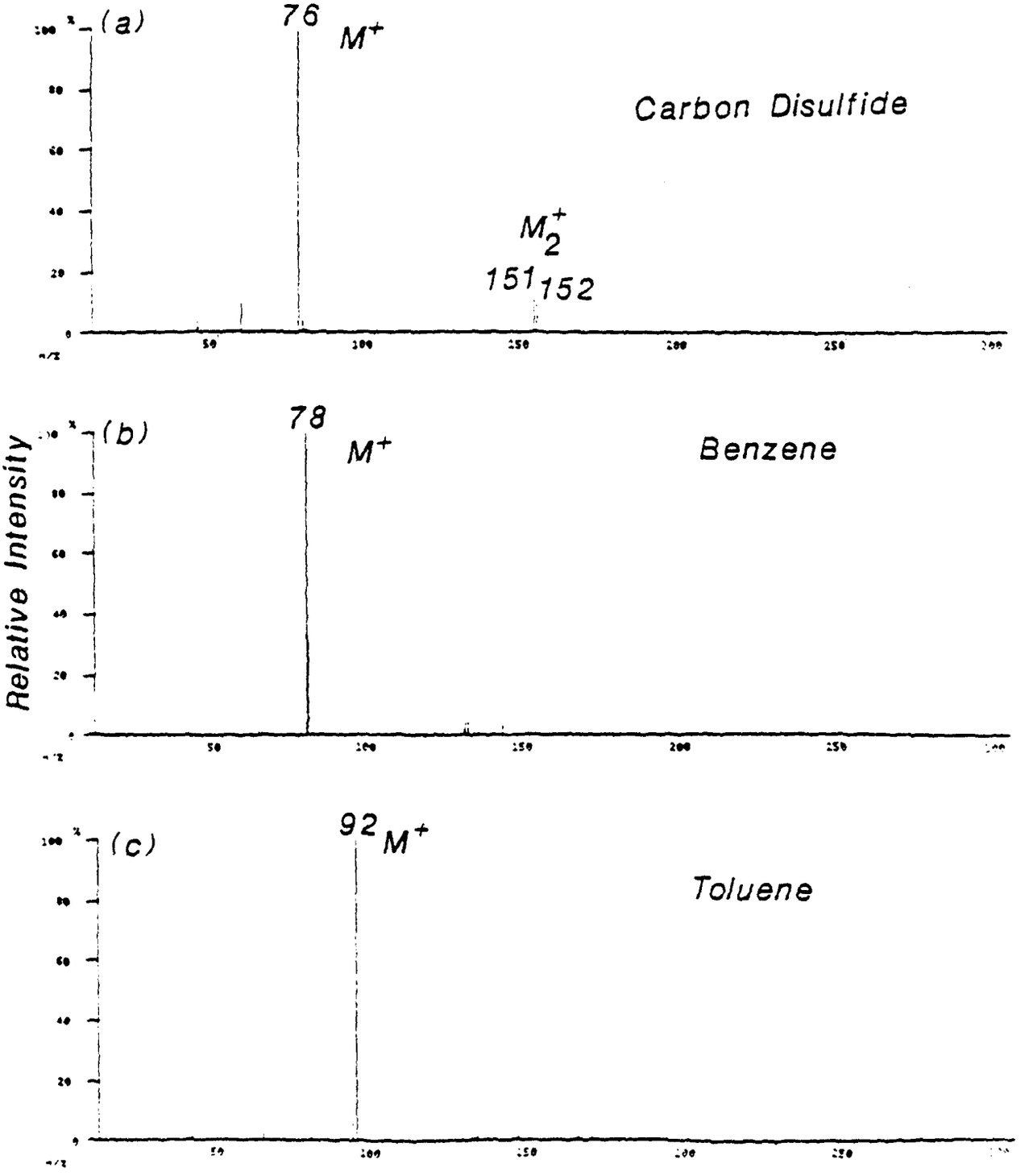
(a)
76
M+
Carbon Disulfide
M2+
151
152
(b)
78
M+
Benzene
Relative Intensity
(c)
92
M+
Toluene

(with a grounded orifice and a voltage-regulated power supply) while performing direct atmospheric monitoring of representative compounds which undergo charge exchange ionization in the API source, carbon disulfide (MW 76), benzene (MW 78), and toluene (MW 92), respectively. These compounds each form almost exclusively the M^+ molecular ion, with carbon disulfide forming a small amount of the M_2^+ dimer ion. Figure 4.2 (a) - (c) shows mass spectra obtained (with a grounded orifice) while performing direct atmospheric monitoring of representative compounds which undergo proton transfer ionization in the API source, acetone (MW 58), ethyl acetate (MW 88), and methanol (MW 32), respectively. Acetone and ethyl acetate both form almost exclusively the $(M+H)^+$ pseudo-molecular ion. The most predominant ion for methanol is the $(M_2+H)^+$ protonated dimer ion. While the signal obtained under these conditions for these samples was not sufficient to perform tandem mass spectrometry (MS/MS), these results demonstrate that this API source can reduce clustering significantly.

Figure 4.3 shows the reconstructed ion current (RIC) traces for the two most predominant background ions (when the instrument is tuned for large amounts of declustering and analysis is performed by bringing caps of solvent bottles near sampling tube of API source) (a) $(H_2O)_2H^+$ (m/z 37) and (b) $(H_2O)_3H^+$ (m/z 55), two representative sample ions (c) $C_6H_6^+$ and (d) $(CH_3CO_2C_2H_5)H^+$, and (e) all the ions. In normal EI mass spectrometry, sample ionization occurs by the bombardment of the sample molecules with electrons from a filament. In positive CI mass spectrometry, ionization occurs through charge exchange or proton transfer with ions created from a reagent gas. Usually, however, these

Figure 4.2

Direct atmospheric monitoring/API/MS of compounds that undergo proton transfer ionization (a) acetone, (b) ethyl acetate, and (c) methanol.

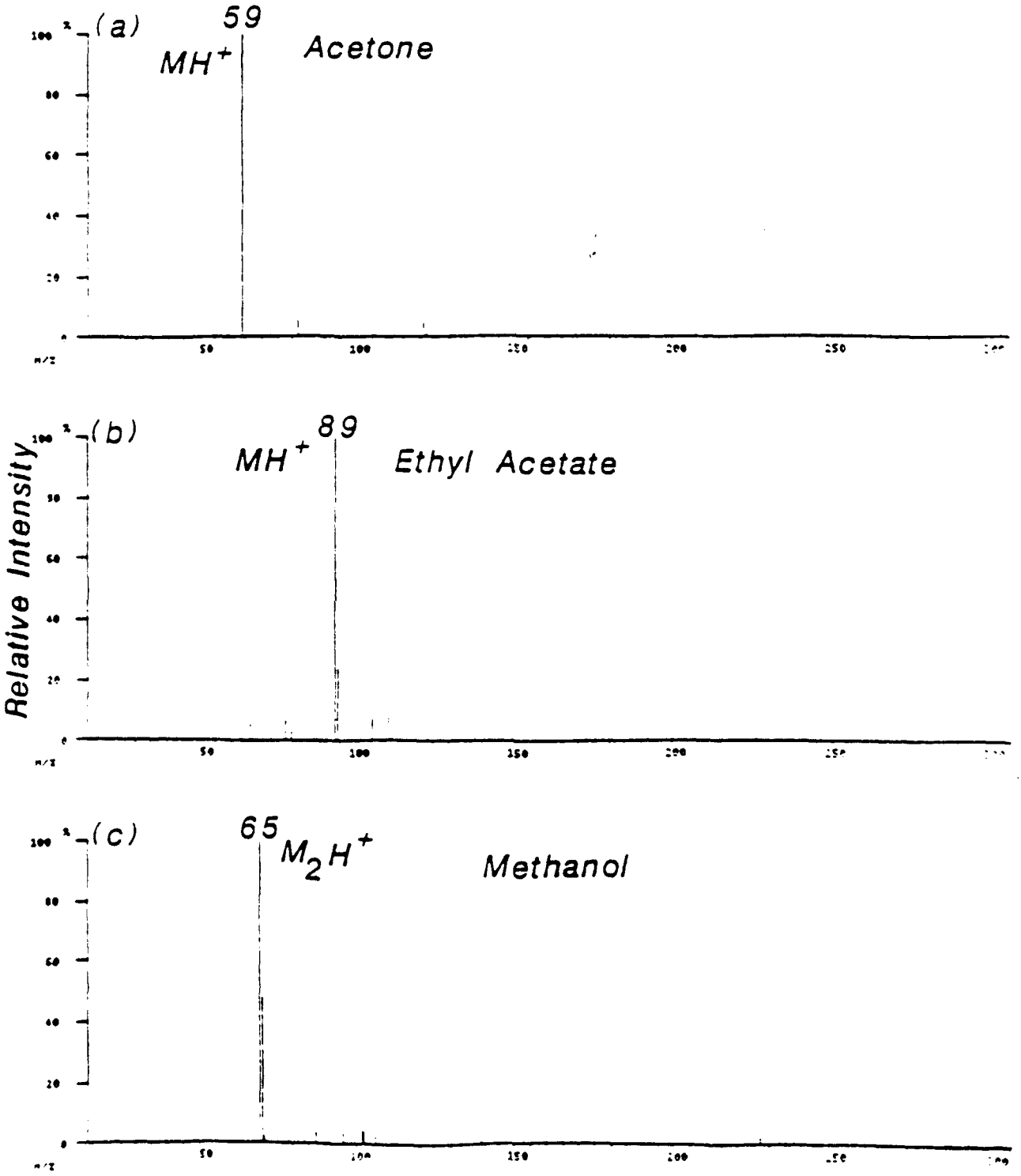
(a)
59
MH+
Acetone
(b)
89
MH+
Ethyl Acetate
Relative Intensity
(c)
65
M2H+
Methanol

Figure 4.3

RIC traces for the two most predominant background ions (a) $(H_2O)_2H^+$ and (b) $(H_2O)_3H^+$, two representative sample ions (c) $C_6H_6^+$ and (d) $(CH_3CO_2C_2H_5)H^+$, and (e) all the ions.

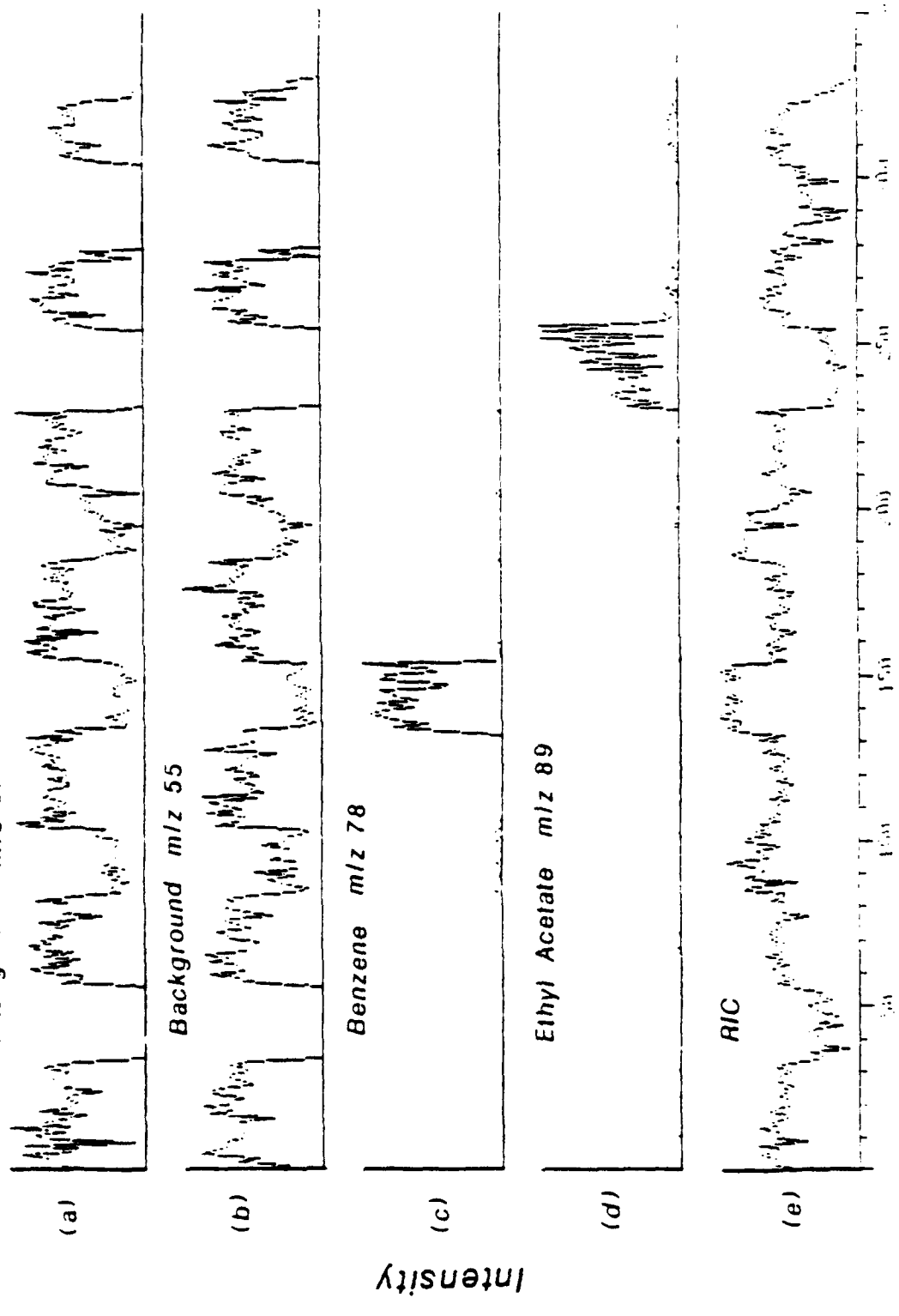
Background m/z 37
Background m/z 55
Benzene m/z 78
Ethyl Acetate m/z 89
RIC
(a)
(b)
(c)
(d)
(e)
Intensity
Scan #

reagent ions are low in m/z value and the mass spectrometer can be set up to pass only ions of a greater mass. Ionization in API mass spectrometry occurs in a similar fashion to CI mass spectrometry (see Chapter 1). In direct atmospheric monitoring mass spectrometry, air serves as the reagent gas, generating N_2^+, H_2O^+, and H_3O^+ ions (equations 1.2 - 1.5). Sample molecules (M) can react with the reagent ions through charge exchange or proton transfer reactions to form M^+ molecular or $M+H^+$ pseudo-molecular ions. The kinetics of the production of ions in discharges at atmospheric pressures has been studied by Shahin [10] and Kebarle [44]. Shahin stated that for direct atmospheric sampling (or for any samples with even a small quantity of water vapor) the production of H_2O^+ (by charge exchange with the initial N_2^+ ions) and H_3O^+ ions would be the dominant reactions. In the case of either charge or proton transfer ionization reactions, the intensity of the reagent ions is reduced as the sample is ionized. Samples that undergo proton transfer ionization may totally deplete the population of the background ions, while samples that undergo charge transfer ionization reduce but do not deplete that population. Figure 4.4 shows the relationship between the intensity of the reagent ions with respect to the time allowed for reaction. Equations 4.1 - 4.3 [44] give the rate constants for the production of H_2O^+, H_3O^+, and $H(H_2O)_n^+$.

$$N_2^+ + H_2O \rightarrow N_2 + H_2O^+ \quad k = 1.9 \times 10^{-9}\ cm^3 \cdot molecule^{-2} \cdot s^{-1} \qquad (4.1)$$

$$H_2O^+ + H_2O \rightarrow H_3O^+ + HO \quad k = 1.8 \times 10^{-9}\ cm^3 \cdot molecule^{-2} \cdot s^{-1} \qquad (4.2)$$

$$H_3O^+ + nH_2O \rightarrow H(H_2O)_{n+1}^+ \quad k \approx 10^{-27}\ cm^3 \cdot molecule^{-2} \cdot s^{-1} \qquad (4.3)$$

Figure 4.4

The kinetics of the production of ions in corona discharges at atmospheric pressure. Generated with the results from a BASIC program utilizing the kinetics of the reactions in Equations 4.1 - 4.3. Study limited to generation of termolecular water cluster.

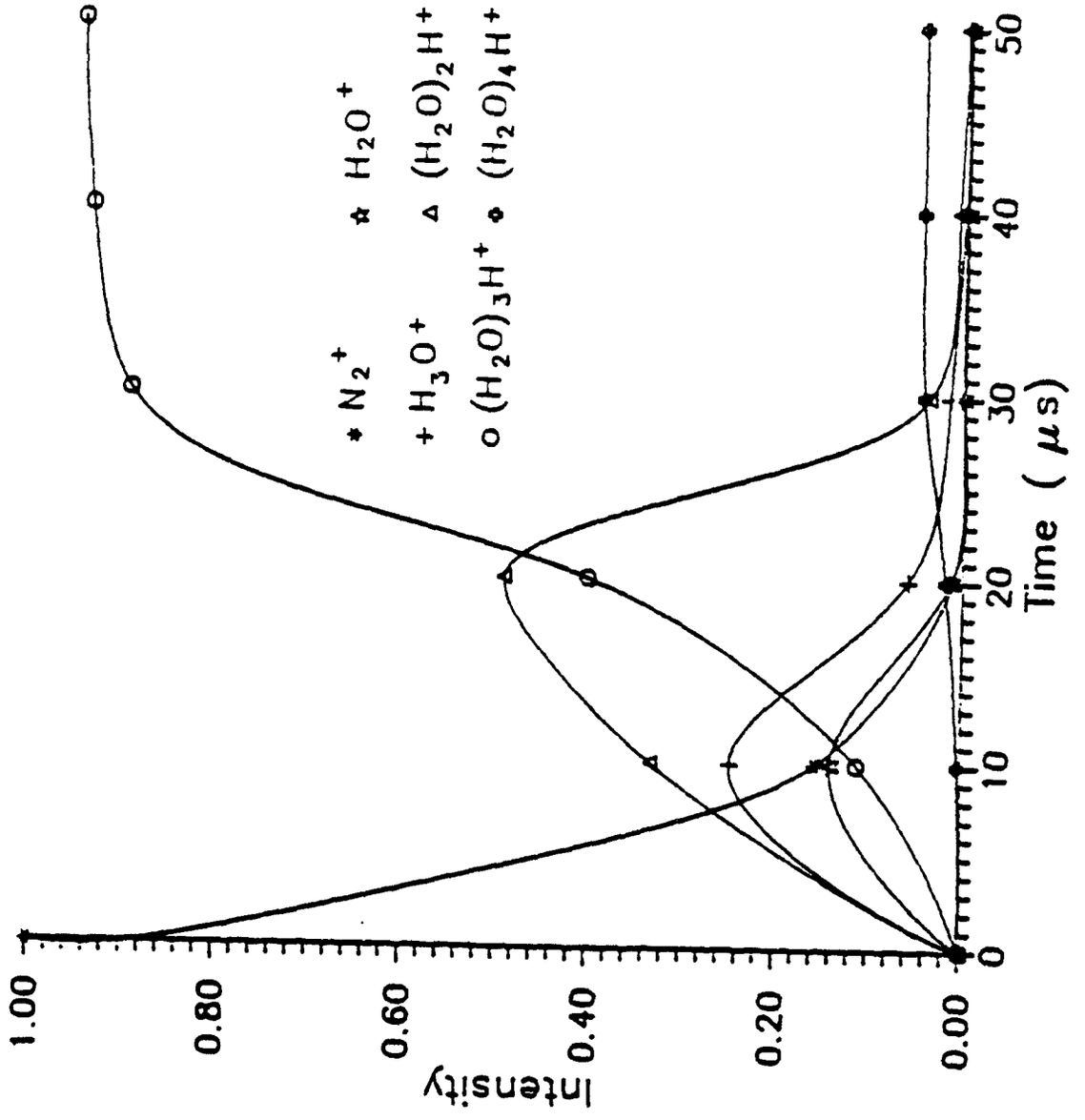
1.00
0.80
0.60
0.40
0.20
0.00
Intensity
0
10
20
30
40
50
Time (μs)
* N_2^+
☆ H_2O^+
+ H_3O^+
△ $(H_2O)_2H^+$
○ $(H_2O)_3H^+$
◆ $(H_2O)_4H^+$

sample molecules with H_2O^+ and H_3O^+ are on the order of 3 x 10^{-9} $cm^3 \cdot molecule^{-2} \cdot s^{-1}$ [45]. Proton transfer reactions with sample molecules will thus consume H_3O^+ before it can further react to form $(H_2O)_2H^+$ (m/z 37) and $(H_2O)_3H^+$ (m/z 55). Charge transfer reactions with sample molecules cannot consume all the H_2O^+ before some of it can be converted to H_3O^+ and therefore, the population of $(H_2O)_2H^+$ (m/z 37) and $(H_2O)_3H^+$ (m/z 55) will be reduced but not depleted.

Memory effects

The RIC traces for the benzene molecular and ethyl acetate pseudo-molecular ions (Figure 4.4) show that, as the sample is brought to the sampling tube, the signal immediately increases and as it is removed, the signal decreases rapidly to zero. This would indicate that memory effects have been minimized with this source; however, it should be pointed out that this source has yet to be applied to trace analysis, and this application would give a much better indication of memory effects.

Orifice Clogging

Orifice clogging proved to be a severe problem with both the Finnigan developed API source and the one developed in this work for the Finnigan 4500 quadrupole mass spectrometer. The major reasons for this problem was that there was no way to prevent particulate matter in the sample gas stream from reaching the orifice. With the addition of the gas jet near the orifice, this problem has been almost eliminated. When the orifice does become clogged (maybe once or twice a day), a gas jet of relative high pressure (≈ 20 - 40 psi) may be directed at the orifice to dislodge any matter. Occasionally, when all else has

failed, the instrument has needed to be vented to atmospheric pressure and the orifice removed and cleaned with an appropriate solvent (methylene chloride). The diaphragms are surprisingly rugged and a single diaphragm has been used for several months of source development and sample analysis while the API source has been installed on the TSQ 70.

Analytical Potential

Compound Identification

An instrument must be able to distinguish between different compounds to be of analytical use. This may be done by separating compounds in time and using a universal detector, by analyzing all compounds at the same time with a detector that provides a different response for each compound, or by some combination of both of these techniques. A single stage of mass analysis can be used with low energy ionization techniques (such as CI, fast atom bombardment, or API) to determine the molecular weight of a compound, or with high energy ionization techniques (such as EI) to provide fragment ions which can be used for structure elucidation. Therefore, mass spectrometers are commonly used with some type of pre-separation step before mass analysis, such as GC, LC, or MS. When API/mass spectrometry is used for direct atmospheric monitoring, by definition there is no opportunity for any pre-ionization separation.

Methyl benzoate (MW 136) and methoxy benzaldehyde (MW 136) are examples of compounds with the same empirical formula and the same

molecular weight that form ions with the same m/z value. Both of these compounds produce an intense $M+H^+$ pseudo-molecular ion (m/z 137), as well as some less intense fragmentation ions when ionized by this API source with the potential difference of the supersonic jet expansion region set at ≈ 50 V (Figure 4.5 (a) and (b)). In a normal API/MS system, it would be difficult to determine the presence of one or both of these compounds and distinguish between them (or other compounds that have MW 136 and form ions through proton transfer reactions). However, because the TSQ 70 is an MS/MS instrument, the pseudo-molecular ion can be fragmented in the center quadrupole to obtain a daughter spectrum (spectrum of fragment ions from a parent ion) of the m/z 137 ion. Figure 4.6 (a) and (b) show the daughter spectra (each under the same conditions of collision energy = 15 eV and pressure of nitrogen collision gas = 2 torr) for methyl benzoate and methoxy benzaldehyde, respectively. Major daughter ions observed for the API-generated $M+H^+$ ion from methyl benzoate are m/z 59 $[(M+H)-C_6H_6]^+$, 77 $[(M+H)-CH_3COOH]^+$, 91 $[(M+H)-HCOOH]^+$, 93 $[(M+H)-CH_3CHO]^+$, 105 $[(M+H)-CH_3OH]^+$, and 109 $[(M+H)-CO]^+$. Major ions observed for the $M+H^+$ ion from methoxy benzaldehyde are m/z 77 $[(M+H)-CO-CH_3OH]^+$, 94 $[(M+H)-CO-CH_3]^+$, and 109 $[(M+H)-CO]^+$. There is a clear difference in these daughter spectra, and thus the compounds can be distinguished.

A concern about API has been its ability to analyze mixtures of samples. Figure 4.7 shows a spectrum of a solvent mixture composed of benzene (MW 78), ethyl acetate (MW 88), benzaldehyde (MW 106), and methoxy benzaldehyde (MW 136), obtained when the API source was used with a floated orifice (potential difference of supersonic jet

Figure 4.5

Direct atmospheric monitoring/API/MS spectra of (a) methyl benzoate and (b) methoxy benzaldehyde.

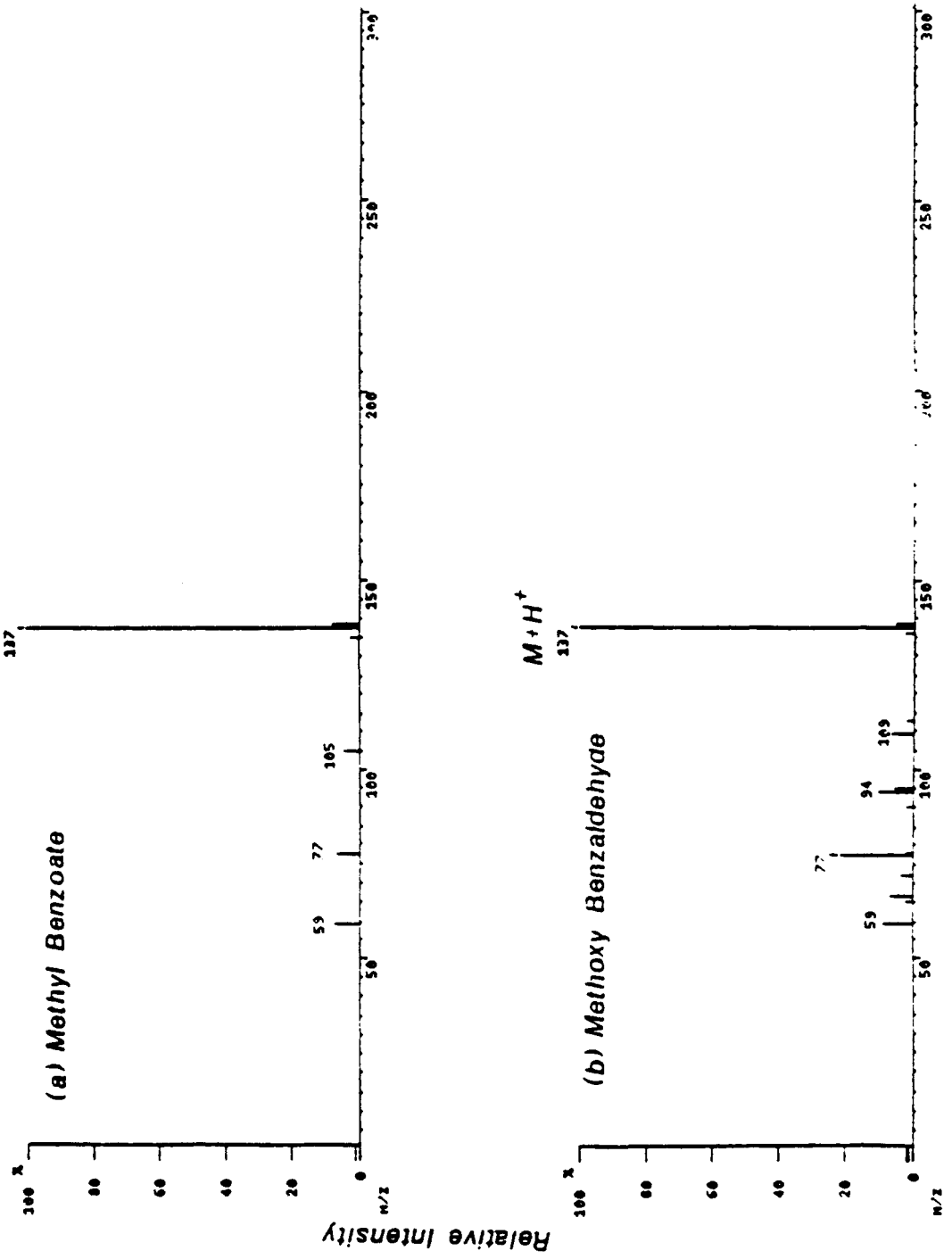
(a) Methyl Benzoate
M+H+
137
105
77
59
(b) Methoxy Benzaldehyde
M+H+
137
105
94
77
59
Relative Intensity
m/z

Figure 4.6

Direct atmospheric monitoring/API/MS/MS spectra of (a) methyl benzoate and (b) methoxy benzaldehyde with collision energy = 20 eV and collision pressure = 2 torr N_2.

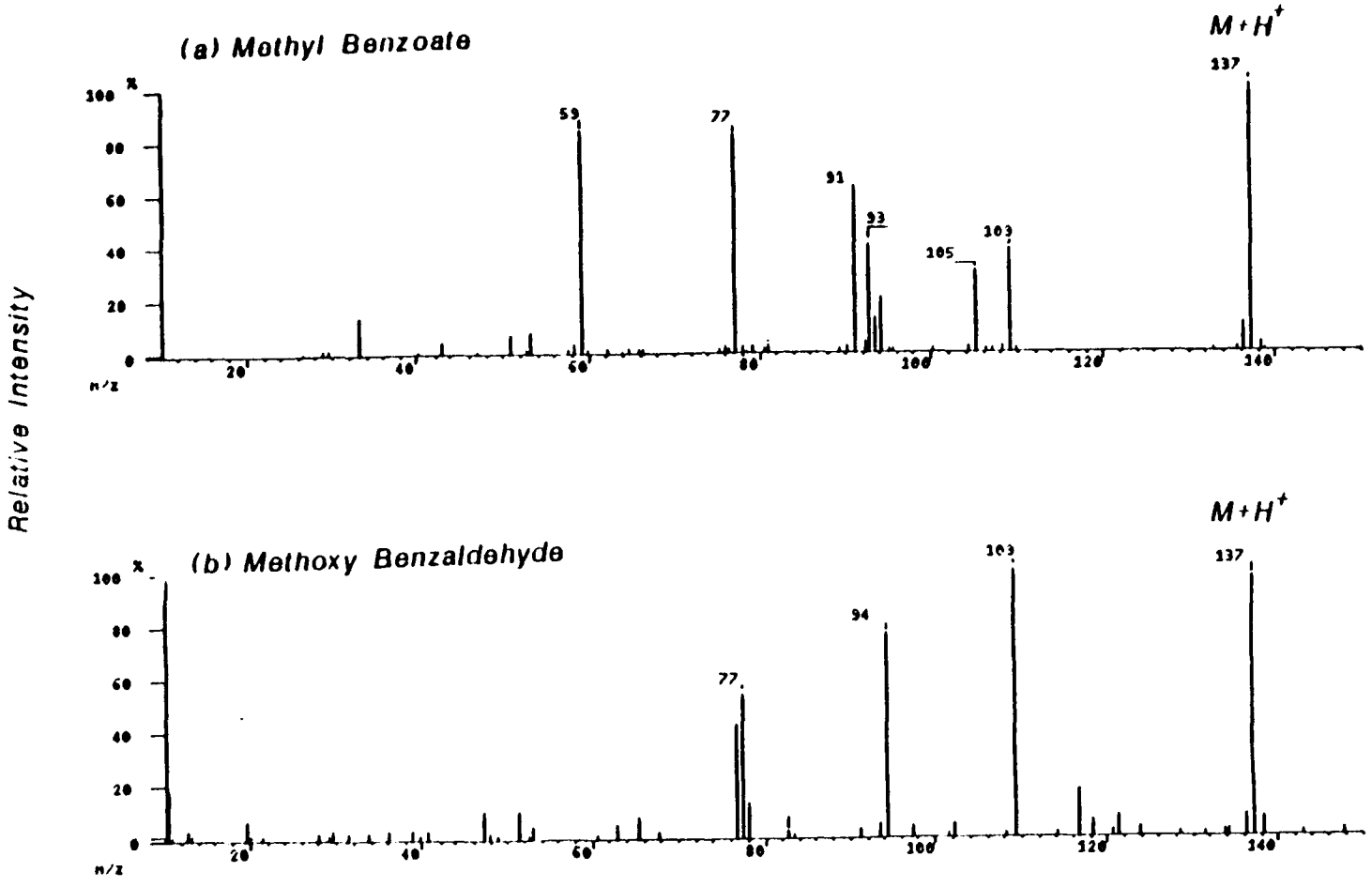
(a) Methyl Benzoate
M+H+
137
59
77
91
93
105
103
100
80
60
40
20
0
%
m/z
20
40
60
80
100
120
140
Relative Intensity
(b) Methoxy Benzaldehyde
M+H+
103
137
94
77

Figure 4.7

Direct atmospheric monitoring/API/MS spectra a solvent mixture composed of benzene (MW 78), ethyl acetate (MW 88), benzaldehyde (MW 106), and methoxy benzaldehyde (MW 136).

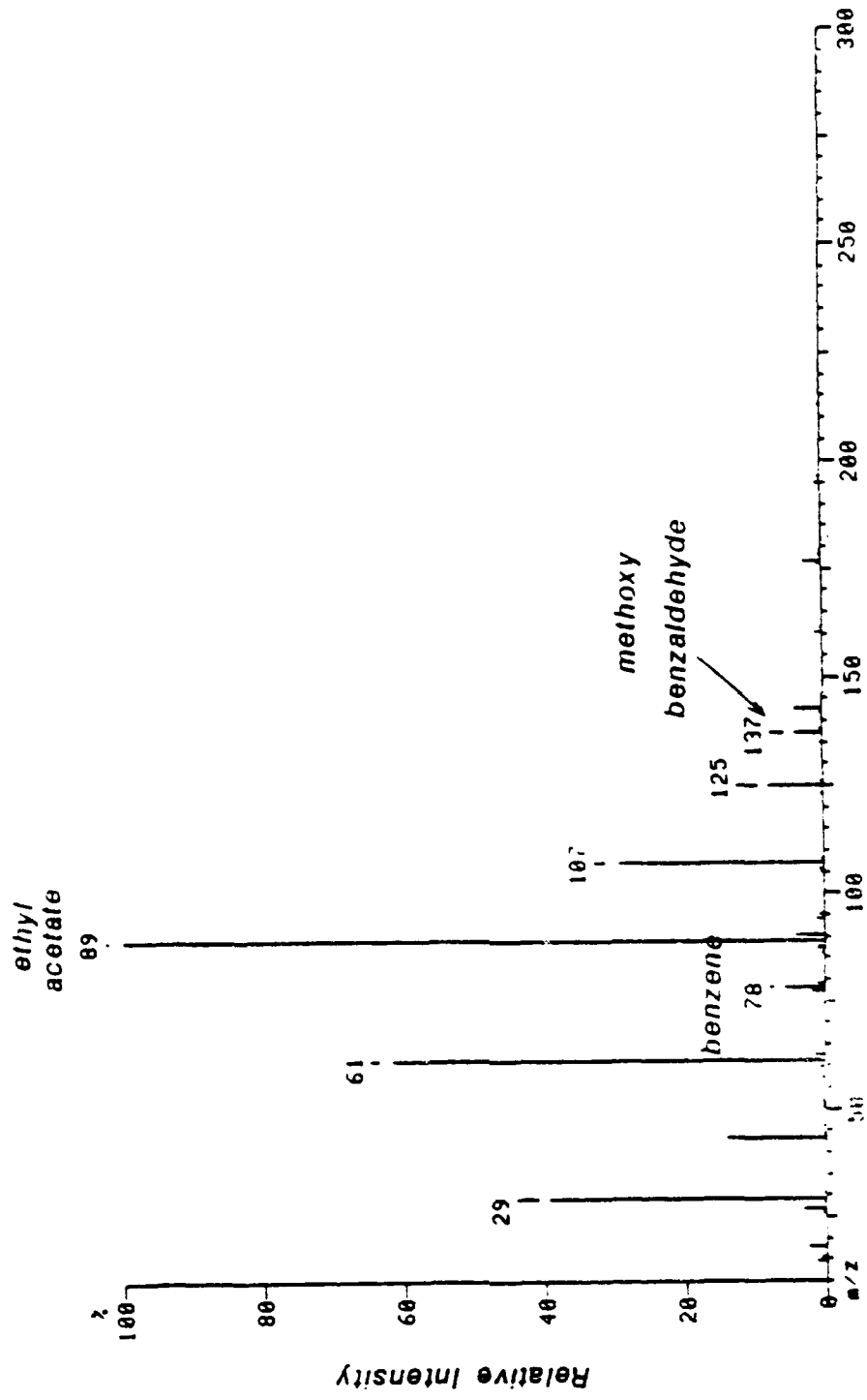
Relative Intensity
%
100
80
60
40
20
0
m/z
29
61
78
89
107
125
137
ethyl acetate
benzene
methoxy benzaldehyde
100
150
200
250
300

expansion region ≈ 50 V) and tuned for a high degree of declustering. The pseudo-molecular ion (m/z 89) from ethyl acetate clearly dominates the spectrum and a small quantity of the protonated dimer (m/z 177) is present. Fragment ions of ethyl acetate are also observed at m/z 29 ($C_2H_5^+$) and m/z 61 ($CH_3COCH_2^+$). However, ions from benzene (m/z 78) and methoxy benzaldehyde (m/z 137) are clearly present. There is some confusion as to the identities of m/z 107 and m/z 125. Because of the large intensity of ethyl acetate it is possible that these ions are cluster ions of ethyl acetate ($M+(H_2O)H^+$ and $M+(H_2O)_2^+$) or that they are related to benzaldehyde ($M+H^+$ and $M+(H_2O)H^+$). Unfortunately, the low intensity of these ions made it difficult to obtain their daughter spectra, and therefore, this uncertainty was left unresolved.

Sensitivity

The sensitivity of this API/MS/MS instrument can be roughly estimated from the daughter spectrum of methoxy benzaldehyde, which has a vapor pressure at room temperature and atmospheric pressure conditions of ≈ 0.2 torr [46]. The concentration (mol/mol) of methoxy benzaldehyde in air above a bottle cap can be approximated to be,

$$0.2 \text{ torr}/760 \text{ torr} = 0.0003. \qquad (1)$$

Neglecting the slightly reduced pressure near the entrance to the glass tube (this occurs because air is being drawn through the tube) and the dilution of the concentration with the air flowing through the system, the API source has detected and positively identified by a full-scan daughter spectrum methoxy benzaldehyde at a concentration of 300 parts

per million (ppm) in room air. Given an air sampling rate of 100 mL/min and an MS/MS acquisition time for the daughter spectrum of 5 s, this corresponds to 15 μg of methoxy benzaldehyde. Clearly, the resultant daughter spectrum has a high enough signal-to-noise ratio that one or two orders of magnitude less of the compound could still be identified. Furthermore, selected reaction monitoring of one or more parent ion-daughter ion pairs, would provide even lower detection limits.

CHAPTER 5

CONCLUSIONS AND FUTURE WORK

Summary of Results

The original purpose of this work was to design and develop a new atmospheric pressure ionization (API) source for a turbomolecularly-pumped triple stage quadrupole (TSQ) tandem mass spectrometer (MS/MS). This API source could be used to study API and direct atmospheric monitoring by mass spectrometry. To accomplish this, the work initially evaluated a commercially developed [1], but never marketed API source, which was developed as a GC-detector. This API source was characterized on a Finnigan 4500 single quadrupole mass spectrometer. Even as a GC-detector, the Finnigan-developed source suffered from memory effects (because of a small source region) and severe clustering of ions with molecules in the supersonic jet expansion of the post-orifice region. Because of these effects, direct atmospheric monitoring with this source was essentially impossible.

Therefore, a new API source was designed, which would be compatible with a commercial turbomolecularly-pumped mass spectrometer, and which would reduce or eliminate the problems of clustering and memory effects. This source was at first developed to be compatible and interchangeable with the Finnigan 4500 mass spectrometer used to

evaluate the Finnigan-developed API source; however, because of its design, this API source suffered from vacuum integrity problems. Even with these problems, ions were obtained with reduced, but not eliminated, clustering. Because of this clustering effect, this source was not viable for use as a direct atmospheric monitor.

This API source was redesigned to be compatible and interchangeable with a state-of-the-art triple stage quadrupole (TSQ) tandem mass spectrometer (MS/MS), the Finnigan TSQ 70. The modifications included moving all junctions between parts of the source canister outside of the vacuum chamber of the mass spectrometer, thus reducing some of the vacuum integrity problems. A new interfacing flange was designed to mate the source with the mass spectrometer. This flange contained the diaphragm seat, which now became the only interface between the atmospheric pressure source region and the vacuum of the mass spectrometer, and allowed the orifice to be electrically floated. Replaceable diaphragms were obtained with laser-drilled orifices, and a diaphragm with a 70 μm diameter orifice was installed in the interface place. This interface flange maintained vacuum integrity to near theoretical levels calculated from fluid-flow theory.

Unfortunately, moving all source components outside of the vacuum chamber resulted in a greater distance between the orifice and the first quadrupole. An ion optical modeling program (SIMION) was employed to model the region between the orifice and the first quadrupole. Although the model, which the program utilized, did not take into consideration the inelastic collisions of ions in the supersonic jet expansion in the post-orifice region, it proved

invaluable in the actual design of two lenses. These lenses increased the fraction of ions which were transmitted to the quadrupoles.

This new version of the API source employed a small tube near the orifice to provide a gas jet in the discharge region. This gas jet served to keep particulate matter away from the orifice (to prevent orifice clogging) and reduced the amount of water vapor which entered the post-orifice region (to reduce clustering).

A new current-regulated power supply, which was adjustable between 0.5 and 4.5 μA with a discharge voltage between 3 and 4.8 kV, was developed that generated a stable corona discharge. Along with this power supply, a ±500 V low output impedance power supply was developed to electrically float the orifice. The ability to electrically float the orifice allowed for an increased sensitivity and a strong declustering capability by creating a potential difference between the orifice and the first conical lens. The combination of these effects provided the ability to minimize clustering with or without the gas jet. The gas jet still served, however, to prevent orifice clogging.

Direct atmospheric monitoring was accomplished for various common laboratory solvents by sampling vapors from the caps of the solvent bottles. The orifice and lens potentials could be tuned such that the molecular or pseudo-molecular ion was the predominant ion in the mass spectrum for each solvent (methanol being the only exception).

Evaluation as Direct Atmospheric Analyzer

The API/MS/MS instrument was applied to differentiating a pair of

solvents with the same molecular weight which generated pseudo-molecular ions of the same m/z value. MS/MS was used to fragment each of the pseudo-molecular ions and generate daughter spectra which were easily distinguishable.

Electrical floating of the orifice caused a larger spread in the kinetic energy of the ions generated. Clustering and fragmentation occurred simultaneously, which in true mixture analysis would make the interpretation of mass spectra more difficult. While the API source was shown to detect compounds directly in the atmosphere at the ppm concentration range (≈15 μg of methoxy benzaldehyde), the potential of the sensitivity of the API source remains to be evaluated.

Suggestions for Future Work

Consideration of Supersonic Expansion Theory

The large body of work which has been performed to study the effects of a supersonic jet expansion of gases for the production of molecular beams has been reviewed by Bossel [47]. Most of the associated theory has been derived for systems with an "effusion source". An effusion source is one in which the diameter of the orifice is less than or equal to one mean-free-path of the species on the high pressure side of the orifice. This assures that no more than one molecule passes through the orifice at a given time. The mean-free-path for nitrogen (the major constituent of air) is 6.56×10^{-2} μm [48] or 656 nm. Clearly, an orifice of this size would reduce sensitivity and suffer from frequent clogging. However, this theory

can be used to calculate the velocity which the ions and molecules obtain in the supersonic jet expansion when they reach the plane of the aperture of the first conical lens. Equation 5.1 [38] can be used to calculate Mach number (the velocity of the molecule or ion relative to the speed of sound) at that point in the supersonic jet expansion.

$$M \approx \left[\frac{\gamma+1}{\gamma-1}\right]^{(\gamma+1)/4} \times \left[\frac{z}{d}\right]^{(\gamma-1)} \qquad (5.1)$$

For nitrogen γ (C_p/C_v) = 1.4 [38], and for this system the diameter of the orifice, d, is 0.00276" (70 μm) and the orifice-to-first conical lens (CL1) distance, z, is 0.075" (1900 μm). Using these values, M can be calculated to be 11.0. The ions and molecules are therefore moving at 8360 mph (3740 m/s). For a molecule of mass 100 g/mole, accelerated to 8360 mph, with a charge of 1, the kinetic energy can be calculated from equation 5.2.

$$K.E. = 0.5 \cdot m \cdot v^2 \qquad (5.2)$$

Applying the values above ($m = 1.66 \times 10^{-25}$ kg/molecule and $v = 3.40 \times 10^{-2}$ m/s), the kinetic energy can be calculated to be 7.2 eV. As the gas expands from the orifice, fluid dynamics predicts that the thickness of the beam of gas will be equal to one orifice diameter for a distance of approximately one orifice diameter [38]. To efficiently sample the beam of gas, CL1 should then have the location of its projected apex within one orifice diameter of the orifice. Figure 5.1

shows the relationship between the Mach number M, the orifice-to-CL1 distance z, and the required diameter of the aperture on CL1 D (see below). Sciex has stated [34] that if z is less than 50D then a potential field may be applied between the lens and the orifice to focus the ions while increasing the kinetic energy spread of the ions by less than 2 eV (for an electrically grounded orifice). Figure 3.8 shows a kinetic energy spread of less than 1 eV with this system for z ≈ 27D. However, for a floated orifice, the kinetic energy spread is much greater (Figure 3.10 shows a value of ≈ 10 eV). Therefore, by applying the knowledge of supersonic jet expansion theory, it may be possible to reduce this energy spread by reducing the size of the conical lens aperture and reducing z.

Bossel also reviews the need for finely machined conical lenses [47]. The front of the cone should come to as sharp an edge as possible. This reduces the production of a shock wave at the plane of cone aperture, termed a "mach disk", which can reduce the transmission of ions through the cone. The conical lenses used in this work lack this precise machining. Therefore, new conical lenses should be obtained. Several companies specialize in the production of molecular beam skimmers for supersonic expansion, two of which are Beam Dynamics [49] and Custom Service Technologies [50].

Requirements for Future Work

For the future development of this source, several components should be modified or replaced. Sciex has shown [34] that varying the needle-to-orifice distance can affect the relative intensities of the ions produced. This may be useful for providing additional selectivity

Figure 5.1

Relationship between the Mach number, M, the distance between the orifice and the plane of the aperture of the first conical lens, z, and the diameter of the aperture, D, required to allow efficient sampling of the ions exiting a 70 μm diameter orifice.

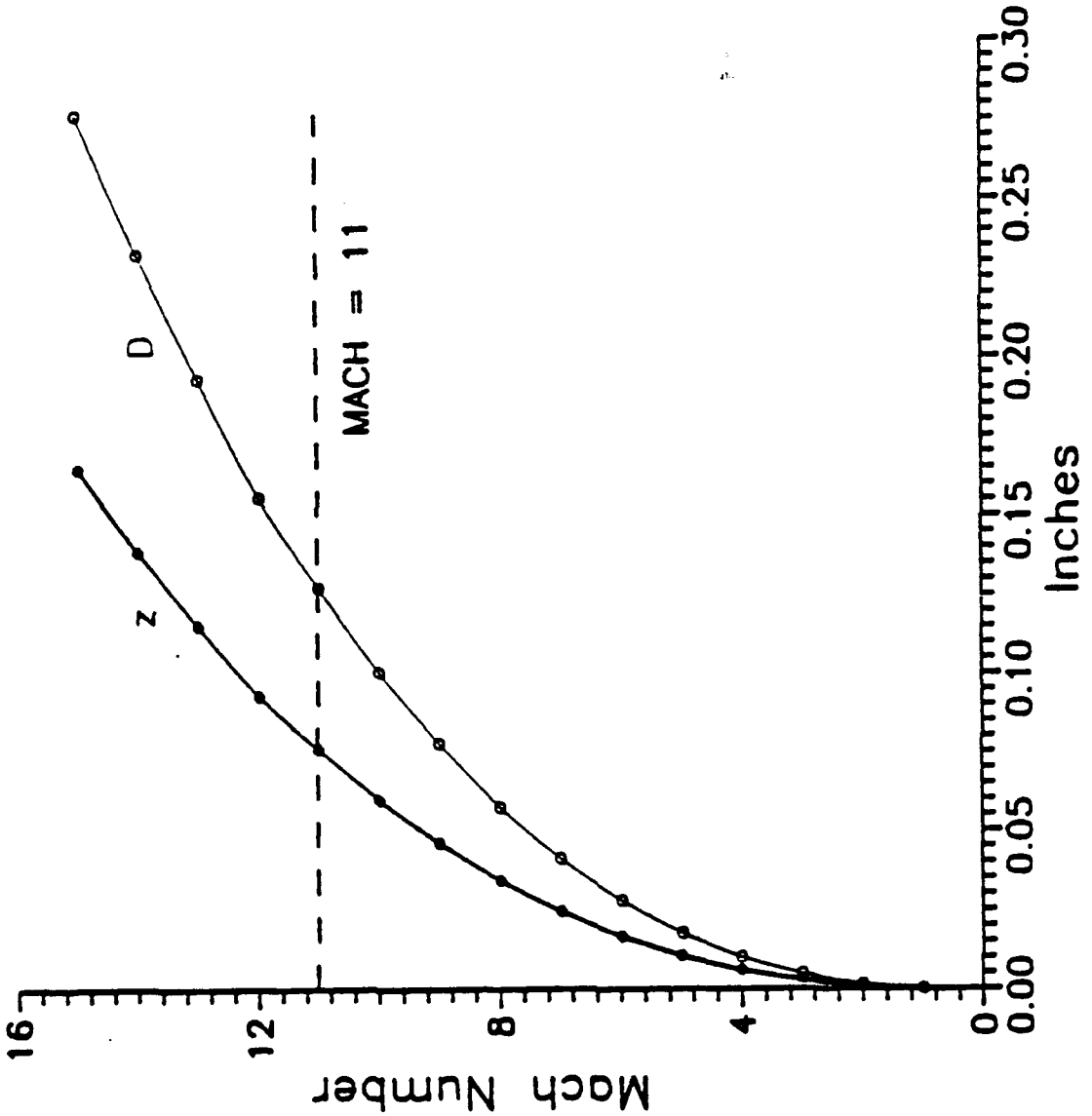
Mach Number
16
12
8
4
0
0.00
0.05
0.10
0.15
0.20
0.25
0.30
Inches
MACH = 11
D
Z

for the ionization process. Although the new corona discharge power supply has served to generate a stable corona discharge, the needle-to-orifice separation has been limited. For a given current, a larger needle-to-orifice distance requires a larger voltage from the power supply. The current power supply is limited to 5 kV. This has limited the needle-to-orifice separation to a few millimeters, and therefore it is proposed that a new discharge power supply be constructed based on a 10 kV power supply.

The vacuum system has proved inefficient in handling the large gas loads provided by the API source. When a normal gas load is put on the system, the forepump pressure (the pressure at the entrance to the mechanical pumps) is a few mtorr. With the API source installed, this pressure increases to approximately 400 mtorr. On the TSQ 70, one mechanical pump serves as the backing-pump for both turbomolecular vacuum pumps. For future work, the turbomolecular pump for the analyzer region should be provided with an independent backing-pump. This may allow for pressures closer to the theoretical value for the analyzer region and may allow the size of the orifice to be increased, increasing the sensitivity of the instrument.

The API source canister for this work was designed to allow flexibility in its configuration. Since the one-orifice system has been shown to perform adequately, a new, second-generation source canister should be built that has a larger diameter source region, is shorter, and provides micrometer control over the needle position. The walls of the original canister are approximately 0.5" thick stainless steel. This makes the source heavy and cumbersome. Therefore, the

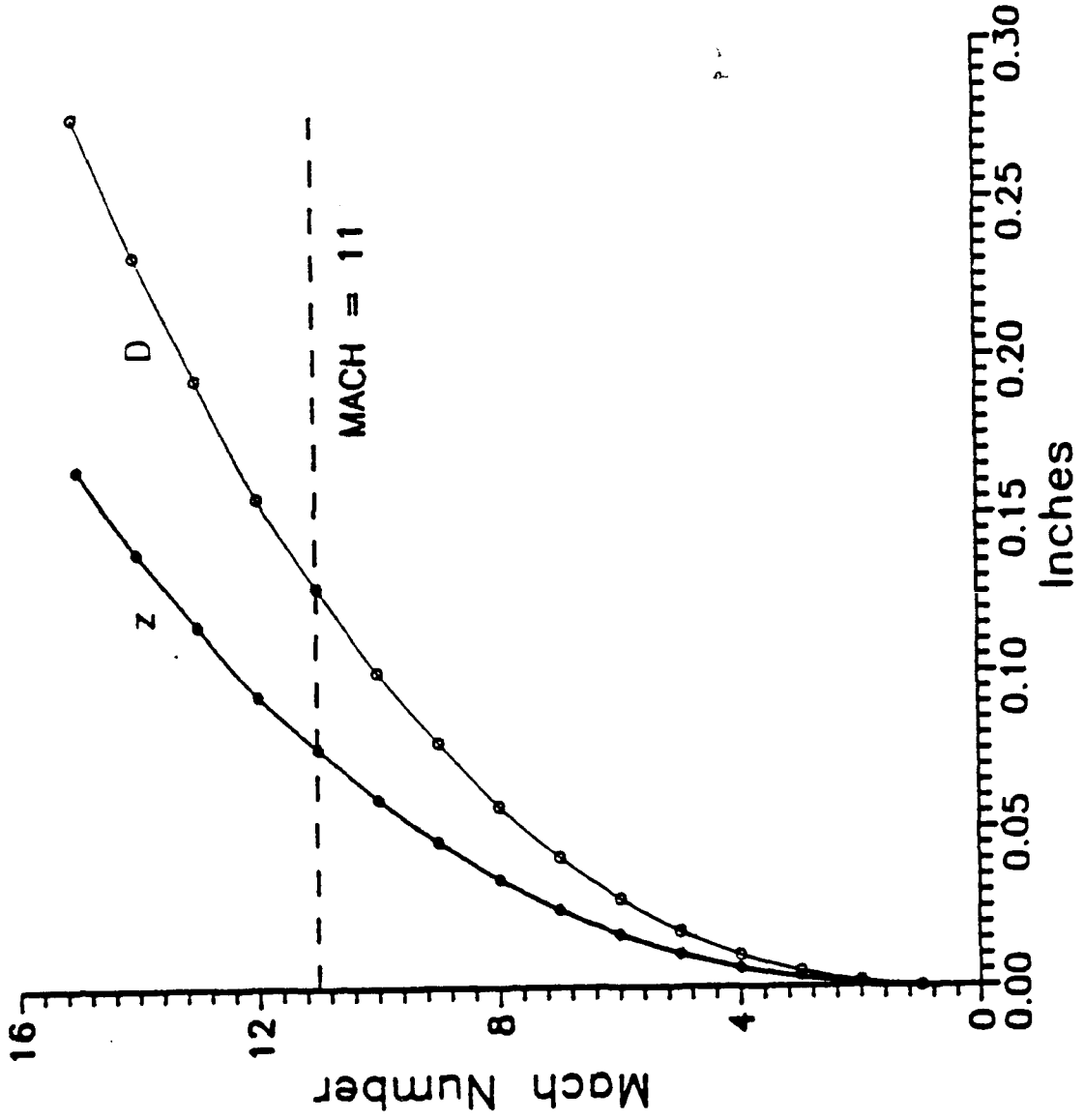
Mach Number
16
12
8
4
0
0.00
0.05
0.10
0.15
0.20
0.25
0.30
Inches
MACH = 11
D
Z

for the ionization process. Although the new corona discharge power supply has served to generate a stable corona discharge, the needle-to-orifice separation has been limited. For a given current, a larger needle-to-orifice distance requires a larger voltage from the power supply. The current power supply is limited to 5 kV. This has limited the needle-to-orifice separation to a few millimeters, and therefore it is proposed that a new discharge power supply be constructed based on a 10 kV power supply.

The vacuum system has proved inefficient in handling the large gas loads provided by the API source. When a normal gas load is put on the system, the forepump pressure (the pressure at the entrance to the mechanical pumps) is a few mtorr. With the API source installed, this pressure increases to approximately 400 mtorr. On the TSQ 70, one mechanical pump serves as the backing-pump for both turbomolecular vacuum pumps. For future work, the turbomolecular pump for the analyzer region should be provided with an independent backing-pump. This may allow for pressures closer to the theoretical value for the analyzer region and may allow the size of the orifice to be increased, increasing the sensitivity of the instrument.

The API source canister for this work was designed to allow flexibility in its configuration. Since the one-orifice system has been shown to perform adequately, a new, second-generation source canister should be built that has a larger diameter source region, is shorter, and provides micrometer control over the needle position. The walls of the original canister are approximately 0.5" thick stainless steel. This makes the source heavy and cumbersome. Therefore, the

canister should be built out of a lighter material such as aluminum, or the wall thickness should be reduced where possible.

To achieve total computer control of the API/MS/MS instrument, digital-to-analog (DAC) converters should be implemented to control the corona discharge current, the ±500 V orifice potential, and the potentials for the additional lenses that the API lens system has added to the mass spectrometer.

To sample gases, the sample must currently be brought near the entrance to the glass sampling tube. A larger capacity gas sampling fan should provide the ability to sample from greater distances.

Applications

Finally, the applications of API/MS/MS with this instrument should be extended. While this instrument has been applied to simple mixtures, it has not be applied to any "real" samples. With improvements listed above, the sensitivity of the instrument should be significantly increased. Also, this instrument has yet to be applied to samples which are more amenable to negative ionization.

The research presented in this thesis has demonstrated the ability to develop a functional API source for a commercial, turbomolecularly-pumped tandem mass spectrometer. The future research proposed here should prove this combination to be a viable method for the direct atmospheric monitoring of trace compounds.

LITERATURE CITED

1. Finnigan-MAT Corporation, 355 River Oaks Parkway, San Jose, CA 95134-1991.

2. Knewstubb, P. F.; Sugden, T.M. Nature 1958, 181, 474.

3. Knewstubb, P. F.; Sugden, T.M. Ibid. 1958, 181, 1261.

4. Knewstubb, P. F.; Sugden, T.M. 7th International Symposium on Combustion (Oxford, 1958) Butterworth, London, 1959, 247.

5. Knewstubb, P. F.; Sugden, T.M. Proc. R. Soc. London 1960, A255, 1920.

6. Kebarle, P.; Hogg, A. M. J. Chem. Phys. 1965, 42, 688.

7. Hogg, A. M.; Kebarle, P. Ibid. 1965, 43, 449.

8. Hogg, A. M.; Haynes, R. N.; Kebarle, P. J. Am. Chem. Soc. 1966, 88, 28.

9. Kebarle, P.; Searles, S. K.; Zolla, A.; Scarborough, J.; Arshadi, M. Ibid. 1967, 89, 6393.

10. Shahin, M. M. J. Chem. Phys. 1965, 45, 2600.

11. Carroll, D. I.; Dzidic, I.; Horning, E. C.; Stillwell, R. N. Appl. Spectrosc. Rev. 1981, 17(3), 337-406.

12. Mitchum, R. K.; Korfmacher, W. A. Anal. Chem. 1983, 55, 1485A-1499A.

13. Horning, E. C.; Horning, M. G.; Carroll; D. I., Dzidic, I.; Stillwell, R. N. Anal. Chem. 1973, 45, 936-943.

14. Dzidic, I.; Carroll, D. I.; Horning, E. C. Anal. Chem. 1976, 48, 1763-1768.

15. Carroll, D. I.; Dzidic, I.; Horning, M. G.; Horning, E. C. Anal. Chem. 1974, 46, 706-710.

16. Mitchum, R. K.; Althaus, J. R.; Korfmacher, W. A.; Moler, G. F. Advances in Mass Spectrom. 1980, 8B, 415-421.

17. Mitchum, R. K.; Althaus, J. R.; Korfmacher, W. A.; Rowland, K. L.; Nam, K.; Young, J. F. Biomed. Mass Spectrom. 1981, 8, 539-545.

18. Tsuchiya, M.; Taira, T. Int. J. Mass Spectrom. Ion Phys. 1980, 34, 351-359.

19. Carroll, D. I.; Dzidic, I.; Stillwell, R. N.; Haegele, K. D.; Horning, E. C. Anal. Chem. 1975, 47, 2369-2273.

20. Scott, R. P.; Scott, C. G.; Munroe, M.; Hess, J. J. Chromatogr. 1974, 99, 395.

21. Arpino, P. J.; Dawkins, B. G.; McLafferty, F. W. J. Chromatogr. Sci. 1974, 12, 574.

22. Yost, R. A.; Fetterolf, D. D. Mass Spectrom. Rev. 1983, 2, 1-45.

23. Caldecourt, V. J.; Zackett, D.; Tou, J. C. Int. J. Mass. Spectom. Ion Phys. 1983, 49, 233-251.

24. Extrel Corporation, P.O. Box 11512, Pittsburgh, PA 15238.

25. Sciex Inc., 55 Glen Cameron Rd, Thornhill, Ontario, L3T 1P2 Canada.

26. Bruins, A. P.; Covey, T. R.; Henion, J. D. Anal. Chem. 1987, 59, 2642-2646.

27. Bruins, A. P.; Weidolf, L. O.; Henion, J. D. Anal. Chem. 1987, 59, 2647-2652.

28. Henion, J.D.; Weidolf, L. O.; Lee, E. D.; Covey, R. C. 35th Annual Conference on Mass Spectrometry and Allied Topics 1987, 15-16.

29. Snyder, A. P.; Kremer, J. H.; Liebman, S. A.; Yost, R. A. 35th Annual Conference on Mass Spectrometry and Allied Topics 1987, 181-182.

30. Davidson, W. R.; Shusan, B. I.; Fulford, J. E.; Thomson; B. A.; Tanner, S. D.; Ngo, A. 32nd Annual Conference on Mass Spectrometry and Allied Topics 1984, 7.

31. Thomson, B. A.; Davidson, W. R.; Lovett, A. M. Environ. Health Perspectives 1980, 36, 77.

32. Glish, G. L.; McLuckey, S. A. 35th Annual Conference on Mass Spectrometry and Allied Topics 1987, 290-291.

33. French, J. B.; Reid, N. M.; Buckley, J. A. U. S. Patent No. 4,023,398, May 17, 1977.

34. French, J. B.; Reid, N. M.; Buckley, J. A. U. S. Patent No. 4,121,099, October 17, 1978.

35. Bertan Associates, 121 New South Road, Hicksville, NY 11801.

36. Karasek, F. W. Anal. Chem. 1974, 46, 710A-720A.

37. Precision Aperture, P.O. Box 10863, Fort Wayne, IN 46803.

38. Fite, W. L. Research note #1, Extranuclear Laboratories, Inc. January, 1971.

39. Levy, D. L. Sci. Amer. 1984, 250, 96-109.

40. Emco High Voltage Co., 11126 Ridge Rd., Sutter Creek, CA 95685.

41. Product and Vacuum Technology Handbook; Leybold-Heraeus, Inc.: San Jose, CA 1986.

42. McGilvery, D. D. Latrobe University, Department of Physics and Chemistry, Bundoora Victoria, Australia, 1977.

43. Dahl, D. A.; Delmore, J. E. Idaho National Engineering Laboratory, EG&G Idaho, Inc., P.O. Box 1625, Idaho Falls, ID 83415.

44. Good, A.; Durden, D. A.; Kebarle, P. J. Chem. Phy. 1970, 52, 212-221.

45. Harrison, A. G. Chemical Ionization Mass Spectrometry; CRC Press Inc.: Boca Raton, FL, 1982.

46. Jordan, T. E. Vapor Pressure of Organic Compounds; Interscience Publishers, Inc.: New York, NY, 1954.

47. Bossel, U. "Investigation of Skimmer Interaction Influences on the Production of Aerodynamically Intensified Molecular Beams", thesis, University of California-Berkeley, 1968.

48. Barrow, G. M. Physical Chemistry; McGraw-Hill Book Company: New York, NY, 1979.

49. Beam Dynamics, Inc., 708 E. 56th St., Minneapolis, MN 55417.

50. Custom Service Technologies, 4300 N. W. 23rd Ave, Suite 289, Gainesville, FL 32602.